APPLICATION OF DIGITAL IMAGING IN MEASURING CROSS TRACK DRIFT OF VESSELS ENTERING A PORT

by

Sahil Ramesh Patel
BScEng (Civil)

Submitted in fulfilment of the requirements for the degree of Master of Science in Engineering
In the
Civil Engineering Programme
University of Natal

Durban
2002

ABSTRACT

Durban is the busiest container port in Africa and there are plans for significant expansion during the next few years. This expansion includes the widening of the port entrance channel to accommodate larger "post-panamax" vessels. Complex crosscurrents near the port entrance, coupled with severe wind and wave conditions, may lead to the intermittent closure of the port which in turn could lead to significant economic implications. Information on the nature of the crosscurrents and how they affect the ships could assist harbour pilots in developing their skills and reduce the risks associated with steering ships into the port.

The research involved a case study to develop an innovative new method for directly measuring the effect of wind, waves and crosscurrents on ships entering the port. The technology is based on the application of digital image processing to track the position of ships as they manoeuvre in the port approach channel. The key innovation of this research is the extraction of the heading direction of the ship from the image data. The angle between this heading direction and the true velocity vector (the "crab angle") is then a direct measure of the cross-track drift velocity (CTDV) due to the combined effects of wind, waves and currents. The crosscurrents are usually the main contributing factor to the cross-track drift. The aim of this research was to develop a fully automated image processing system for real-time ship monitoring, and to determine cross-track drift within a wide range of weather conditions and ship parameters.

The methodology presented in this research allows the spatial structure of the CTDV along the harbour approach channel to be studied. The relationship of the CTDV to local surface winds was analysed. For deep draught vessels, measured CTDVs were found to be poorly correlated to surface winds. The spatial structure of the measured CTDVs shows distinct regions along the approach channel where vessels experience significantly larger drift velocities.

In summary, with the software tools developed by this research, digital images can be captured automatically and analysed to produce ship tracks and crab angles. From this information an extensive database for ship manoeuvring in the approach channel can be developed and the safety and efficiency of port operations improved.

PREFACE

The work described in this dissertation was carried out in the Centre for Research in Environmental Coastal and Hydrological Engineering, School of Civil Engineering, Surveying and Construction, University of Natal, Durban, from February 2000 until December 2001 under the supervision of Professor D.D Stretch, and is in accordance with the requirements of the University for the award of Master of Science in Engineering.

These studies represent the original work by the author and have not otherwise been submitted in any form for any degree or diploma to any tertiary institution. Where use was made of the work of others it has been duly acknowledged in the text.

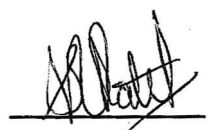

S.R Patel

As the candidate's supervisor I have/~~have not~~ approved this dissertation for submission

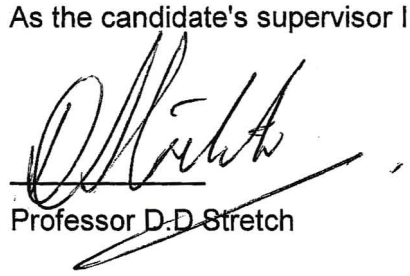

Professor D.D Stretch

02/21/02

ACKNOWLEDGEMENTS

I would like to thank Professor Derek Stretch, for his motivation and guidance throughout this research project. He has been a great supervisor to work with, and his inspiration and enthusiasm encouraged me to strive harder and achieve better results.

I would also like to thank Professor Chris Roebuck for his guidance and financial assistance provided on behalf of the Eastern Centre of Transport Development, a subsidiary of the Department of Transport.

I would like to thank PORTNET, the local port authorities, especially Port Engineers Dorian Bilse and Vishaal Lutchman for their kind assistance.

To postgraduates Guy Laister and Karan Venayagamoorty for their support and guidance, and to my girlfriend Anushka for her patience, and many hours of help.

To my family, especially my Mom and Dad, a hearty thanks goes out to you, for your love and encouragement throughout this challenge.

Finally I would like to thank God for providing me with the strength to succeed.

CONTENTS

LIST OF TABLES

LIST OF FIGURES

LIST OF PLATES

LIST OF SYMBOLS

Chapter 2

A_a	projected surface area of the vessel exposed to crosswinds (m^2)
A_w	projected surface area of the vessel exposed to crosscurrents (m^2)
C_a	coefficient of friction in water
C_w	coefficient of friction in water
F_a	force due to crosswinds (N)
F_w	force due to crosscurrents (N)
f	focal length
k_1	developed distortion coefficients
k_2	developed distortion coefficients
m_{ij}	direction of cosines of orthonormal rotation matrix
u_w	speed of crosscurrents (m/s)
u_a	speed of crosswinds (m/s)
u_o	x-coordinate of image centre (pixel)
U	image at time t
V	image at time t+Δt
v_o	y-coordinate of image centre (pixel)
x_e	distance measured from principal point to right hand edge of image (pixel)
X	x-coordinate for world (m)
X_c	x-coordinate for optic centre of camera (pixel)
Y	y-coordinate for world (m)
Y_c	y-coordinate for optic centre of camera (pixel)
Z	z-coordinate for world (m)
Z_c	y-coordinate for optic centre of camera (pixel)
δ	field of view of camera (deg)
ϕ	angle of rotation (deg)
λ_u	horizontal scale factor
λ_v	vertical scale factor
ρ_a	density of a air (kg/m^3)
ρ_w	density of water (kg/m^3)
σ	camera roll (deg)
τ	camera tilt (deg)

Chapter 3

B	point perpendicular to the horizon line
CTDV(t)	Cross Track Drift Velocity vector at time t
$CTDV_S(t)$	magnitude of the CTDV at time t (m/s)
$CTDV_D(t)$	bearing of CTDV(t) calculated from true north in a clockwise direction (deg)
D	point at which photograph is exposed
D_P	straight-line distance between camera and reference point (m)
D`	ground nadir point
Δs	arc length (m)
ΔH_θ	horizontal angular variation (per unit pixel) (deg/pixel)
ΔV_θ	vertical angular variation (per unit pixel) (deg/pixel)
H_θ	horizontal angle of view of the camera (deg)
H_D	heading direction (deg)
L_{OA}	overall Length of ship (m)
L_{SS}	length of ship from the bow to the smoke stacks (m)
L_{PROJ}	projected length of the ship (m)
O	centre of the earth
R_H	distance from camera location to Horizon (m)
R_P	location of reference point
R_O	mean radius of the earth (m)
S	chosen target object
S'	chosen target object on horizon line
S(t)	position of ship at time *t*
S(t-1)	position of ship at time *t-1*
Δt	time increment (s)
V_θ	vertical angle of view of the camera (deg)
V_D	direction of velocity vector (deg)
$V_D(t)$	direction of velocity vector at time t (deg)
V_{DV}	actual current velocity (m/s)
V_S	magnitude of velocity vector (m/s)
$V_S(t)$	magnitude of velocity vector at time t (m/s)
V_V	velocity vector
$V_V(t)$	velocity vector at time t
V_w	velocity of the ship relative to the water (m/s)

V_{DVH}	component of the actual current velocity vector, resolved parallel to the ship heading direction (m/s)
x_o	x-coordinate of image centre (pixel)
x_P	x-image coordinate of Reference Point (pixel)
x_S	x-coordinate of ship on image (pixel)
x_{TOT}	total number of horizontal pixels in an image (pixel)
X_C	X-ground coordinate of camera (m)
X_P	X-ground coordinate of reference point (m)
X_S	X-coordinate of ship on ground (m)
X_1	X-ground coordinate of bow of ship (m)
X_2	X-ground coordinate of smoke stacks of ship (m)
X`	X-ground coordinate of target object measured from O (m)
y_o	y-coordinate of image centre (pixel)
y_H	y-image coordinate of apparent horizon (pixel)
y_P	y-image coordinate of reference point (pixel)
y_S	y-coordinate of ship on image (pixel)
Δy_R	difference in y coordinate between horizon and reference point (pixel)
y_{TOT}	total number of vertical pixels in an image (pixel)
Y_C	Y-ground coordinate of camera (m)
Y_P	Y-ground coordinate of reference point (m)
Y_S	Y-coordinate of ship on ground (m)
Y_1	Y-ground coordinate of bow of ship (m)
Y_2	Y-ground coordinate of smoke stacks of ship (m)
Y`	Y-ground coordinate of target object measured from O (m)
Z_C	Z-ground coordinate of camera (m)
Z_P	Z-ground coordinate of reference point (m)
α	angle measured from North to reference point (deg)
β	angle measured from the right hand edge of the image to the object (deg)
θ	crab angle (deg)
θ_s	crab angle due to ship slip (deg)
ρ	angle measured from the right hand edge of the image to the reference point (deg)
τ	angle measured from Horizon to object position on the water plane (deg)
ω	angle measured from North to object (deg)

ω_1	angle measured from North to bow (deg)
ω_2	angle measured from North to smoke stacks (deg)

Chapter 4

X_S	x-ground coordinate of camera (m)
Y_S	y-ground coordinate of camera (m)
H_S	altitude of camera (m)
σ	camera roll (deg)

Chapter 5

H_θ	horizontal angle of view of the camera (deg)
X_C	X-ground coordinate of camera (m)
X_P	X-ground coordinate of reference point (m)
x_P	x-image coordinate of reference point (pixel)
x_{TOT}	total number of horizontal pixels in an image (pixel)
y_H	y-image coordinate of horizon (pixel)
y_P	y-image coordinate of reference point (pixel)
Y_C	Y-ground coordinate of camera (m)
Y_P	Y-ground coordinate of reference point (m)
y_{TOT}	total number of vertical pixels in an image (pixel)
Z_C	Z-ground coordinate of camera (m)
Z_P	Z-ground coordinate of reference point (m)
μ	mean (m)
μ_x	mean in the x-direction (m)
μ_y	mean in the y-direction (m)
σ	standard deviation (m)
σ_x	standard deviation in the x-direction (m)
σ_y	standard deviation in the y-direction (m)

Chapter 6

μ	mean
σ	standard deviation

LIST OF ABBREVIATIONS

ADCP	Acoustic Doppler Current Profiler
asl	above sea level
BMP	Bitmap file format
CCC	Cross Correlation Coefficient
CCD	Charge Coupled Device
CSIR	Council for Scientific and Industrial Research
CTDV	Cross Track Drift Velocity
DV	Digital Video
DOF	Degrees of Freedom
FFT	Fast Fourier Transform
GCP	Ground Control Point
GPS	Global Positioning System
GUI	Graphical User Interface
ICPMRDT	International Conference on Port and Maritime Reconstruction and Development and Technology
IDL	Interactive Data Language
IEEE	Institute of Electronic and Electrical Engineers
JPEG	Joint Photographic Experts Group
KBps	Kilobytes per second
Mbps	Megabits per second
msl	mean sea level
NPA	National Ports Authority of South Africa
PC	Personal Computer
PCI	Peripheral Computer Interface
PIANC	Permanent International Association of Navigation Congresses
PTZ	Pan, Tilt and Zoom
RGB	Red, Green and Blue
ROI	Region of Interest
SSA	Search Strategy Area
USACE	US Army Corps of Engineers
VCCC	Vector Cross Correlation Coefficient

CHAPTER 1

INTRODUCTION

1.1. Motivation

The Port of Durban is located on the eastern seaboard of South Africa, handling some thirty-one million tonnes of containerised cargo annually making it the busiest container port in Africa. With Durban being situated along one of the mainstream shipping routes, increasing demands are being placed on its container handling capacity annually. The National Port Authority of South Africa has realised that changes to the existing Port infrastructure are necessary in order to keep up with international standards. Failure to do so could result in the Port of Durban and South Africa suffering huge financial losses.

With this is mind, the port authorities, in 1997, commissioned the Council of Scientific and Industrial Research (CSIR) to undertake a study to determine the optimum increased width of the Durban's entrance channel. An increased width would result in the present one-way traffic changing to two-way traffic. In addition, the Port of Durban would then be able to host larger "post panamax" vessels that currently cannot enter the port due to physical constraints.

The widening of any entrance channel is a complicated process, with natural features like the wind, waves and currents playing an instrumental part in determining the optimum width. Too narrow a channel would lead to unacceptable risks, while too wide a channel would lead to increased dredging and costs. The South African continental margin is one of the most dynamically active meteorological and oceanographic regions in the world (Segal, 2001). Colliding currents, large standing waves and variable and intense wind fields can provide enormous challenges for Captains of large ocean vessels. The safety and efficiency of port operations relies on the skill of experienced harbour pilots who guide the ships into the port. Information on the nature of the crosscurrents and how they affect the ships could assist pilots in developing their skills and help reduce the risks associated with guiding ships into the port under adverse conditions. If the complexities of currents, winds and waves are misunderstood and applied hastily to the optimum width design process, shipping operations could become hazardous, eventually leading to catastrophic results.

1.2. Problem Statement

The design of the optimum width for the Durban Harbour entrance channel relies specifically on the behaviour of ships in extreme weather conditions. Ship simulators are commonly used to validate a selected width, by means of a probabilistic analysis, for a variety of weather conditions. Ship simulators model a ship's response to environmental forcing mechanisms using empirically derived coefficients. Ship tracks produced with these simulators are therefore questionable. An important factor not considered by most simulators is the spatial structure of crosscurrents, and its variation with depth. It is well known that at Durban the most limiting factor for harbour pilots who steer ships into the Port is the crosscurrents. There is currently no physical instrument outside the entrance channel of the Durban Harbour that regularly measures currents. However, growing pressures are being placed on the local port authorities to install some kind of measuring device. These measuring devices would usually be located at fixed positions, thus only giving current information at that position. Due to the significant spatial variability of crosscurrents a fixed point measuring system may not be adequate for improving the safety of ship operations. The cost of deploying and maintaining such devices is also high, hence other more cost effective solutions are required.

1.3. Present Investigation

An innovative new method for measuring the direct effect of wind, waves and crosscurrents on ships entering the port has been developed in this investigation. The technology is based on the application of digital image processing to track the position of ships as they manoeuvre in the port approach channel. The key innovation is the extraction of the heading direction from the image data. The angle between this heading direction and the true velocity vector (the "crab angle") is then a direct measure of the cross-track drift velocity (CTDV) due to the combined effects of wind, waves and currents. Using automated image processing techniques coupled with real-time monitoring, the CTDV for a wide range of weather conditions and ship parameters can be measured at any location along the ship tracks. This new and innovative technique can be used:

1. For long term monitoring of actual ship tracks under actual weather conditions. The ship track plots from this investigation can be used to validate the ship track plots from a ship simulator for similar conditions.
2. For providing spatially distributed information about crosscurrents and their affect on ship manoeuvring, so that it may assist pilots in maintaining safe entry operations.

3. For the training of new harbour pilots, who can use these recorded ship tracks to learn about general patterns of entry as well as identify key visual aids used by the more experienced harbour pilots.

1.4. Objective

The objective of this research was to develop a fully automated image processing system that would monitor and automatically track ships entering the harbour on a real time basis and produce a database of ship track and CTDV data for a wide range of weather conditions and ship parameters.

1.5. Aims

The specific aims of this investigation were to:

1. further develop and validate a new technology, using digital imaging, to track ships entering the port and measure the direct effects of winds, waves and crosscurrents on ship manoeuvres.
2. use the above technology to investigate the preferred entry patterns used by pilots at the Durban harbour, and investigate its dependency on weather conditions.
3. use the above technology to investigate the spatial structure of the cross track drift experienced along the Durban approach channel, and to investigate if regions along the approach channel exist where dominant drifts can be expected.
4. develop software to automate the process of monitoring and tracking ships into the harbour in real time.

1.6. Publications

The work presented in this investigation was presented at the International Conference on Port and Maritime Reconstruction and Development and Technology (ICPMRDT), in Singapore (Patel & Stretch, 2001). The preliminary results were also presented (at a seminar) to the port Captain and engineers of Durban (the case study site), during January 2002.

1.7. Structure of this Dissertation

In **Chapter 2** a brief review into port entrance channel design, with a focus on how ship simulators are used for channel width design is discussed. Basic ship dynamics and the effects of winds, waves and currents are also reviewed. Coastal Imaging principles are reviewed, with a focus on machine vision and image correlation techniques.

In **Chapter 3** the methodology, of the proposed imaging technology is derived and discussed. The key innovation of extracting a ship's heading direction from an image as well as how an actual ship track plot can be determined by using imaging techniques is shown.

Since it was not clear that the proposed imaging technology would work, **Chapter 4** discusses how this method evolved from using a portable digital still camera to a fixed video camera system. Preliminary results of the methodology are presented, with the difficulties experienced for each stage of the evolution process discussed. The results of a validation of the proposed technology are also presented and discussed.

Specific ship tracking software that was developed for automating the imaging techniques proposed in Chapter 3 and Chapter 4 are presented and discussed in **Chapter 5**. Specific features of this software are described, with focus on the feature tracking function. Limitations of the proposed software are also discussed.

Chapter 6 presents ship track data and drift measurements that were determined using the proposed technology. An overview of the data is presented and discussed. The results of a conditional analysis of the data are presented with key observations highlighted. The results presented in this chapter are specific to the Durban Harbour (the case study site).

Chapter 7 summarises and discusses the new technology as well as the key findings of the work carried out for this investigation. Recommendations for future work are made.

CHAPTER 2

LITERATURE REVIEW

2.1. Introduction

Note that the technology that forms the subject of this dissertation is new. No literature about the tracking of ships using digital imaging was found. A patent concerning this new technology is under investigation (Stretch, 2001).

This chapter reviews some key concepts relevant to the present investigation. The key concepts that will be discussed are:

1. Port Entrance Channel design
2. Ship dynamics due to winds, waves and currents
3. Measurement of currents and their association with wind
4. Coastal Imaging using digital video
5. Machine vision with object tracking

The general design of an entrance channel is discussed, with a focus on the channel width design parameter and how ship simulators are often used to optimise the width. The present investigation presents a method that can be used to validate the results of ship simulators by using actual observed ship tracks instead of simulated ones.

Weather conditions like wind, waves and currents and their affects on ship movements are discussed as these natural forces, when coupled, can result in complicated and risky conditions for ships negotiating entry into a port.

According to studies carried out by the Council for Scientific and Industrial Research (CSIR) the most critical environmental factor with respect to ship manoeuvring in the Durban entrance channel are crosscurrents (CSIR, 1999b). A review with respect to how currents are generated as well as how they are measured is summarised. This investigation presents a technique to measure the spatial distribution of a component of drift, which is primarily due to currents.

A brief review is carried out on the ship drift phenomenon. Richardson (1997) used ship drift measurements to obtain currents by subtracting a ship's heading vector from its true velocity vector, over time scales measured in hours. These vectors were recorded on computers on board the vessels. The method used in the present investigation uses digital imagery to extract heading and velocity vectors, but over very short time intervals (seconds), thus focusing on higher spatial resolution drift information.

Since this investigation uses digital imagery, the recent applications of digital video to coastal imaging are summarised. Areas reviewed include rectification methods and basic photogrammetric principles, where rectification is defined as the transformation of image coordinates (pixels) to world coordinates (metres).
Machine vision or pattern matching techniques are reviewed since this investigation uses these concepts for the development of automated ship tracking software. Cross correlation techniques, are also investigated as they have been proven to be useful in similar applications.

2.2. Entrance Channels

An entrance channel is a channel section beginning in the open sea and extending through a tidal inlet or between breakwaters (Kriebel et al, 2000). When a vessel is out in the open ocean, it has virtually unlimited space in which to manoeuvre. While the chances of a ship actually colliding with a landmass is small, the ship may be subjected to waves and swells, blown off course by winds or affected by currents. While approaching a harbour, these factors may still be present, but to ensure a safe entry the vessel has to follow an accurate course to avoid collisions with the breakwaters or grounding on the shores. A harbour pilot is generally used to ensure a safe entry of a ship into the Port under adverse weather conditions. The width of the entrance channel is of critical importance as the wider the entrance the easier the task becomes for the harbour pilot. However the wider the entrance channel, the larger the effects of wave energy on the vessels (Harlow, 1981).

At present the design of entrance channels is based on the international design guideline and manuals of the Permanent International Association of Navigation Congresses (PIANC, 1997). Various countries have adopted this guideline but have adapted the design parameters to suit their needs. The United States standard practice with respect to the design of entrance channels is based on the standards set by the U.S. Army Corps of Engineers (USACE, 1995). The South African standard practice for harbour design is based on PIANC guidelines but has been modified by the National Ports Authority of South Africa to suit local conditions. Presently, the Durban harbour entrance channel has a bed width opposite the head of the main breakwater of about 170 m, and tapers to 140 m at the central part of the entrance channel (CSIR, 2000).

2.3. Design of Entrance Channels

The following sub-sections summarise the basic design philosophy used in the design of entrance channels. More detailed analysis is available in PIANC (1997) or USACE

(1995) design manuals. The design philosophy is reviewed here in order to demonstrate where in the channel design process, the technology presented in this investigation can be used.

Channel design is normally considered to be a two-stage process consisting of a conceptual design and a detailed design. The conceptual design is the initial design stage where physical parameters of the proposed channel - width, depth and alignment - are determined from physical environmental data.

The detailed design is a more elaborate process where the results of the conceptual design are evaluated and refined. The methods used in detailed design commonly rely on computer simulation models to determine the dimensions of the entrance channel and the manoeuvring areas. A risk and cost estimate analysis may also be carried out. For this investigation the detailed design stage is discussed with specific attention to ship simulators and its relevance to the channel width design process. The first stage of the design process is to select a suitable design ship.

2.3.1. Design Ship Concept

A design ship is chosen to ensure that it, and all other ships using the channel can navigate safely within the entrance channel. The design ship may be based on one or more of the following criteria (PIANC, 1997):

1. Poor inherent manoeuvrability.
2. Very large in the context of Port operations.
3. Excessive windage.
4. Transportation of hazardous cargo.

If the channel is to cater for a wide range of ship types, it may well be appropriate to consider more than one design ship. In such cases a deep-draught design ship might be used to determine the channel depth while a shallow draught ship with a large windage might be used for channel width. There are also some interactions between these variables. For example, the ship length and beam can affect the channel depth if the ship is rolling or pitching in waves. The ship draught also affects the channel width, since ship manoeuvrability is degraded when the depth-to-draught ratio diminishes and approaches unity. The next stage of the design process involves determining the channel width, depth and alignment.

2.3.2. Channel Width

The design of the optimal channel width should ensure the safe movement of all ships expected to use the channel. In the conceptual design stage, channel width is determined primarily from the beam of the design ship. For the detailed design phase, the channel width is checked using ship simulation (Kriebel et al, 2000).

In 1997, the CSIR was commissioned by the National Ports Authority of South Africa (NPA) to undertake a study to determine the optimum width of the entrance channel, which could accommodate fully laden post-panamax container vessels. The CSIR reported that, based on the PIANC guidelines, the conceptual design width for Durban's entrance channel should be about **five** times the design ship's (single transit post-panamax container vessel) beam width (CSIR 2000).

PAINC (1997) recommends that ship-manoeuvring simulations be carried out to refine the conceptual design width, and quantify the safety and risk level of the final channel width determined. PIANC (1997) defines a ship manoeuvring simulation as a mathematical model, installed on a computer, which reproduces the manoeuvring behaviour of the ship. Standard detailed design practice utilizes a real time simulator to manoeuvre the design ship through the channel under various environmental conditions. Numerous simulated runs are carried out to determine the transverse deviation (or offsets) of the ship normal to the entrance channel axis. The assumed channel width is confirmed if the safety requirements of the simulated runs are satisfied. This is part of a probabilistic design approach.

There are generally three types of ship simulators, the full mission simulator, mini simulator and the micro simulator (CSIR, 2001). The full mission simulator is the most expensive (and most realistic) simulator, and has a full reproduction of the bridge of a ship - with all ship controls. The users view is a projection of the harbour environment, with a full view around the ship (360 degrees) or only the foremost view sector (225 degrees). The smallest type of simulator is the micro simulator, which runs on a standard PC, with manoeuvring control by keyboard. The users view for this simulator is from above the ship (birds eye view).

The simulator used by CSIR during their investigations at the Port of Durban was a micro simulator known as PORTSIM. PORTSIM was developed by SSPA in Gothenburg, Sweden. The simulator is equipped with numerous functions including automatic pilot, course keeper control and direct manual control settings. It is capable

of determining a ship's motion with up to six degrees of freedom. The simulator programme has the capability of accepting wind, wave and current measurements. By varying these weather parameters, both simple and complicated ship manoeuvres can be simulated for a range of channel layouts. The probabilistic design method adopted by the CSIR used a ship simulator to manoeuvre a design vessel through the channel under extreme design conditions (CSIR, 2000). At various sections along the channel the spreading of the simulated ship tracks was computed, from which the standard deviation of the ship's swept path was calculated. Probability functions like the Gaussian distribution function was used to determine the probability of exceedance. For an accepted percentage of exceedance of 1.24%, a width of at least **six** times the design ship's beam width was determined for the simulated data for Durban (CSIR, 2000). This is the basis of the design of the optimum width.

For the present investigation actual ship tracks under a range of weather conditions are recorded and can be statistically analysed to produce the transverse deviations of the ship from the channel axis. This analysis can then, for similar weather conditions, be compared to the results produced by the CSIR simulation analysis in order to validate the simulator.

2.3.3. Channel Layout

The USACE (1995) and PIANC (1997) both recommend aligning a channel with the predominant tidal currents and with the natural channel bathymetry. This generally helps to minimize maintenance dredging. In addition, tidal currents will generally follow a path in line with the channel, which is preferred for navigation as opposed to having currents crossing the channel at right or oblique angles. The predominant wind and wave directions are also considered in channel alignment, as a channel aligned with these directions simplifies ship manoeuvring. Channels should be aligned so that ships can maintain speed and control while transiting through areas where they may be exposed to high winds, waves, and currents. This requirement precludes the use of sharp turning angles in exposed locations. Ship dynamics are such that, when under manual control, they sweep a path, in the absence of all external forces from wind, waves, current etc., which exceeds their beam width by a certain amount. This must also be taken into account in channel alignment and width.

The entrance channel to the Port of Durban has an orientation of 215.5° as can been seen in Figure 2-1. This is within the range of values of the dominant wind directions, which are from the north-east and south-west directions. Wind forces therefore have only small direct effect on ship movements in the entrance channel. It is the

crosscurrents that have the most influence on the safe entry of vessels into the port. Previous studies, (CSIR, 1999a and b), concerning the entry of vessels into the harbour have concluded that north-westerly currents have a greater influence on ships than south-easterly currents. Note that the convention is to specify currents by the direction **towards** which they are flowing, unlike winds that are specified by the directions **from** which they blow.

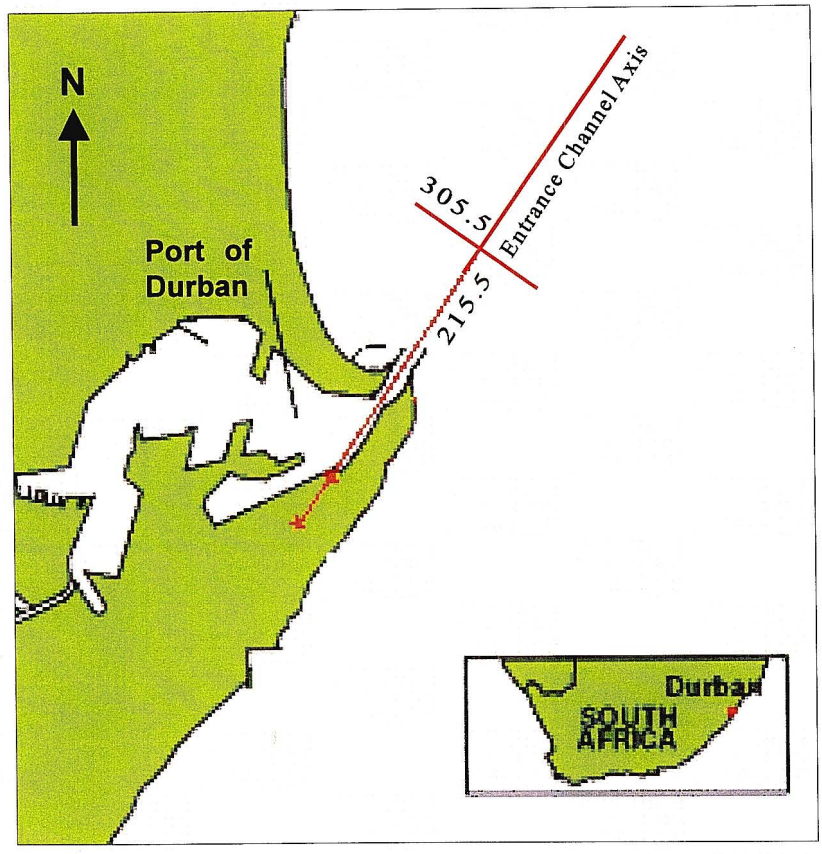

Figure 2-1: Map of the Port of Durban and entrance channel

2.4. Wind Effects on Ships

PIANC (1997) states that cross winds will affect ships at any speed, with the greatest effect experienced by ships at low speeds. A ship will drift laterally due to cross winds and thus increase the width required for manoeuvring. Under crosswinds a ship travelling at low speeds will be unable to maintain a fixed course, forcing the pilot to steer the ship into the wind, resulting in an oscillatory course. Figure 2-2 illustrates this course, which has been exaggerated for clarity. Cross wind effects primarily depend on the windage of the vessel, the wind speed and direction relative to the ship and the depth/draught ratio. PIANC (1997) states that as the depth/draught ratio decreases towards unity, a ship becomes more directionally stable and, consequently, more sluggish in its response. The improvement in directional stability is an advantage in straight channels as long as the ship is not deflected off its proper course. If it is

deflected, its sluggish response will result in handling problems, which will increase the manoeuvring space required.

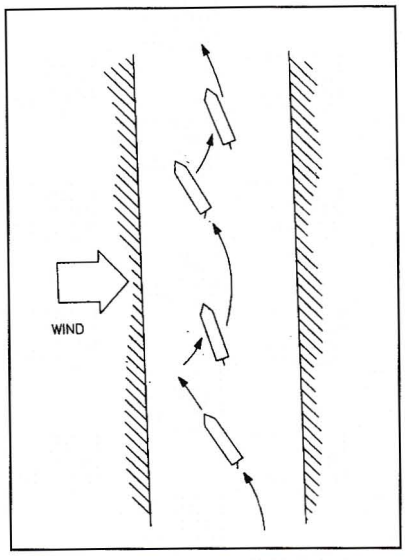

Figure 2-2: Handling of a vessel in a strong wind (from PIANC, 1997)

CSIR (1999a) analysed wind data for the Port of Durban, and concluded that the two dominant wind directions for high wind speeds (larger than 10 m/s) are NE (42% of the time, with an additional 12% from N and 9% from E) and SW (20% of the time, with an additional 13% from S). The present orientation of the port lies within the sector of the dominant wind directions (NE = 45° and SW = 225°). This implies that the dominant extreme winds will blow in line with the ship as it enters the port. CSIR (1999b) converted the wind speeds to an elevation of 10 m above sea level, and found that a one-minute average wind speed of 12 m/s is exceeded during about 10% of the time and that a speed of 16 m/s is exceeded during about 1% of the time. It can, therefore be expected that the influence of the extreme wind conditions on entry manoeuvres is not severe. A typical wind rose for winds experienced around Durban is shown in Figure 2-3. This wind rose was based on wind data over a five-year period (1998-2002) and was provided by the CSIR. The wind data used in this wind rose was recorded at the Durban Port Control weather station. The results presented by CSIR are qualitatively consistent with this wind rose, with the higher wind speeds predominantly blowing along the entrance channel axis.

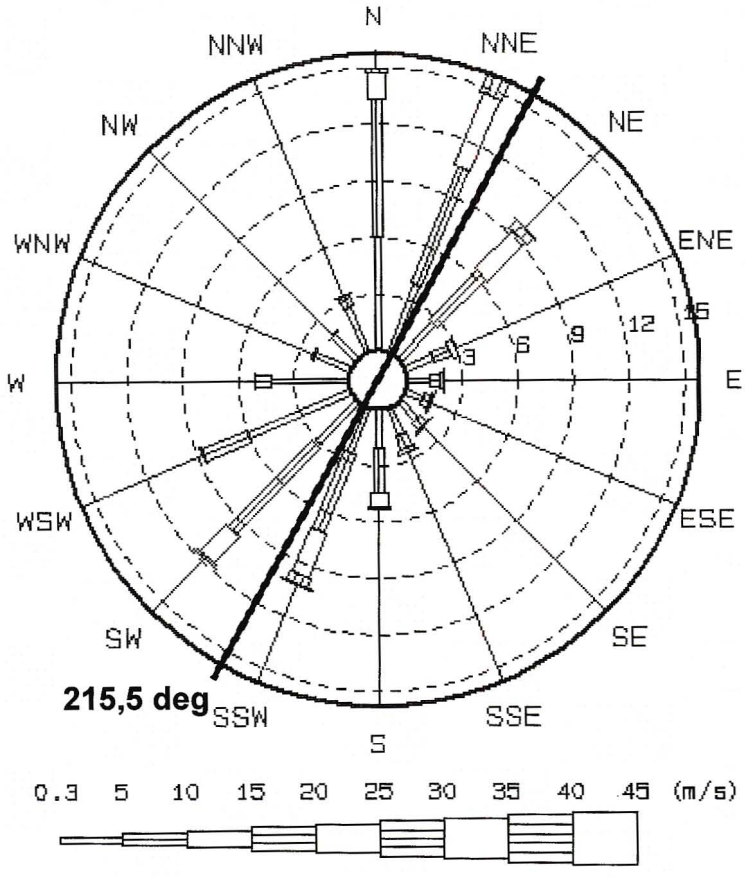

Figure 2-3: Typical wind rose for Durban from the Durban Port Control weather station, for 5 years of data – 1998 to 2002 (unpublished from CSIR)

2.5. Wave effects on ships

Wave information is an important aspect in the design and operation of entrance channels. This information deals with vessel motions and manoeuvring characteristics. A ship can undergo wave-induced motion with six degrees of freedom (DOF) as shown in Figure 2-4 from Demirbilek & Sargent (1999). In general, six DOF motions apply to any rigid body. Three of the DOF's are in the vertical plane (heave, roll, and pitch), while the remaining DOF's are in the horizontal plane (surge, sway, and yaw)

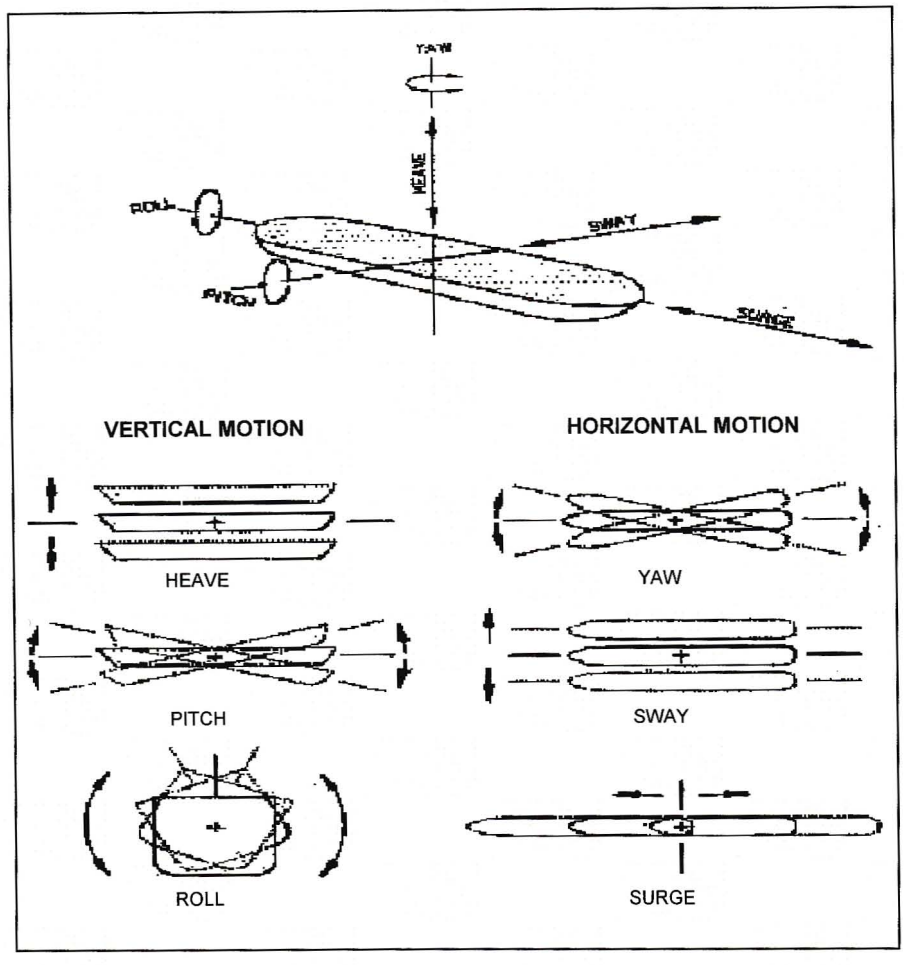

Figure 2-4: The six degrees of freedom that can be induced by wave action on a vessel (from Demirbilek & Sargent, 1999)

The vertical motion of some point on the ship is determined by, the heaving, pitching and rolling motions. The motion of a ship depends upon the size of the ship relative to the waves. One can consider these motions being equivalent to a mass-spring dynamic system (Bijker and Massie, 1978). These systems have a natural frequency. The displacements can be large even though the waves are of small amplitude. These vertical motions can be important in the design of channel depths and underkeel clearances.

The horizontal ship movement is determined by swaying, surging and yawing motions. The horizontal motion components of yaw and sway are caused by either rudder or wave action and are important in determining the required manoeuvring areas and channel widths (Bijker & Massie, 1978).

2.6. The effect of current on ships

Longitudinal currents affect a ship's ability to manoeuvre and stop whilst crosscurrents affect the ship's ability to maintain a set course. PIANC (1997) recommends that in

order for a vessel to avoid the effects of strong crosscurrents (of order 2 knots) over a short section of the channel, the ship may have to pass through this section as rapidly as possible to avoid deviation from its path.

Monitoring and forecasting of waves and currents are helpful for activities such as ship navigation and for routine operation of ports and offshore platforms. Statistics derived from long-term current measurements are often used to calculate probabilities of extreme conditions likely to be encountered at specific locations. Thus such monitoring is essential for designing and planning purposes (Lane et al, 1999).

The tidal currents in the port of Durban's entrance channel are not considered a problem for manoeuvring ships, since they are in line with the ship's path (CSIR, 1999b). These tidal currents were measured by CSIR (1999a) and were found to be about 0.8 m/s (1.6 knots). The major problem is associated with strong currents that occur across the entrance channel just beyond the breakwater. These crosscurrents are generated either directly by local wind and wave action or are associated with large-scale current patterns along the coastline. Figure 2-5 illustrates the dominant currents common around the Durban entrance channel (CSIR, 1995).

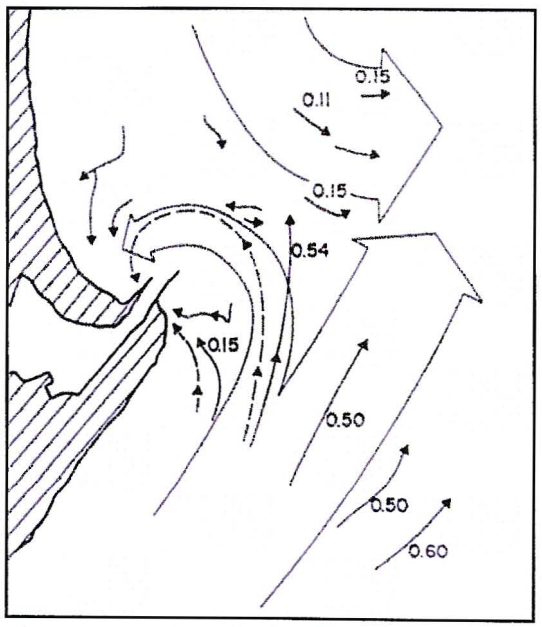

Figure 2-5: Flow distribution around the Durban Harbour entrance channel derived from Buoy Tracks (from CSIR,1995)

From the current patterns shown it appears that the largest currents are north-westerly with average magnitudes equal to 0.5m/s (refer Figure 2-5). CSIR (1999c) identified two key circulation cells around the entrance channel, an anticlockwise "Bight eddy" (shown as the south-easterly current in Figure 2-5) and a clockwise "Bluff eddy" (shown as the north-westerly current in Figure 2-5). The measurements shown in

Figure 2-5 were derived from wave buoys with the inferred current being along the surface. Unfortunately currents around the port entrance have a complicated structure, varying both spatially and with depth, and depend strongly on the weather conditions over short time scales. Information on how these currents vary with depth is useful for understanding the difficulties of manoeuvring in the entrance channel.

2.7. Wind Driven Currents

Currents are driven either by winds or waves or a combination of the two. Wind driven currents, as the name implies, are currents that are created by the force of the wind exerting a shear stress on the water surface. This stress causes the surface water to move and this movement is transmitted to the underlying layers of the water. The depth to which the stress induces the movement is dependant on the strength and persistence of the wind. Wind induced currents are common in oceans. The current is generally in the wind direction at the surface with a counter current flow direction at some depth below the surface (Wu & Tsanis, 1995). Many measurements have been made under various wind conditions and it was found by Wu (1975) that the current near the water surface follows a Karman-Prandtl (logarithmic) velocity distribution. It was also found that the current immediately below the water surface varies linearly with depth. Figure 2-6 illustrates this profile of the velocity distribution of wind-induced currents, and how the current varies with depth through the water column. The variation of direction with depth is associated with Coriolis effects and the phenomenon is known as the Ekman Spiral. From Figure 2-6 one can see that the direction and magnitude of wind-induced currents in the upper surface layers of the water column varies from that of the subsurface layers.

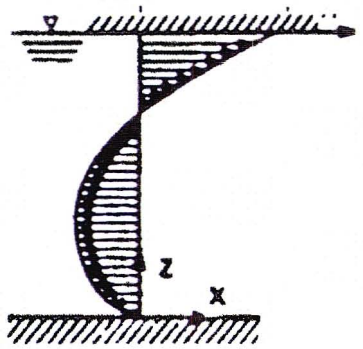

Figure 2-6: Velocity Distribution varying with depth. (from Tsanis, 1989)

2.8. Current Measurements

Current velocities in estuaries and coastal waters have traditionally been measured by means of a combination of float tracking for surface waters and various types of impeller or other forms of mechanical current meter deployed at specified depths within the water column (Wewetzer et al, 1998). These techniques determine only the horizontal components of flow velocity. During recent years, the three-dimensional velocity structure of coastal and estuarine systems has increasingly been investigated by means of Acoustic Doppler Current Profilers (ADCP).

An ADCP can be used to measure current velocities and directions through the water column, and can be used to determine their effect on a design ship. Current measuring devices are usually located at fixed positions, thus only giving current information at that position. Due to the significant spatial variability of crosscurrents a fixed point measuring system may not be adequate fro improving the safety of ship manoeuvring. Lane et al (1999) conducted experiments with a towed ADCP (located at the base of a vessel), with the advantage that currents could be measured over a larger area with the use of one instrument only. Although this method yields detailed current information, trying to equip every maritime vessel with this type of current measuring system is costly and impractical.

The CSIR (1999a) carried out similar research to investigate the spatial structure of currents along the Durban Harbour Port approach channel, extending from the end of the southern breakwater to a distance approximately 3 kilometres offshore. This involved using an ADCP fixed to a vessel, which was used to measure the vertical and horizontal structure of the currents below a depth of four metres from the ocean surface. A typical transect indicating the vertical structure of the current along the approach channel is shown in Figure 2-7. The currents shown are in centimetres per second and extend from the head of the southern breakwater to a distance three kilometres offshore. Note that contours marked with a negative sign in Figure 2-7 imply a south-easterly flowing current as defined by CSIR (1999a).

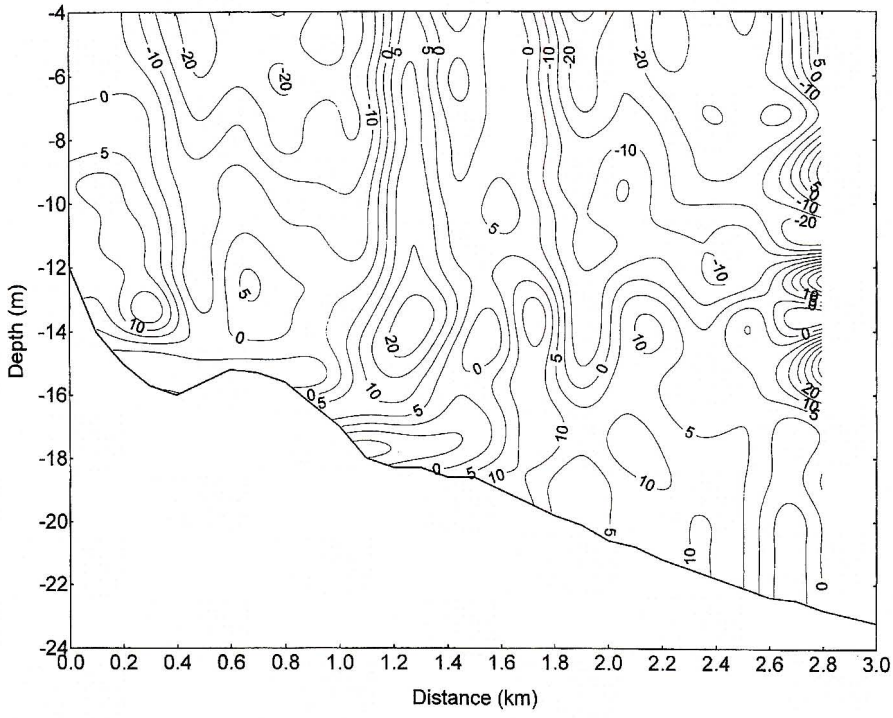

Figure 2-7: Transect of the spatial structure of the crosscurrents normal to the ship track path followed (from CSIR, 1999a).

Figure 2-8 illustrates the horizontal structure of the currents from the same transect at a depth of seven metres below the water surface. In total, CSIR (1999a) presented fifty-seven transects which were used for their analysis. Unfortunately due to the complex structure of the crosscurrent data no consistent relationships between the measured crosscurrents, winds and wave conditions could be found. Nevertheless, CSIR (1999a) recommended that the National Ports Authority install an ADCP at approximately 750m north-east of the southern breakwater, since this was the region where large crosscurrents were regularly measured (refer Figure 2-8 b). Due to the shallow sea depth at this position and the risk of damage due to deep draught vessels, the CSIR suggested placing the ADCP at a position just east of the channel (refer Figure 2-8 b - Position X).

An ADCP was temporarily deployed at this position for a period of thirty days (February to March 1999). This data was analysed by Mardon & Stretch (2002), and the key results are shown in section 2.9.2.

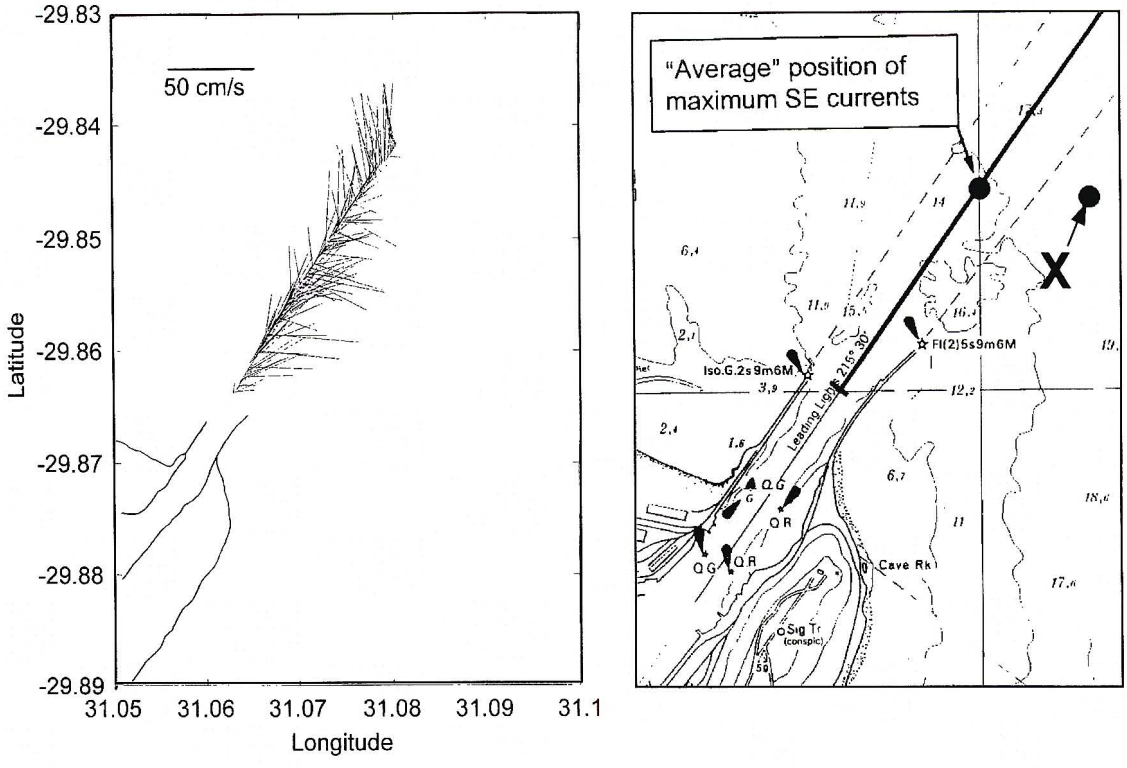

Figure 2-8: (a) Plan view of the horizontal structure of the currents transect with the crosscurrents transverse to the path followed (b) Plan view of the entrance channel showing the region where the average maximum currents were measured. (from CSIR, 1999a)

2.9. ADCP measurements around the Durban entrance channel

2.9.1. Background

The primary purpose of an ADCP is the measurement of horizontal components of current velocities up to ranges of about 500m from the instrument (Haren, 2001). In the past decade a secondary application of an ADCP has been the measurement of surface waves (Pinkel & Smith, 1987), wind speed and direction (e.g. Schott, 1989) and sea level variations (Visbeck and Fischer, 1995).

An ADCP uses the Doppler principal to measure the relative velocity between different objects. A review of ADCP principles is given by Wewetzer et al (1998) and Gordon (1996).

2.9.2. Typical Vertical Profiles from an ADCP

Mardon & Stretch (2002) carried out an analysis of ADCP current data provided by the CSIR. The aim was to determine at what depths near-shore currents were driven by local wind patterns, and at what depths they were unaffected by local wind patterns but rather driven by larger scale ocean circulation or weather patterns. Figure 2-9 shows a typical vertical ADCP current profile from Mardon & Stretch (2002). This figure illustrates seven curves plotted on one set of axis. These curves show the structure of the crosscurrent over a one-hour period between 8:00am and 9:00am on 10 February 1999. The component of the total current in the direction of 305.5 degrees (positive) and 125.5 degrees (negative) was calculated and plotted on the x-axis with the corresponding depth shown on the y-axis as defined by Mardon & Stretch (2002). From Figure 2-9 it is evident that from the mean sea water level to a depth of four metres, large changes of current magnitudes are observed. From the four metre depth downwards, current measurements remain similar (0.4m/s) with little variation.

Crosscurrents near the water surface are driven by shear stress associated with surface winds and thus depend on wind direction and duration. The time scales for setting up these currents is of order a few hours (Mardon & Stretch 2002). In contrast, sub-surface currents at greater depths are not linked to local wind patterns (i.e. have non-local forcing) and are generally more persistent with longer time scales (Mardon & Stretch 2002).

A schematic of a ship of varying draught is overlaid on Figure 2-9. From the vertical current structure shown, it is evident how currents found in the top four metres of the water column may dominate the drift experienced by shallower draught vessels. For deeper draught vessels sub-surface currents could dominate the resultant drift experienced.

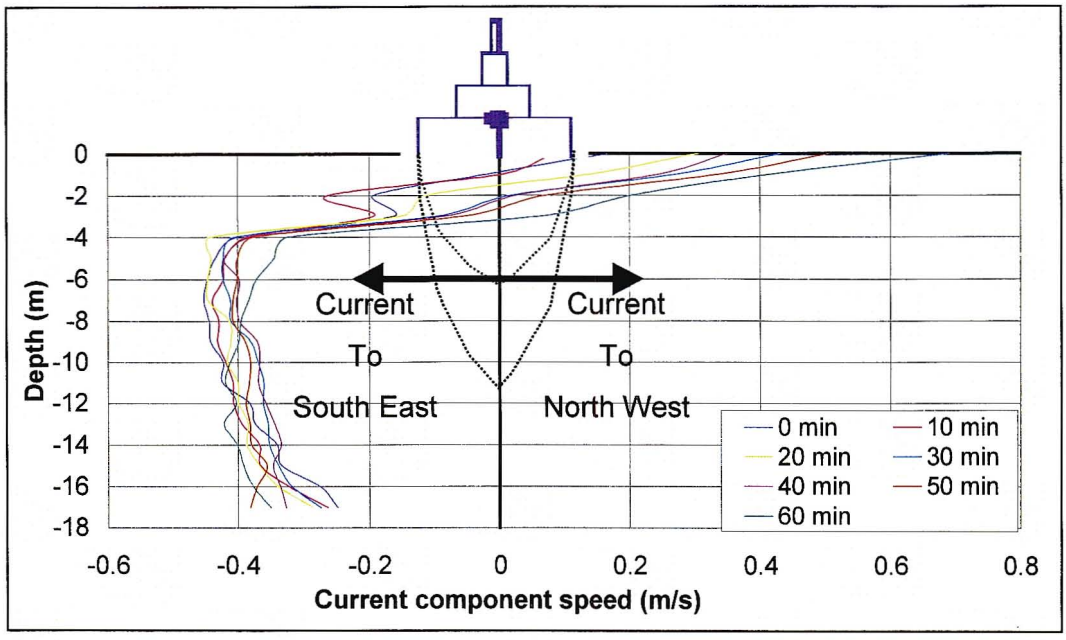

Figure 2-9: Cross Section of a typical vertical current profile outside the Durban Harbour (adapted from Mardon and Stretch, 2000)

2.10. The relative importance of wind and currents on ship drift

> *"Does the lateral drift experienced by a ship depend more on the forces due to cross winds or to crosscurrents?"*

This is a common question asked by both mariners and port engineers. This section will discuss and attempt to answer this question.

Any solid body moving through a fluid experiences a drag or a resistance to its motion. Part of the drag results directly from the shear stress on the surface and is termed **skin friction** drag. In the case of non-streamlined or 'bluff' body shapes, drag force may also be associated with the pressure distribution due to crosswinds and crosscurrents around the body and is called **form** drag. With respect to the lateral drift experienced by a vessel, the form drag component is expected to dominate because of the non-streamlined shape in the cross track direction.

For this discussion it is assumed that a vessel acts like a bluff body, with the length to draught or length to windage ratios being about two, having very large Reynolds numbers based on the overall length of the vessel. Thus the ratio of the windage to draught height is assumed to be two. From PIANC (2002), ratios calculated between a fully-laden vessel's super structure and submerged structure range from 0.5 to 1 for general cargo ships, bulk carriers and oil tankers, with container ships and gas tankers having factors ranging from 1.5 to 1.9. Since the port of Durban receives mainly

container handling vessels a factor of 2 is appropriate. The force due to crosscurrents (F_w) acting on the projected area of the ship below the waterline may be written as:

$$F_w = \frac{1}{2}\rho_w u_w^2 A_w C_w \tag{2.1}$$

where ρ_w is the density of water, u_w is the speed of crosscurrents, A_w is the projected surface area of the vessel exposed to crosscurrents and C_w the coefficient of friction. Similarly the force due to crosswinds (F_a) acting on the part of the ship above the waterline may be expressed as,

$$F_a = \frac{1}{2}\rho_a u_a^2 A_a C_a \tag{2.2}$$

where ρ_a is the density of air, u_a is the speed of crosswinds, A_a is the projected surface area of the vessel exposed to crosswinds and C_a the coefficient of friction.

The ratio of the cross track drag due to wind and currents therefore follows as:

$$\frac{F_w}{F_a} = \frac{\rho_w}{\rho_a}\left(\frac{u_w}{u_a}\right)^2 \frac{A_w}{A_a}\frac{C_w}{C_a} \tag{2.3}$$

If the Reynolds number is large then the drag coefficients C_w and C_a are expected to be similar. If it is initially assumed that areas A_w and A_a are similar, it follows that:

$$\frac{F_w}{F_a} \cong \frac{\rho_w}{\rho_a}\left(\frac{u_w}{u_a}\right)^2 \tag{2.4}$$

Since the density of water is approximately 1000 times higher than air it follows from equation 2.4 that for the drag forces due to wind and current to be equivalent, would require a crosswind velocity about thirty (30) times larger than the crosscurrent velocity. This holds so long as the projected areas and the coefficients of drag are the same. If the projected area of the ship above the water is twice the projected area of the ship below the water, as in the case of container handling vessels then the factor reduces from 30 to 20.

We can now return to the question asked in the beginning of this section. Crosscurrents velocities are typically 1 knot (0.5m/s) at the Durban port entrance (CSIR, 1999a). For crosswinds to have a comparative affect on the ship, would therefore require wind speeds perpendicular to the channel of 20-30 knots. The

probability of a 20 to 30 knot wind blowing perpendicular to the channel is small. Figure 2-3 illustrates the dominant wind patterns around the Durban Harbour. Wind speeds perpendicular to the channel axis rarely exceed 6m/s (12 knots). The main contributing factor to the cross track drift experienced by a vessel at Durban is therefore expected to be crosscurrents and not the crosswinds.

2.11. Shipdrift

Surface currents in the oceans can be determined from historical shipdrift velocity data. Richardson (1997) obtained shipdrift data by subtracting the velocity vector based on measured ship position fixes, from the estimated dead reckoning velocity vector (heading vector) over the same interval of time. Figure 2-10 illustrates this vector diagram. The heading vector is a combined measurement of the ship's speed through the water by the ship's log and the direction of the ship's course by compass.

From Figure 2-10, the measured surface current vector is a combination of the actual surface current and leeway vectors. Richardson (1997) describes the 'leeway vector' as one used to describe the transverse drift through the water or the sideslip of the ship off her course due to wind, wave and current forces. He concluded that surface current measurements from shipdrift data required correction with respect to leeway in order to have a useful data set of surface current measurements. Richardson (1997) investigated how 'leeway vectors' varied with ship speed and local wind velocity using model ships in towing tanks and wind tunnels.

The method used in the present investigation uses similar concepts by applying digital imagery to extract the heading and velocity vectors, over very short time intervals (seconds), thus focusing on high spatial resolution drift information.

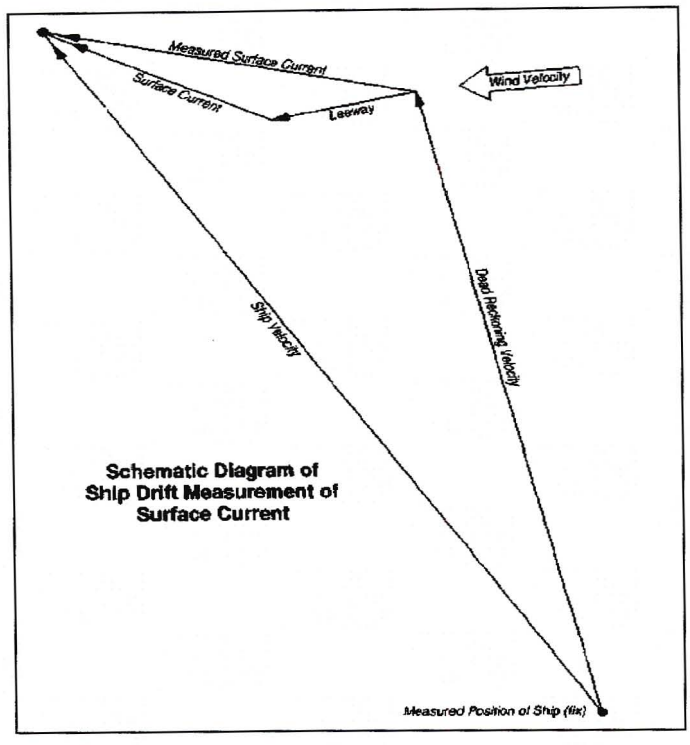

Figure 2-10: Schematic diagram of a shipdrift measurement of surface current. In the figure the surface current and leeway vectors are exaggerated (from Richardson, 1997).

2.12. Coastal Imaging

Holman et al. (1993) describes the application of digital video imagery for coastal applications and how an understanding of the transformation between image and real-world coordinates is required for the quantitative use of video image processing. Since this investigation uses a similar method of transforming digital images to real-world coordinates to the one used by Lippmann & Holman (1989) and Holland et al (1997) a brief review into these methods is presented here.

Holland et al (1997) derived the necessary equations used in the transformation method. The process of deriving field coordinates from image coordinates is called 'rectification'. This rectification process consists of a large number of geometrical calculations, depending on the number of image points or 'pixels'. A pixel is the smallest single point in a graphic image. Pixels are arranged in rows and columns, and appear to be joined since they occur so close together.

The location of any object in an image is a function of the spatial orientation of the camera in relation to the ground geometry. When transforming from ground coordinates to image coordinates, the geometric relationships are relatively easy to determine and solve. However transformation from image to ground coordinates renders equations that are underdetermined, since image coordinates are 2-

dimensional and ground coordinates are 3-dimensional. This is overcome by assuming one dimension to be known. For near shore related problems it is reasonable to assume the vertical coordinate to be at sea level (Aarninkhof, 1996). With a known elevation, the mapping of all of the pixel coordinates within a region of an oblique image, to a rectified planar image in world coordinates, can be determined.

Holland et al (1997) developed a distortion-free camera model, which was used in their camera calibration procedure. Let (X,Y,Z) represent the 3-dimensional spatial coordinates of visible point relative to the Cartesian world coordinate system and (u,v) represent the 2-dimensional pixel coordinates of the same point in a digitised image. The idealized image plane is at a distance, *f* from the optical centre (X_c, Y_c, Z_c) of the camera. The coordinates of the image centre are given by (u_0, v_0). These parameters are illustrated in Figure 2-11. By using the parameters defined here the transformation between image and world coordinates can be derived in terms of the following 'collinearity equations' (Wolf, 1974), under the condition that the camera centre, the image point and the object point all lie in a straight line:

$$u - u_0 = -\frac{f}{\lambda_u}\left[\frac{m_{11}(x-x_c)+m_{12}(y-y_c)+m_{13}(z-z_c)}{m_{31}(x-x_c)+m_{32}(y-y_c)+m_{33}(z-z_c)}\right] \quad (2.5)$$

$$v - v_0 = -\frac{f}{\lambda_v}\left[\frac{m_{21}(x-x_c)+m_{22}(y-y_c)+m_{23}(z-z_c)}{m_{31}(x-x_c)+m_{32}(y-y_c)+m_{33}(z-z_c)}\right] \quad (2.6)$$

In equation 2.5 and 2.6, λ_u and λ_v are horizontal and vertical scale factors, which are assumed to be 1 in this investigation. These scale factors are used to cater for the effects of radial distortion in the digital images. For this investigation these effects were ignored. The individual elements m_{ij}, of the 3 x 3 orthonormal rotation matrix are directional cosines and can be derived in terms of three successive rotations about the angles τ (tilt), ϕ (azimuth), and σ (roll). These angles in the orthonormal rotation matrix have been defined by Wolf (1974); Moffit & Mikhail (1980) and Holland et al (1997).

From Lippmann & Holman (1989) field measurements of tilt (τ) may be awkward and inaccurate and the focal length (*f*) of a zoom lens may be difficult to estimate. The focal length can be calculated by counting the number of pixels from the screen and relating them to the field of view of the camera (δ). An expression for *f* is,

$$f = \frac{x_e}{\tan\left(\frac{\delta}{2}\right)} \quad (2.7)$$

where, x_e represents the distance measured (in pixels) from the image centre (u_0, v_0) to the right hand edge of the image and δ is the field of view of the camera. Unfortunately the field of view δ is another feature of lenses, which is not easily measured accurately in the field. In general, the angle that the beach makes with the x-axis of the image (azimuth,ϕ) and the angle the image makes with the horizon (the roll, θ) are also needed.

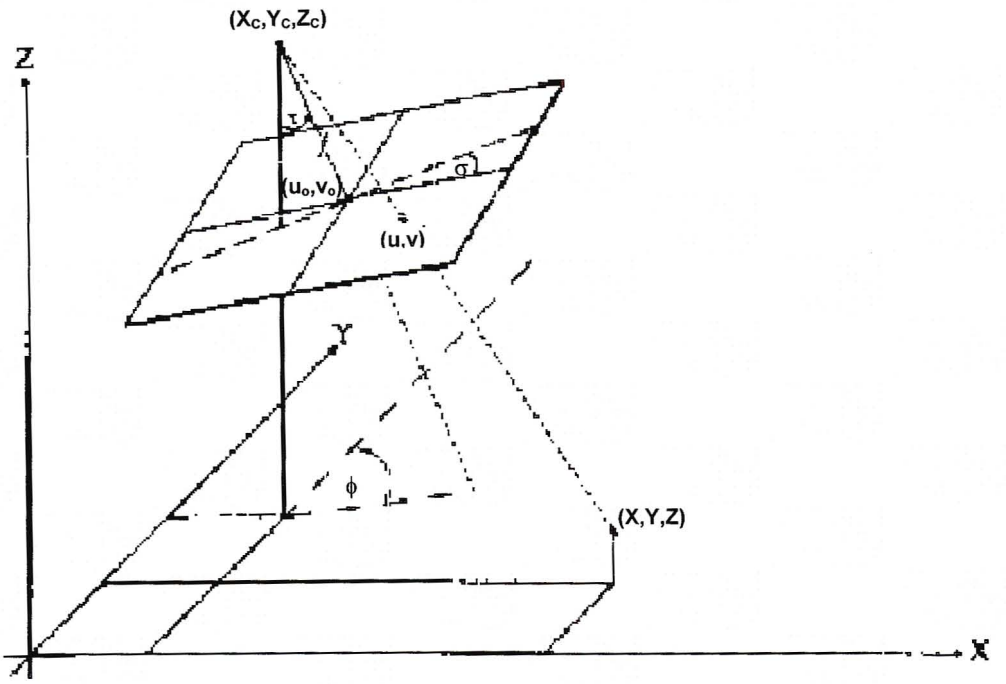

Figure 2-11: Collinearity relationship between camera (X_c,Y_c,Z_c) and image (u,v) and world (X,Y,Z) coordinates and rotation angles (ϕ, τ and σ) used in the orientation definition. (from Holland et al, 1997)

The three rotation angles ϕ,τ and σ as well as the camera centre world coordinates, X_c, Y_c, Z_c and the focal length f yield seven unknowns. The collinearity equations can be used to solve for the unknown parameters using a standard iterative minimization technique. By constraining the camera coordinates (X_c, Y_c, Z_c) to predetermined values, in particular by fixing Z_c, the number of unknowns is reduced to four and the system can be uniquely determined given two ground coordinate points, whose locations are known in image as well as world coordinates. These are so-called Ground Control Points (GCP's). Note that on flat terrain, typical for this investigation, the scale is approximately constant along any line in the x-direction (along any line parallel to the true horizon), while it continually varies along any line in the y-direction (along any line parallel with the principal line or perpendicular to the true horizon line).

In summary the application of photogrammetry in the field requires the accurate knowledge of four camera related parameters δ,τ,ϕ and σ. Holland et al (1997) reported that lens distortion significantly affects the results of the rectification procedure. Radial symmetric lens distortion (distortions along radial lines from the centre of the image) was shown to be the largest source of distortion error, and was thus accounted for in their model. They developed distortion coefficients (k_1 and k_2), by laboratory calibrations and measured the deviations between observed and predicted image coordinates due to lens distortion.

This investigation used a similar rectification technique to perform transformations from image coordinates to real world coordinates, which will be described in chapter 3.

2.13. Machine Vision

Crowley and Coutaz (1995) describe the application of machine vision and interaction and how computer vision provides a powerful tool for the interaction between man and machine. Many computer vision techniques require matching parts of images. Examples include registering images to determine the shift and deformation for reconstruction and motion, matching to a reference for recognition, verification and event detection. Pattern matching is thus fundamental to computer vision (Martin & Crowley, 1995). The correlation of a source image to a template image is an extension of the basic tools used in signal processing and communications theory. Vision researchers believed that the central problem of matching by direct convolution was one of tedious and time-consuming computations. To reduce this time wastage, other techniques were investigated e.g. Fast Fourier Transforms. Although cross correlations by direct convolution were used in the early years of computer vision, it has largely been neglected due to time consuming computations (Martin & Crowley, 1995). Since available computing power has increased rapidly, more interest in the use cross correlation techniques has developed due to its reliability as an image-matching tool.

Let U be an image at time t and V be an image at time $t+\Delta t$ later. Consider an object in image U with pixel coordinates $x(t)$ and $y(t)$. At time $t+\Delta t$ this object may change its pixel coordinates. The goal of pattern matching is to find the location of this object $x(t+\Delta t)$ and $y(t+\Delta t)$ in image V. The two key components to any feature tracker are accuracy and robustness. The accuracy component is related to the local pixel accuracy attached to tracking. The robustness component relates the sensitivity of tracking with respect to changes in: (1) the orientation of the object, (2) the ambient

lighting conditions, (3) the size of the object as well as (4) the quality of the images used i.e. noise.

This investigation will discuss cross correlation methods and how they were used and applied for matching and tracking features in image sequences. The results of this technique will be presented in chapter 6.

2.14. Summary

This review has outlined background information for key concepts used for the present investigation.

The design of entrance channels was briefly outlined with a focus on the channel width design parameter and how ship simulators are used to finalise the optimum width. Later in this dissertation actual observed ship tracks will be presented, which can be used to compliment and validate the results of a ship simulator.

The movement of vessels under the influence of wind, waves and current has been discussed. Important conclusions are that wind is responsible for driving the surface currents, while sub-surface currents can be independent of local wind patterns. The cross track drift experienced by vessels entering the Port of Durban is mainly due to crosscurrents and waves and is not strongly affected by winds.

ADCPs are useful tools for measuring current through the water column but current measured in this way, is usually at a fixed point only. To assume that the current measured at a point is representative over the entire approach channel may be incorrect. This investigation presents a technique to measure the cross track drift of a vessel spatially, which can be used to validate the measurements from an ADCP.

The rectification of oblique digital images can be used to extract qualitative information from photographs. It will be shown in chapter 3 how this information is used to measure a ship heading direction and eventually the ship's drift as a function of time.

Machine vision, and particularly the application of cross correlation techniques, will later be used as a tool for automating tasks proposed for the development of this new technology. The results will be shown in Chapter 6.

CHAPTER 3

CONCEPTUAL FRAMEWORK

3.1. Introduction

In this chapter, a method of measuring a ship heading direction as well as its true velocity vector (magnitude and direction) over very short time intervals (seconds), is presented. This is used to determine a cross track drift for the ship. The method involves the use of time-lapsed sequences of digital images, and rectification techniques founded on the principles of photogrammetry. From the difference between the heading and velocity directions a 'crab angle' can be defined and calculated, and together with the magnitude of the true velocity vector (speed of the ship over the ground) a component of the drift can be determined. Richardson (1997) used shipdrift measurements to obtain surface currents by subtracting the velocity vector from the estimated heading vector over the same time interval, the order of hours. The shipdrift measurement presented by Richardson (1997) is averaged over a large area. Richardson (1997) used the term 'leeway' to describe the transverse drift through the water or sideslip of a ship leeward of her course due to wind and wave forces on the ship. For this investigation the term 'cross-track drift velocity' (CTDV) is used to refer to a component of the overall drift.

The rectification method used in the present investigation is simpler but not as accurate as the method suggested by Holland et al (1997), but for the application presented here it will be shown to be adequate.

3.2. Basic Concept

It is well known that in the presence of crosscurrents, a ship's heading direction will differ from the direction of its true velocity vector. This is shown schematically in Figure 3-1. The angle formed between the heading (H_D) and velocity vector (V_V) directions, which for this investigation has been referred to as the crab angle (θ), is a direct measure of cross-track drift velocity (CTDV) which is measured perpendicular to the velocity vector and arises due to the combined effects of wind, waves and currents.

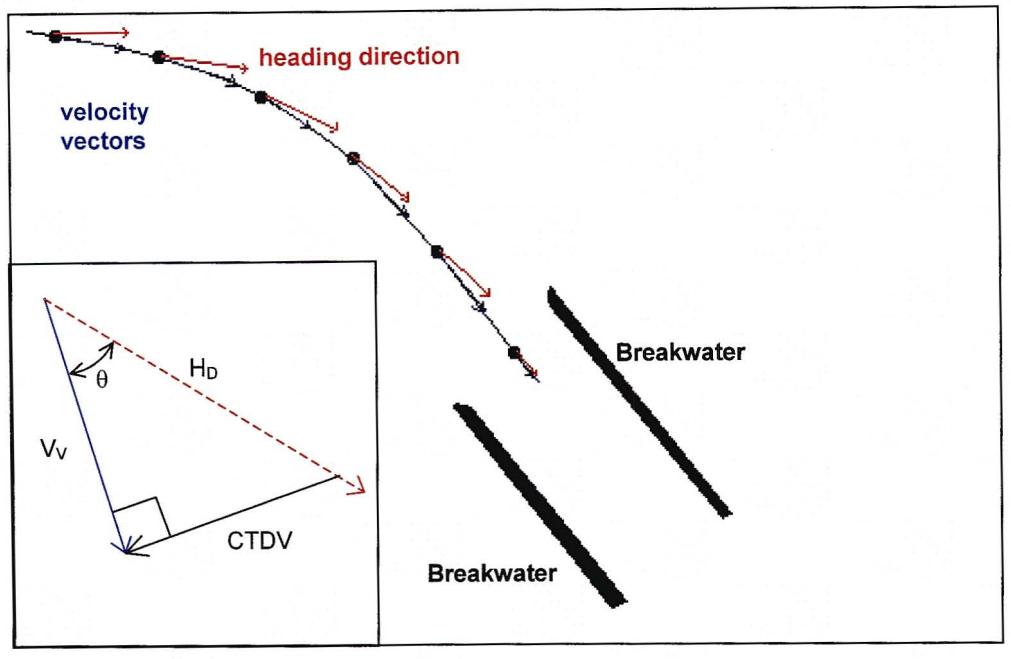

Figure 3-1: A schematic plan view of a ship approaching the harbour entrance along with the heading and velocity vector over time.

When interpreting CTDVs one should not assume that the CTDV is equivalent in magnitude and direction to the ship's actual drift velocity. To determine the actual drift vector requires knowledge of the ship's speed relative to the water, which the imaging technology cannot measure directly. The technology does allow calculation of the CTDV, which is a vector representation of the crab angle (θ) and ship speed over the ground (V_V). Referring to Figure 3-2, if the velocity of the water and the velocity of the ship relative to the water are represented as vectors V_{DV} and V_W respectively, then as V_W increases from zero, the magnitude and direction of V_{DV} tends towards the measured CTDV. For small θ and $V_W \cong V_V$ the CTDV is approximately equal to the actual drift velocity experienced by the ship. The CTDV is in fact equal to the difference between V_{DV} and a component of the current velocity vector resolved parallel to the ship heading direction (V_{DVH}). If $V_W \cong V_V$, then the component of the current along the heading direction is small i.e. $V_{DVH} \cong 0$.

There is a simple relationship between the CTDV vector, the crab angle (θ) and the speed of the ship over the ground (V_V) i.e.

$$CTDV = V_V \tan(\theta) \qquad (3.\ 1)$$

For small θ, $\tan(\theta) \cong \theta$, thus a linear relationship would exist between these variables, so if both the speed and the crab angle are doubled, the resulting CTDV will increase by a factor of 4.

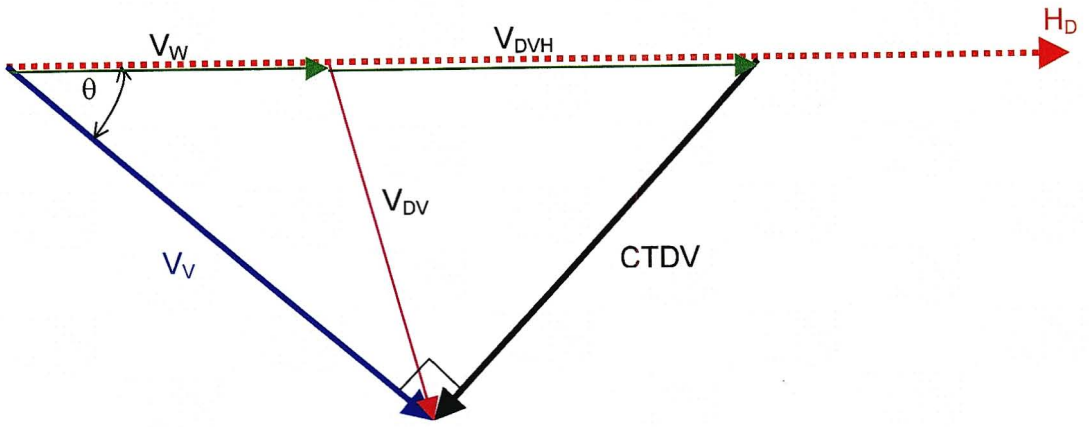

Figure 3-2: Vector representation of the heading direction (H_D) and the velocity vector (V_V) of a ship. Also shown is an assumed actual current velocity (V_{DV}) and speed of ship through water (V_W)

In summary the definition of relative terms used and shown in Figure 3-1 and Figure 3-2 are:

H_D	- Heading direction	- the direction that the pilot steers the ship
V_V	- Velocity vector	- actual speed and direction that the ship follows
θ	- Crab angle	- angle formed between the Heading and Velocity vector directions
CTDV	- Cross Track Drift Velocity	- a representation of drift perpendicular to the velocity vector

and,

V_{DV}	- actual current velocity
V_W	- velocity of the ship relative to the water
V_{DVH}	- component of the actual current velocity vector resolved parallel to the ship heading direction

The CTDV drift component is due to external natural forces i.e. winds, waves and currents as well as the lateral slippage of the ship in the water due to rudder induced turning movements. Let this slip be characterised by an angle θ_s. This slip experienced by ships, if large enough, will increase the magnitude of the crab angle, which will

result in an increase in the measured CTDV. The slip experienced by ships depends on the turning rate of the ship and the depth to draught ratios. The turning rate of a ship is influenced by the speed of the ship over the ground as well as the rudder angle used by the pilot to turn the vessel. For a specific type of ship the larger the turning rate the smaller the turning radius of the ship and thus the larger θ_s would be. Smaller depth to draught ratios result in more directionally stable ships with θ_s small. The contribution to CTDV due to sideslip will be reviewed in more detail in section 3.9.

As reviewed in section 2.9 currents vary with depth, therefore the net drift experienced by shallower draught vessels is influenced more by surface currents while deeper draught vessels are probably influenced by sub-surface currents. Surface currents respond rapidly to changes in wind stress, while deeper sub-surface currents may have distinctly different forcing mechanisms. It is thus possible for the currents to change direction with depth, which makes it difficult to predict the response of ship's of various displacements and draughts. Ship dynamics may also be sensitive to water depth, particularly in the shallower waters of a port approach channel. The proposed method of analysing ship movements avoids these complications by directly measuring the response of the ships (i.e. the crab angle).

The CTDVs measured and presented in this investigation are thus the net effect of all the currents and waves acting perpendicular to the projected surface area of a ship below the water surface. The smaller the time interval used to determine the CTDVs the higher the spatial resolution of the CTDVs measured. The main advantages of the proposed technology are,

1. that a measurement of ship response to currents and waves is determined directly rather than using current or wave data measured at a fixed point and trying to infer the ship's response.
2. the spatial structure of the drift velocities can be determined.

A disadvantage to the proposed technology is that currents and waves cannot be measured directly, due to the limited information. The technology can be used and applied to any port around the world. The remainder of this chapter will discuss how this technology was customised for a local case study at the Port of Durban.

3.3. Summary of the Methodology

The essential elements of this methodology can be summarised as follows:

(a) Use digital imaging to record ships entering the port.

(b) Process the digital images to determine the actual positions of the ships as a function of time i.e. to obtain "ship tracks" and true velocity vectors.

(c) Process the images to determine the ship's heading direction and thus the crab angles at various positions along the ship track.

(d) From the true velocity vectors of the ship's and their crab angle data, infer the cross-track drift velocities (CTDVs) along the ship tracks (see Figure 3-1 and Figure 3-2).

Initially a suitable vantage point needs to be selected from where sequenced images of ships entering the harbour are recorded. For this case study the Durban Bluff Signal Station was used as this vantage point. The Signal Station is situated at approximately 101.3 metres above mean sea level and is on a bluff. Plate 3-1 indicates the position of this Signal Station as well as the North and South Piers that flank the entrance channel.

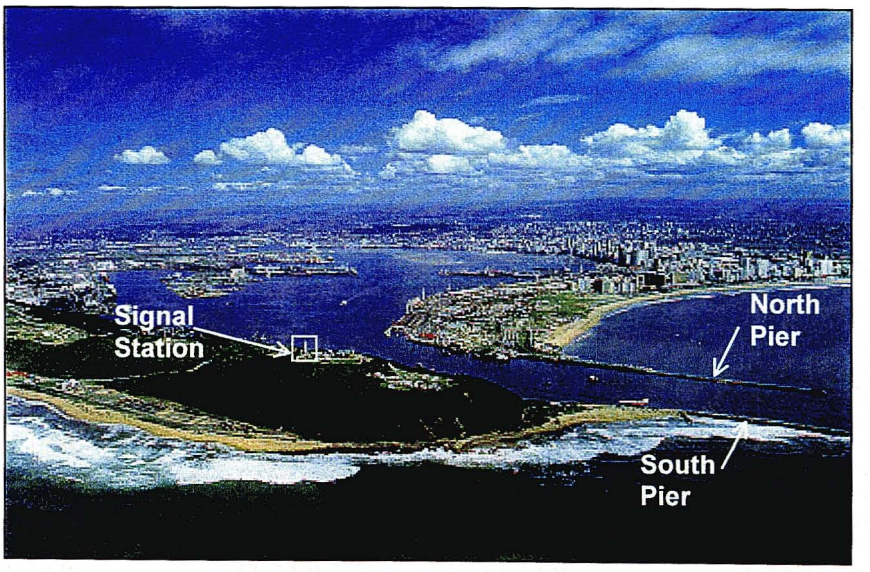

Plate 3-1: Image showing the Durban Harbour in the background and the Bluff in the foreground. Also shown is the entrance channel flanked by the North and South Piers (from http://www.portnet.co.za/durban/home.html)

During this investigation two methods of acquiring images were used. Initially a portable digital still camera was used. Later a fixed video camera was introduced. In either case a time-lapse sequence of images of ships entering the harbour was obtained. These sequenced images, were processed on a personal computer. Once

analysed the data produced was in the form of heading directions, velocity vectors, crab angles and CTDVs for each position of the ship as a function of time. Figure 3-3 summarises the methodology used.

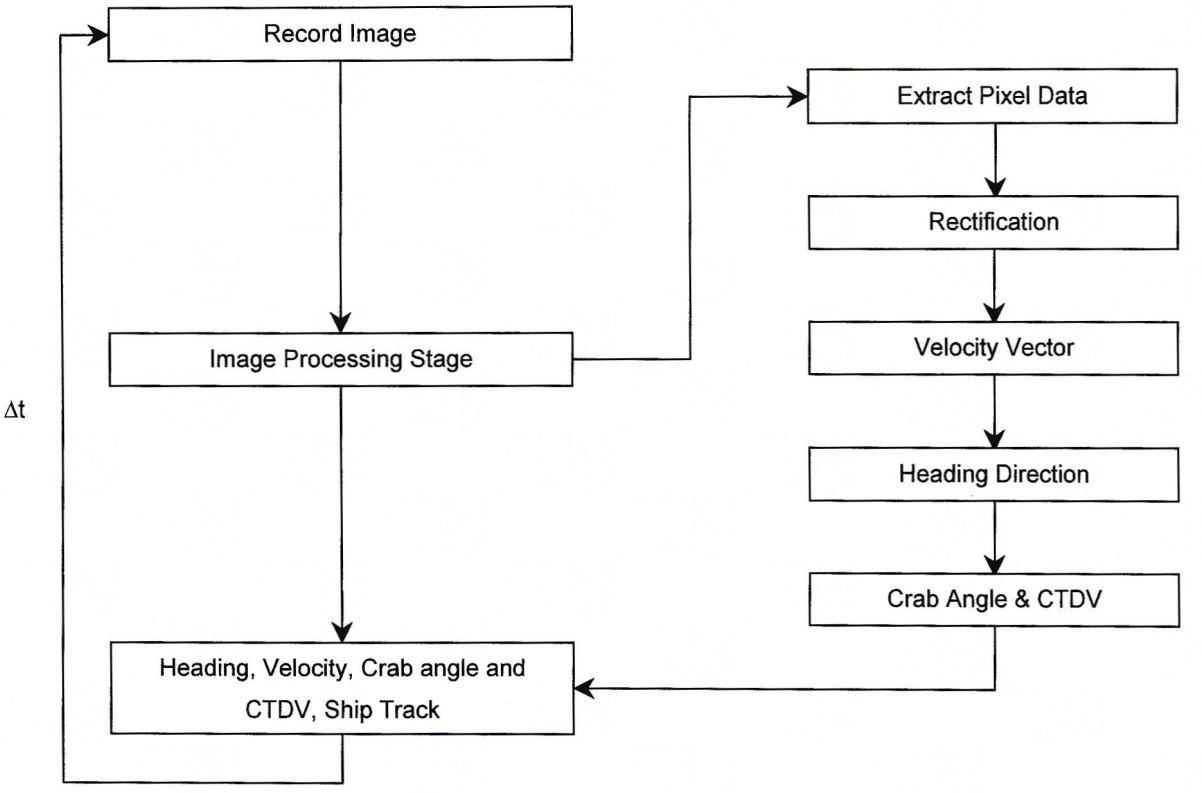

Figure 3-3: Flow Diagram illustrating the essential elements of the methodology used

The image processing stage is divided into five sections as shown in Figure 3-3. These sections are discussed in greater detail in the following sections.

3.4. Extraction of Pixel Data

The first step in determining the heading direction and velocity vector and ultimately CTDVs, is to select key points from an image of a ship entering the harbour. These points are located on the ship and the choice of these specific points is key to the method. The pixel coordinates of two points are required for the calculation of the heading, velocity and CTDV vectors for every position of a ship. These two points are shown graphically on Figure 3-4, and are explained as follows:

Point 1 - Intersection of a vertical line drawn from the bow of the ship (yellow) and intersecting a horizontal line drawn at the water surface (pink).

Point 2 - Intersection of a vertical line drawn from the smoke stacks of the ship (green) and intersecting the horizontal line drawn at the water surface extending from the bow (pink).

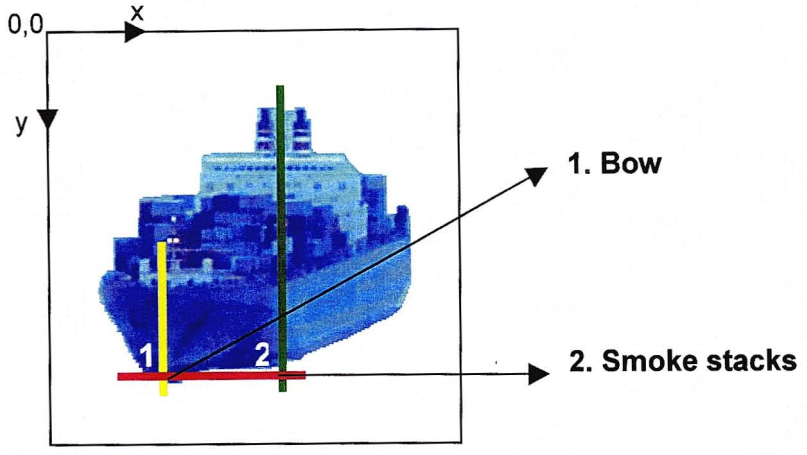

Figure 3-4: Pixel data required per image that is used in the calculation of the CTDVs.

The pilot on board uses the bow as a visual guide for ensuring the ship is moving in the correct direction. If the pilot decides that the vessel is in fact off course, a decision to correct the ship's heading will be taken based on the direction faced by the bow. Directly below the bow at the intersection with the water plane lies point 1. This point, which is at a known elevation (the water plane) is used to determine the position of the ship at each time step. The rectified coordinates of point 1 as a function of time are used for calculating the velocity vector at each position.

The second point (point 2) is chosen because the smoke stacks of the ship are usually situated close to the centre line of the vessel and towards the stern of the ship. The x-pixel offset between points 1 and 2 is used for calculating the heading direction.

In summary two sets of pixel coordinates are extracted per image of a ship entering the harbour, and are used to determine the heading and velocity vectors. Plate 3-2 is a typical snap shot of a ship entering the Durban harbour with these two points shown.
The y-pixel coordinate of the horizon and the (x,y) pixel coordinates of another ground reference point (the south pier lights in Figure 3-2) are used to rectify the pixel coordinates of point 1 and 2 to obtain the corresponding world coordinates. This is described in the next section.

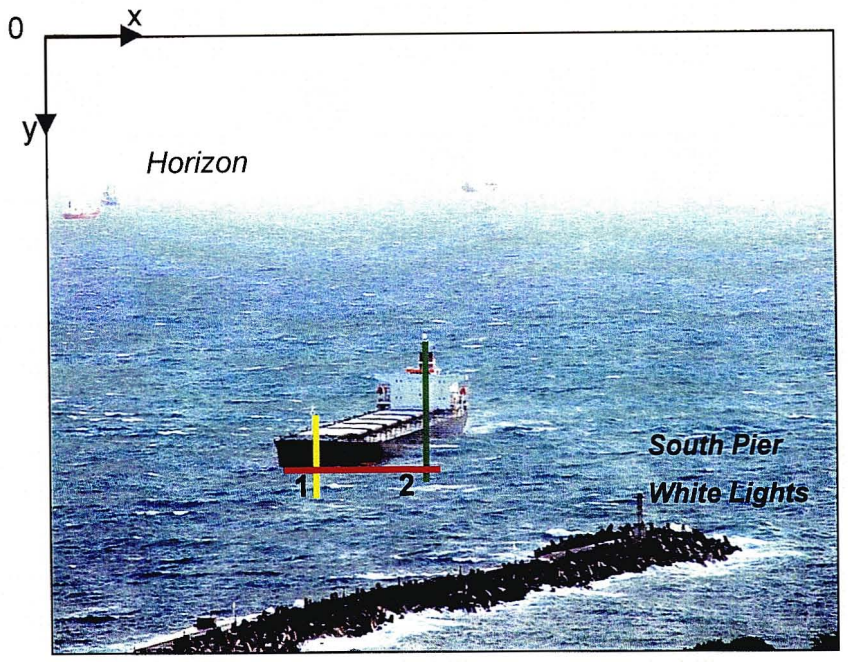

Plate 3-2: Image showing a ship in Durban's approach channel as it enters the port.

3.5. Rectification

As noted by Wolf (1974) with high oblique photos with a flat reference plain (as in this case) the ground distance represented by each pixel continually varies along any line perpendicular to the horizon line. The closer a pixel is to the horizon the larger the ground distance it represents.

As noted in the review of section 2.12 the process of deriving field coordinates from image coordinates is called 'rectification'. Holland et al (1997) derived rectification equations, which are applicable to this application. They also noted that the 3-dimensional coordinates of a 2-dimensional pixel location cannot be estimated because the system of equations is underdetermined They suggested two alternatives: (1) either constrain at least one spatial dimension of the world coordinate system or (2) sample additional images of the same object space from different camera viewpoints. For this investigation the first option is a natural choice since the water plane provides a known reference elevation.

The rectification method used in this investigation was specifically derived for this application. It is similar to the technique used by Holland et al (1997) but is simpler and less accurate. The procedure was divided into two stages: (1) Range Calculation and (2) Position Calculation. These stages are reviewed in the following sub-sections.

3.5.1. Range Calculation

Input parameters required for the range calculation include the world coordinates of the camera location (X_C, Y_C, Z_C), the world coordinates of at least one known reference

point located in the images and the y-pixel coordinates of the horizon in the images. For this investigation the South Pier White Lights (see Plate 3-2) is used as the reference point (X_P, Y_P, Z_P) as it is the only known point that was visible in the field of view of the camera. The pixel coordinates of the South Pier White Lights and the y-pixel coordinate of the horizon are denoted as (x_p,y_p) and (y_H) respectively. The x- and y-pixel dimensions of the images (constant throughout) are also required (x_{TOT} ,y_{TOT}). The mean radius of the earth (R_O) is a constant also required for this calculation. Wolf (1974) and Moffit & Mikhail (1980) give a typical value of R_O as 6370320 metres.

Another two variables required for the rectification procedure were the horizontal and vertical angles of view (H_θ and V_θ) of the camera. The angular variations per unit pixel can be calculated as:

$$\Delta H_\theta = \frac{H_\theta}{x_{TOT}} \qquad (3.\ 2)$$

$$\Delta V_\theta = \frac{V_\theta}{y_{TOT}}$$

Both angles of view are dependant on the focal length used. The horizontal angle of view is determined by means of a calibration process. Patel (1999) developed a simple method of calibrating a camera to determine this angle of view for various zoom settings. The method is applicable to any camera device and involved placing two physical objects at known distances apart and at a known distance from the camera device. These objects were then photographed at various focal length settings i.e. at various angles of view. Increasing the focal length of the camera lens decreases the angle of view of the camera. Patel (1999) reviewed typical results from this calibration process. This calibration procedure can be carried out in any situation where the world coordinates of at least two reference points within the angle of view are available.

The vertical angle of view was determined in the field as follows. From Figure 3-5 a photograph is exposed at *D* located at a height of Z_C relative to the mean sea level (msl). In this investigation the camera is located on the Bluff Signal Station. The South Pier white lights (the reference point used in this investigation) is located at R_P a height Z_P above mean sea level. The mean sea level is the spatial dimension constrained for the rectification process. By constraining this elevation parameter all pixel coordinates within the image that are located at mean sea level, may be rectified to world coordinates.

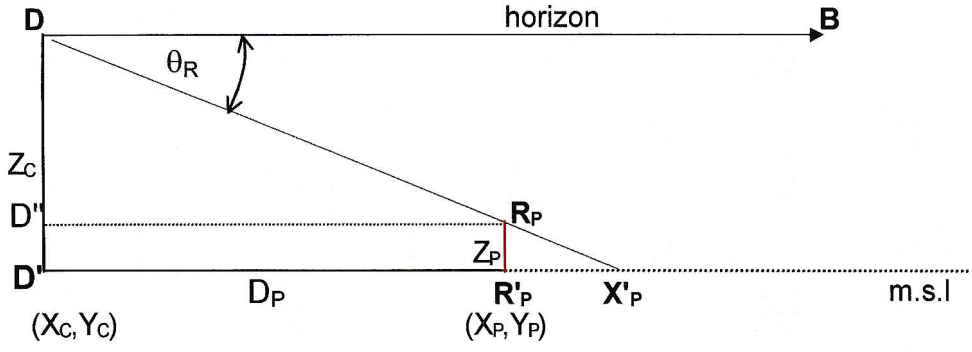

Figure 3-5: Vertical angle of view calculation

From Figure 3-5, Line *DB* is the horizon line drawn tangent to the earth's surface (refer also Plate 3-2). The point *D'* is the ground nadir point, which is a point on the reference plane directly below the imaging station. Line DR_P is an imaginary ray drawn from the camera to the reference point at height Z_P above the msl. Since the X-, Y- and Z-ground coordinates of both the camera and the reference point are known the straight line horizontal distance between these points can be calculated (D_P). This distance is equivalent to lines $D'R'_P$ and $D''R_P$. By geometry, distance $D'X'_P$ can be calculated where X'_P is the point where ray DR_P intersects with the reference plane. Using distance $D'X'_P$, angle θ_R can be calculated as,

$$\theta_R = 90 - \mathbf{arctan}\left(\frac{D'X'_P}{Z_C}\right) \tag{3. 3}$$

The difference between the y-pixel coordinates of the horizon and the reference point R_P is,

$$\Delta y_R = y_R - y_H \tag{3. 4}$$

From equations (3.3) and (3.4) the vertical angular variation per pixel may be obtained as,

$$\Delta V_\theta = \frac{\theta_R}{\Delta y_R} \tag{3. 5}$$

Note that if the camera is moved or the zoom setting changed, re-registration of the coordinates of the reference point, the horizon, as well as the new horizontal and vertical angles of view of the camera are required from the image before rectification.
The geometric solution will now be reviewed. The objective of this solution is to calculate the distance from the camera position to any point on the reference plane.

An image is obtained from *D* at a height of Z_C above the mean sea level. Referring to Figure 3-6, *O* is the centre of the earth, and is taken as the origin of the coordinate X'- and Y'-axis, and R_O is the mean radius of the earth. *S* is a chosen target object that is located at mean sea level, whose world coordinates with respect to the origin (O) are (X'_S, Y'_S). This sketch represents a plane containing *D*, *S*, and *O*. Note that the relative scales are grossly exaggerated, and since the angle subtended at the centre of the earth by the area of view is small (less than 0.05 degrees typically), the line DD' is essentially perpendicular to the horizon line DB to close approximation.

The object at *S* is visible from the photograph with corresponding pixel coordinates of (x_S, y_S). Line *DB* is the horizon line drawn tangent to the earth's surface. The angle τ is measured from the horizon line down towards point *S*. The point *D'* is the ground nadir point directly below the imaging station. Line *OS* is drawn from the earth centre to point *S*. Line *OB* is drawn from the earth centre to a point perpendicular to the horizon line. Let the angle at *O* subtended by arc *BS* be ϕ. By geometry the angle at *SBS'* is equal to $\phi/2$. Let the arc length *SB* be Δs.

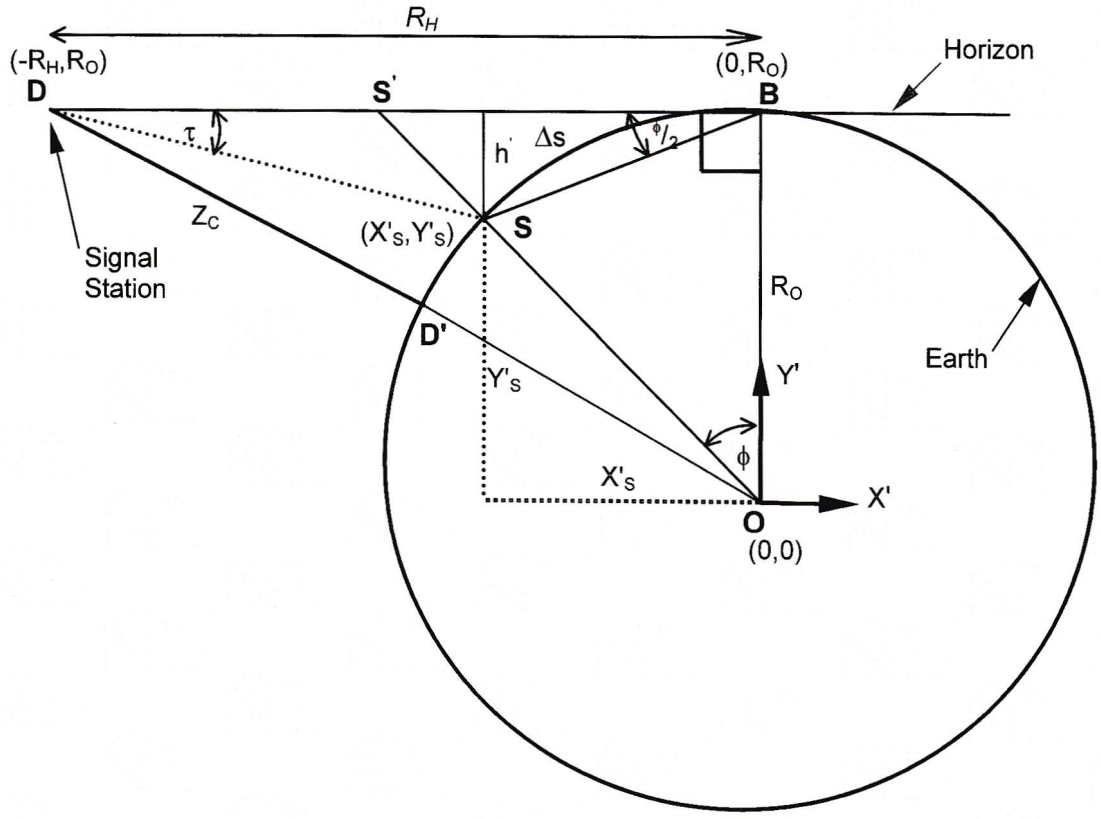

Figure 3-6 : Section (DB) through the earth and the signal station (not to scale)

The aim is to determine the D'S between the camera position and the target object on the reference plane. From Figure 3-6, the coordinates of point D are $(-R_H, R_O)$ where,

$$R_H = \sqrt{(R_O + Z_C)^2 - R_O^2}$$

The gradient of the line *DS* is given by,

$$m = \left(\frac{Y'_S - R_O}{X'_S + R_H} \right) \tag{3. 6}$$

The equation of line *DS* follows as,

$$Y' = m \cdot X' + R_O + m \cdot R_H \tag{3. 7}$$

Assuming the earth to be circular the equation of a circle with centre at the origin and radius R_o is,

$$X'^2 + Y'^2 = Ro^2$$

At the intersection between the circle and line *DS* at *S*, it follows that,

$$Y'_S = \left(Ro^2 - X'^2_S \right)^{1/2} \tag{3.8}$$

Substituting back into equation 3.7, it follows,

$$\underline{m^2 \cdot \left(X'_S + R_H \right)^2 + 2 \cdot m \cdot R_O \cdot \left(X'_S + R_H \right) + X'^2_S = 0} \tag{3.9}$$

Angle τ is determined by using the angular variation per pixel of the camera (ΔV_θ) together with the measured difference between the y-image coordinates of the horizon (y_H) and of the object *S* (y_S). The angle τ is measured below the horizon line (DB), and is taken as negative. Equation 3.6 can then be written:

$$m = \tan(\tau) = \tan\left((y_H - y_S) \Delta V_\theta \right)$$

Substituting for *m* in equation (3.9) the X-world coordinate (X'_S) of an object at point *S* can be calculated, as it is the only unknown. The Y-world coordinate (Y'_S) also follows (equation 3.8). These ground coordinates of point *S* are measured relative to the centre of the earth, which in this case was the origin *O*.

In order to calculate the coordinates of this point relative to the position of the camera at *D*, distance *D'S* is calculated using a simple transformation. Referring to Figure 3-6, we note that $h' = R_O - Y'_S$ and $\Delta s = R_O \phi$, where Δs is the arc length measured from *B* to *S* and angle ϕ is measured in radians.

Since angle ϕ is very small, it can be assumed that arc length Δs is approximately equal to chord length *BS*. For example a viewpoint at a height of 100 metres above mean sea level yields angle $\phi \cong 0.005$ radians (0.3 degrees). It therefore follows that,

$$\frac{\phi}{2} \cong \frac{h'}{\Delta s} = \frac{h'}{R_o \phi}$$

$$\phi = \sqrt{\frac{2h'}{R_O}}$$

Furthermore,

$$BS' = R_o \tan(\phi) \cong R_o \phi$$

By geometry distances *DS'* and *D'S* follow as (for small ϕ),

$$D'S \cong DS' = R_H - R_o \phi \qquad (3.10)$$

The above procedure determines the horizontal ground distance of any object located on the reference plane relative to the camera location. Note that this procedure determines a distance in the plane containing *D*, *S* and *O*. All object distances determined this way need to be resolved into X- and Y-components, in the world coordinates, relative to a new origin at point *D'* the ground nadir point to *D*. This calculation is described below.

3.5.2. Position Calculation

Figure 3-7 represents a plan view of an image exposed from a camera located at *D*, with the horizontal angle of view (H_θ) defining the horizontal extents of the image boundaries. The naming notation used here is consistent with the notation used in Figure 3-5 and Figure 3-6. Section *DBO* shown in Figure 3-6 is represented in plan as line *DB* in Figure 3-7.

This figure will be used to determine the X- and Y- ground coordinates (X_S,Y_S) of an object located at *S* in the image plane with image coordinates (x_S,y_S). Note that the X- and Y-ground coordinates of this object are measured relative to the camera, at point *D'*. Note also that the x- and y-image coordinates are measured from the top left hand corner of the image (point G). The horizontal distance to the reference point (south pier lights) located at R_P is distance D_P from point *D'*. The angle α is measured from true north in a clockwise direction to this reference point (R_P), and is relative to the camera

position. This angle α is indicated on Figure 3-7. Line D'F forms the right hand boundary edge of the image where the x-pixel coordinate is fixed at x_{TOT}.

Section 3.5.1 determined the horizontal ground distance to an object located at *S*. Since distance *D'S* is known, by geometry the X- and Y-ground coordinates of an object at *S* can be calculated as follows:

Let the image centre coordinates be (x_0,y_0). The horizontal angular variation per pixel of the camera (ΔH_θ) can be determined as shown in equation 3.2. Let ρ and β be the angles $R_PD'F$ and $SD'F$ respectively. These angles are determined as,

$$\rho = \Delta H_\theta.(x_{TOT} - x_P)$$

$$\beta = \Delta H_\theta.(x_{TOT} - x_S)$$

The angle ω measured to the object at *S* follows in terms of α,ρ and β as,

$$\omega = (\rho + \alpha) - \beta$$

The X- and Y- ground coordinates of an object at position *S* can be calculated relative to the viewing point at point *D'* by,

$$X_S = D'S.\sin(\omega)$$

$$Y_S = D'S.\cos(\omega)$$

The complete rectification procedure has been reviewed and can now be applied to determine the X- and Y- ground coordinate points (relative to D) of any number of objects that are at mean sea level.

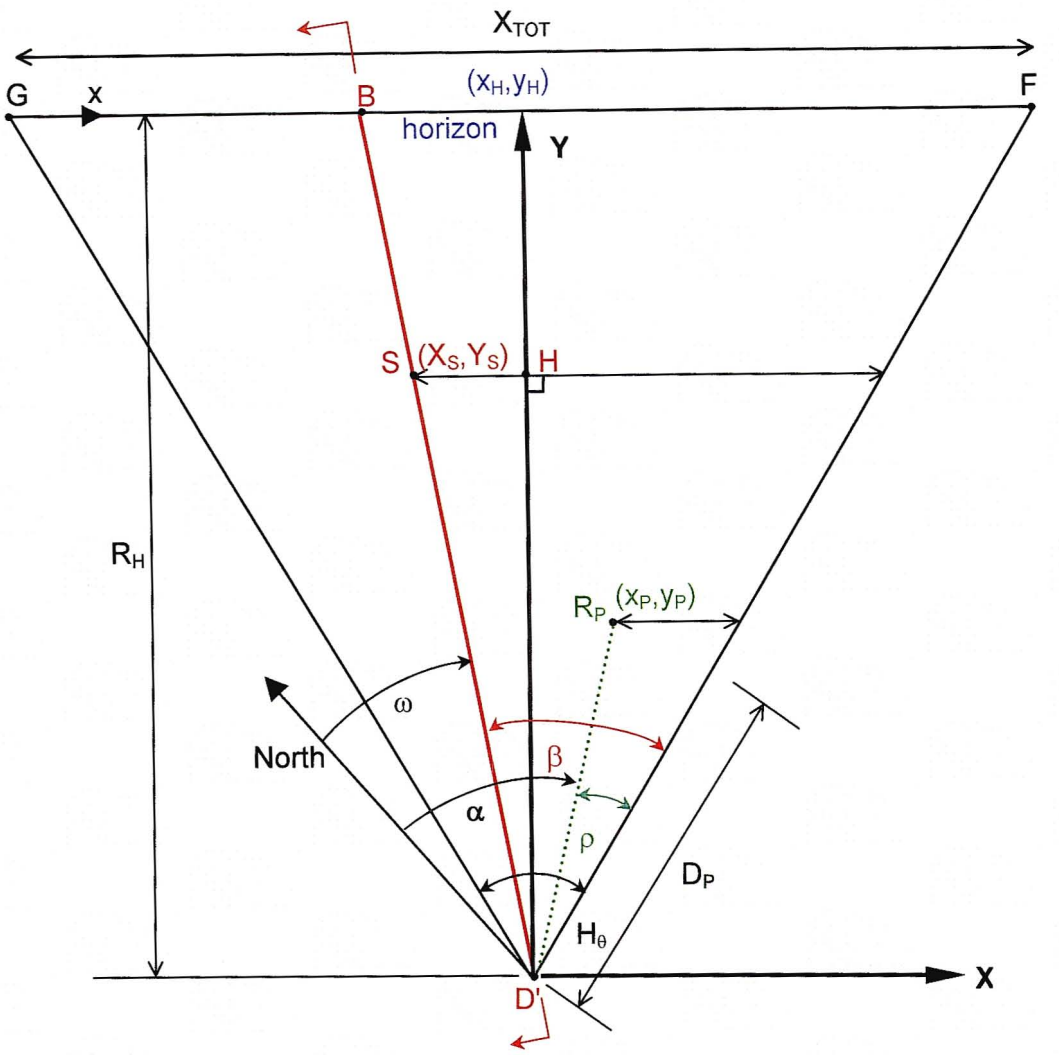

Figure 3-7: Plan view of the cameras horizontal angle of view and is used to illustrate how the X and Y coordinates of an object relative to the viewpoint is calculated.

3.5.3. Assumptions and limitations

The rectification procedure presented and used in this investigation, was formulated based on the following assumptions:

Whereas Holland et al (1997) used collinearity equations to determine variables like the azimuth (ϕ), tilt (τ) and roll (σ), for the procedure used here it was assumed that σ was zero. It was thus assumed that the camera was mounted with the x-image axis parallel to the horizon.

Furthermore whereas Holland et al (1997) considered the effects of distortion by calculating distortion coefficients based on the camera focal lengths, which for this investigation was ignored. An exercise was carried out to validate the results of the rectification procedure used in this investigation. The results of this validation exercise are presented in section 4.6.

3.5.4. Rectification application

In Section 3.4 it was noted that two points on the vessels were recorded, in order to determine the heading direction velocity vector. These were (refer Figure 3-4) defined as point 1(the bow) and point 2 (the smoke stacks).

Both these physical features were projected vertical down onto the reference plane, and the corresponding pixel coordinates were recorded and used for rectification.

From the rectification procedure three variables were obtained for each rectified point. They are the world coordinates relative to D' (X,Y) as well as a direction (ω) measured from true north. This is discussed in the following sections.

3.6. Heading Direction Calculation

For the heading direction calculation the X- and Y-ground coordinates of points located at the 'Bow' (X_1,Y_1) and the 'Smoke Stacks' (X_2,Y_2) are required as well as the angle measured from true north to the these points on the reference plane i.e. ω_1 and ω_2. The horizontal length of the ship measured from the bow to the smoke stacks (L_{SS}) is also required. This variable can be determined in two ways. L_{SS} may be determined either from common ship registers e.g. Ned Lloyds Shipping Register or by simple imaging techniques as long as the overall length of the ship is known.

Assuming that the overall length of the ship (L_{OA}) is known, the length of that part of the ship measured from the bow to the smoke stacks (L_{SS}) can be calculated, if a side view of the ship exists. Plate 3-3 is a typical example of a side view, with both the total length (L_{OA}) and the length from bow to the smoke stacks shown (L_{SS}). L_{SS} can easily be determined by proportion based on pixel count ratios.

Plate 3-3: This is a side view of the ship Africa Star that entered the Durban Port on 19th July 2000. This image was used to calculate the length of the ship measured from the bow to the smoke stacks.

During a ship's entry manoeuvre the length of the ship between the bow and smoke stacks appears smaller due to the position of the camera and the angle of the ship entry. For this investigation this variable is termed the projected length of the ship during entry (L_{PROJ}). From a plan view as depicted in Figure 3-8, both the L_{SS} and L_{PROJ} are visible.

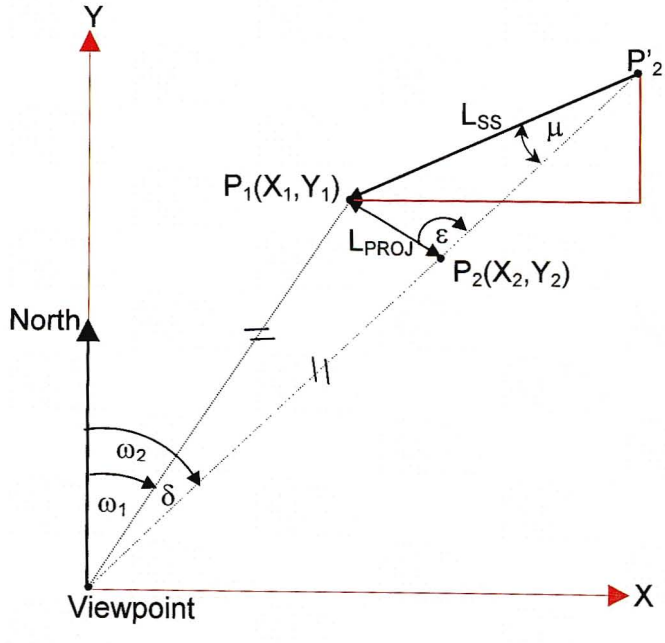

Figure 3-8: Annotated Heading direction calculation

From Figure 3-8 since the coordinates of both P_1 and P_2 are known, therefore L_{PROJ} can be calculated as,

$$L_{PROJ} = \sqrt{(X_1 - X_2)^2 + (Y_1 - Y_2)^2}$$

The angle δ is equal to the difference between ω_2 and ω_1. Since the ground distances from *D* (the view-point's nadir) to P_1 and P_2 are approximately equal, ε can be expressed as,

$$\varepsilon = \frac{\delta}{2} + 90$$

This implies that for a small angle δ, angle ε tends to 90 degrees. Angle μ is calculated by using the Sine Rule Law as,

$$\sin(\mu) = \frac{L_{PROJ} \cdot \sin(\varepsilon)}{L_{SS}}$$

With angle μ determined the heading direction of the ship is easily calculated from true north in a clockwise direction as,

$$H_D = (\mu + \omega_2) + 180 \qquad \text{If } X_1 <= X_2$$

$$H_D = (\mu - \omega_2) + 180 \qquad \text{If } X_1 > X_2$$

The heading direction calculation can be summarised in a flow chart in Figure 3-9.

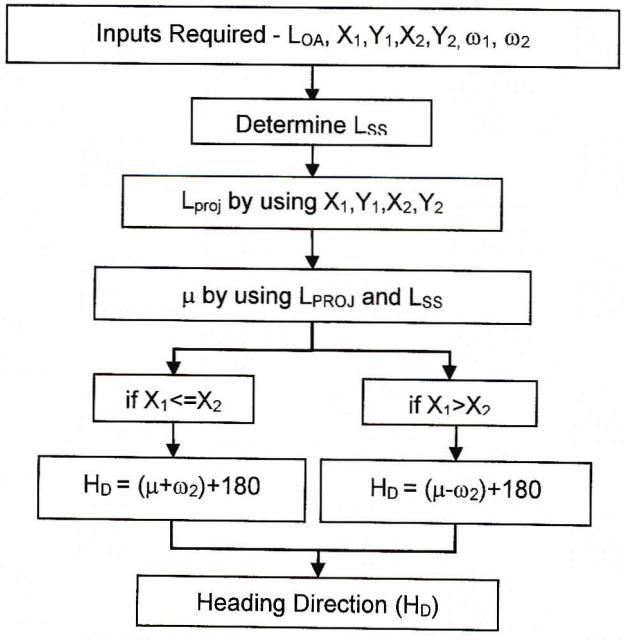

Figure 3-9: Flow chart summarising the calculation of the heading direction.

With the heading direction known the magnitude and direction of the velocity vector may be calculated. This is discussed in the next section.

3.7. Velocity Vector Calculation

Using the rectification procedure for a set of time exposed images, X- and Y-ground coordinates can be calculated for a ship as the time series of its position. This set of ground coordinates represents the position of the bow of the ship projected down onto the reference plane over time. For the present investigation these ground coordinates were used to represent the actual position of the ship.

A schematic of a possible ship track is shown in Figure 3-10. In this figure the present position of the ship at time *t* is shown as *S(t)* with the position of the ship at times *t-1* and *t+1* also shown. Ideally to determine the velocity vector at *S(t)* ground coordinates of a ship at position *S(t-1)* and *S(t+1)* should be used. However for real-time applications this is obviously not possible.

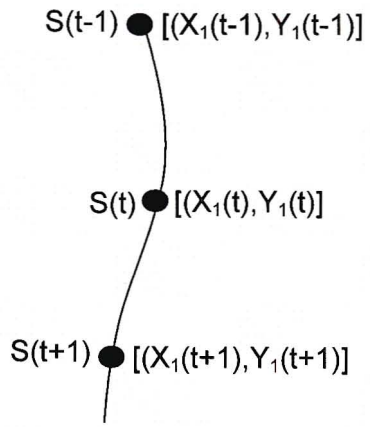

Figure 3-10: Schematic illustrating the position of the ship as a function of time

Therefore, for this investigation, the velocity vector was determined using *S(t)* and *S(t-1)*. The time derivative of the position between these two points was determined using a backward difference approximation to yield the velocity vector at time *t*.

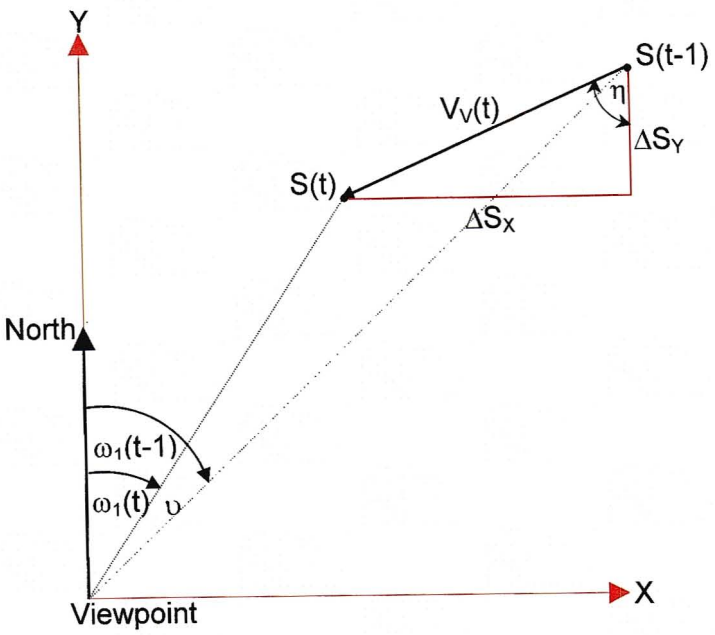

Figure 3-11: Plan view of ship at two consecutive positions along its ship track

Referring to Figure 3-11, the true velocity vector is given by,

$$V_V(t) = \left(\frac{\Delta S_X}{\Delta t}, \frac{\Delta S_Y}{\Delta t} \right)$$

where, $\Delta S_X = X_1(t-1) - X_1(t)$ and $\Delta S_Y = Y_1(t-1) - Y_1(t)$.

The direction of the velocity vector at *S(t)*, can be determined from angle η defined in Figure 3-11 and is given by,

$$\eta = \mathbf{arctan}\left(\frac{\Delta S_X}{\Delta S_Y} \right)$$

The direction of the velocity vector measured from true north in a clockwise direction is,

$$V_D(t) = \eta + 180$$

The magnitude of the velocity vector (the speed of the ship over the ground) at time *t* is,

$$V_S(t) = \sqrt{\left(\frac{\Delta S_X}{\Delta t} \right)^2 + \left(\frac{\Delta S_Y}{\Delta t} \right)^2}$$

3.8. Crab Angle and CTDV Calculation

As reviewed in section 3.2 the crab angle (θ) is the difference between the heading (H_D) and velocity vector directions (V_D). This section will use the crab angle as well as the magnitude of the velocity vector ($V_S(t)$) to calculate the Cross Track Drift Velocity (CTDV) of a ship at time *t*. As reviewed earlier the CTDVs measured and presented in this investigation are the net effect of all the currents and waves acting perpendicular to the projected surface area of a ship below the water surface, (over a known time-interval) The directions of these vectors are illustrated in Figure 3-12.

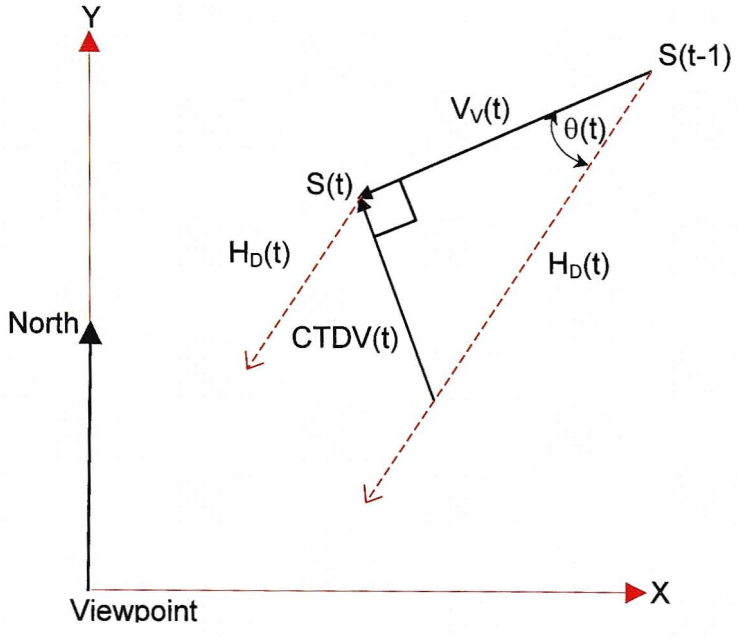

Figure 3-12: Vector diagram for calculation of the CTDV component

The crab angle (θ) at time *t* was calculated as the difference between the velocity and heading directions,

$$\theta(t) = V_D(t) - H_D(t)$$

The magnitude of the CTDV at time *t* is determined as,

$$CTDV_S(t) = \tan[\theta(t)].V_S(t)$$

The direction of the CTDV(t) vector, $CTDV_D(t)$, is calculated from true north in a clockwise direction as,

$$CTDV_D(t) = V_D(t) - 90 \qquad \text{If } \theta(t) < 0$$

$$CTDV_D(t) = V_D(t) + 90 \qquad \text{If } \theta(t) > 0$$

Note that when the crab angle (θ) equals zero, the CTDV equals zero. Note also that the direction convention used for cross track drift, is the same as that for currents i.e. currents are specified by the direction *towards* which they are flowing. So for this investigation the direction calculated for the CTDV is the direction that the ship is drifting *towards*. The procedure used to calculate the magnitude and direction of the CTDV can be summarised, in the flowchart shown in Figure 3-13.

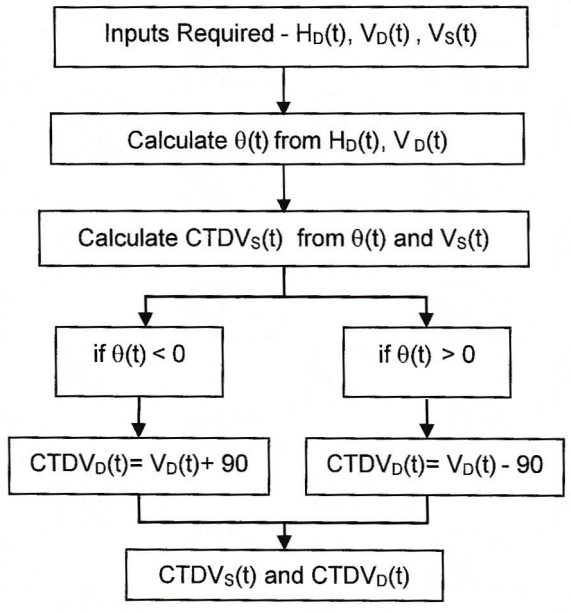

Figure 3-13: Flowchart illustrating the procedure followed to calculate the CTDV magnitude and direction.

3.9. Ship Slip due to manoeuvring

As mentioned in the latter parts of section 3.2 the crab angle (θ) experienced by vessels can also depend on the sideways slip of the vessel in the water. The contribution of ship slip to the measured crab angle was unknown and required further investigation. It was initially assumed that under calm weather conditions (i.e. no winds, waves or currents) a ship will have a crab angle equal to zero (for a fixed rudder setting). This section will show that ships do have a crab angle under such conditions, which is due to the sideways slip of the vessel through the water, and depends on the turning radius of a ship at specific water depths. An investigation to calculate the contribution of slide slip to the overall crab angle was undertaken by using the PORTSIM simulator, the same simulator used by CSIR (1999b).

The PORTSIM simulator programme had the capability of accepting wind, wave and current measurements, which for this exercise were set to zero. By varying the speed and the rudder settings of a selected design ship, turning circles of various magnitudes would result along with a corresponding crab angle due to slip. Figure 3-14 is a typical

example of a plan view of a ship plot for a Post Panamax vessel travelling at a fixed rudder setting and speed. The ship plot shows the ship travelling in a counter clockwise direction, with the ship's position shown every 60 seconds. It can be seen that the ship's heading direction (bow) is different to the velocity direction at every point along the ship plot, with the ship's bow pointing towards the inside of the turning circle. This is illustrated in Figure 3-15.

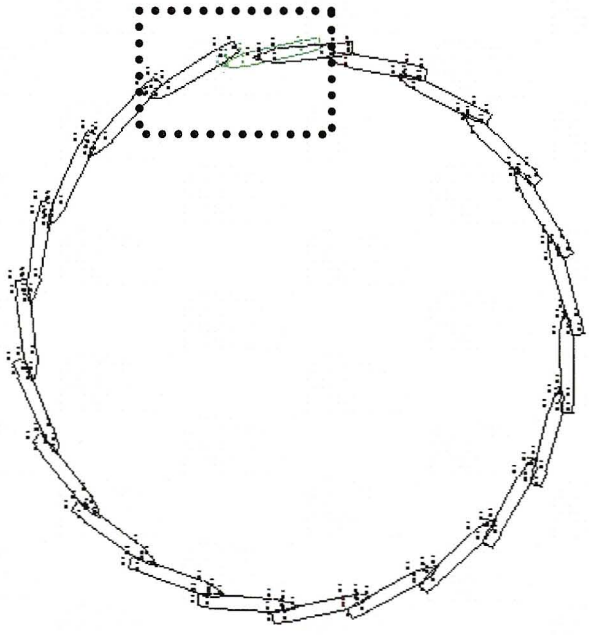

Figure 3-14: Ship track plot of a Post Panamax vessel steered at a constant rudder angle of 45 degrees at a speed of 6 knots

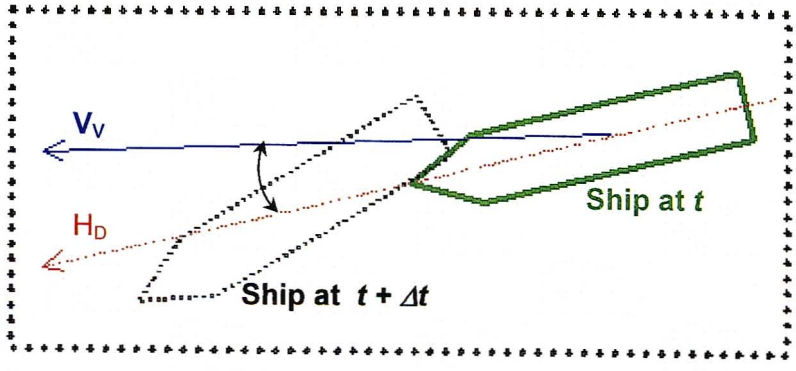

Figure 3-15: Magnified illustration of part of the ship plot shown in Figure 3-14

If this component of the crab angle due to slip is known for specific turning radii, it can be used to correct the measured crab angle and more accurate measurements of the CTDV due to wins, waves and currents would result. Using the PORTSIM simulator three design vessels were investigated i.e. car carriers, post panamax vessels and product tankers. Ship characteristic data for these three ships can be found in Appendix E. Simulations were carried out with these three vessels at varying ship

speeds and rudder settings. Figure 3-16 to Figure 3-18 illustrates the results of these simulations carried out for three ships i.e. car carriers, post panamax vessels and product tankers respectively. The data used to generate these figures can be found in Appendix E.5. It is evident from these figures that a large radius of curvature will result in a small crab angle due to slip. If two out of the three following variables are known; 1.Radius of Curvature; 2.Rudder angle; 3.Water depth, interpolation of an approximate value for the crab angle due to slip can be determined from the simulated data. Application of these results correcting the CTDV data will be shown later in sub-section 6.5.2.

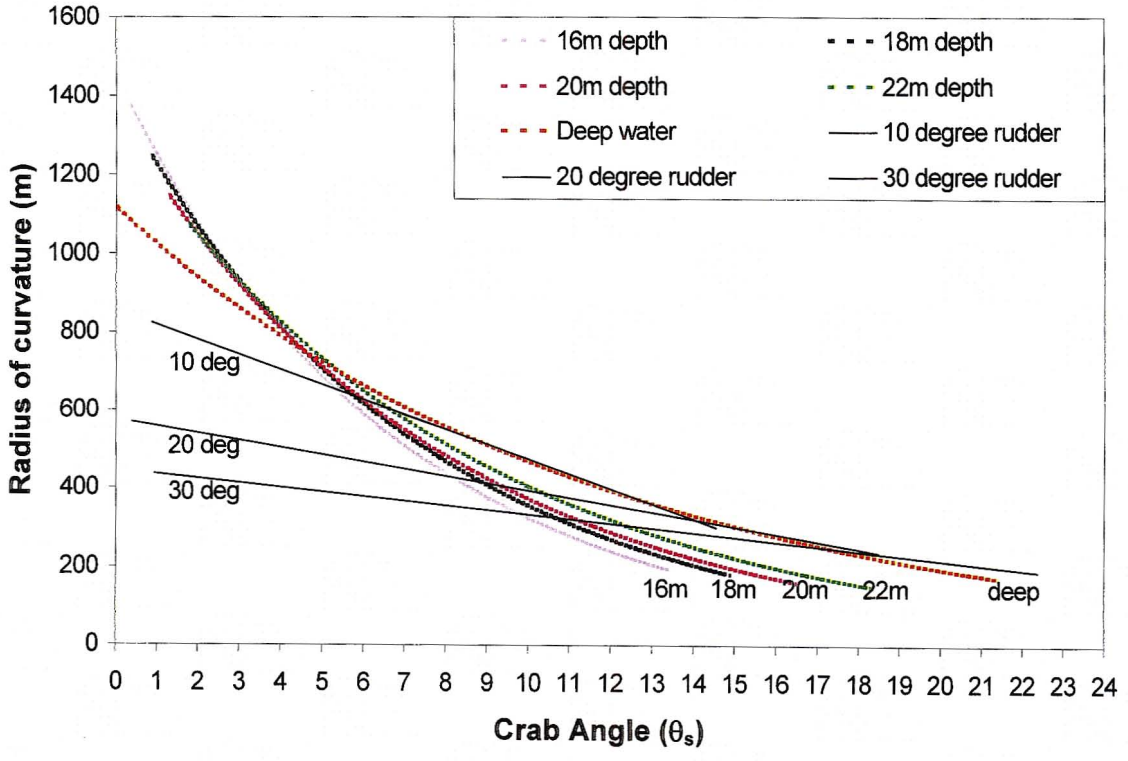

Figure 3-16: Graph illustrating how the crab angle due to slip (θ_s) varies with changing ocean depths, rudder settings and turning radii's for Car Carrier type vessels

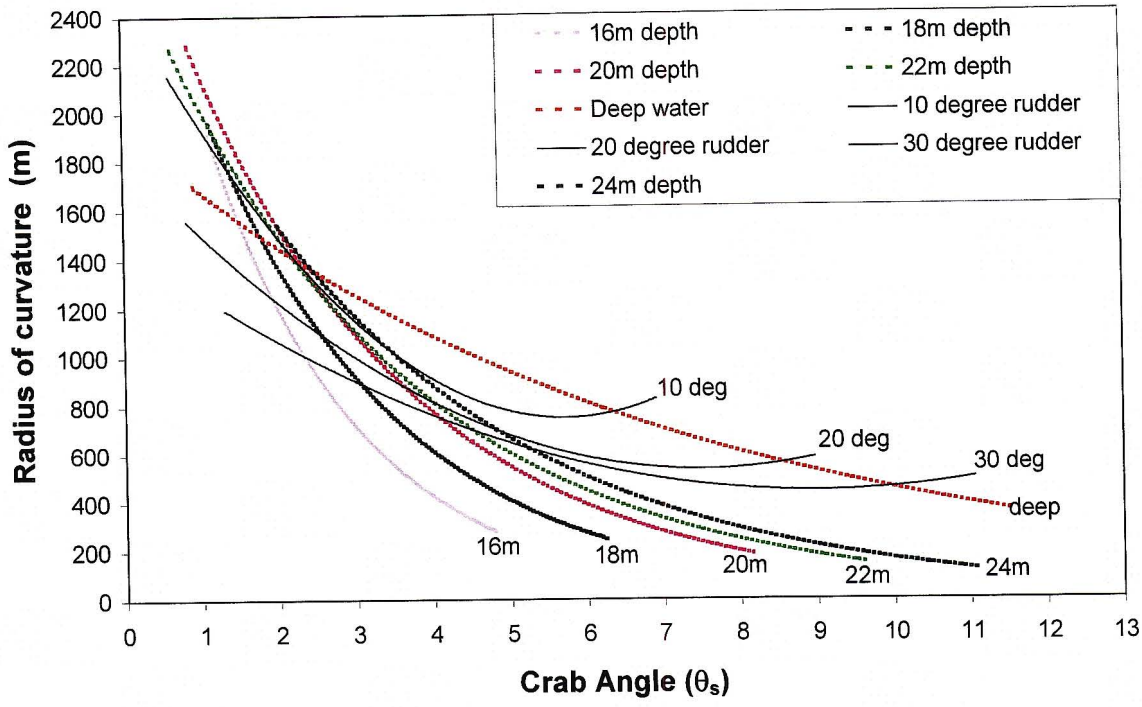

Figure 3-17: Graph illustrating how the crab angle due to slip (θ_s) varies with changing ocean depths, rudder settings and turning radii's for Post Panamax type vessels

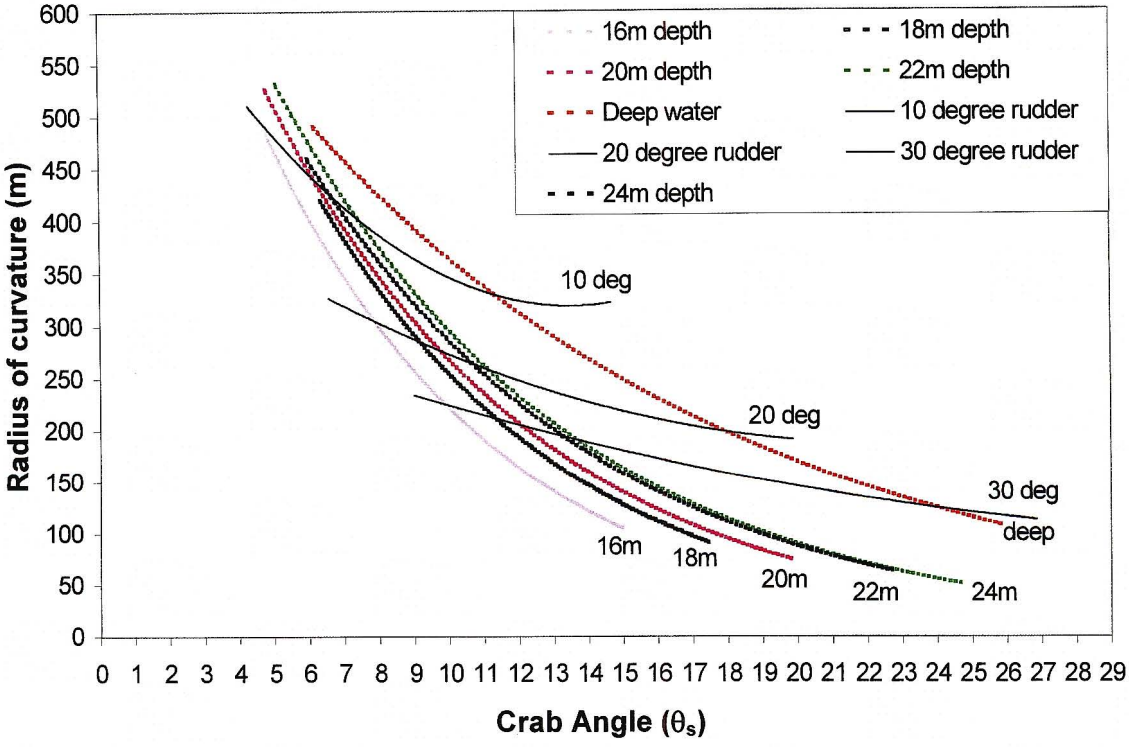

Figure 3-18: Graph illustrating how the crab angle due to slip (θ_s) varies with changing ocean depths, rudder settings and turning radii's for Product Tankers type vessels

3.10. Summary

This chapter has explained the basic concept as well as the key innovations of the present investigation. Sections 3.4 to 3.8 explained the procedures used in processing images to yield the Heading Directions, Velocity Vectors, Crab Angles and CTDVs. In section 3.9 it was shown that a vessel with a specific turning radius would generally have a crab angle (θ_s) due to lateral slippage in the water associated with rudder induced turning movements.

In chapter 4 the application of the concepts discussed in this chapter to actual images is described to illustrate that the concept works in practice.

CHAPTER 4

TESTING AND EVOLUTION OF THE METHODOLOGY

4.1. Introduction

The concept of processing images to obtain a ship's heading and velocity were explained in chapter 3. It was not clear whether the proposed method was practical. It was unknown whether the imaging resolution would be adequate or whether the spatio-temporal resolutions used would be sufficient. This chapter discusses the application of the concept to actual images of ships entering the harbour at our case study site. The viability of the approach is assessed.

A portable digital still camera was initially used in a preliminary study to determine whether the basic concept was feasible. Later, video cameras were applied. This chapter will discuss the testing and evolution of the methodology.

4.2. Portable Digital Still Camera

A portable digital still camera was used for image acquisition between 17th August and 17th September 1999 (see Patel, 1999). During this time eighteen ships were successfully tracked into the harbour using this camera under varying weather conditions.

4.2.1. Field Set-up

The digital still camera used was a Sony Mavica FD-88. This camera was cost effective, and could quickly and easily provide initial results. The camera has the following features:

- Storage of captured images by means of $3^1/_2$ inch removable diskettes
- Time and date recording features.
- Optical Zoom settings (which would allow the field of view to be varied)
- Resolution up to 1280 pixels x 960 pixels

The camera was mounted on a tripod and positioned on the main platform of the Bluff Signal Station at approximately 100m above mean sea level, facing the harbour entrance. Images were recorded and saved to diskette using the built in disk drive in the camera. The images were saved in JPEG format. A JPEG is a graphic image file created using a suite of compression algorithms developed by the Joint Photographic Experts Group. Consecutive images could be recorded at a minimum of 10-second

intervals, but for this preliminary study a 30 second interval was used. Between 9 and 11 images could be saved to each diskette at the 1024 x 768 resolution setting. A fixed zoom setting with an image resolution of 1024 x 768 pixels was used to ensure adequate quality images for identifying key features on the ship during the image processing stage. These key features included the bow and smoke stacks of the ships discussed earlier. With a complete set of time lapsed images recorded, post processing of the images was performed manually, using the method explained in chapter 3.

4.2.2. Initial Results

Plate 4-1 is a sample of superimposed time-lapse images of a ship entering the port during 1999.

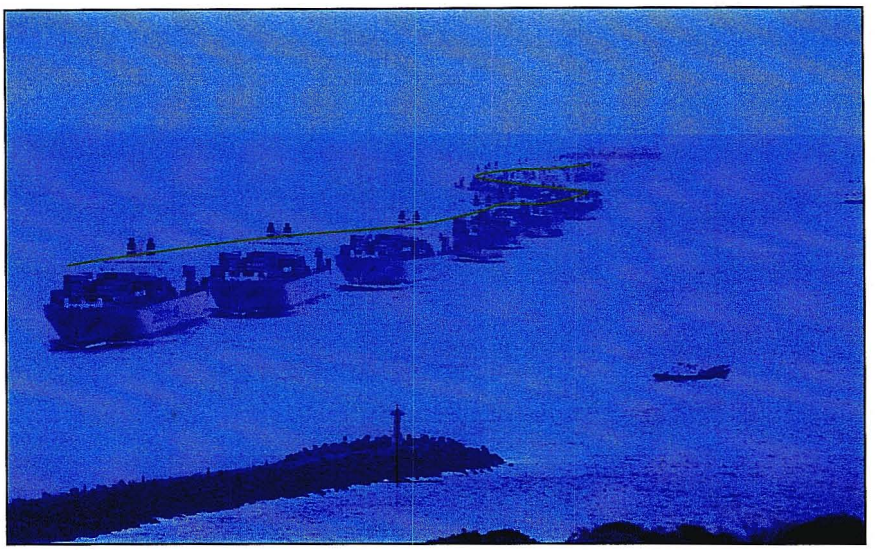

Plate 4-1: Superimposed time-lapse images of the "Del Kalahari" entering the Durban Harbour on 24th August 1999

The rectified track is shown in Figure 4-1. The calculated CTDVs were determined and are shown as arrows perpendicular to the ship track. The CTDVs are drawn to the scale indicated in the figure. The maximum measured CTDV is about 1.2m/s (2.4 knots) and is a North-westerly drift.

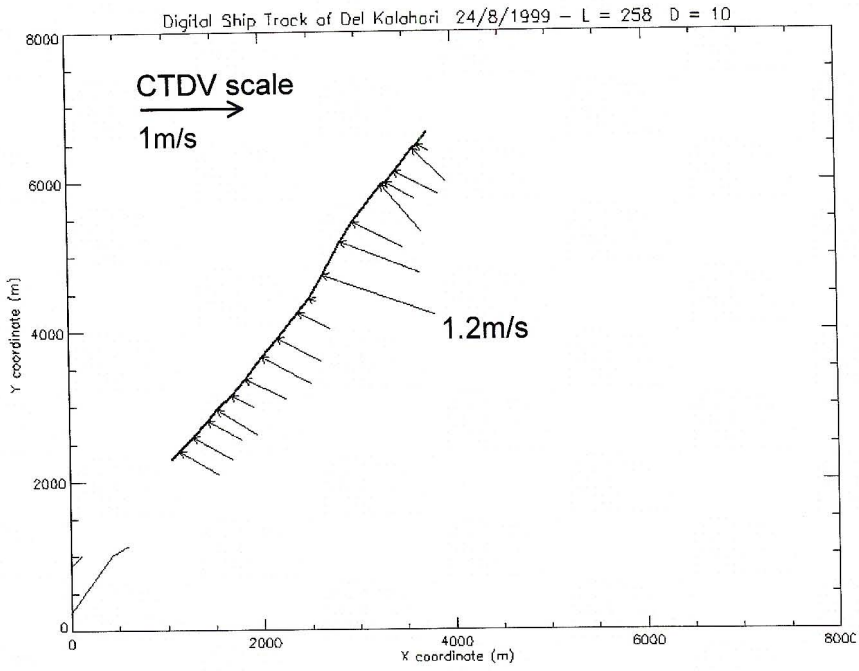

Figure 4-1: Transformed ship track of the Del Kalahari

Plate 4-2 is another example of superimposed time-lapse images of a ship entering the port during 1999. For this example more complicated turning manoeuvres, can be seen.

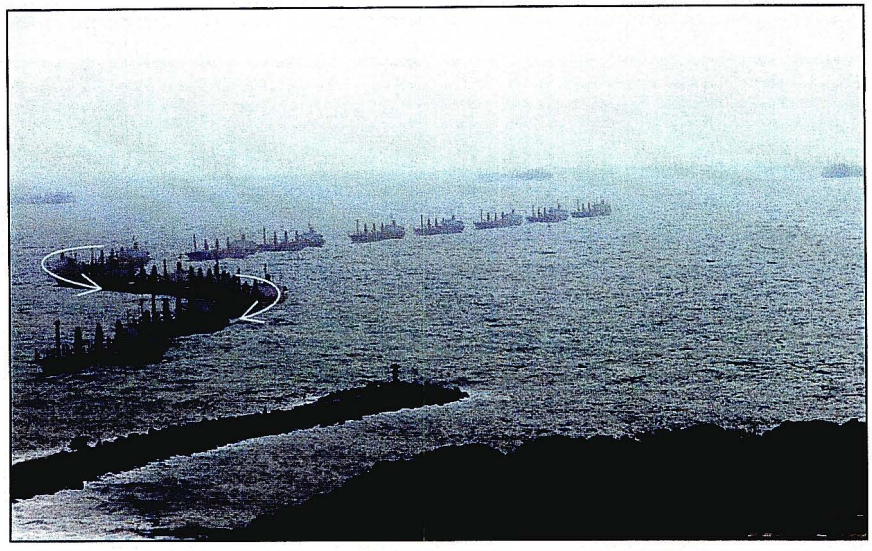

Plate 4-2: Superimposed time-lapse images of the "Salinthip Naree" entering the Durban Harbour on 3rd September 1999

Rectification of the time-lapsed images shown in Plate 4-2 yielded the transformed ship track shown in Figure 4-2. From the ship track in this figure it is evident that a relatively larger CTDV (0.4 m/s = 0.8 knots) occurred during a sharp turning manoeuvre about 600 metres outside the south breakwater. As discussed in section 3.9, it is incorrect to

assume that this measured CTDV results only from winds, waves and currents. A contribution due to slip (θ_s) would also be included in this CTDV, i.e. the larger the slip (θ_s) the larger the crab angle (θ) thus the larger the measured CTDV. Corrections to the CTDV data to allow for slip could be required. Section 6.5.2 discusses how the corrections affect the results.

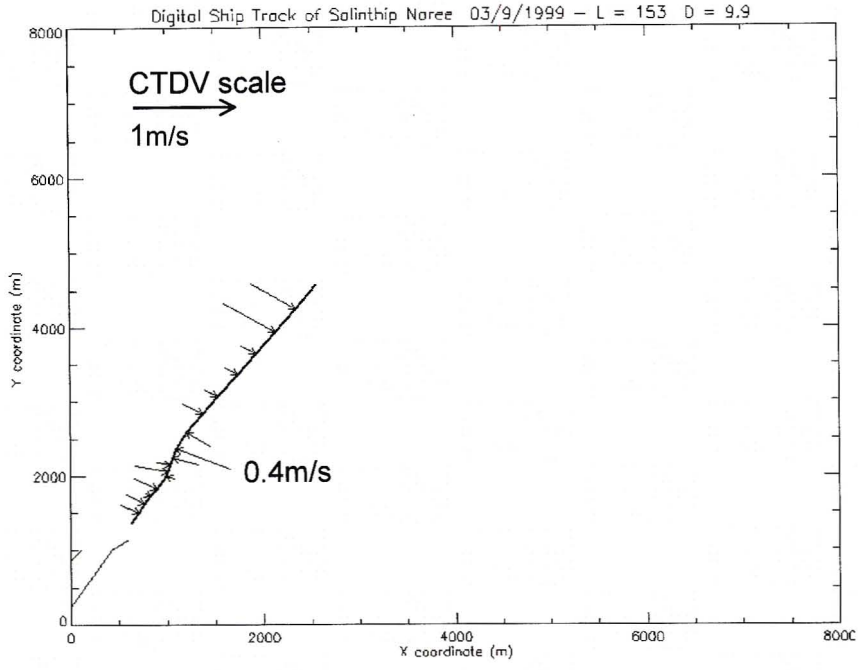

Figure 4-2: Transformed ship track of the Salinthip Naree.

4.2.3. Difficulties encountered with the still camera option

The difficulties experienced during this preliminary investigation are summarized below:

Shipping at a busy harbour is an intense and (to some extent) unpredictable activity. Ships enter the port only when the shipping agents are ready to accommodate them at available berthing stations. The schedule for ships entering the port on any given day is thus only decided early each morning, which made the recording of ship tracks difficult. Added to this problem was the distance between the University of Natal and the Bluff Signal Station (about 20km) that equates to a 20-minute drive. This made the recording of ship tracks a time consuming activity.

The process of replacing the diskettes during a recording sequence resulted in small jostling movements of the camera. This meant that the reference points in the image moved their positions, which made post-processing of the images more tedious.

Images were manually recorded and captured to a diskette. Due to the manual process, images could not be recorded at precise and regular time-intervals.

As stated earlier, images were captured approximately every 30 seconds. During this time the ship could traverses a large distance through the water. The spatial accuracy of the heading and velocity data along the ship track was thus reduced. Due to this limitation, velocity vectors were determined by fitting a 5^{th} order polynomial through each position along the ship's track (using a least squares approach). With the equation of this polynomial known, the time derivative of the ship's position was determined and the velocity vector at each point calculated. The large time-intervals between images resulted in the spatial structure of CTDVs being poorly resolved. It also resulted in poorly resolved ship track plots, which decreased the overall accuracy of the results especially during rapid turning manoeuvres.

Manual post-processing of the captured image sequences was carried out. As explained in Section 3.4, for every image, two sets of pixel coordinates were extracted. This involved the drawing of the three lines on the image (refer Figure 3-4). From the intersection of these lines two sets of pixel coordinates could be extracted. The manual digitisation of this pixel data was a time consuming process.

A complete set of pixel coordinates for each ship track was stored and used for the rectification process. Rectification calculations were performed on a spreadsheet. A Visual Basic sub-routine was developed by Patel (1999) that semi-automated the rectification procedure as well as the calculation of the CTDVs. Limitations to this routine were:

(a) Only a maximum of 18 images could be rectified per ship track.
(b) Velocity vectors were determined manually with their accuracy questionable due to large time-intervals between consecutive images.

4.2.4. Improvements to the still camera system

From the challenges encountered during this part of the investigation the following improvements were suggested:

Firstly, it was evident that using a video camera instead of a still camera would yield significant benefits to the pre-processing stage. It would enable a more complete time sequence of images to be recorded and saved. The need to manually trigger the capture of images would be eliminated, as the entire image sequence would be saved

on cassette. The sequence of images recorded would be accurately time and frame stamped for later extraction. The user would only be required to start and stop the camera at the beginning and end of the capture sequence with no interference during the ship entry manoeuvre. This would reduce the problem of jostling movements of the camera. Images later extracted from the recording could be captured at smaller time intervals, thus having ship tracks with higher spatio-temporal resolution. The velocity vectors at each point along the ship's track could then be more accurately determined. This would result in more accurate calculation of the spatial distribution of the measured CTDVs.

The key problem associated with the post-processing stage was the tedious and time-consuming task of manually extracting two sets of image coordinates from each image in a sequenced ship track. This problem could be addressed through image processing software written in a more powerful programming language.

4.3. Portable Digital Video Camera

Following the initial experiments with a digital still camera, a portable digital video camera was purchased. This video camera was used to acquire ship tracks from 4th February till 19th July 2000. The primary aim in using a video camera was to increase the resolution of the ship tracks.

4.3.1. Technical Information

Video Images are generally rectangular with the ratio between horizontal and vertical dimensions being 4:3. Since there are approximately 480 active horizontal lines in standard video signals, the number of horizontal pixels is typically 640. These dimensions can vary depending upon the capabilities of the imaging system. The image resolution used for the video camera system thus was less than that used for the still camera (1024 x 768). That is, for the same field of view, the video images will have a lower spatial resolution than those for the still camera. This lower resolution makes identification of key features in the images (e.g. the bow and smoke stacks of the ships) less accurate. Unfortunately maintaining a high resolution from a video-based system was not economically feasible, thus a trade-off between the higher temporal resolutions of video capture and high spatial resolution of still imaging was necessary.

The digital video camera used was a Panasonic AG-EZ 35. This camera had the following features:

- Storage of captured images by means of digital video cassette (mini-DV standard)
- Time and date recording features.
- Optical Zoom settings up to 12
- Resolution of 720 pixels x 576 pixels

The field set-up of the video camera was similar to that of the still camera. The ship's video sequences were stored onto cassettes for later extraction of still images.

A personal computer connection kit made it possible to interface the camera directly to a computer and capture still frames from the video. The video camera could be connected to a PC via the standard RS-232C serial port. Initially images were captured using software that was acquired with the video camera (Panasonic "DV Studio" Software). This software allowed the user to define the beginning of a video sequence from which frames would be captured and stored, at user defined time intervals. For example, if the user required images to be captured every ten seconds, the video sequence was first initialised, and then the software would take control of the camera and play and stop the video at ten second intervals. An image will then be grabbed and transferred across to the PC at approximately 14 kilobytes a second (KBps). A standard digital video image is about 140 kilobytes in size, thus the time taken to transfer an image from the video camera to the PC is about 10 seconds. This method proved to be time consuming and unreliable, as images could be "lost" during the transfer process. A faster and more efficient method of capturing images from the video source was thus investigated.

The video camera is equipped with an IEEE 1394 ("Firewire" ™) digital interface, which allows the direct transfer of video to a personal computer. An IEEE 1394 ("FireWire" ™) interface card was installed in the PC, which allows the transferring of digital video data at speeds of 100, 200, or 400 megabits per second (Mbps). With such high data speeds the full-motion video could be viewed directly on the monitor of the PC. Commercial software ("Moto DV" by Digital Origin) was used for the process of viewing, extracting and saving images from the video sequence at user defined time intervals. With a complete set of time-lapsed images saved directly to the PC hard disk, post processing of these images could then be performed.

4.3.2. Initial Results

Ten ships were successfully tracked into the harbour under varying weather conditions using the digital video method. The time interval chosen for acquisition of images from the sequence was set at 10 seconds. The acquisition process was accurate within an error of ±3 frames with frames 40 milliseconds apart, i.e. accuracy of ±120 milliseconds. Plate 4-3 is a sample of superimposed time-lapse images of a ship captured entering the port with the digital video camera.

Plate 4-3: Superimposed time-lapse images of the "Ned Clarence" entering the Durban Harbour on 16th May 2000.

Note that Plate 4-3 consists of only a few of the sequence of images recorded from the video source. On average 45 images per ship track were recorded and analysed for each ship track. Programming code was written and developed to make the post-processing of images more efficient. A mathematical software package ("Mathematica"™) was used to develop this programming code. This code added more flexibility and automation to the post-processing stage of the images. Figure 4-3 is a sample result of the rectified ship track shown in Plate 4-3. The CTDVs shown in this figure are drawn to scale (shown in Figure 4-3) and have been magnified for illustrative purposes. The transformed ship track shown in Figure 4-3 is more accurately resolved then the transformed ship track shown earlier in Figure 4-2. This is due to the larger number of images available during the post-processing image stage. With this larger data set, the spatial structure of the CTDVs was more accurately resolved and appears to be more variable.

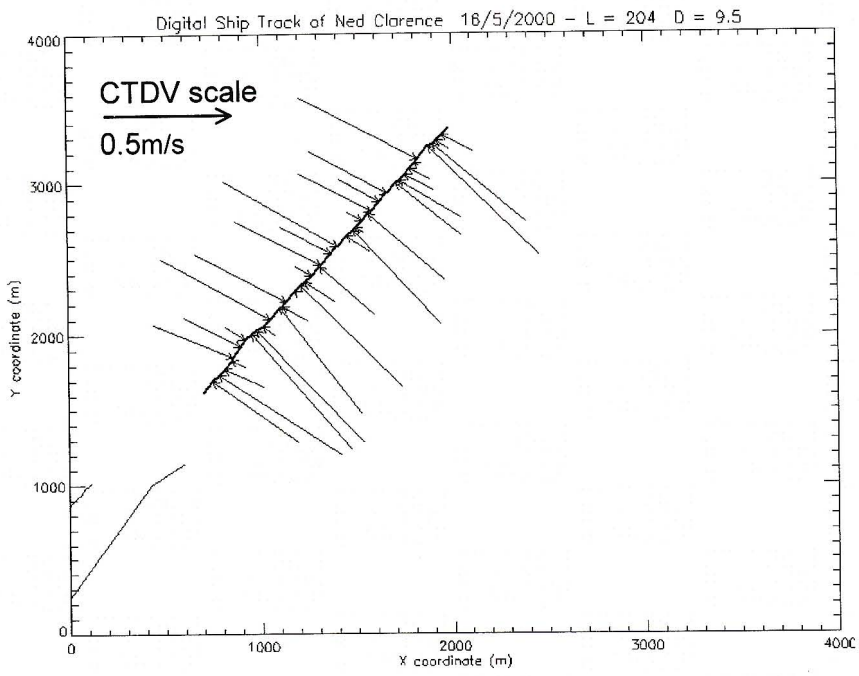

Figure 4-3: Transformed ship track of the Ned Clarence

For this specific ship track, it appears as if the CTDVs are not consistent in direction. Presently the reasons for these inconsistencies are not clear and should be further investigated. It is believed that they may, in part, be due to rapid rudder turning manoeuvres (refer section 6.5.2).

4.3.3. Comments on the video camera system

The major difficulty as explained earlier was the time spent travelling between the Signal Station on the Bluff and the University of Natal as well as the accessibility of shipping schedules. Smaller time-intervals between consecutive images helped in improving the accuracy of the measured CTDVs during rapid turning manoeuvres of the ship. However the effects of lateral slippage of the vessel would still need to be addressed. The main problem associated with the post-processing process remained the time taken to manually extract the pixel coordinates.

4.3.4. Improvements to the portable DV camera

It was decided that the installation of a fixed base video camera at the Signal Station with a live video and telemetry link to the university would be undertaken. This would be the most efficient imaging system since digital images of ship tracks could be captured, stored and analysed real time. Since the video camera would be permanently fixed to the Signal Station during capture, the only uncontrolled movements of the camera would be due to strong winds. Reference points (used for rectification) within

the angle of view of the camera would remain fixed at all times for specific focal lengths.

4.4. Fixed Video with Microwave Link and Telemetry

A permanent colour CCD (Charged Coupled Device) digital video camera was installed at the Bluff Signal Station with a live video and telemetry link to the University of Natal. This was a collaborative effort between the local port authorities (PORTNET), CSIR and the University of Natal. The camera (the Ultradome KD6) was used for this investigation from March 2001.

4.4.1. Field-setup

This video camera was mounted on the Bluff Signal Station and is equipped with pan, tilt and zoom capabilities. This camera is located at coordinates X_S = 306345.58, Y_S = -5572.39m, and altitude H_S = 101.3m above sea level (asl), measured in the Transverse Mercator coordinate system (a conformal Gaussian mapping) using LO31 Cape Datum (31° longitude) as the reference system. The camera was equipped with telemetry to allow remote PTZ control, and images were transmitted to University of Natal via a microwave link. Plate 4-4 shows pictures of the antennas used for transmitting and receiving the analogue video signals and data telemetry.

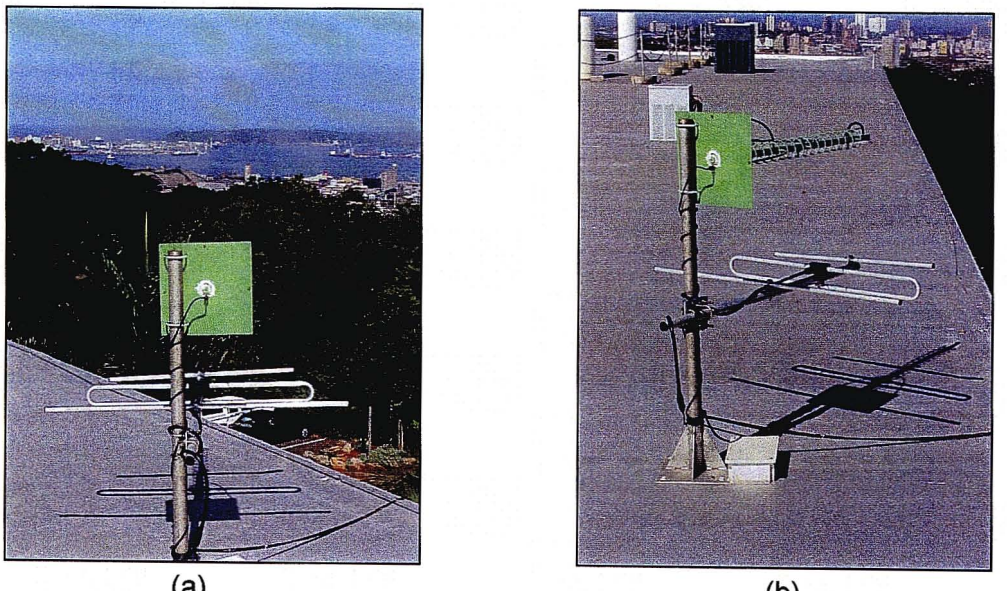

(a) (b)

Plate 4-4: (a) View of the antennas on the Civil Engineering building with the Bluff in the background. (b) Side view of the VHF Telemetry Transmitter (green) and the Microwave Receiver

Live video was transmitted to the University and viewed on a standard monitor. The camera was equipped with 100 programmable preset positions, and all captures were taken with the camera at a specific preset setting. These presets are repeatable to within 0.5 degrees (according to the manufacturers specification). The PC located at the University of Natal was then used to capture sequences of ships entering the harbour using an "ELLIPS RIO" frame grabber. Programming code was developed to perform this capture. Figure 4-4 schematically illustrates the set-up of the system.

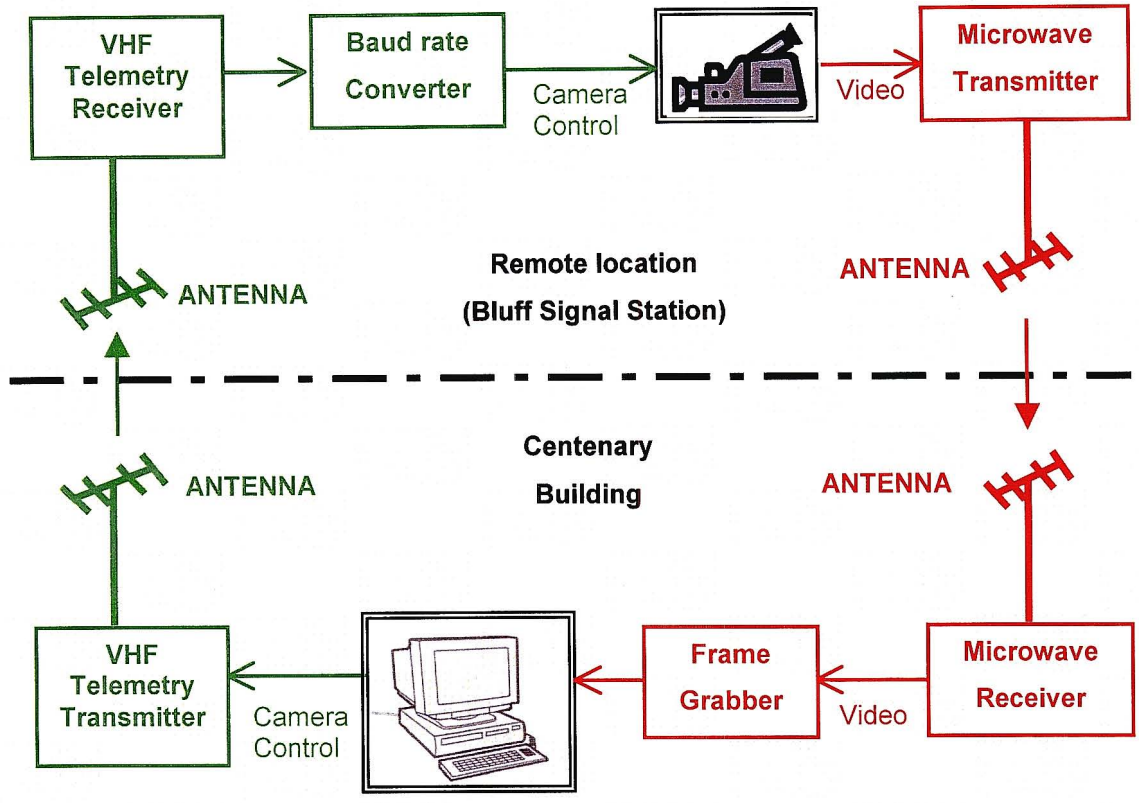

Figure 4-4: Schematic set-up of the CCD camera and the microwave link installation between the Signal Station and the University of Natal (adapted from Basson, 1999)

The Ellips Rio frame grabber is a high performance PCI (Peripheral Component Interconnect) component, which is normally targeted at real-time industrial image processing applications. It is designed to work with most S-Video/composite colour or monochrome cameras. A software library (developed in Microsoft Visual C++) accompanied the Rio Ellips frame grabber board. Custom software to control the image acquisition process was developed using that library and is described in chapter 5.

4.4.2. Initial Results

Approximately sixty ships were successfully tracked into the harbour under varying weather conditions using this microwave link. Approximately thirty of these ship tracks were captured using a time-interval between images of ten seconds whilst the

remainder were captured at two-second time-intervals. Out of the thirty ships captured at ten second intervals, eighteen were analysed and processed for this investigation. Plate 4-5 is a typical panoramic view of the Port entrance channel from the CCD camera located on the Bluff Signal Station. From this plate both the north and south piers are visible. The Durban beach coastline is seen running along the left edge of the plate.

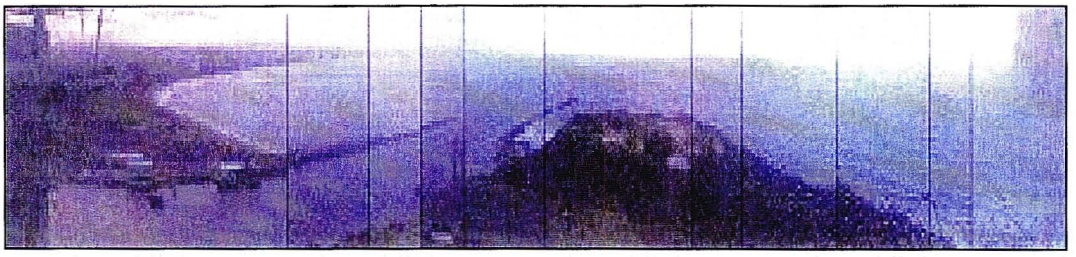

Plate 4-5: Panoramic View from the CCD camera located on the Bluff Signal Station.

With this installation, the port entrance channel could be remotely and continuously monitored from the University of Natal. The resolution of the imaging system was 768 by 576. Although this resolution is slightly higher than the resolution of the portable digital video camera, an analogue video signal was now being transmitted, with an overall reduction in quality. A standard preset PTZ setting was used for capturing sequences of ships entering the port as shown in Plate 4-6. The horizontal angle of view of the camera was 11.1 degrees, as calibrated in the field, using two surveyed ground control points within the angle of view as explained in chapter 3.

Plate 4-6: Standard preset used for capturing sequences of ships entering the harbour.

Figure 4-5 is a typical transformed ship track captured using the new fixed video imaging system. In this figure the direction of a few CTDV vectors appear to be incorrect (marked). For these cases, the distance travelled by the ship along the

channel between consecutive images was small, with the sideways movement large. This resulted in the digitised y-pixel coordinate being the same over a fixed time-interval resulting in quantization errors. The digitised x-pixel coordinate offsets between these images would be larger thus influencing the direction of the CTDV vectors. As a result the crab angle produced in these cases were high and led to spuriously high magnitudes for the CTDVs. Spurious data of this type is later removed from the full data set, after which analysis is carried out (see Section 6.3.1).

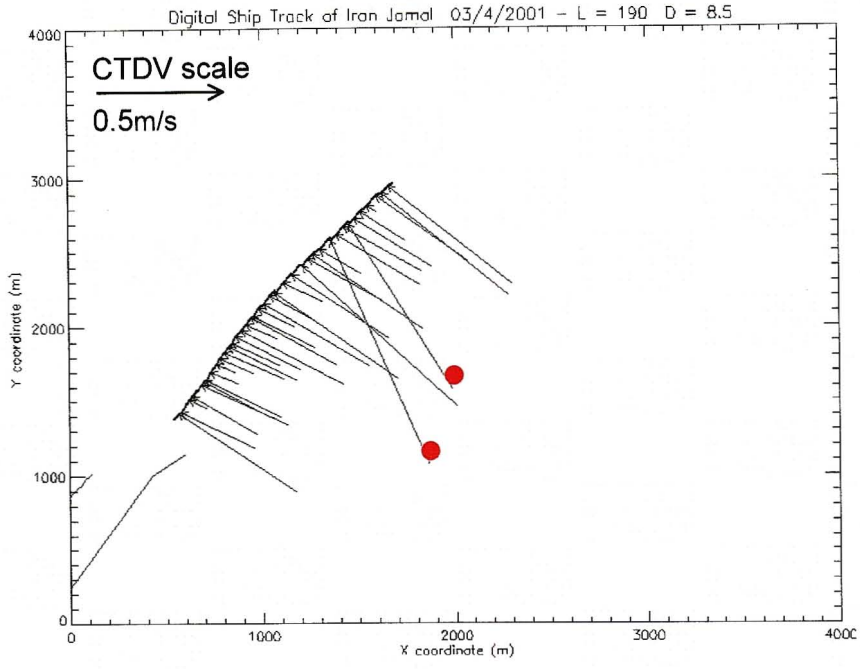

Figure 4-5: Transformed Ship Track of the Iran Jamal

With images continually available from the Signal Station, software was now required to complete the automation of the process.

4.5. Automation required

The primary aim of this investigation was to automate the procedure of tracking ships into the Port of Durban. This automated procedure would detect a ship about to enter the port and trigger a capture sequence to record the ship's entry manoeuvre. When the ship left the field of view of the camera the capture routine should cease and return to a dormant mode waiting to be triggered by the next incoming vessel.

The problem associated with the image post-processing stage (as already explained) was the time-consuming task of extracting pixel coordinates of key features. This problem could be addressed by having a system that can automatically track features like the smoke stacks and the bow of the ship. During this tracking process these image coordinates can be rectified to produce graphical plots of the ship track and

CTDVs. To incorporate such techniques, requires the application of machine vision technology such as pattern matching and feature tracking methods.

4.6. Validation of Rectification method

During 2001, an undergraduate research assistant was recruited to assist in investigating the accuracy of the ship tracking technology presented in this investigation. Nundlall (2001) validated the rectification procedure by using simultaneous GPS (Global Positioning System) measurements. This procedure involved using a portable hand held GPS, which was taken on board the ships by the harbour pilots. The harbour pilots used the GPS to capture waypoints during ship entry procedures at twenty (20) second intervals. During this time, images of the incoming ship were digitised and saved using the microwave based imaging system. The images were processed, and rectified. The ground coordinates of the ship were then compared to the corresponding GPS coordinates. Nundlall (2001) was able to obtain simultaneous GPS and imaging information for three ships that entered the harbour. These three ships were:

(a) Bella Lontra - 30th August 2001
(b) Global Mombasa - 11th September 2001
(c) Alam Senang - 18th September 2001

Data about these ship's can be found in Appendix B. Figure 4-6 to Figure 4-8 illustrates the ship track plots. The video imaging tracks are shown as the blue curve with the actual GPS track shown as the red curve. Tables D.1 to D.3 tabulates X and Y ground coordinates for all three ships and can found in Appendix D.

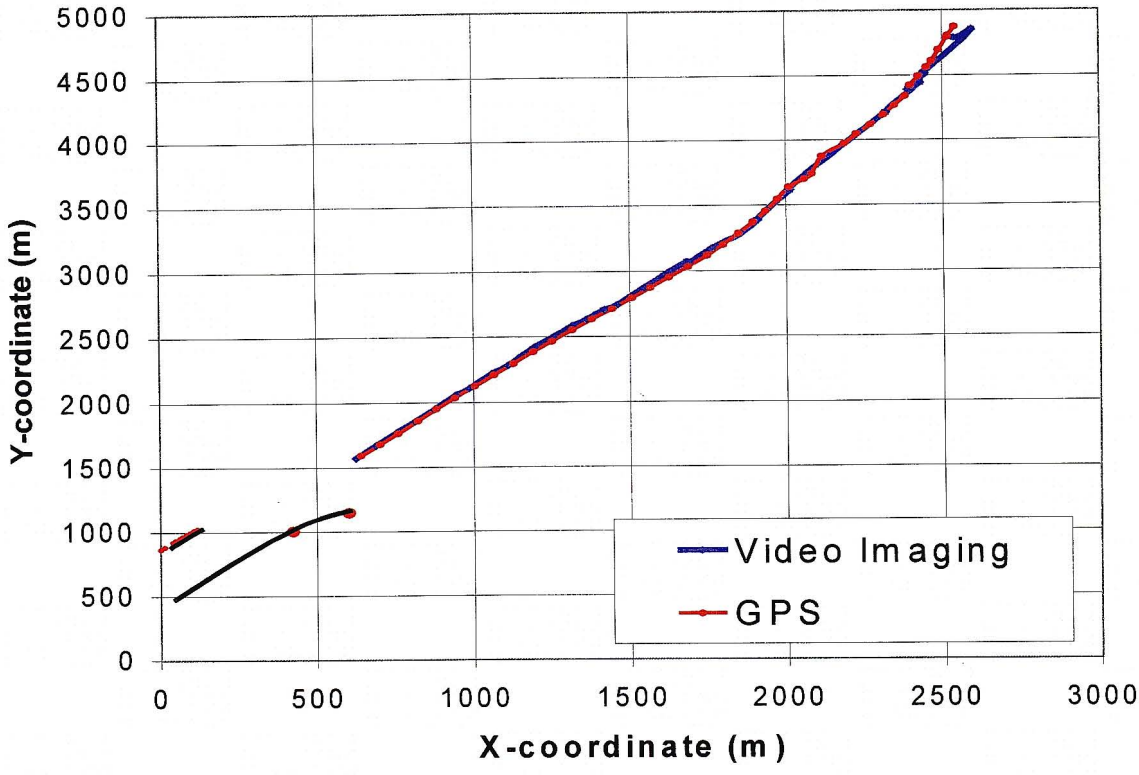

Figure 4-6: Ship Track plots comparing the GPS and video imaging coordinates for the Bella Lontra

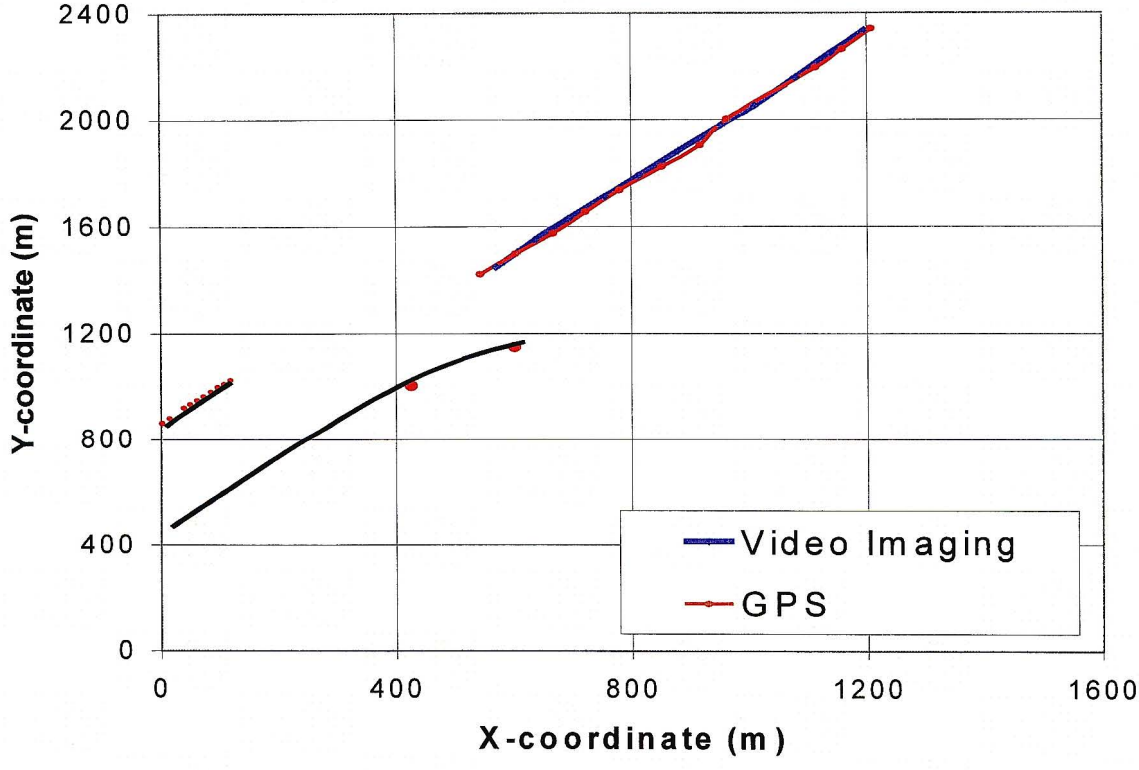

Figure 4-7: Ship Track plots comparing the GPS and video imaging coordinates for the Global Mombasa

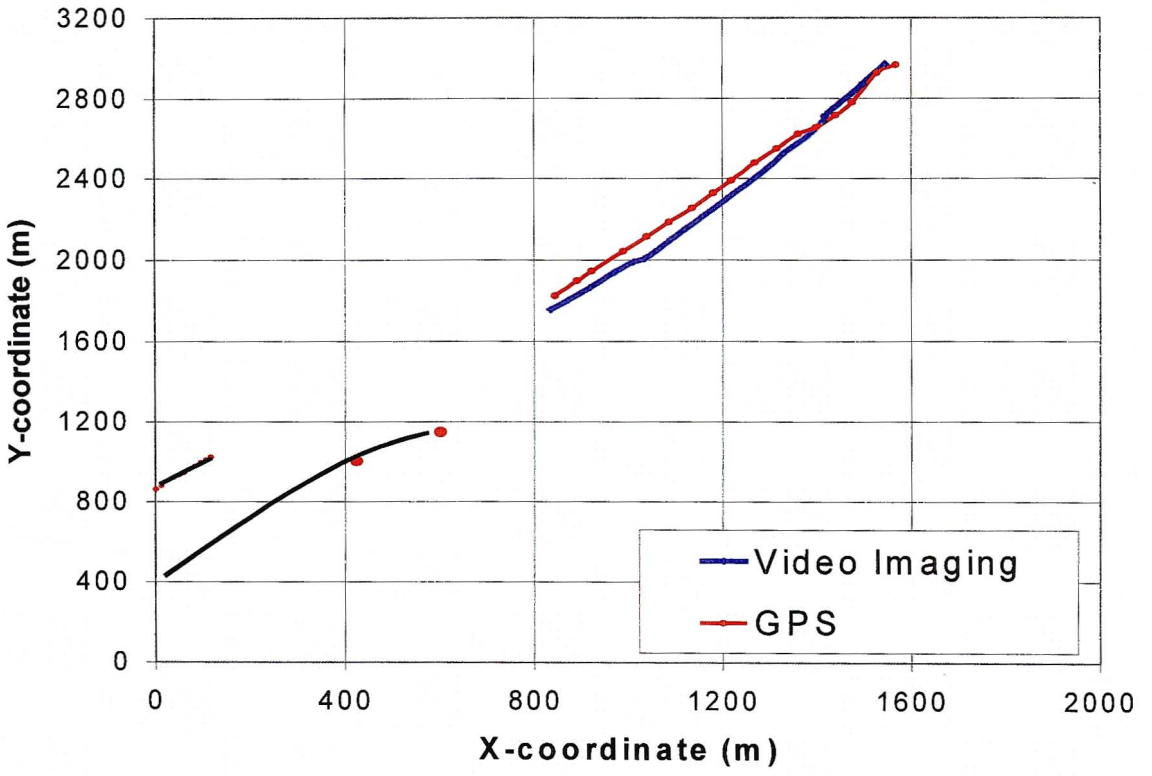

Figure 4-8: Ship Track plots comparing the GPS and video imaging coordinates for the Alam Senang

By studying the graphs shown above it is apparent that the GPS and video imaging track appear similar, however the points on both tracks are unsyncronised. Since there was no direct contact with the harbour pilots during the capture sequence, this type of problem was prone to occur.

The X and Y-ground coordinates of the GPS and video imaging tracks were compared, by first fitting a best fit polynomial through the video imaging ship track, and outputting an equation. This equation was used to calculate a new set of Y-coordinates for the video-imaging track by substituting the X-coordinate of the GPS data. The difference between new Y-coordinates of the video imaging and GPS tracks were found and the average absolute error in the Y-direction was calculated. This procedure was repeated for calculating errors in the X-direction. The results of this comparison are shown in Table 4-1. The overall average error calculated was 21 metres in the X-direction and 35 metres in the Y-direction. This is equivalent to 1 percent error at a range of four kilometres. The errors calculated and shown are possibly due to the following reasons:

1. The accuracy of the hand held GPS used. The GPS was only accurate to at best 5 metres, and depends on the strength of the signal. Weak and intermitant signals resulted in poor results.

2. The assumption that the camera roll (σ) angle is zero i.e. the horizon is located at a fixed y-pixel coordinate.
3. Digitisation errors since the rectification procedure used in this investigation ignored errors due to lens distortion

Table 4-1: Average absolute errors in both the X and Y directions between the GPS and Video imaging track data

NAME	ΔX	ΔY
(a) Bella Lontra	17	32
(b) Global Mombasa	11	16
(c) Alam Senang	35	57

The errors between the actual GPS and the video imaging coordinates were considered to be acceptable for the purposes of this application. Further more accurate validation exercises could be carried out, where more accurate GPS devices can be used e.g. a Differential GPS system (accurate within centimetres). By maintaining radio links with the pilot during the capture sequences and using smaller time-intervals between waypoints, the accuracy of results should also improve.

4.7. Summary

This chapter has summarised how the methodology presented in chapter 3 has evolved from capturing sequenced images of ships entering the Durban Harbour using portable to fixed video cameras. Typical results of the rectification process have been shown, with specific anomalies explained. Simultaneous GPS measurements have been shown to validate the ship tracking methodology to an acceptable accuracy for this application. In the next chapter software to automate the ship tracking process is described.

CHAPTER 5

SHIP TRACKING SOFTWARE

5.1. Introduction

The first stage of the automation process was to have a continuous feed of video to the University of Natal. This was made possible by a microwave link. The next stage was the development of software to automate the image capturing and processing. Initial testing and development of the prototype software was carried out using a high level-programming environment - Interactive Data Language (IDL). The final software was developed using Microsoft Visual C++, with a Graphical User Interface (GUI) designed to execute image capturing and processing. This GUI makes it possible for any user to make use of routines written in C++ without having to know how to call the routines with all their parameters, or without even having to know how to write program code. The GUI places all available options in the form of check boxes, text boxes, and menus on screen. This chapter will discuss key features of this GUI as well as explaining the algorithms developed for triggering capture sequences and feature tracking.

5.2. Background

The tracking software developed was based on object orientated programming techniques. A C++ library of driver software accompanied the "RIO ELLIPS" frame grabber board, was the primary reason for developing this software in Visual C++. The flowchart shown in Figure 5-1 summarises the basic procedure to be automated.

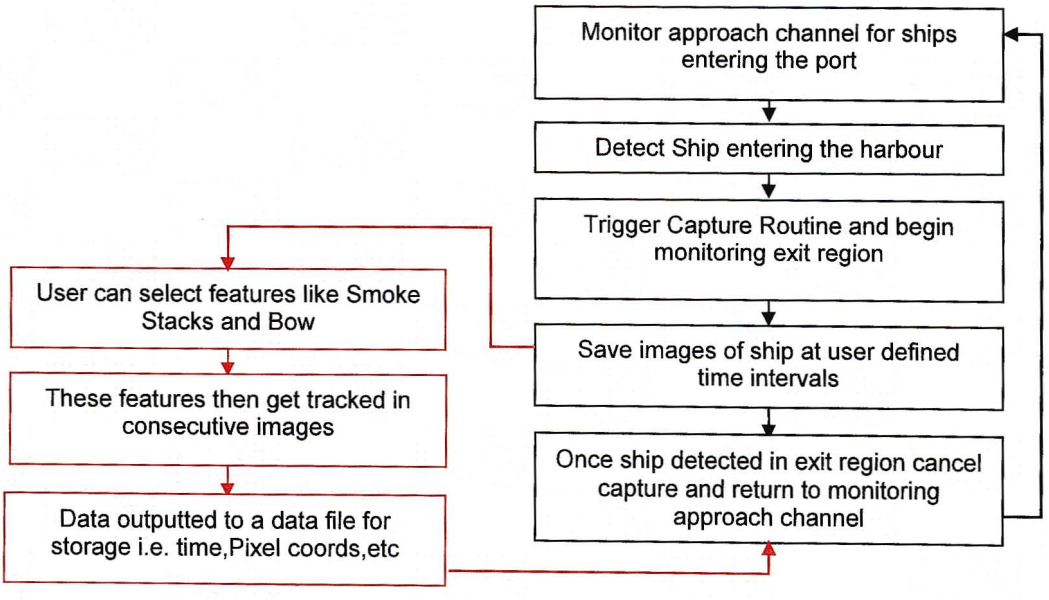

Figure 5-1: Flowchart summarising the basic automation procedure.

5.3. A Graphical User Interface for Ship Tracking

'Ship Tracking' was the name given to this software which when executed opens a window with a Graphical User Interface (GUI). This GUI's dimensions are designed to accommodate a video image of 768 pixels by 576 pixels. The user can change the window size by using the mouse pointer tool. When first started, the main window is blank but by selecting the **Grab Picture** button an image will be grabbed from the video source and displayed in this window. Figure 5-2 illustrates an image that has been grabbed from the video source and displayed on the GUI.

Figure 5-2: Graphical User Interface for ship tracking application developed.

A number of functions have been implemented in the ship tracking application and are accessed from the GUI's drop down menus. A description of these options is given in Table 5-1.

Table 5-1: Table illustrating features of the software accessed from the drop down menus

MENU ITEM	OPTIONS	DESCRIPTION
File	Exit	Shuts down and exits the GUI.
Edit	ImageProp	Allows the user to set the following image settings Brightness Contrast Saturation Hue Gain
View	Toolbar	Turns on the Tool Bar displaying all the buttons
	Status Bar	Turns on the Status Bar displaying status fields
Help	About Ship Track	Displays an about box with the name of the application as well as the designers name and version number
Options	File Format	Displays a box where various options are provided Format to save files Time Interval settings Region of Interest dimension settings
	Transformation	Contains reference point data required for the Rectification process
	TriggerParam	Contains parameters for setting the location of entry and exit regions for the trigger process
	Reset Default	Resets all parameters to their default settings

Note that the features available from the **Options** menu are used in conjunction with buttons located on the menu bar. These features when selected produce dialogue boxes with text fields for input parameters. These parameters are required as input for specific functions used in the Ship Tracking application. With these parameters correctly defined, subroutines associated with individual buttons can operate appropriately. Table 5-2 lists these buttons, their names, and a brief description of their functions.

Table 5-2: Illustration and description of buttons implemented in the Ship Tracking application.

BUTTONS	NAME	DESCRIPTION OF BUTTONS
	**About**	Displays window with information with respect to the application i.e. version number and developers name
	**Grab Picture**	Captures the most recent image from the video source and displays it on the GUI's main window.
	**Trigger**	Sets the application into a dormant trigger mode, which triggers a capture sequence when a ship is detected entering the port, and returns to this dormant trigger mode once the ship, has entered.
	**Manual**	This Manual button allows the user to manually capture images of a ship entering the harbour at pre-defined time intervals.
	**Streaming**	This Streaming button grabs continuous video footage from the video source and displays the images in the GUI's main window.
	**Crosshairs**	When selected allows the user to right (or/and) left click on the main window drawing a spanning cross/es with a pre-defined Region of Interest box size. If selected again the spanning crosshairs is turned off.
	**Tracking**	Initiates the tracking sequence and tracks the position of selected features over time.
	**Stop**	The stop button is used to stop any function that is operating i.e. Trigger, Manual, Streaming and Tracking functions

5.3.1. General Dialogue Boxes

An **Image Colour Properties** dialogue box show in Figure 5-3 displays the image colour properties. The user can vary these properties to improve the quality of the images being captured. In this dialogue box five fields are available for input. The five field parameters are: (1) Brightness, (2) Contrast, (3) Saturation, (4) Hue and (5) Gain. Note that input into any of these fields is required to be in integer format, with an automatic conversion to the conventional scales shown in the greyed fields alongside the input fields. Table 5-3 gives a list of default settings for these parameters as well as the minimum and maximum integer restrictions.

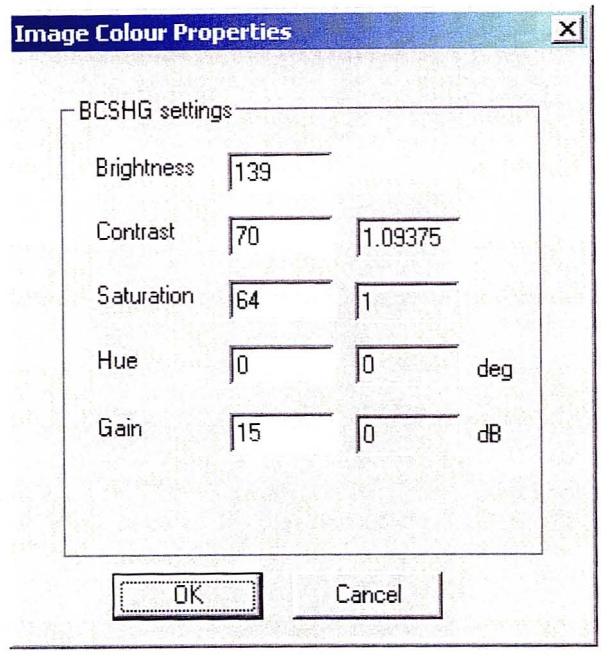

*Figure 5-3: Dialogue box for option **Image Colour properties**.*

*Table 5-3: List of default as well as minimum and maximum settings for input parameters for the **Image Colour properties** dialogue box.*

INPUT PARAMETERS	DEFAULT	MIN	MAX
Brightness	139	0 - dark	255- bright
Contrast	70 = 1.09 inverse	-128 = -2 inverse	127 = 1.99 inverse
Saturation	64 = 1 inverse	-128 = -2 inverse	127 = 1.99 inverse
Hue	0 = 0°	-128 = -180°	127 = 178.6°
Gain	15 = 0 dB	0 = -2.82 dB	63 = 9dB

The **Format and time setting** dialogue box is shown in Figure 5-4 and displays parameters associated with image capturing and saving. Other parameters include the initial region of interest (ROI) size used for feature tracking, as well as optional features related to specific buttons on the menu bar i.e. **Crosshairs** and **Manual** buttons. These buttons and their functions will be explained in greater detail in sub-section 5.3.3.

The first radio button shown in Figure 5-4 allows the user to choose the format at which images are saved. Two options are made available in this application. The user can either save images in the default JPEG format or in the uncompressed windows 24-bit bitmap format (BMP).

The next three radio buttons in the dialogue box offers the user options to accept or decline three specific features. These three features are:

1. The choice of saving images to hard disk during the streaming or tracking processes.
2. The choice of resetting the coordinates of the spanning cross every time the crosshairs button is switched off.
3. The choice of using a procedure which stops the manual capture button automatically once a ship is detected in the exit region.

The default setting for all three of these radio button options is 'No'. The next two options concern information about the time-intervals. The first field holds the value of the time-interval at which to capture and save images. The second field holds the value of the time-interval used in the Triggering process for monitoring consecutives images and triggering when a ship is detected entering the harbour. It is also the time interval used between consecutive images for tracking the movements of selected features e.g. smoke stacks, bow etc.

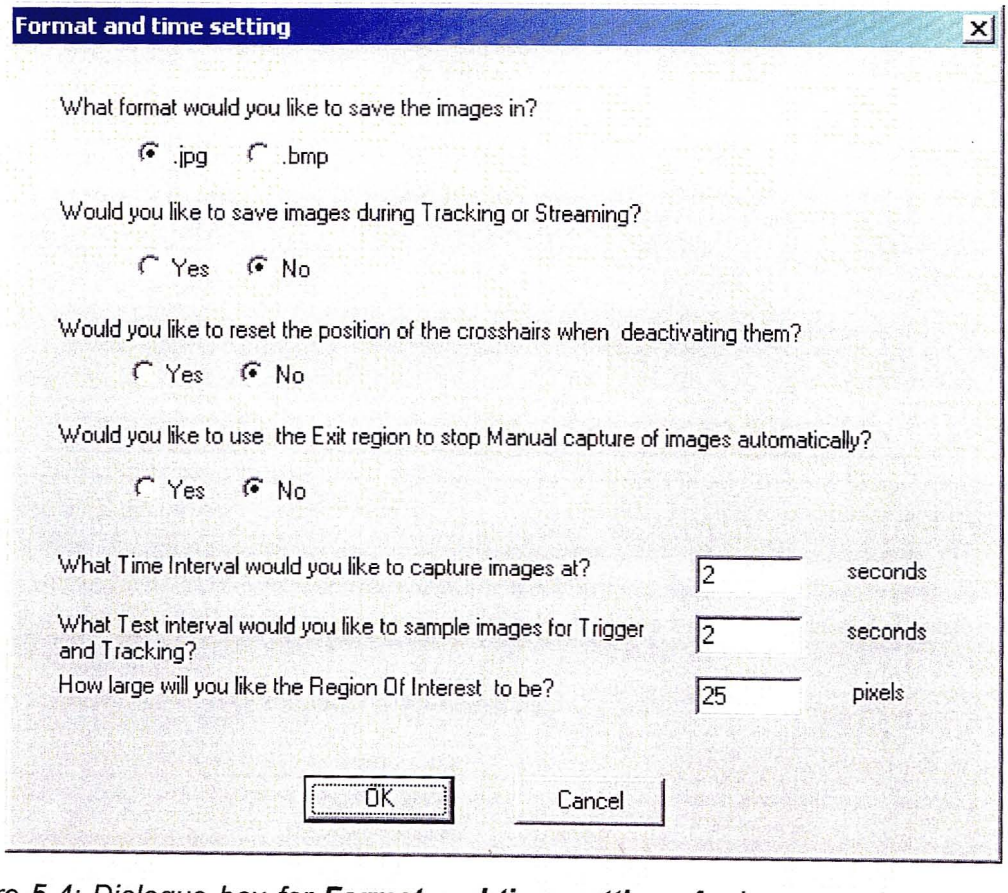

*Figure 5-4: Dialogue box for **Format and time settings** for image capture as well as feature tracking.*

The last field shown in this dialogue box allows the user to select an initial size of the ROI. This ROI is fixed as a square box with the desired point to be tracked located at its centre. The default setting for this input parameter is 25 pixels. Note that the larger the ROI the slower the processing time associated with tracking.

A **Default Settings** dialogue box sets all parameters back to the default or initial settings. By selecting the **Default Settings** from the **Options** menu, a window will appear confirming that the user wants to reset all parameters to their default settings. An example of this window is shown in Figure 5-5.

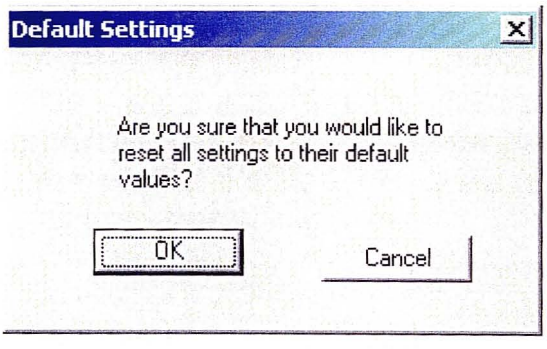

*Figure 5-5: **Default Settings** dialogue box, which resets parameters to their default values.*

An **About Box** dialogue box can be selected either using the **About** button from the menu bar or the **About Ship Track** option from the **Help** drop down menu. The information window shown in Figure 5-6 will appear with information about the name of the application, the date developed as well as the developers name and version number.

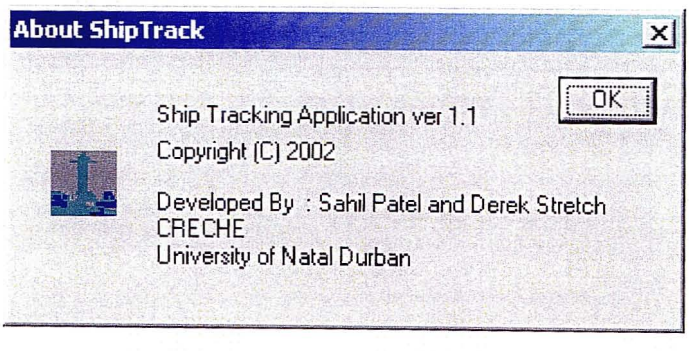

Figure 5-6: About box displaying information about the application and the developer's name.

5.3.2. Specific Dialogue Boxes

Rectification parameters are set using the **Transformation** dialogue box shown in Figure 5-7, which has twelve input fields that are required for the rectification procedure. The first six fields hold the X, Y and Z ground coordinates of the camera (X_C,Y_C,Z_C) and the reference point (X_P,Y_P,Z_P) which for this investigation was the South Pier White Lights. The coordinates given here are based on the LO31 Cape Datum coordinate system. The next three fields hold the image coordinates of the reference point (x_p,y_p) as well as the y-pixel coordinate of the horizon (y_H). All image coordinates are referenced to an origin at the top left hand corner of the image. The next field shown is the horizontal angle of view of the camera at a specific zoom setting (H_θ). This angle can be determined either in the field or in a laboratory and as explained in section 4.4.2 was determined in the field using two known GCP's within the angle of view of the camera. The last two fields represent the image dimensions (x_{TOT},y_{TOT}). These fields and their purposes are explained in Section 3.5.1. The values shown in Figure 5-7 are the default settings required for Durban.

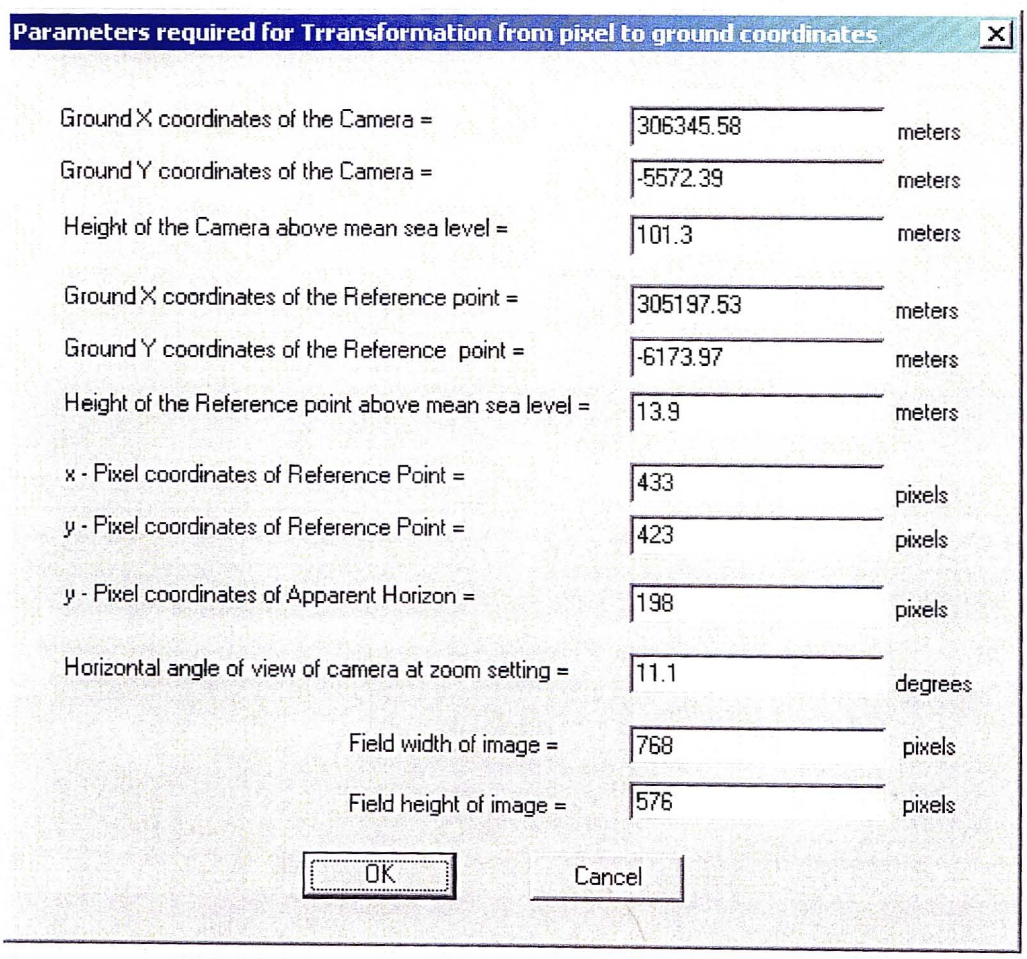

Figure 5-7: ***Transformation*** *dialogue box holding text fields required for the rectification procedure.*

The information in this dialogue box is linked directly to the tracking algorithm (that is activated by the **Tracking** button) where the transformation from image to ground coordinates is carried out as features are tracked.

The **Trigger parameters** dialogue box shown in Figure 5-8 consists of seven fields. The first six fields contain pixel coordinates whilst the last field is a dimensionless value. The first two fields allow the user to define the position and size of the entry region where monitoring will take place to trigger the capture sequence. The next four fields permit the user to define the position of the exit region, where monitoring begins only when a capture sequence has been initiated. Once the ship is detected in the exit region the capture sequence stops, and the application returns to monitoring the entry region. The values shown for these fields in Figure 5-8 are the default settings.

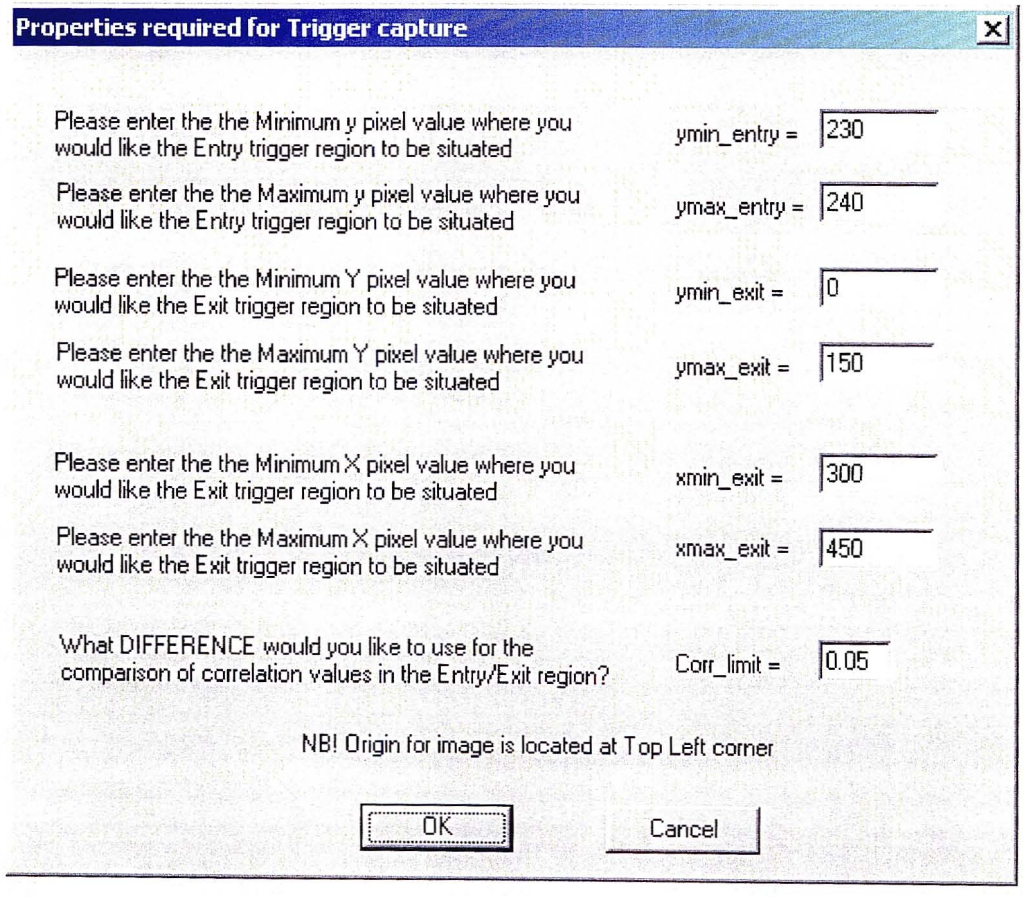

*Figure 5-8: **Trigger Capture** dialogue box used for setting and defining the entry and exit regions used for the trigger capture routine.*

The last field shown is the correlation leeway allowed in the trigger region with its default set at 0.05. This implies that if two consecutive images, when compared to a template image, have a cross correlation coefficient difference of more than the default

value than the trigger is activated. By changing this value the affects of poor visibility and quality of picture can be accounted for.

5.3.3. Menu Bar Buttons

The **Trigger** button ■ is used to place the application into a dormant trigger mode. During this mode a specific entry region is monitored for ships at pre-defined time-intervals. The default time-interval is 2 seconds and is set in the **Format and Time setting** dialogue box.

When a ship is detected in the entry region the capture sequence is triggered and images are captured and stored to hard disk. Figure 5-9 shows this entry region as a line of sixteen (16) white boxes with a red box shown on the right hand edge of the main window. Changing the first two fields of the parameters for **Trigger Capture** dialogue box can alter the size and location of these boxes. When a ship passes through this region the capture sequence will be triggered. Images of the ship's entry are then captured and stored to hard disk at user-defined time-intervals. The format at which images are stored as well as the time interval between consecutive images is specified in the **Format and Time setting** dialogue box.

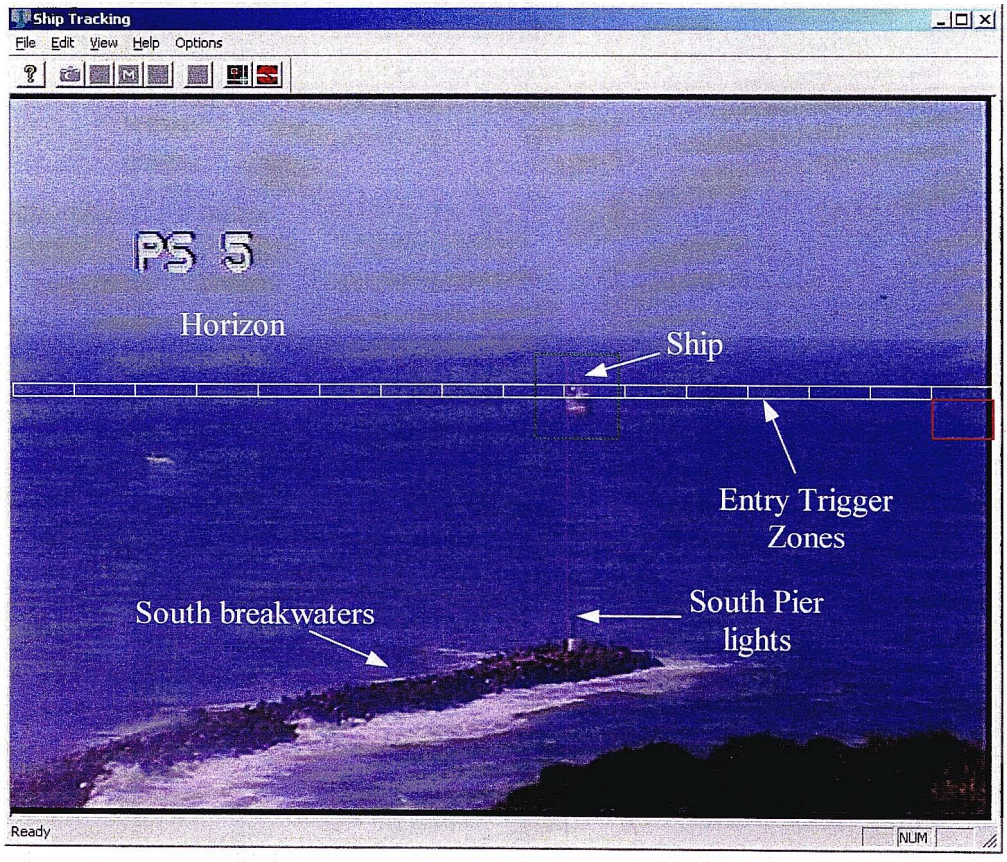

Figure 5-9: Entry region set at default settings with a ship passing through and triggering capture.

Once the capture sequence is triggered, monitoring of the exit region begins. Figure 5-10 shows a ship in the exit region. The exit region with dimensions as specified in the **Trigger Capture** dialogue box is drawn on the main window (illustrated by a red box). When the ship is detected in the exit region the capture sequence comes to an end and the software returns to monitoring the entry region for the next incoming ship.

Figure 5-10: Exit region set at default settings with a ship approaching the entrance channel.

The **Streaming** button S1 grabs and displays images continuously on the GUI window in real time (full motion video at 25 frames per second). The user is given the option of saving these images to hard disk (at a reduced frame rate) when using the streaming button. This option is available from the **Format and Time setting** dialogue box.

The **Tracking** button T allows the user to track features within the viewing window. The default setting for this feature is set at 2 seconds. The user has the option of saving images during the tracking routine in either a BMP or JPEG format. The user can also choose to vary the size of the Region Of Interest (ROI) box used for tracking. The ROI used in this application is square and set to a default value of 25 pixels for

tracking. The default values may be changed in the **Format and Time setting** dialogue box shown in Figure 5-4.

The features used in ship tracking were the smoke stacks and the bow of the vessels. In order to track these features a drawing tool is required to select the chosen feature. By selecting the **Crosshairs** button, the user is able to left or right click on the main window where a spanning cross with a ROI will be drawn. These lines will only be visible when the next image is grabbed and updated in the window. It is best to use the **Crosshairs** button during normal streaming capture as the GUI window is continuously updated with the most recent image. Once the user has selected the feature or features to track, the user must then stop the Streaming capture process and select the **Tracking** button, to initiate feature tracking. For accurate tracking results these steps must be carried out before the object being tracked has moved out of the ROI. An example of these spanning crosses is shown in Figure 5-11. The red spanning cross drawn is a result of using the left mouse button whilst the white spanning cross is a result of using the right.

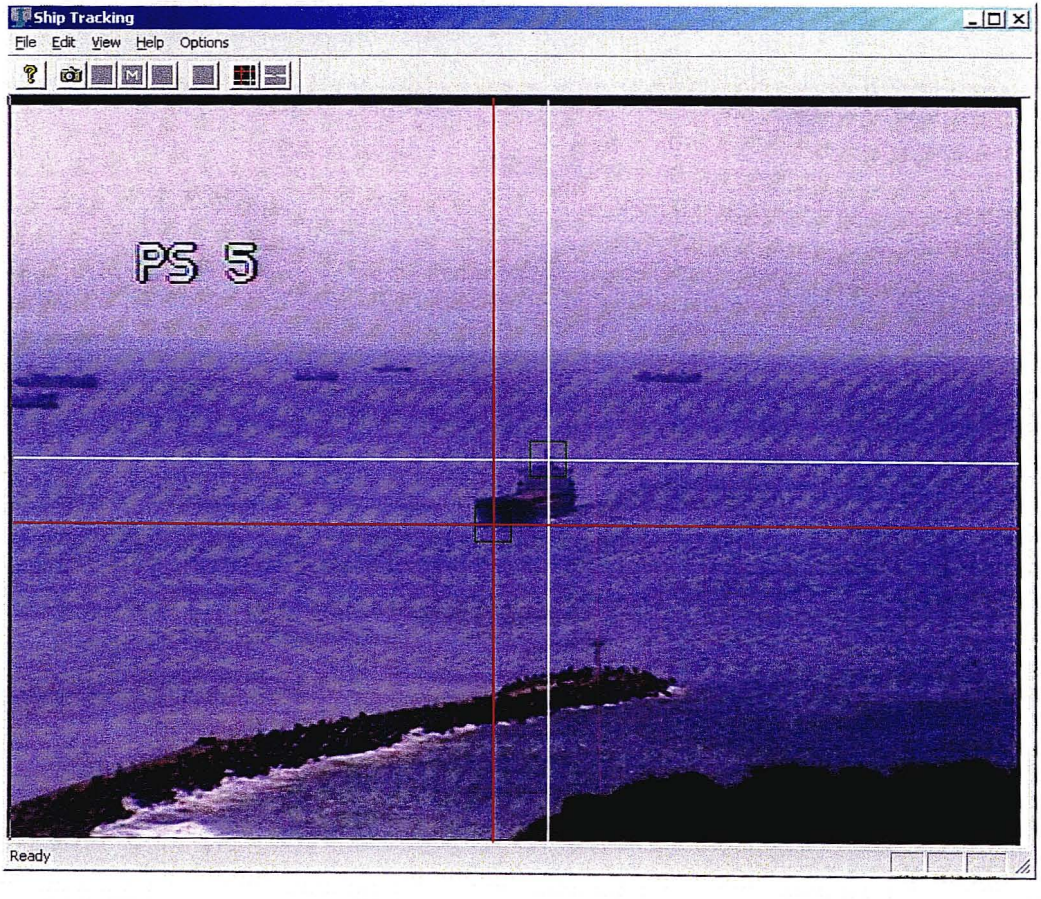

Figure 5-11: Illustration of a ship entering the harbour with the smoke stacks (white cross) and the bow (red cross) of the vessel selected for tracking.

Note that the **Tracking** button will be greyed out until the user clicks on the main window, with the **Crosshairs** button turned on. Once activated the tracking routine will track one or two objects selected in the window, depending on whether the user has used both the left and right hand mouse buttons. Features will continuously be tracked until the user selects the Stop button. Note that this feature is not linked with the exit trigger routine.

Note that the **Crosshairs** button when turned off will store in memory the present location of the spanning cross (or crosses). The user may decide to reset the spanning crosses and this is achieved by selecting the option available from the **Format and Time setting** dialogue box.

Manual Button

The **Manual** button  allows the user to initiate a capture sequence manually. This button is generally used when a ship is entering the harbour and the trigger mode is not in operation. The user manually triggers the capture sequence and images are grabbed and stored on the PC's hard disk. The time interval at which images are captured and stored can be changed in the **Format and Time setting** dialogue box in Figure 5-4.
The time associated with a general entry manoeuvre is about twenty minutes. If the user does not want to wait to manually stop the capture sequence, it is possible to use the automated trigger option to stop the capture sequence. This option is available from the **Format and Time setting** dialogue box shown in Figure 5-4.

5.4. General algorithms

The programming code for the general algorithms used for this software can be found in Appendix G.

5.4.1. Saving Images

Visual C++ can be a difficult programming language to work with, since it is sensitive to memory allocation. It was found that if memory is not deallocated correctly, the system could become unstable resulting in the PC crashing. This was the primary problem associated with the development of an algorithm to save images. These images are grabbed from the frame grabber board, and displayed on the main window of the GUI. In order to save an image displayed on the main window to the hard disk the following steps are required (summarised in psuedo code):

```
1     lock memory for Direct Memory Access (DMA) transfer
2     grab image from board and saves it to ImageBufferHandle
3     save image in ImageBufferHandle to ##.bmp or ##.jpg in
      directory
4     update latest image on GUI
5     unlock memory for DMA transfer
```

The actual process of saving the 'ImageBufferHandle' to a file is simplified by the use of the MST Image C++ Library (Musatenko, 2000). This library is used to convert the image stored in the 'ImageBufferHandle' to a memory stream, which is written in either windows BMP or JPEG format. The saving routines offered by this library were efficient, and easy to use. A normal 24bit colour image (786 by 576) could be saved to hard disk using BMP format in 32 milliseconds and using JPEG format in 280 milliseconds (system dependant). This is implies that 31 BMP images or 3 JPEG images can be saved per second. This large time difference is expected since the time spent applying compression algorithms to a JPEG file is higher then the time spent transferring a BMP files to disk storage. This is the case although BMP files are three times the size of JPEG files.

Images are saved to folders created by the application on the local hard disk. If the local hard disk is known as the C:\ drive then the following folders will be created in this format *C:\yyyy\mon\dd* where:

- *yyyy* is the year e.g. 2001
- *mon* is the month e.g. Nov
- *dd* is the day e.g. 07

Each image grabbed is assigned a timestamp which is the name given to the file when saved to the above directories. These file names are in the following format *hhmmss.ext* where:

- *hh* is the hour e.g. 00 till 24
- *mm* is the minutes e.g. 00 to 60
- *ss* is the seconds e.g. 00 to 60
- *ext* is the format e.g. BMP or JPEG

The programming code that was developed for the subroutines described in this section can be found in Appendix G.1.

5.4.2. Time-delay algorithm

This saving algorithm is called continuously at user defined time intervals to store images regularly to hard disk. A simple while loop statement is used for this time delay sub-routine. Once the time delay is complete a new image is grabbed and saved to disk.

A problem associated with loop statements, especially with respect to GUI's is that once they are run, they will continue until completion. During this time the GUI is frozen and inaccessible. This means that the user is forced to wait while the operation completes. Once the time delay routine is run the user may not be able to stop the routine and images will be saved indefinitely. This routine will end only when the while statement condition is no longer satisfied. A better solution was desired and was achieved by using multi-threaded software. Multi-threading provides a solution to keeping the GUI active while a computation is being performed. Threads were written for four routines in the Ship Application GUI, so that their computations could be intercepted using the **Stop** button  . These four threads run independently of each other, with only one thread being active at any given time. Threads were written for the following buttons: (1) **Trigger**, (2) **Manual**, (3) **Streaming**, (4) **Tracking**.

5.5. Trigger algorithms

The Trigger capture subroutine is explained by the flowchart shown in Figure 5-12.

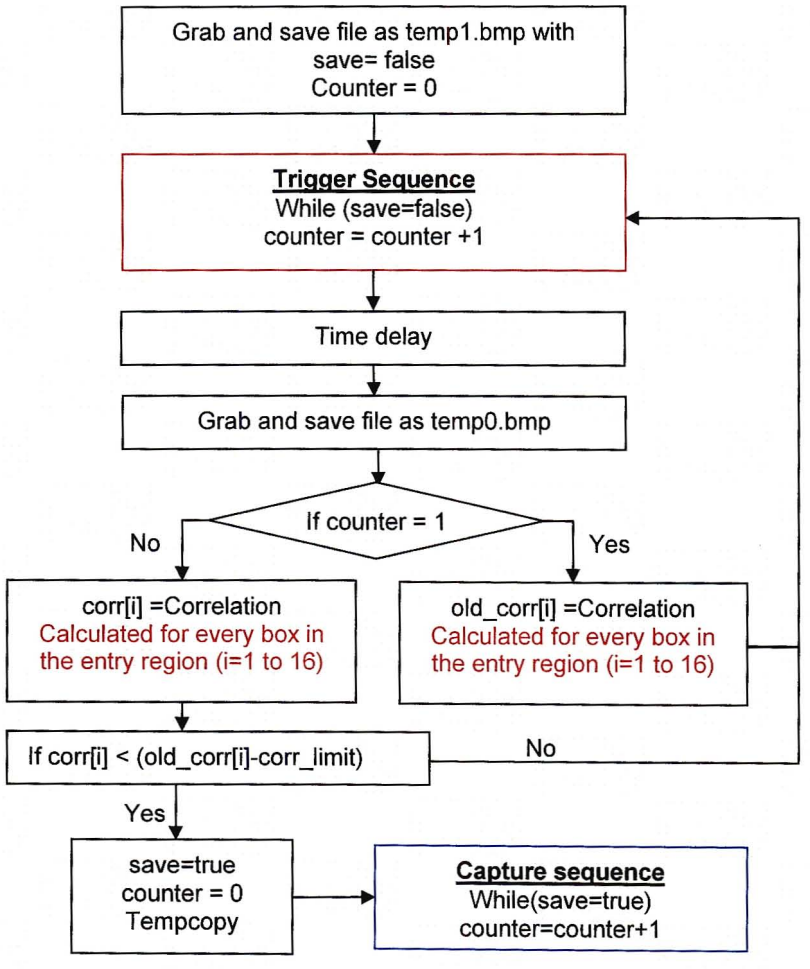

Figure 5-12: Flowchart of algorithm used for triggering the start of a capture sequence

This exit region subroutine is explained by the flowchart shown in Figure 5-13. The cross-correlation algorithm used for the trigger entry and exit routines can be found in Appendix G.2.

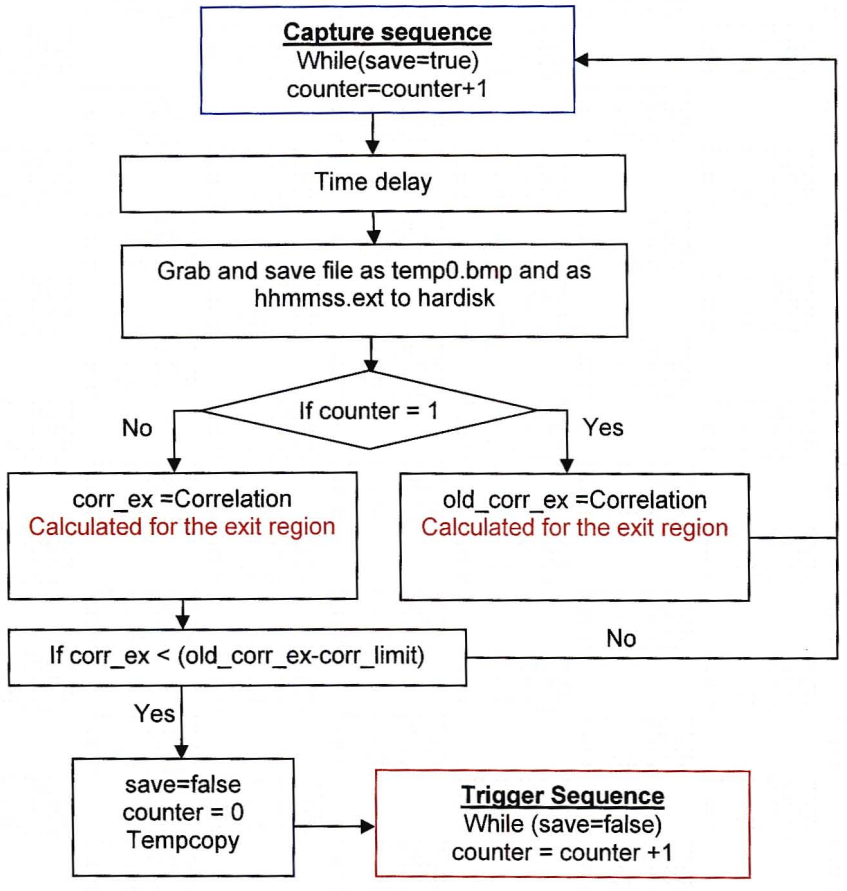

Figure 5-13: Flowchart of algorithm used for triggering the cessation of the capture sequence

5.6. Tracking algorithm

In order to automatically track a specified feature from one image to the next, an algorithm based on the cross-correlation (or convolution) of the images was used. This is a standard image processing methodology for feature tracking (Martin & Crowley, 1995 and see section 2.13). The method is described using a simple illustrative example in the following section.

Cross-correlation coefficients between images are usually computed between two data sets comprising scalar values e.g. a grey scale value for each pixel. However, note that each pixel in a full colour image comprises information for the three primary colour channels - red, green and blue (RGB). Every pixel in an image thus has a specific colour characterised by three scalar RGB values. In this investigation cross correlations were determined using the full colour information by considering each pixel as a 3-component vector valued quantity. The cross correlation formulation is derived in Appendix A, and the programming code implementing the algorithm is given in Appendix G.2. Two methods of implementing object tracking were experimented with.

Initially correlations between images were computed using Fourier transforms while later they were computed by direct convolution.

Two-dimensional Fast Fourier Transforms (FFT) are commonly used in the field of image processing. To obtain correlations between two images, they are first transformed using an FFT. By multiplying one transform by the other, and inverting the product, an array of cross correlation coefficients can be formed. The position of the maximum cross correlation coefficient between consecutive images can then be used to locate the new position of the object that is being tracked.
Standard FFT libraries (e.g. Press et al, 1992) are only efficient when using data sets of size 2^n (so called radix 2 algorithms). Unfortunately this limits flexibility, with respect to specifying the size of the region of interest (ROI see below). Another limitation to FFT's is that they assume periodicity in the data, which is not true for the actual data in this case, although using zero padding around the data set can cater for these end effects. The lack of flexibility in FFT methods suggested that the case of direct convolution could be a more attractive alternative in the present case. While both methods produced similar results, only the direct convolution approach was focused on.

5.6.1. Illustration of the method

Let U and V be images consisting of pixel data each comprising three scalar (RGB) values: $U = \{U_R U_G U_B\}$ and $V = \{V_R V_G V_B\}$. Figure 5-14 illustrates a 11x9 pixel image (U) at time *t*. Suppose a ship is located at the beginning of an entry manoeuvre in image *U* with its "bow" located at cell 21, with coordinates (x_0, y_0). A region of interest (ROI) is selected (say 5x5 pixels) and centred on it as shown by the shaded border. This ROI defines a 'template' of the target object that is to be tracked in the next image of the sequence.

1	10	19	28	37	46	55	64	73	82	91
2	11	20	29	38	47	56	65	74	83	92
3	12	21	30	39	48	57	66	75	84	93
4	13	22	31	40	49	58	67	76	85	94
5	14	23	32	41	50	59	68	77	86	95
6	15	24	33	42	51	60	69	78	87	96
7	16	25	34	43	52	61	70	79	88	97
8	17	26	35	44	53	62	71	80	89	98
9	18	27	36	45	54	63	72	81	90	99

y_0

x_0

Figure 5-14: An example of an image (U) with a region of interest located around the point of interest

Continuing to the next image in the sequence, image *V* at time t+Δt *(*for small Δt*)*, the ship would not have moved more than a few pixels. For this example assume that the ship has moved from cell 21 (x_0, y_0) in image *U* to cell 60 (x_f, y_f) in Image *V*. This is illustrated in Figure 5-15.

1	10	19	28	37	46	55	64	73	82	91
2	11	20	29	38	47	56	65	74	83	92
3	12	21	30	39	48	57	66	75	84	93
4	13	22	31	40	49	58	67	76	85	94
5	14	23	32	41	50	59	68	77	86	95
6	15	24	33	42	51	60	69	78	87	96
7	16	25	34	43	52	61	70	79	88	97
8	17	26	35	44	53	62	71	80	89	98
9	18	27	36	45	54	63	72	81	90	99

y_0

y_f

x_0 x_f

Figure 5-15: An example of an image (V) with the original location of an object and its location after time Δt.

Starting at (x_0, y_0) and shifting the ROI over each cell in image *V*, cross-correlation coefficients are determined between the initial template region and the new image. The idea is to search for the displacement that will maximise the cross-correlation coefficient. The cross-correlation values for all displacements on the grid around cell 21 (x_0, y_0) can be determined (i.e. every point in the image) but this method would be time consuming. A systematic search strategy was therefore used to decrease the number

of cross-correlation computations and to converge to the point of maximum correlation quickly and efficiently.

The strategy involved first defining a search strategy area (SSA) either larger or smaller than the original ROI (5x5). For this example let this SSA region be smaller then the original ROI i.e. 3x3 pixel array. This array was centred over the initial object position (x_0, y_0) in image *V*. This set-up is shown in Figure 5-16.

1	10	19	28	37	46	55	64	73	82	91
2	11	20	29	38	47	56	65	74	83	92
3	12	21	30	39	48	57	66	75	84	93 y_0
4	13	22	31	40	49	58	67	76	85	94 y_1
5	14	23	32	41	50	59	68	77	86	95
6	15	24	33	42	51	60	69	78	87	96
7	16	25	34	43	52	61	70	79	88	97
8	17	26	35	44	53	62	71	80	89	98
9	18	27	36	45	54	63	72	81	90	99
		x_0	x_1							

Figure 5-16: An example of an image (V) with the original location of an object and its initial search strategy box region.

The idea of this strategy is to displace the initial 5x5 array and position it over all cells located within the SSA. Cross correlation coefficients (CCC) were calculated at each of these positions. Initially a set of nine (9) cross correlation coefficients were calculated, which included the zero displacement cross correlation at (x_0, y_0). The largest CCC was then selected from this set, and a new SSA is then located around the coordinates of this maximum. The process is iterated until a local maximum coincides with the CCC value of the most recently centred point.

For the example shown in Figure 5-16, suppose that cell 31 (x_1, y_1) has the largest CCC from all nine CCC's calculated initially. A new SSA is now located around this point and the process of calculating CCC's is repeated. The speed of the algorithm is increased by not recalculating the CCC for cells that were already calculated in the previous iterations. For example for the second iteration CCC's for cells 21,22,30 and 31 need not be recalculated, with CCC's determined only for cells 23,32,,39,40 and 41. A new set of nine cross correlations will result (5 new and 4 old), with the largest CCC selected as the position for the next iteration. This iterative procedure essentially

guesses the approximate direction of motion of the ship by using the local maximum CCC values as a guide.

Figure 5-17 illustrates this search strategy and how it moves from the initial position at (x_0, y_0) to the final maximum CCC value at (x_f, y_f). By using the search strategy, calculation of only twenty-five CCC's were required to locate the overall maximum, as compared to ninety-nine CCC's had there been no such strategy.

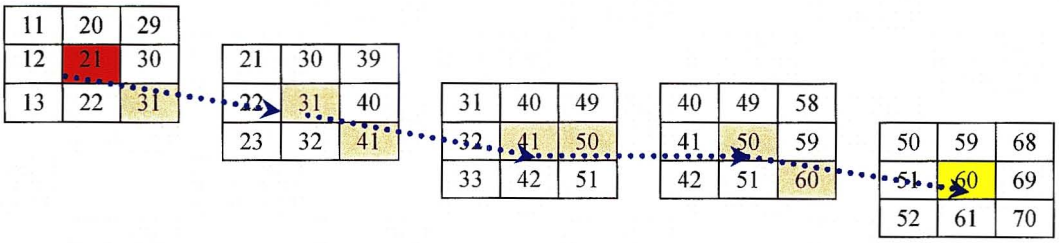

Figure 5-17: An example of an image (V) with the original location of an object at time *t and its location at t +Δt.*

5.6.2. Variable Region Of Interest (ROI) size

Over time the imaged ship increases its apparent size due to perspective effects. An enlargement of the Region Of Interest (ROI) with time was used. The increase in the ROI size was made to be inversely proportional to the distance between the object being tracked and the camera position. This means that the target object within the ROI maintains its size ratio with respect to the ROI size. By allowing the ROI to increase in this manner the results of the tracking procedure become more accurate (see section 5.7.3)

5.7. Optimum settings for ship tracking

An analysis was carried out with the aim of determining the optimum settings for tracking ships into the Durban harbour. The variables that affect the speed and the results of the tracking algorithm most are:

- The time-interval between images
- Initial size of ROI
- The ROI's increase in size over time associated with the relative increase in size of the object
- The size of the SSA used to determine the maximum CCC

The next sections will present these results. Note that for this analysis, the position of the bow of the ship at the water surface was the point used for tracking purposes as

shown in Plate 5-1 (a to f), which illustrates a time-lapse sequence frames of a ship entering the harbour.

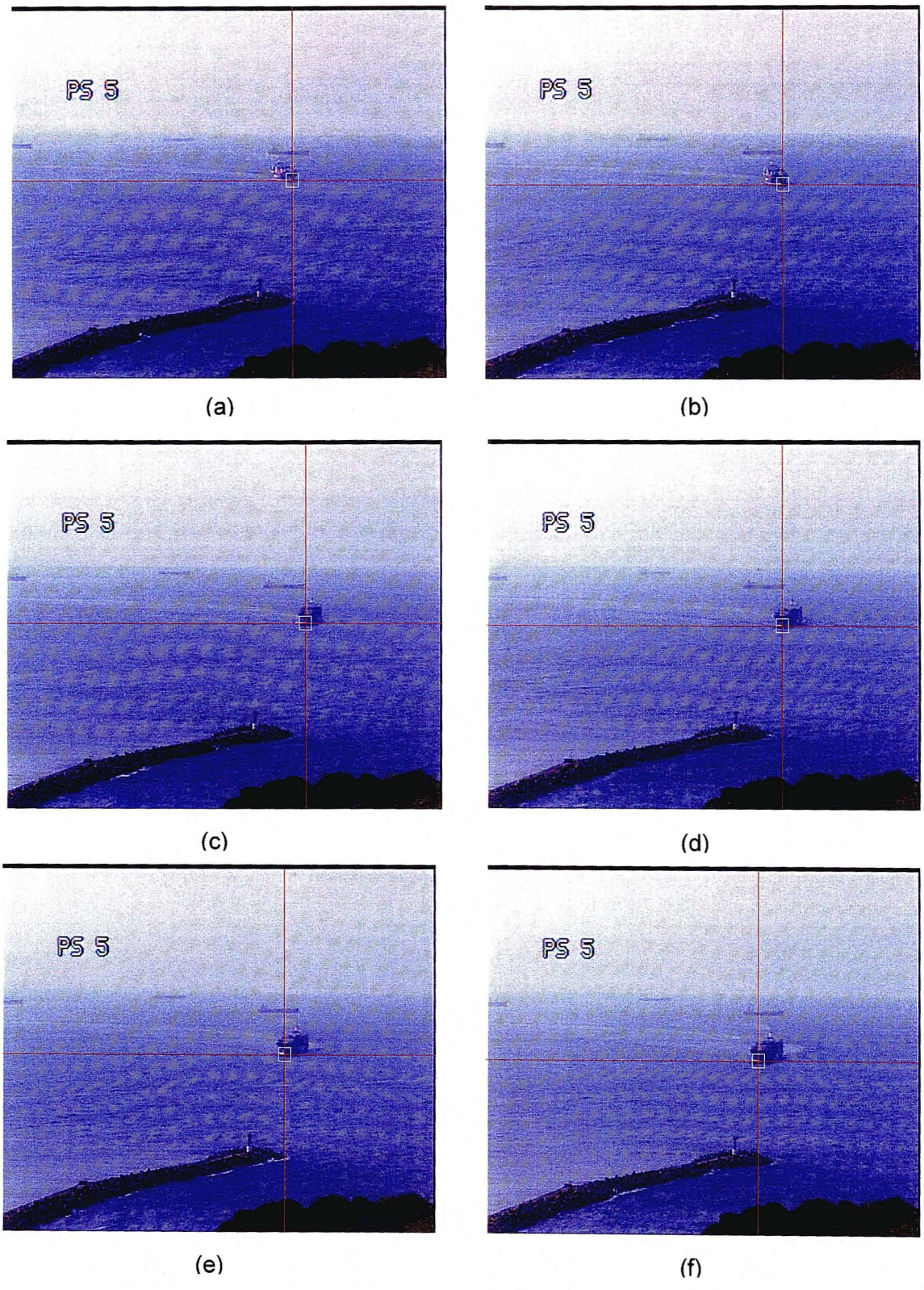

Plate 5-1: (a) to (f) A time lapsed image sequence of a ship entering the Durban Harbour at 40-second time intervals. The crosshairs show the result of the feature-tracking algorithm

The time interval between these frames is 40 seconds. Spanning crosses along with ROI's are shown, which were used for the tracking of the bow of the ship over time. A benchmark set of ship positions data was created by manually digitising the ship position in each image. This was then used to assess the performance of the automated tracking algorithm using different user supplied parameters.

5.7.1. Time interval

By having a very large time interval between images, the results of the feature tracking was found to become inaccurate, since the template image did not compare well to the next image in the time sequence. Over this time-interval the imaged ship increases its apparent size due to perspective effects, and may change its orientation. However, having very small time intervals between images can also result in poor feature tracking. Some of the results are shown in Figure 5-18 (a) to (d), where a comparison of actual and automated ship track data for varying time-intervals is shown. The blue curve shown in the plots is the actual ship track (from manual digitisation). The red curve shown in the plots were determined by using the tracking software to automatically extract the pixel coordinates. The absolute difference in errors between the X- and Y- ground coordinates for the two tracks were calculated. The inserts shown on the top left hand corner of each plot represents the mean (μ) and standard deviation (σ) values for these errors in the X and Y directions. From these statistics it can be seen that small (2 seconds) and large (10 seconds) time-intervals resulted in poorer tracking results. The optimum time interval was around 5 seconds, as shown in Figure 5-18 (b). Note that for this analysis the size of the initial ROI as well as the SSA were kept constant.

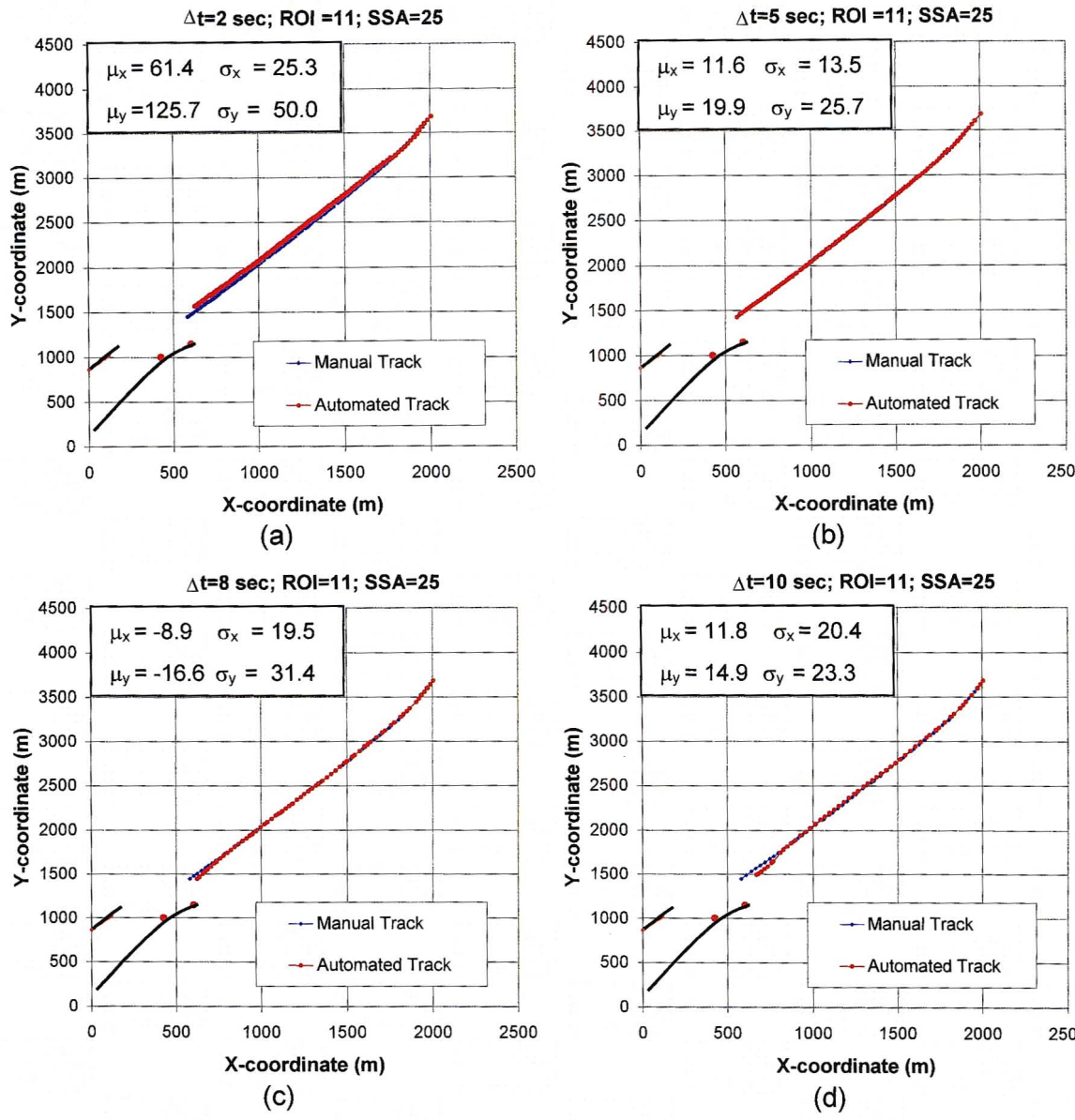

Figure 5-18: Comparison of actual and automated ship track data for varying time-intervals for ROI=11x11and SSA=25x25. The inserts show the mean and standard deviations of the errors between the manual and automated methods in the X and Y directions.

5.7.2. Initial Region Of Interest (ROI)

The choice of the initial ROI used depends on the size of the object being tracked. It was expected that a larger initial ROI would result in greater accuracy. However having an unnecessarily large ROI may include objects other than the target object within the ROI, which results in poorer tracking. Another disadvantage of having a large ROI is that the computation takes longer, which makes real time tracking more difficult to achieve. The plots shown in Figure 5-19 (a) to (d) illustrate the analysis carried out at 5-second intervals for a varying initial ROI.

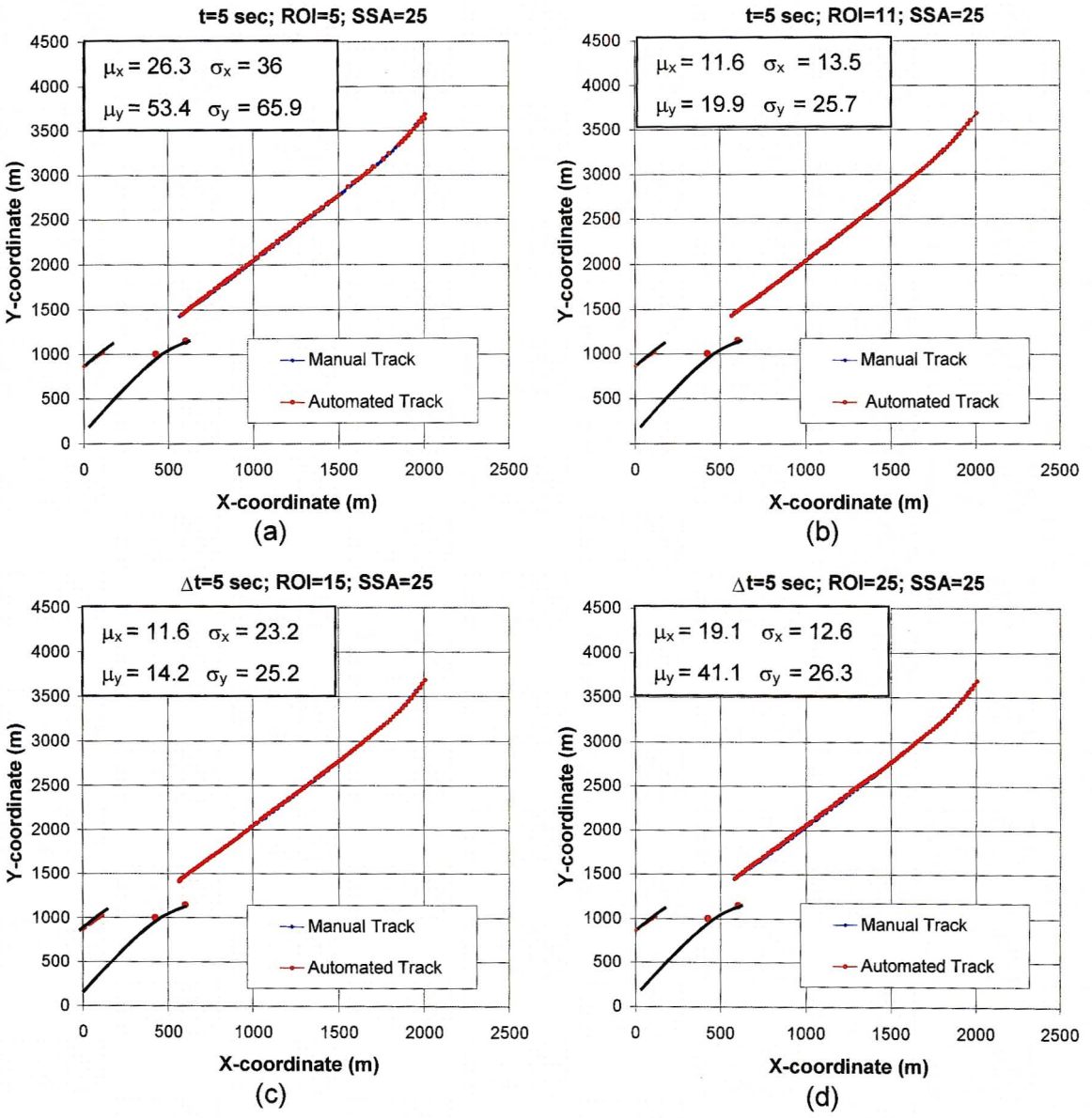

Figure 5-19: Comparison of manual and automated ship track data for varying initial Region of Interest (ROI) for Δt = 5sec and SSA=25x25. The inserts show the mean and standard deviations of the errors between the manual and automated methods in the X and Y directions.

From the mean and standard deviations of the errors one can deduce that for very small or very large initial ROI, the accuracy of the tracking results decreases. For this example the optimum size of the initial ROI at a distance of four kilometres from the Signal Station was a (11 x 11) -pixel ROI.

5.7.3. Effects of Region Of Interest (ROI) inflation

The effect of inflating the size of the ROI as the ship got closer to the viewpoint is illustrated in Figure 5-20 (a) and (b). Figure 5-20 (a) illustrates the results of the tracking algorithm where the ROI was not allowed to inflate as the ship came closer. The results shown in Figure 5-20 (b) are for an inflating ROI size. From the mean and standard deviations shown, it is clear that by allowing this gradual increase in ROI size there is an overall improvement in tracking accuracy in both the X and Y directions. A 24% and 33% improvement for the mean values in the X and Y direction respectively was obtained.

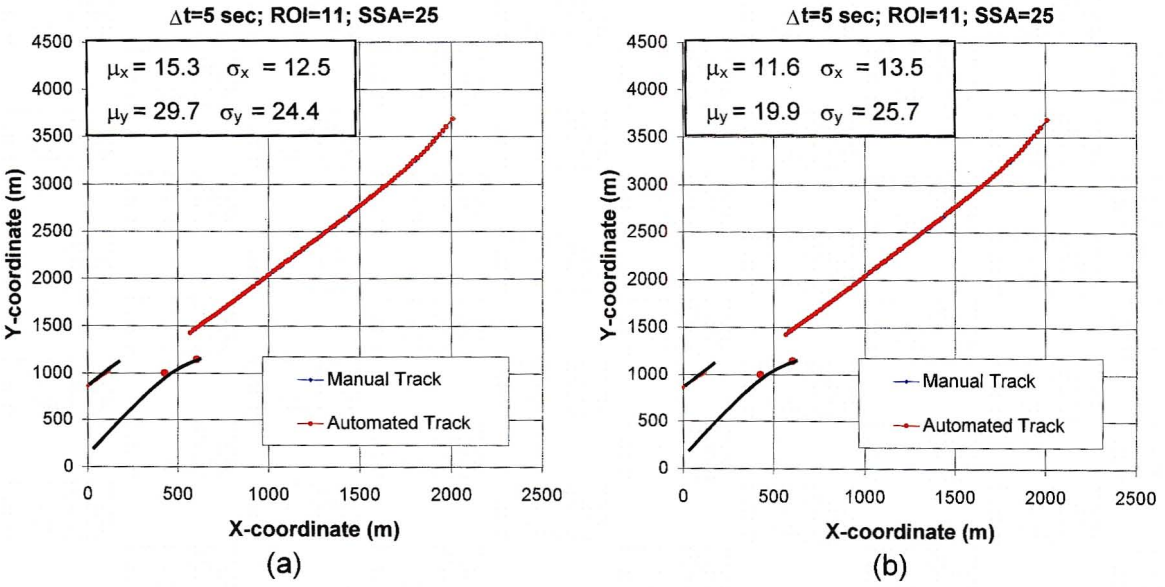

Figure 5-20: Comparison of tracking results between (a) fixed ROI (b) gradually increasing ROI for Δ t = 5sec; ROI = 11x11; SSA=25x25. The inserts show the mean and standard deviations of the errors between the manual and automated methods in the X and Y directions.

5.7.4. Effect of Search Strategy Area (SSA)

The size of the search area used influences the time spent searching for the point of maximum correlation. If the search area was initially too large then unnecessary CCC calculations would be carried out thus wasting time. For small time intervals the point of maximum correlation will be in close proximity to the previous maximum therefore the search area can also be small since the object would have only moved a few pixels. Tests were carried out to determine the optimum size of the search area. Figure 5-21 (a to d) illustrates the results.

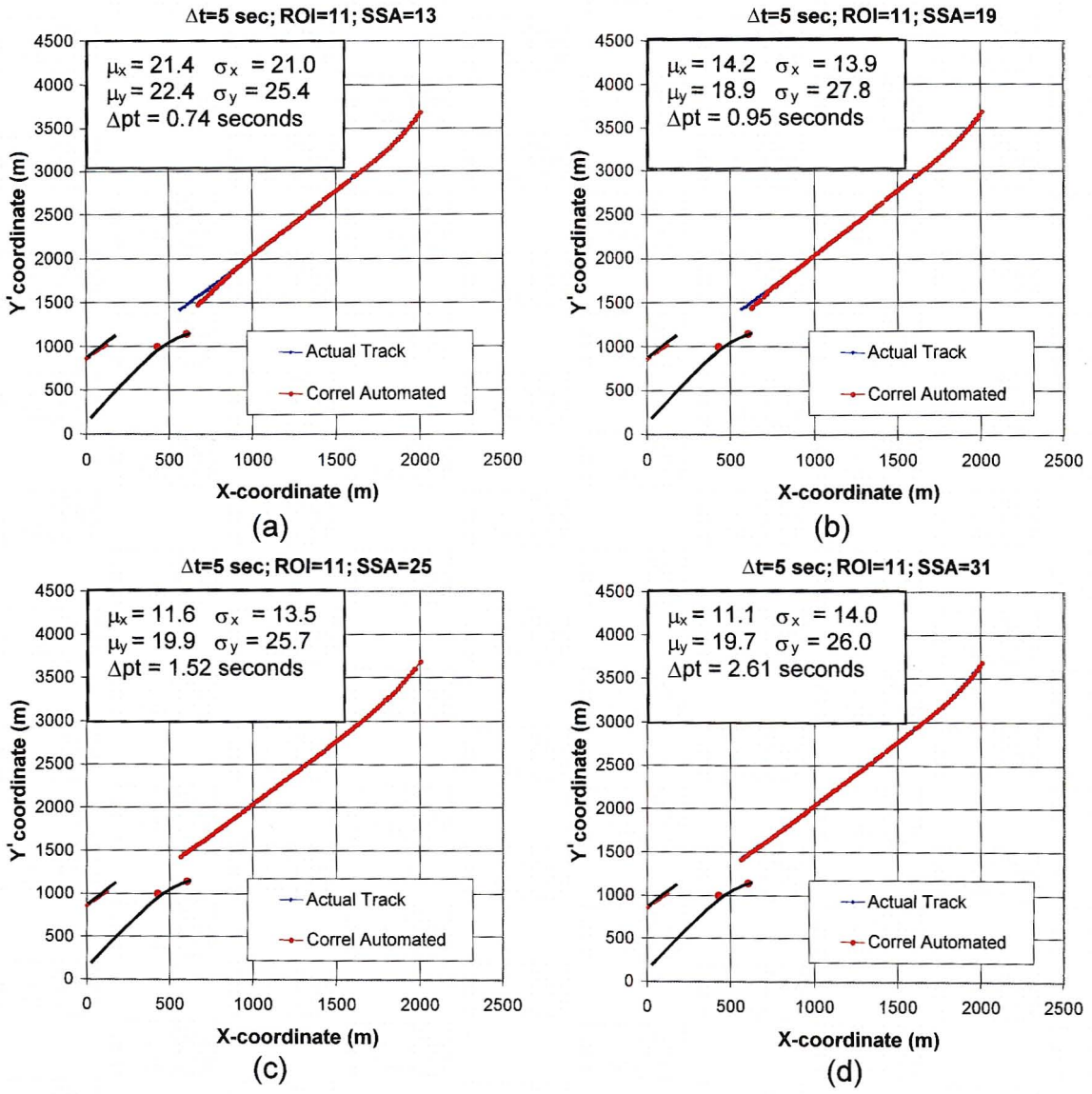

Figure 5-21: Comparison of actual and automated ship track data for a varying search strategy area (SSA) for Δt = 5sec and ROI=11x11. The inserts show the mean and standard deviations of the errors between the manual and automated methods in the X and Y directions. Also shown is the average processing time (Δpt) taken to determine the point of maximum correlation per image.

From the mean error values shown by increasing the SSA from a 13 to 31 pixels, a 12% and 47% improvement is recorded in the X- and Y-directions respectively. The mean error values shown for the 25x25 -pixel SSA appear to be similar to the values shown for the 31x31 -pixel SSA. The larger SSA takes approximately one extra second in processing time for no improvement in accuracy. The optimum results were produced when a 25x25 -pixel search strategy area was used. Figure 5-22 illustrates the processing time spent per image for an increasing search strategy area.

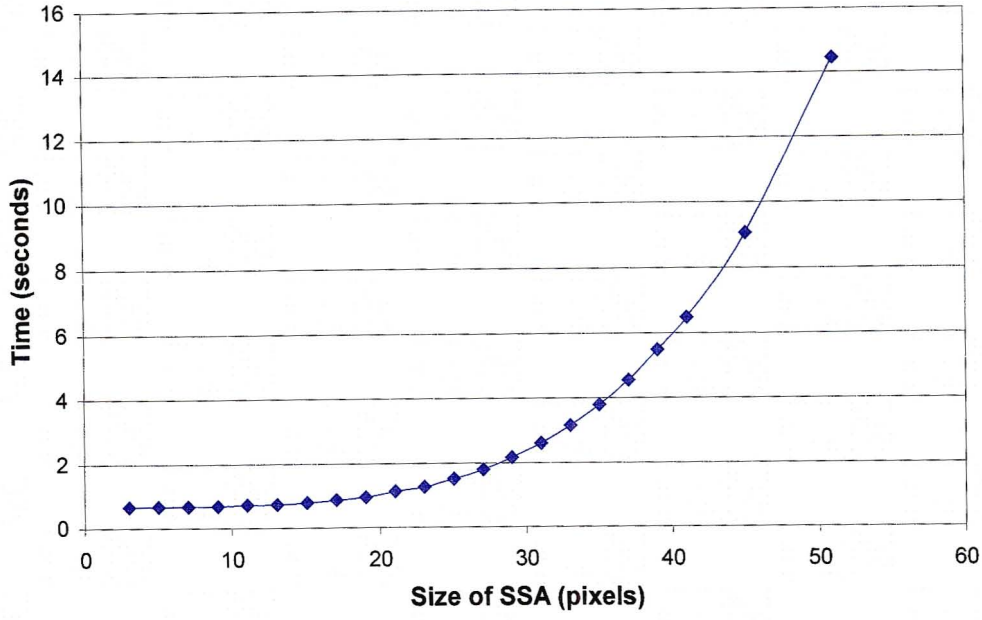

Figure 5-22: Illustration of the processing time required per image for an increasing search strategy area for a ROI=11 and Δt=5seconds

5.7.5. General Validation of Tracking of any point in image

In the previous sub-sections optimum results were presented for tracking the bow of a vessel. This section will present the results of tracking the smoke stacks of the vessels. The same sample of images was used. Most of the optimum settings were maintained, but various ROI sizes were used as it was found to be the most influential variable. The mean and standard deviations of the errors for both the X- and Y-directions are presented in Table 5-4. From the results it appears that the optimum setting of using an initial ROI of (11x11)-pixels does not apply for the tracking of the smoke stacks. The best results for this specific case were achieved by using an initial ROI of (13x13) - pixels. This result suggests that the feature tracking can be sensitive to user specified parameters and should therefore be calibrated for specific applications.

Table 5-4: Mean and standard deviations error values for tracking of the smoke stacks with various initial ROI magnitudes for Δt = 5sec; SSA=25x25.

REGION OF INTEREST	X-DIRECTION		Y-DIRECTION	
	μ_X	σ_X	μ_X	σ_Y
7	-26.0	46.9	-42.7	91.1
11	57.5	50.0	121.4	86.8
13	10.4	33.5	31.3	62.1
15	28.4	37.4	69.1	69.2
25	-26.8	64.4	-20.1	123.4

5.7.6. Object Tracking in Noisy images

Analysis was carried out to determine the robustness of the current tracking algorithm. This involved using the same sample of images, with 'salt and pepper' noise added to the images to decrease their clarity. Varying levels of noise were added to the complete set of images, and then used in the tracking sequence. Noise level were characterised by the number of 'noise' pixels in the image. For example to add 1% of noise to an image that is 100 by 100 in size, 100 pixels were set to extreme colour values. The colour values used were 255 for white (salt) and 0 for black (pepper), and were distributed randomly. The bow of the vessel was the point used for tracking purposes. The mean and standard deviation error values for the tracking results are presented in Table 5-5. From these results it appears that the tracking algorithm can be sensitive to noise, with poor quality images resulting in significantly poorer tracking results.

Table 5-5: Mean and standard deviations for tracking bow of the ship with varying noise levels.

NOISE LEVELS (%)	X-DIRECTION		Y-DIRECTION	
	μ_X	σ_X	μ_X	σ_Y
0	11.6	13.5	19.9	25.7
1	20.6	15.2	51.9	31.9
2	24.6	56.2	61.4	137.9
4	64.7	135.7	128.7	251.9
5	112.4	119.5	159.9	226.9

A 1% level of noise resulted in an increase in mean errors of 78% in the x direction and approximately 157% in the y-direction. This trend continues as the quality of the images decrease. Therefore accurate tracking results require good quality images for the results to be reliable.

5.8. Summary and Improvements

This chapter has outlined the key concepts, used in the development of the automated ship tracking software. The software can trigger capture sequences and save time lapsed images to disk. It is also capable of automatic feature tracking i.e. the ability to track features on the ship over time. Other built in functions include the:

- Ability to vary the location of the entry and exit trigger regions
- Ability to vary the time interval at which images are stored.
- Ability for user to input and change constants used for rectification procedure.

- Pixel registration through tracking, with the rectification procedure carried out in real time.

These functions are available from dialogue boxes, menu bars and buttons found in the Ship Tracking application GUI. Algorithms required for these functions, have also been explained in this chapter.

Analysis was carried out to determine the optimum parameters required for tracking ships. The use of cross-correlation for object tracking worked well as long as the template images used for the correlations were updated regularly at small time intervals (between 5 and 10 seconds). This allowed both the changes in orientation of the object being tracked as well as the apparent lighting conditions to be catered for. Increasing the size of the template ROI over time gave improved tracking results. However by increasing the ROI sizes, the processing time also increased. The sensitivity to size of the search strategy area (SSA) used was small with a similar spread of results achieved for all cases shown. The optimality of the variables used i.e. Δt, ROI, SSA are expected to be case specific.

CHAPTER 6

CASE STUDY: RESULTS & ANALYSIS

6.1. Introduction

The methods of capturing and processing image data to produce cross track drifts and ship tracks have been explained in previous chapters. From these methods and techniques ship tracks and cross track drift data under varying weather conditions can be determined. During this study a total of forty-six ships were successfully tracked into the harbour. From this data set seventeen were captured using a still camera, ten using a portable digital video camera and the remaining nineteen using the microwave video system.

These ship tracks and their CTDV data along with corresponding weather conditions are presented and discussed in this chapter. Note that all this data was obtained from manual digitisation of the images, rather than the automated process. The data is used to qualitatively understand the patterns routinely used by the harbour pilots and the influence of weather patterns. Quantitative results from statistical analysis are also presented.

6.2. Wind Data

Mardon & Stretch (2002) suggests that for wind speeds greater than 3 m/s and for lag times of two hours there is a good correlation between local wind and surface current conditions around the Durban harbour. Therefore only winds at two hours before entry were considered for this investigation. The component of the wind perpendicular to the channel axis i.e. 'crosswinds' shall be used as representative of the local wind or surface current conditions. Wind measurements were recorded for every ship in the data set. This wind data was based on one-hour averages and was measured at 100 metres above mean sea level. The wind data is presented graphically in a wind rose format in Figure 6-1.

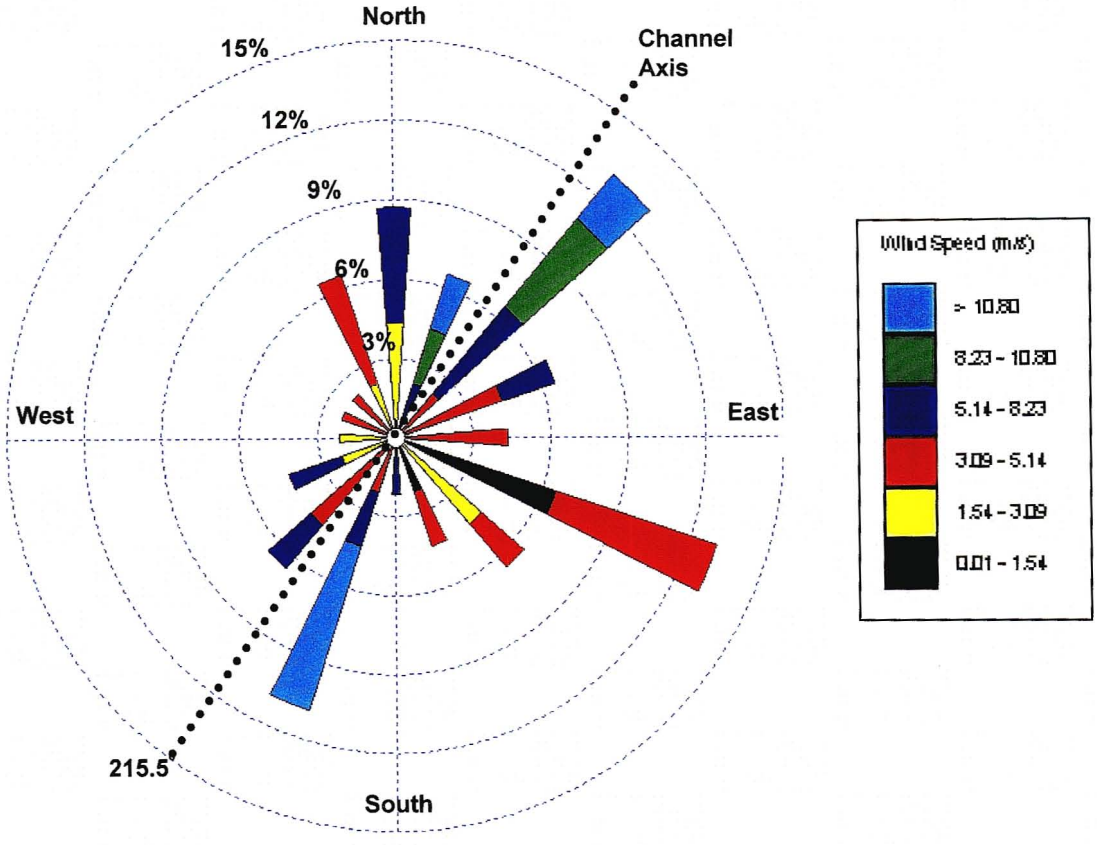

Figure 6-1: Wind rose for wind data recorded at two-hours before entry for all forty -six ship tracks in the data set. The direction of the entrance channel axis is indicated.

From the wind rose shown in Figure 6-1, the dominant wind patterns are generally consistent with the wind rose in Figure 2-3 where wind data for a fourteen-year period around Durban was shown. Winds blowing from the north-easterly and south-westerly sector are prevalent, making up 33% and 24% of the total distribution respectively.
The distribution of crosswinds across the channel axis (shown in Figure 6-1) is small, with south-easterly crosswinds appearing to be more frequent then north-westerly crosswinds. For this data set wind speeds greater than 8.23m/s were only measured in the north-easterly and south-westerly wind sectors.

6.3. Overview of Ship Track Data

6.3.1. General

Figure 6-2 graphically illustrates the ship track data for all ships under all weather conditions on one set of axes. Plots of the raw data for each of the forty-six ships are given in Appendix F. The centre line of the entrance channel axis for the Durban harbour is shown as a dotted line, which is the desired course for a safe entry

manoeuvre (heading 215,5°). At the harbour entrance, the north pier flanks the channel on the north side and by South Pier breakwater on the south side.

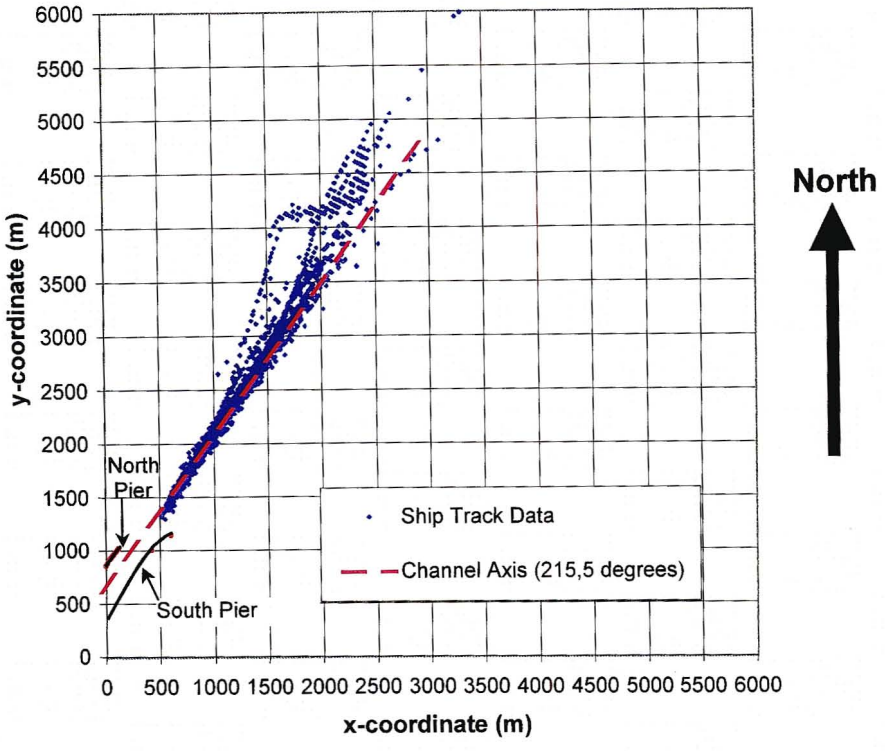

Figure 6-2: Scatter plot of ship track data for 46 ships that entered the Durban Harbour from 1999 to 2001

From Figure 6-2 it is evident that there is an overall bias towards the north-westerly side of the channel axis, with the ship's mean position remaining north-west of the channel axis. This seems to be a preferred pattern adopted by the pilots for entry into the port and probably reflects the prevailing weather and current characteristics of this location.

The speed of the ship relative to the ground was calculated, from the time derivative of its position. Figure 6-3 is a plot of the data, showing the distribution of the ship speeds as they approached the south breakwater. The average speed over the whole approach channel was 5.2 m/s (10.4 knots). As expected there is a general reduction in speed as the ships approach the harbour entrance. Note that some very high speeds are evident in the data. It is obviously unlikely that the ships entering the harbour achieved speeds greater than 10 m/s (20 knots); therefore it appears that some of the calculated speeds are not physically possible and are incorrect. These errors are believed to be due to incorrect registration of pixel coordinates.

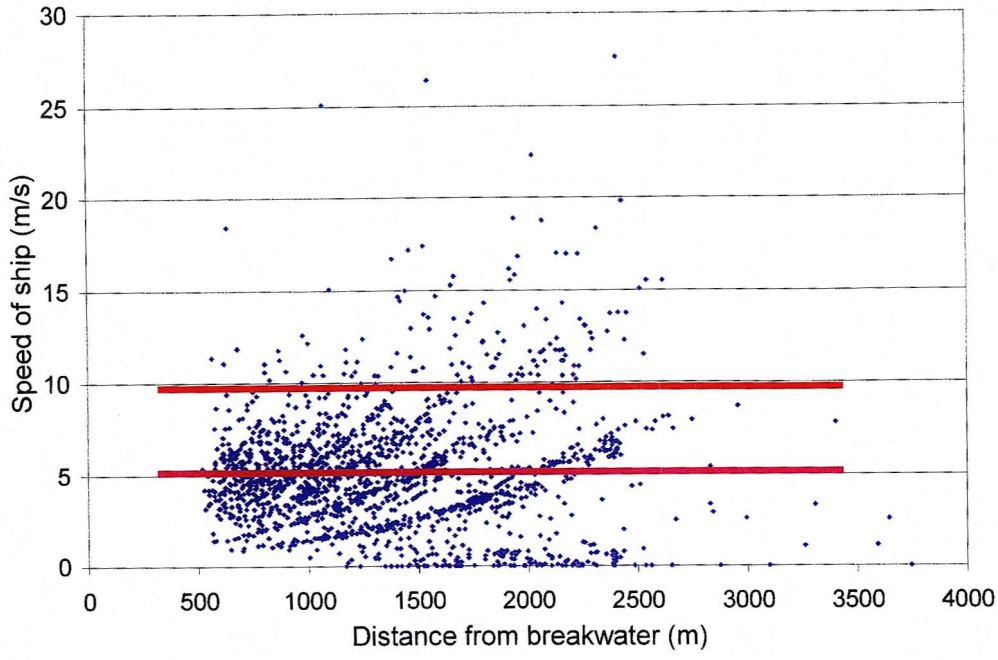

Figure 6-3: Plot of all the ship data, showing the distribution of the velocity of the ship as it approaches the south breakwater. The average and maximum velocities were calculated based on the mean and standard deviations as 5.2 m/s and 9.6 m/s respectively. These velocities are shown as the red and purple lines on the plot.

The ship data was further investigated by using the corresponding CTDV and crab angle data. Figure 6-4 (a) and (b) show the distribution of the crab angle and CTDV along the approach channel. Note that the negative sign on the y-axis represents crab angle data favoured towards the south-east. In the case of the CTDV data it implies drifts from the south-east.

From Figure 6-4 (a) it is evident that crab angles greater than 30 degrees, were obtained. On further investigation, it was found that these spuriously large crab angles (and the associated CTDVs) occurred primarily when the velocity of the ship was small i.e. less than 2 m/s (4 knots) as shown in Figure 6-4 (c) and (d). These data are invalid and arise due to quantization errors as explained in section 4.4.2.

Data points associated with these anomalies i.e. speeds greater than 10m/s, and crab angles greater then 30 degrees (absolute) were subsequently removed before further analysis. In total 14 % of the original ship data was removed from the data set.

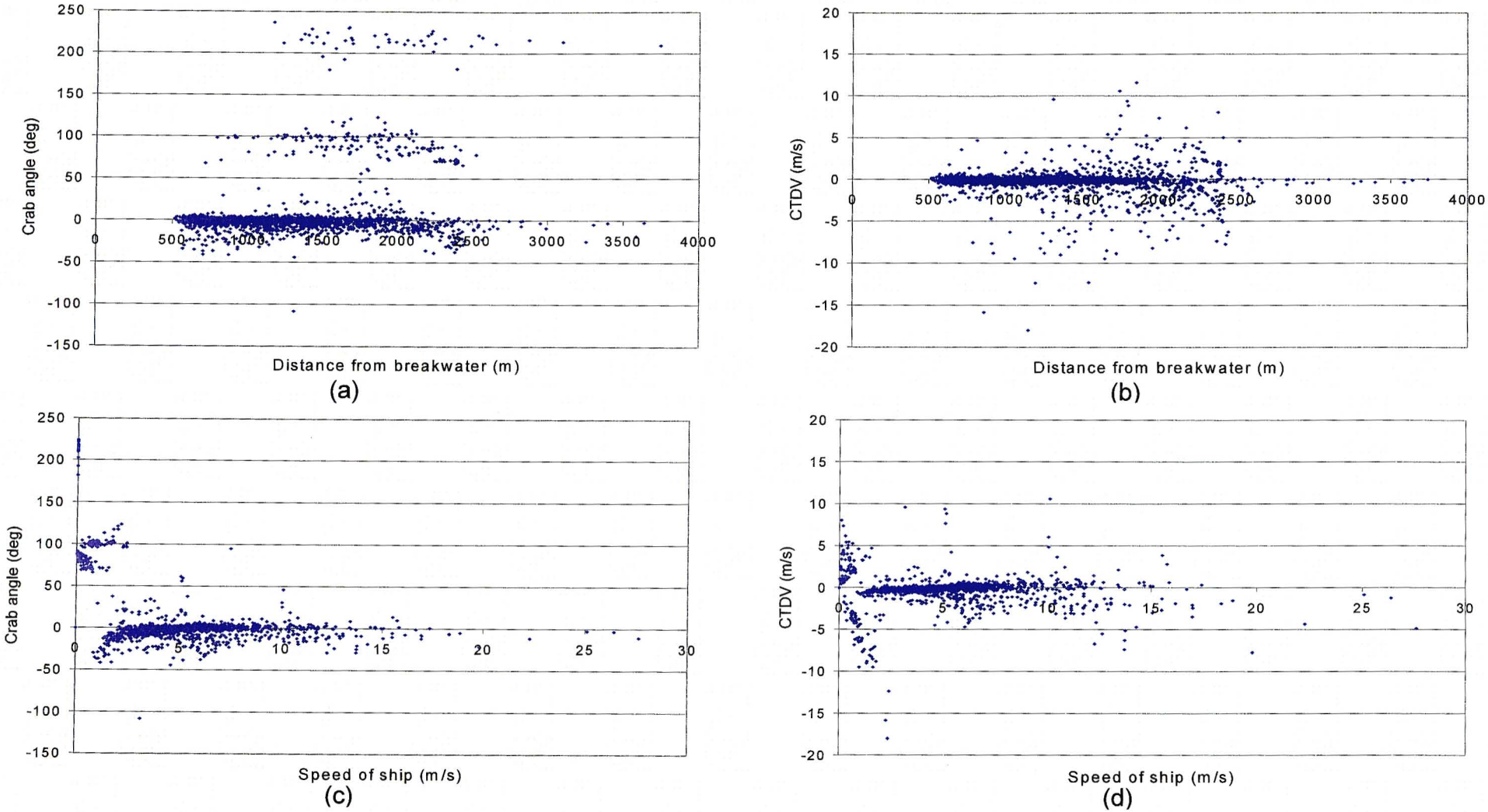

Figure 6-4: Plots of the ship data, showing the distribution of the crab angle and CTDV data (a and b) during the vessel approach to the south breakwater and (c and d) for the distribution of the measured velocity

Conditional tests were carried out on the data set presented in Figure 6-2. These tests filtered the data set into smaller sub-sets based on certain ship and weather criteria. These criteria included crosswinds and the ship draught. The results are discussed in the following sub-sections.

6.3.2. Crosswind effects on Offsets from channel axis

Using hourly averaged wind data at two hours before entry to obtain crosswinds, the data points shown in Figure 6-2 can be filtered into two data sets: the first being for ship tracks where the measured crosswind is south-easterly (125.5 degrees) and the second where the crosswinds are north-westerly (305.5 degrees). Figure 6-5 (a) shows all the ship tracks that have south-easterly crosswinds and Figure 6-5 (b) shows the cases with north- westerly crosswinds.

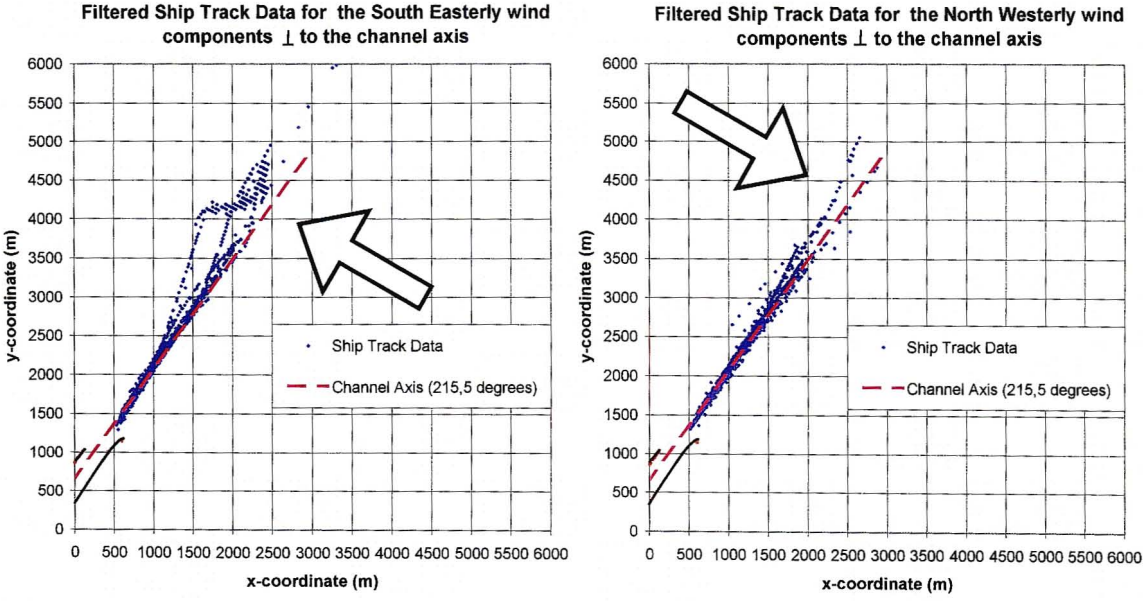

(a) (b)

Figure 6-5: Filtered Ship Track Data for crosswinds (south-east and north-west) at 2-hours before entry.

From Figure 6-5 (a) it can be seen that for winds from the south-easterly sector, larger offsets from the entrance channel axis occurred. Furthermore for south-easterly crosswinds, channel alignment is generally reached when the ship is approximately 1.2 kilometres from the south pier breakwater. For north-westerly crosswinds channel alignment is on average reached at 1.8 kilometres from the south pier breakwaters. These trends probably reflect the prevailing wind, current and wave conditions for this data set.

6.3.3. Ship Draught

The analysis carried out by Patel & Stretch (2001) found that for ship draughts greater than 8.5 metres poor correlations existed between the cross track drift and hourly wind average. Using the ship draught to order the ship track data yields the results shown in Figure 6-6. Figure 6-6 (a) shows the ship tracks for those ships with draught less than or equal to 8.5 metres, while Figure 6-6 (b) shows data for ship draughts greater than 8.5 metres.

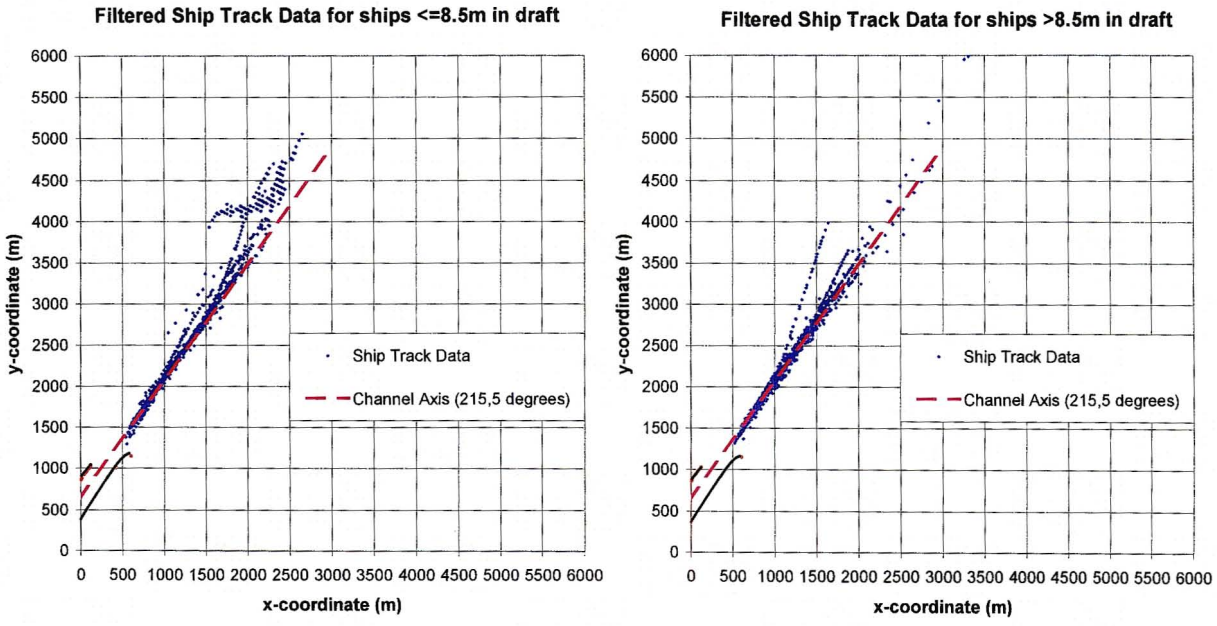

(a) (b)

Figure 6-6: Filtered Ship Track Data for (a) ship draughts less than or equal to 8.5 metres and (b) ship draught greater than 8.5 metres

From Figure 6-6 (a) larger offsets from the channel axis are evident especially from about 2.5 kilometres from the south pier breakwater. From Figure 6-6 (b) it is evident that for vessels of draught greater than 8.5 metres the offsets from the channel axis are small except for one or two exceptions. Investigation has shown that these exceptions were associated with calm weather conditions.

From Figure 6-6 (a) and (b) it can be tentatively concluded that shallower draught vessels have a somewhat larger offset from the channel axis then deeper draught vessels, particularly at distance greater than 3 kilometres from the south breakwater. These offsets are possibly due to the higher risks taken by harbour pilots when entering the port with shallower draught vessels. As reviewed in sections 2.4 and 2.6 the pilot can afford to take such risks, since the depth/draught ratio is high so if the ship

drifted off the desired track, corrections to the ship's track can be made with small response times.

6.4. Statistics of Ship Track Data

Figure 6-2 illustrated a scatter plot of ships tracked into the Durban Harbour from 1999 to 2001. To statistically analyse the data the approach channel was first partitioned into eight sections according to depth. The boundaries of these sections were determined from hydrographical data provided by the local port authorities. The depth measurements recorded along the approach ranged from 15.4 metres at the head of the south breakwater to 27.4 metres at a range of 6 kilometres. Table 6-1 tabulates the depth boundaries used for the eight sections, as well as the ground distance covered by each section.

Table 6-1: Ocean depth boundaries for the eight sections used for the statistical analysis.

SECTION	MINIMUM DEPTH (m)	MAXIMUM DEPTH (m)	AVERAGE DISTANCE FROM SOUTH PIER (m)	SECTION LENGTH (m)
1	15.5	16.7	285.7	590.2
2	16.7	17.9	857.1	580.8
3	17.9	19.1	1428.6	577.5
4	19.1	20.3	2000.0	575.4
5	20.3	21.5	2571.4	573.5
6	21.5	22.7	3142.9	573.3
7	22.7	23.7	3666.7	514.7
8	23.7	27.4	4785.7	1732.1

The depth variations as a function of distance from the breakwater are shown in Figure 6-7. Also shown are the range boundaries of the eight sections used for the analysis.

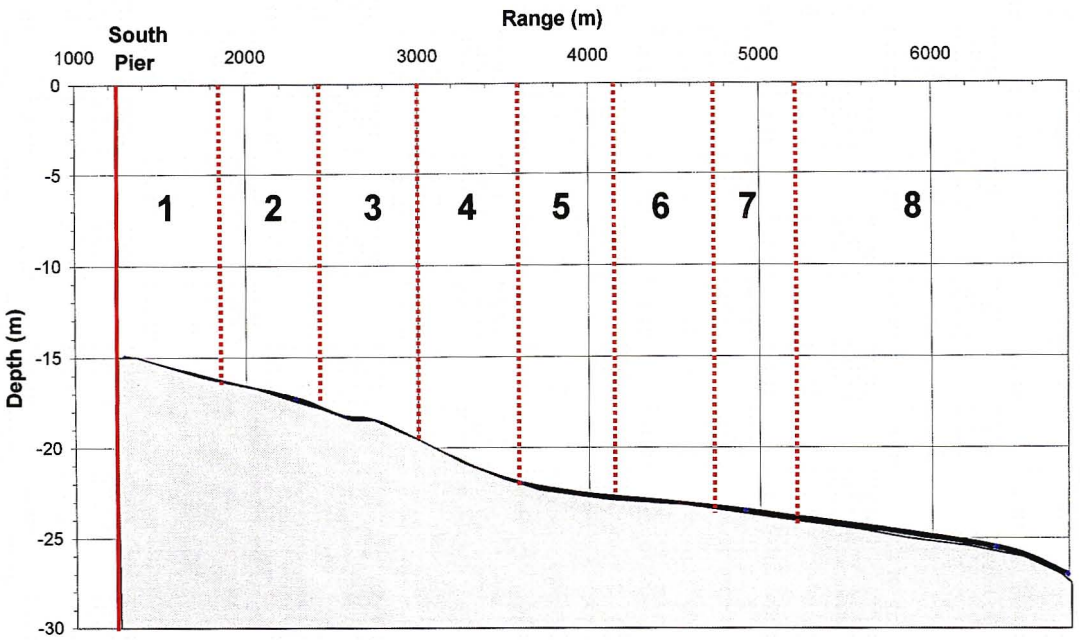

Figure 6-7: Long-section of the entrance channel extending from the South Pier breakwater along the with eight (8) sections used for analysis

The ship data for each section was analysed separately. The offset distances of the ship tracks from the channel axis were computed and analysed. Figure 6-8 (a to d) and Figure 6-9 (a to d) are histograms of the offsets, for sections one to eight. Also shown are the cumulative probability distributions of the deviations. Note that the centre line of the entrance channel axis is shown as the red vertical line. Histogram data to the left of this line represents ship positions located towards the south-east of the channel axis whilst data to the right represents ship positions located towards the north-west (this convention reflects the view of pilots on entering the harbour).

The mean and standard deviation values of the offsets for each section are shown Table 6-2.

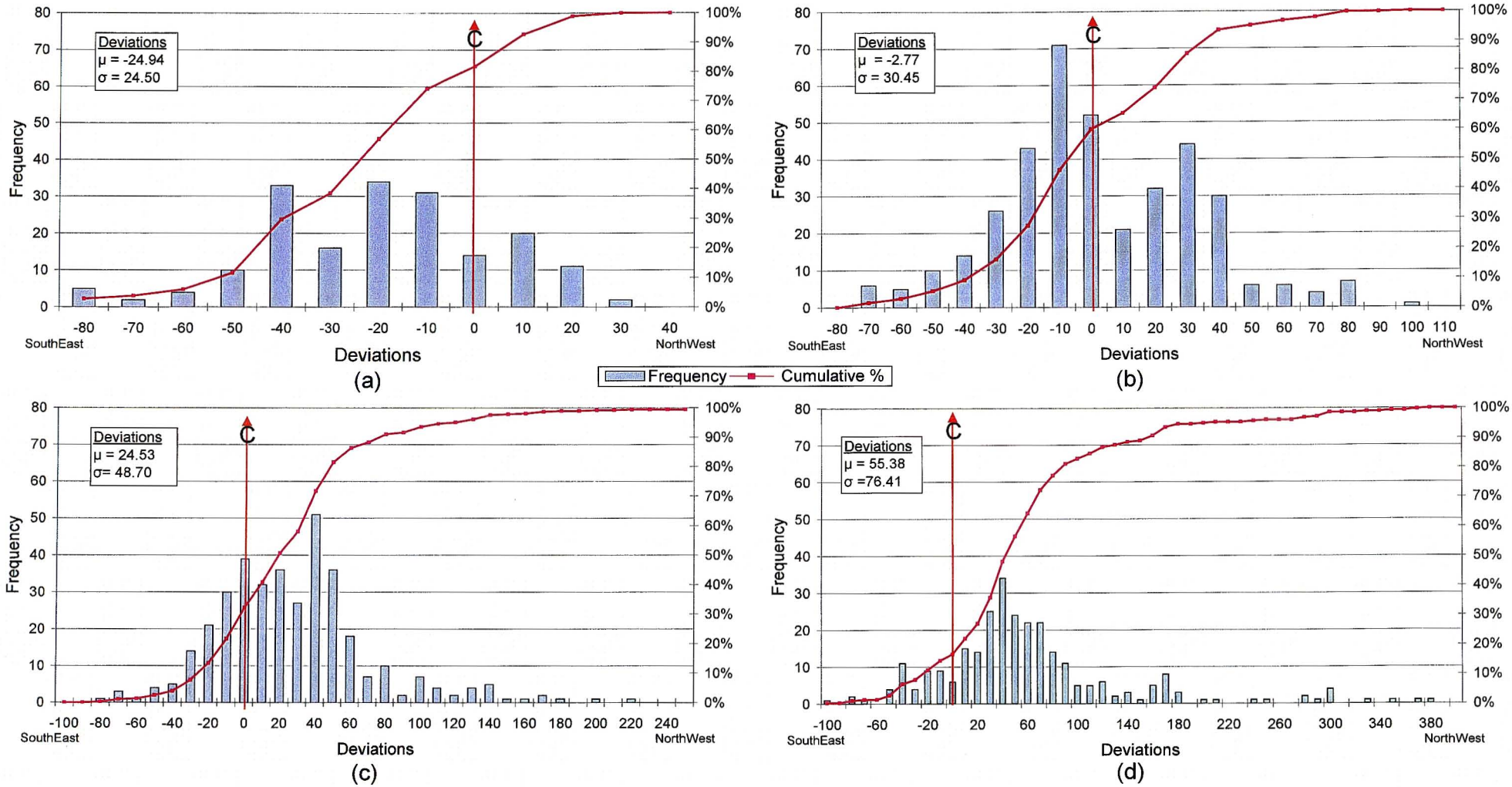

Figure 6-8: Histograms of the offset distances for the ship tracks in sections 1 to 4 of the approach channel (shown as (a) to (d) respectively), with the channel centreline shown as (red line). The inserts show the mean and standard deviations of these offset distances.

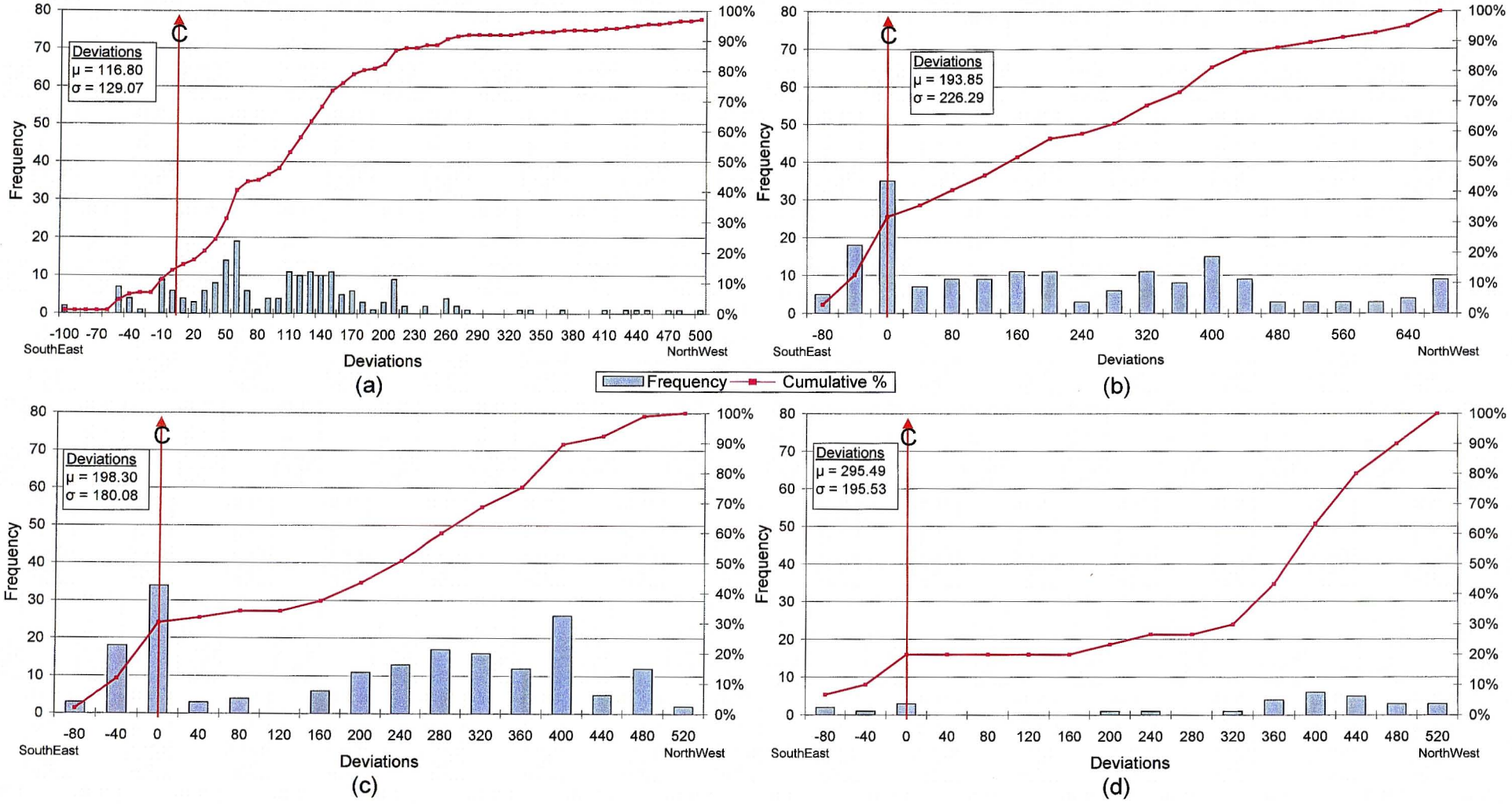

Figure 6-9: Histograms of the offset distances for the ship tracks in sections 5 to 8 of the approach channel (shown as (a) to (d) respectively), with the channel centreline shown as (red line). The inserts show the mean and standard deviations of these offset distances.

Table 6-2: Tabulated mean and standard deviations values for the offsets from the channel axis for each of the eight depth sectors along the approach channel.

SECTION	TOTAL DATA POINTS	μ (m)	σ
1	182	-24.9	24.5
2	378	-2.8	30.5
3	368	24.5	48.7
4	281	55.4	76.4
5	205	116.8	129.1
6	136	193.9	226.3
7	113	198.3	180.1
8	30	295.5	195.5

From Table 6-2 it can be noted that the positive mean values signify an overall bias towards the north-westerly side of the channel axis. The overall mean offset from the channel axis increases from -24.9 metres to 295.5 metres for sections 1 to 8 where the average distance increases from 1.5 to 6,0 kilometres from the Signal Station respectively.

A total of 84% of the ship data points occur between sections 1 and 5 with a sharp decrease in data points from section 6 outwards. Most of the ship data points occurred in sections 2 and 3 contributing 44% of the total data. The mean values for sections 1 and 2 favour the south-east side of the channel axis whilst for sections 3 to 8 the mean values are increasingly biased towards the north-west side. The smallest mean offset is measured in section 2 of the approach channel (-2.8 m). This implies that over this stretch of the approach channel (section 2), ships are most probably aligned with the navigation lights and are following a heading of 215.5 degrees. A deviation of -24.9 metres in section 1 is difficult to understand, as this offset is expected to be similar to, or smaller than, the mean offset experienced in section 2. Possible reasons for this could be that as the ship approached the breakwater there is a transition from a turbulent, transverse flow outside the breakwater to a relatively calm but longitudinal flow moving inside the breakwater. It is speculated that this could result in over correction of the ship tracks by the pilots.

CSIR (1999b) carried out a similar analysis using simulated ship tracks. CSIR (1999b) divided the approach channel into 5 sections beginning from approximately 400m from the south breakwater and extending to where the entrance channel enters the bay. Their analysis was based on 35 simulated ship tracks, with 21 carried out under a fixed north-westerly flowing crosscurrent of 1 knot. Only data from section 1 of the approach

channel i.e. from 0m to 500m from the breakwater could be used for comparative purposes. The mean and standard deviations for sections 1 are tabulated in Table 6-3 for comparison.

Table 6-3: Comparison of the mean and standard deviation of the offsets of ships along the approach channel

SECTION	CSIR		PRESENT	
	μ (m)	σ	μ (m)	σ
1	22.2	27.7	-24.9	24.5

The two sets of data are similar in magnitude but opposite in direction. The estimated sampling error for the mean values is approximately 5 metres. It is speculated that the port entry manoeuvres, as simulated by the Durban pilots on the Portsim simulator (CSIR, 1999b), were not representative of the actual conditions.

6.4.1. Wind effects on channel offsets

It was decided to investigate whether or not crosswinds influence the offset distances from the channel axis. Only sections between 1 and 5 were analysed, to focus on the regions within 3 kilometres from the south breakwater. The data was analysed conditional on the direction of the crosswinds i.e. 125,5 and 305.5 degrees. Tables B.3 and B.4 in Appendix B tabulate the data for ships that satisfied these criteria.

The number of cases for crosswinds in each direction was approximately the same i.e. 49% south-easterly and 51% north-westerly. Table 6-4 tabulates the mean and standard deviation values for the data.

Table 6-4: Tabulated mean and standard deviation offset values for all the ship track data from sections 1 to 5, as well as values conditioned for south-easterly and north-westerly crosswinds

SECTION	SOUTH - EASTERLY		NORTH-WESTERLY		ALL DATA	
	μ (m)	σ (m)	μ (m)	σ (m)	μ (m)	σ (m)
1	-21.7	25.0	-28.0	23.8	-24.9	24.5
2	6.8	29.0	-11.6	29.2	-2.8	30.5
3	32.6	49.2	16.3	46.9	24.5	48.7
4	68.6	84.2	43.2	66.4	55.4	76.4
5	148.7	143.7	85.8	104.8	116.8	129.1

Comparing the mean offsets for the unconditional data to the conditioned data in Table 6-4, an increase in magnitude of the offsets is evident for south-easterly crosswinds,

with the opposite being true for north-westerly crosswinds. It has already been shown that the ships mean offset favours the north-west side of the channel axis, and from the results presented in this section, for south-easterly crosswinds these mean offsets are larger than the mean offsets shown for all the data. It is therefore speculated that these offsets are representative of the local surface current conditions. This means that winds from the south-east result in north-westerly flowing crosscurrents, which in turn result in larger offsets from the channel axis and vice versa for north-westerly winds.

6.4.2. Ship draughts

It was decided to investigate whether large offsets from the channel axis are associated with shallower draught vessels and whether or not the draught of a vessel influences the position where alignment with the channel axis is reached. This analysis used data analysed conditional on draught i.e. either >8.5 metres or <=8.5 metres. Tables B.5 and B.6 in Appendix B tabulate the data for ships that satisfied these criteria along with the corresponding draughts.

The number of cases satisfying each draught criteria were about equal. Table 6-5 tabulates the statistical means and standard deviations for the data.

Table 6-5: Tabulated mean and standard deviation offset values for all the ship track data from sections 1 to 5, as well as values conditioned for ship draughts less than or equal to 8.5 metres and greater than 8.5 metres

SECTION	DRAUGHTS <= 8.5m		DRAUGHTS > 8.5m		ALL DATA	
	μ (m)	σ	μ (m)	σ	μ (m)	σ (m)
1	-19.0	25.8	-30.7	21.9	-24.9	24.5
2	10.6	29.5	-14.6	26.1	-2.8	30.5
3	41.4	47.8	9.8	44.6	24.5	48.7
4	66.6	67.8	44.6	82.7	55.4	76.4
5	113.2	83.7	121.6	172.3	116.8	129.1

Comparing the mean offsets for unconditional data to the conditioned data in Table 6-5, a general increase in magnitude of the mean offsets is evident for shallower draught vessels (except in section 5). It has already been indicated in sub-section 6.3.3 that shallower draught vessels experience larger offsets from the channel axis, and this statement is now corroborated by the data presented in this section.

The smallest mean offsets occurred in section 2 for shallower draught vessels and section 3 for deeper draught vessels. Deeper draught vessels attain their minimum mean offsets in section 3, while shallower draught ships attain this by section 2. This is

expected as deeper draught vessels are more difficult to handle and are more sluggish to respond to directional changes and thus alignment should occur earlier along the approach channel. Both sections 2 and 3 are close to the south breakwater so it is expected that the pilots would attempt to minimise deviations from the axis at these positions to avoid colliding with the breakwater.

6.5. Ship Tracks with corresponding CTDV data

In this section measured ship tracks and corresponding CTDV data will be presented. The complete set of these ship track plots can found in Appendix F. Some of the interesting ship track plots are however presented and discussed in this section.

6.5.1. Vertical Current Structure

As reviewed in section 2.9.2, Mardon & Stretch (2002) found that the structure of crosscurrents near the water surface (up to 4-metre depths) were driven by shear stress associated with surface winds and are thus dependant on wind direction and duration. This section will illustrate and explain how the drift experienced by ships can vary due to the vertical structure of the crosscurrents in a water column using an example of two ships that entered the port within an hour of each other. The two ships were the Silver Star and the Anangel Dignity that entered the harbour on 27 August 1999. Table 6-6 tabulates the ship data of the two ships as well as the crosswinds at two hours before entry. Note that the crosswind components for both ships were similar and blowing from the north-west.

Table 6-6: Ship characteristics together with perpendicular wind components for two ships having deep and shallow draughts

NAME	DRAUGHT (m)	LENGTH (m)	CROSS WIND (m/s)
Silver Star	6.6	106.0	3.1
Anangel Dignity	11.5	182.8	2.9

From the ship track plots shown in Figure 6-10 and Figure 6-11 the Silver Star (draught 6.6m) appears to experience a dominant drift in the direction of the local wind patterns (North West to South East). The Anangel Dignity (draught 11.5m), appears to experience drift in the opposite direction. The drift experienced by the shallower draught vessel (Silver Star) appears to be associated with the surface currents driven by the local winds and the drift experienced by the deeper draught vessel (Anangel Dignity) appears to be associated with deeper sub-surface currents that must have been flowing in the opposite direction

This simple example illustrates the point that currents are complicated and vary with depth. The result presented here provides evidence that the drift experienced by shallower draught vessels is dependent on the direction of the local wind conditions while the drift experienced by deeper draught vessels does not. If actual current measurements were available at the time, further evidence could be provided to support this conclusion.

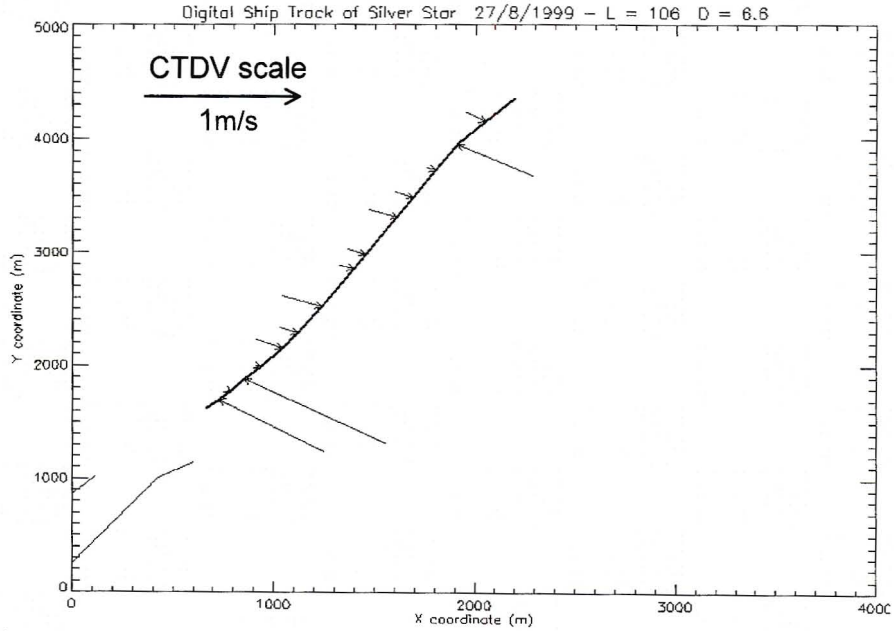

Figure 6-10: Ship Track of the Silver Star that entered the Durban Harbour on 27 August 1999

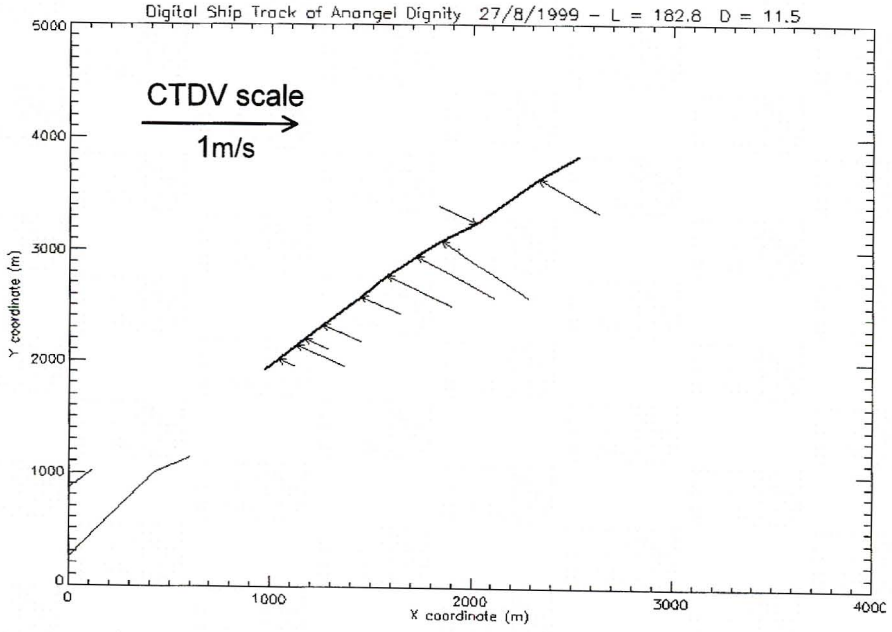

Figure 6-11: Ship Track of the Anangel Dignity that entered the Durban Harbour on 27 August 1999

6.5.2. Correction due to side slip

This section will illustrate the effect sideways slip has on a ship's crab angle as discussed in section 3.9. The ship track plots presented so far in this section have not taken the effect of slip into account i.e. by extracting the crab angle due to slip (θ_s) from the measured crab angles (θ). This section will present examples of ship tracks with and without these corrections and show how this method can be used to generate more realistic data. Note that Figure 3-16 to Figure 3-18 (shown in section 3.9) were used to calculate the crab angles due to slip.

Two types of sideslip crab angles have been defined i.e. a portside slip as shown in Figure 6-12 (a) or a starboard slip as shown in Figure 6-12 (b). In order to calculate θ_s, the turning radius of the ship at every time step is required. The sign convention used was negative for a starboard slip and positive for a portside slip. The turning radius at time t was calculated by using the X and Y ground coordinates of a ship at times t, $t+\Delta t$ and $t-\Delta t$. Three equations with three unknowns will result i.e. (X_a,Y_a,R) which can be simultaneously solved. With the turning radius known, Figure 3-16 to Figure 3-18 were used to calculate the average crab angle due to slip.

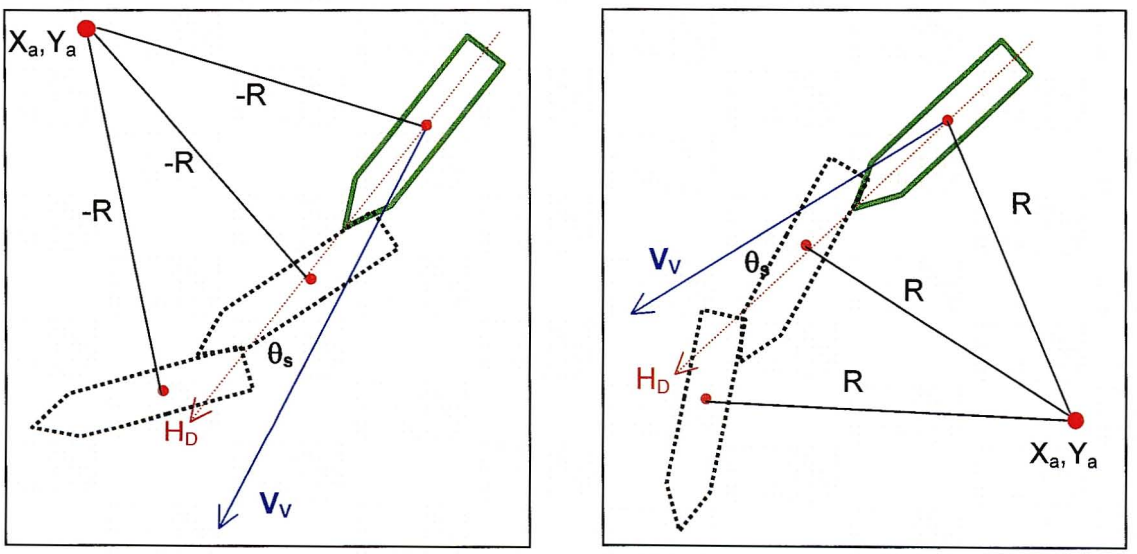

Figure 6-12: Illustration of a ship's turning manoeuvre for (a) portside turn (b) starboard turn

Figure 6-13 illustrates two ship track plots for each of the Salinthip Naree and the Socol 6 with and without sideslip corrections respectively. The ship tracks for each ship are similar, however differences in the crab angles were obtained in specific sections of the

tracks, resulting in varying CTDVs. These differences were generally larger for small turning radii's. In the case of the Salinthip Naree, at approximately 1 kilometre from the south breakwater small turning radii result from rapid turning manoeuvres of the ship. Figure 6-13 (b) illustrates that by correcting the measured crab angle to allow for side slip, more realistic CTDV values in the rapid turning region result.

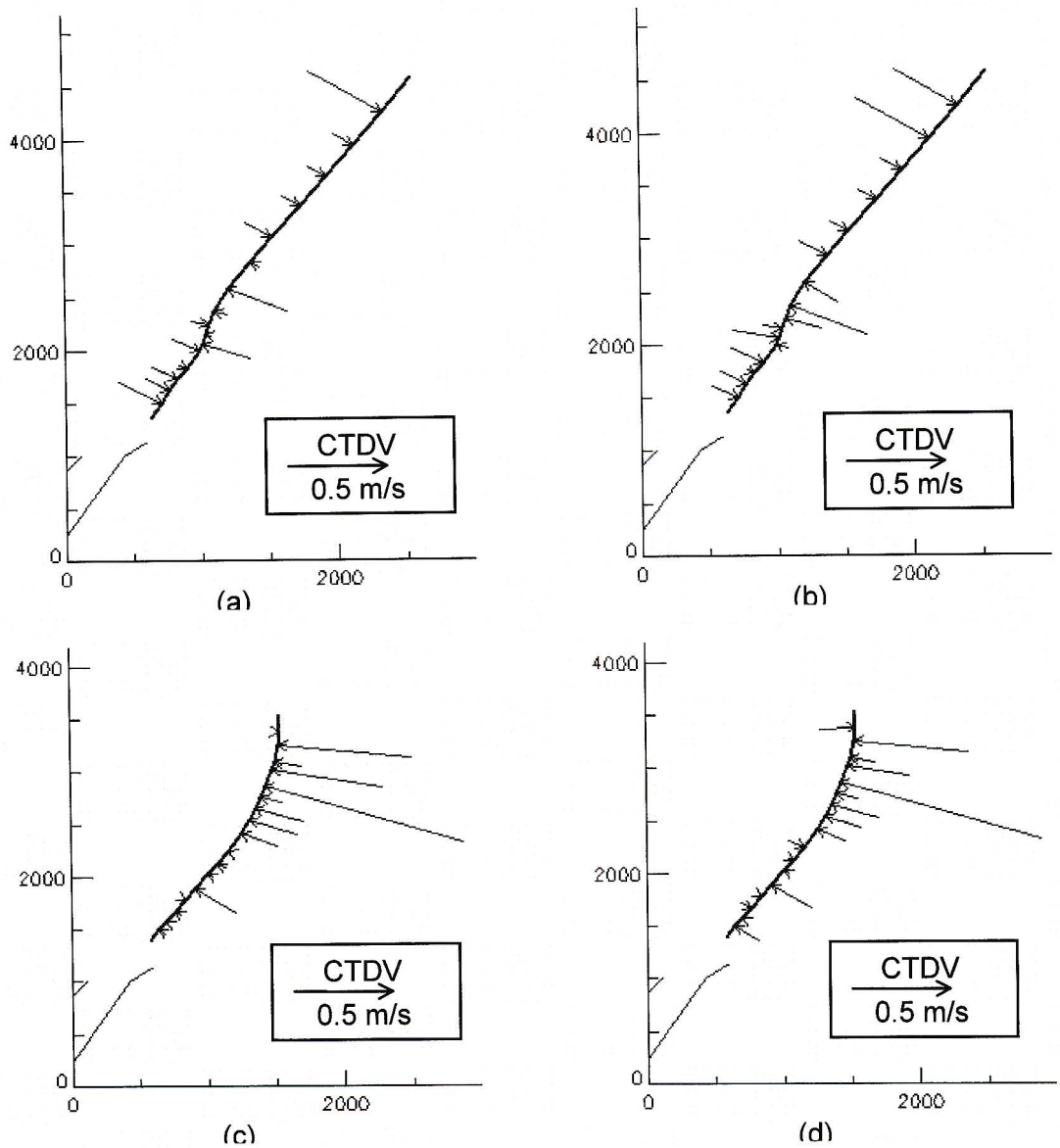

Figure 6-13: Ship Track Plots for two ships, the Salinthip Naree (a & b) and the Socol 6 (c & d) respectively, with and without slide slip corrections.

Similar conclusions can be seen for the ship track plots of the Socol 6 shown in Figure 6-13 (c) and (d). From Figure 6-13 (d) there appears to be a general north-westerly moving CTDV, but some south-easterly moving CTDVs were obtained in the region where the ship was turning. By correcting the measured crab angles for side slip, these

south-easterly moving CTDVs are shown to be erroneous and the corrected CTDVs are more consistent.

The examples shown here illustrate how corrections due to ship slide slip can be accounted for. The corrections used were based on average ship slip crab angles, determined using three vessel types i.e. Car Carriers, Post Panamax vessels and Product Tankers. The crab angle corrections used are questionable as the PORTSIM simulator used was not specifically designed for this purpose. Further investigation into these effects is therefore required.

6.5.3. Summary

The results presented in this sub-section illustrate the vertical current structure, as well as the ship slip concept. Further analysis was carried out to present the CTDV data in a format that can be used for design purposes. This analysis is reviewed in the next section.

6.6. Relationship between CTDVs and crosswinds

The preliminary analysis of the ship track data described in section 6.3 indicated that some extreme data points existed in the ship track data set. As mentioned 14% of these extreme data points were removed from the data set. The analysis carried out on the CTDV data is similar to the analysis carried for the ship track data shown in section 6.4, with the same section depth partitions used along the approach channel. These sections along with the mean and standard deviation values of the CTDV data per section are shown in Table 6-7.

Table 6-7: Mean and Standard deviations for average CTDV data per section along the approach channel

SECTION	TOTAL DATA POINTS	μ (m/s)	σ
1	177	-0.08	0.48
2	365	-0.14	0.49
3	340	-0.15	0.56
4	234	-0.16	0.67
5	161	-0.14	0.85
6	90	-0.52	1.47
7	68	-1.87	1.76
8	25	-1.26	1.78

From Table 6-7 the negative mean values signify an overall bias towards the crosscurrents from the south-easterly side of the channel axis. The overall mean CTDVs remain approximately constant along sections 1 through to 5 i.e. between 0.1 and 0.15 m/s, but a large increase in the average CTDV occurs from section 5 outwards. Only sections between 1 and 5 were analysed, to focus on the regions within 3 kilometres from the south breakwater. Histograms of the CTDVs for sections 1 to 5 are shown in Figure 6-14 (a to e).

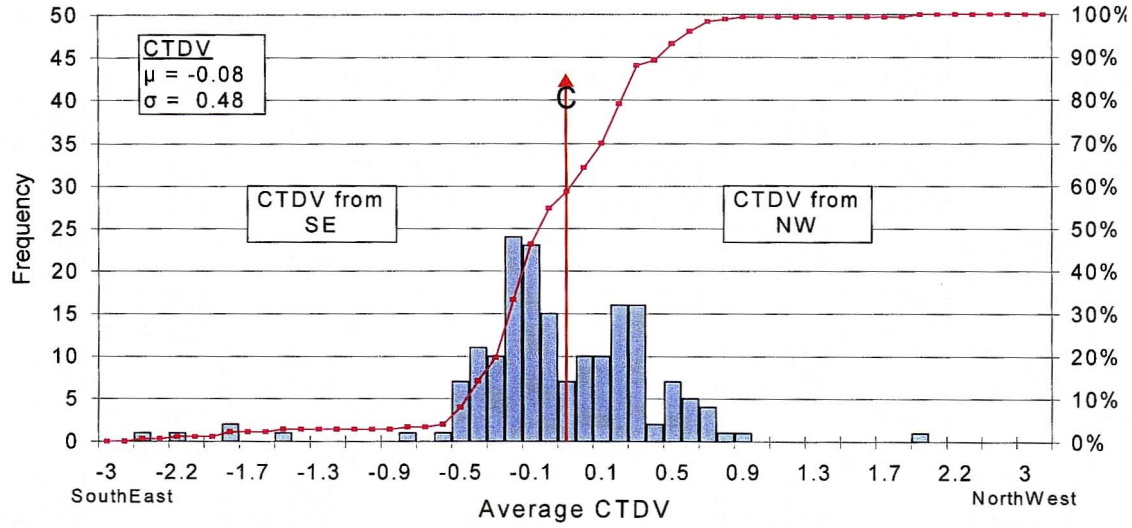

(a)

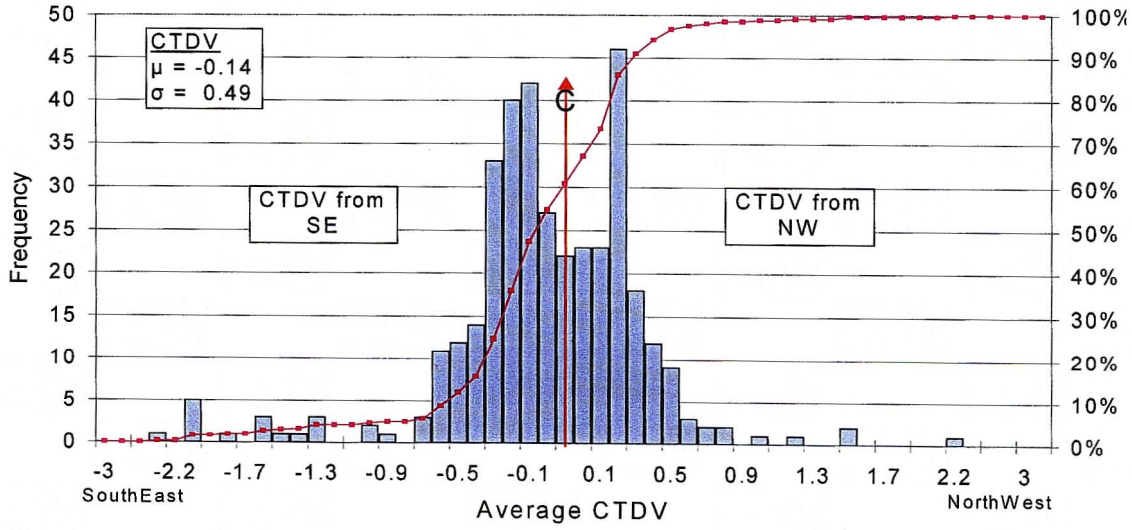

(b)

Figure 6-14: Histograms illustrating the spread of the CTDVs measured over sections 1 (a) to 2 (b) along the approach channel. The inserts show the mean and standard deviations of the CTDVs per section. CTDV data to the left of the channel axis signifies CTDVs moving from the south-east, with CTDV data to the right signifying CTDVs from the north-west. Sections 3 to 5 are shown on the following page

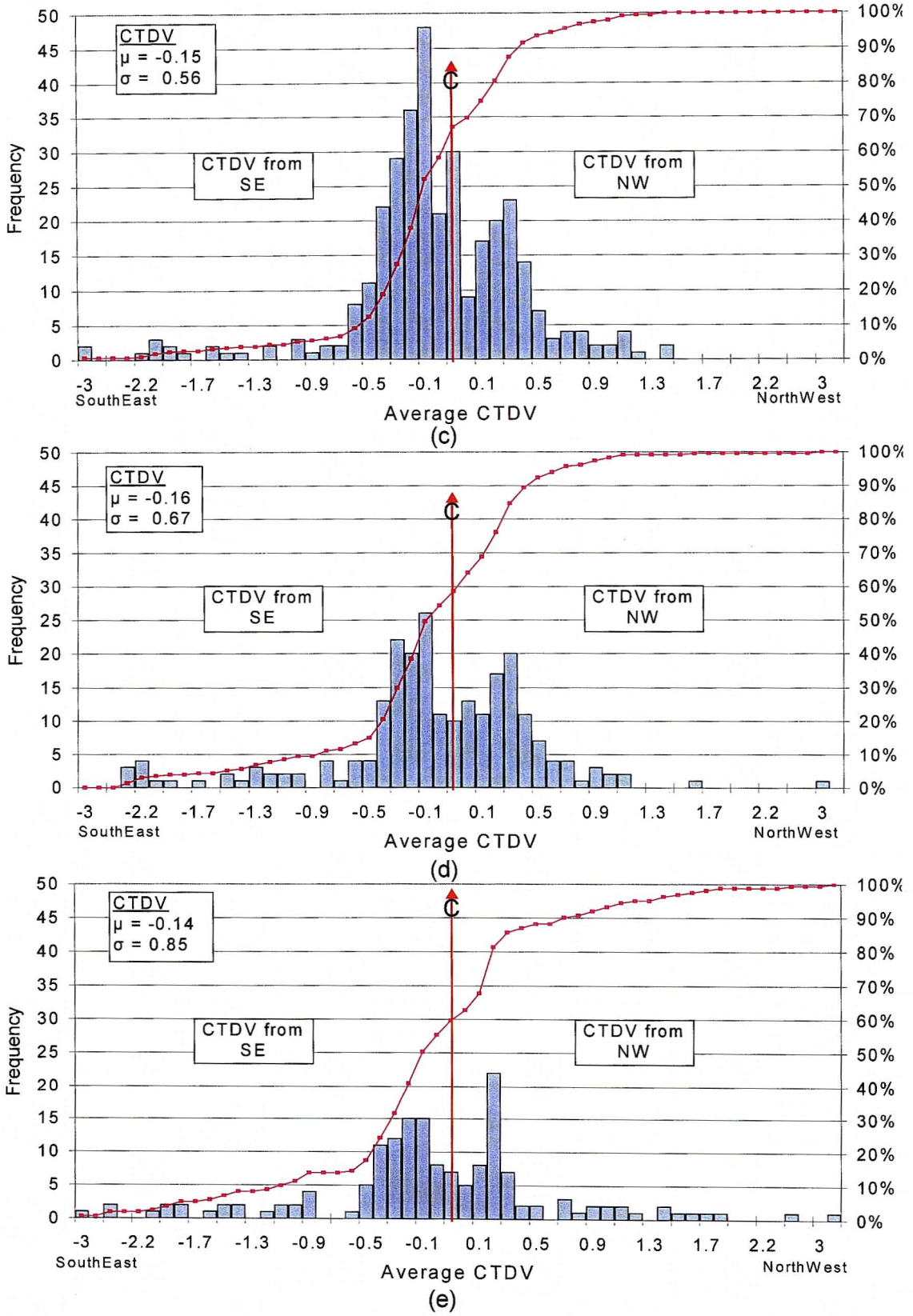

Figure 6-14 continued: Histograms illustrating the spread of the CTDVs measured over sections 3 (c) to 5 (e) along the approach channel. The inserts show the mean and standard deviations of the CTDVs per section. CTDV data to the left of the channel axis signifies CTDVs moving from the south-east, with CTDV data to the right signifying CTDVs from the north-west

Summarising the results presented, there appears to be a general drift pattern around the Durban harbour from the south-east, which is consistent with the currents at the port as reviewed by CSIR (1995).

As shown previously in Table 6-2 the mean deviations of ship tracks from the channel axis are towards the north-westerly side of the channel, while from Figure 6-14 the dominant drift appears to be from the south-east. It thus appears that harbour pilots steer their vessels from the north-west because they are aware of the dominant drift pattern from the south-east and prefer steering into the drift rather than away from it.

In the next sections an attempt will be made to address the following questions using conditional statistical analysis:

1. Which drift direction is more significant to ship manoeuvring along the approach channel?
2. Are there strong correlations between drift directions and crosswinds and if so along which sections are these conditions dominant?
3. Does the drift experienced by deeper draught vessels depend on crosswinds or does the drift have other forcing mechanisms?
4. Do strong crosswinds correlate well with the direction of CTDV experienced by all types of vessels?

6.6.1. Which drift direction is more significant to ship manoeuvring along the approach channel?

This question was addressed by calculating the average CTDV values for both the north-westerly and south-easterly directions in sections 1 to 5 along the channel. The mean and standard deviations of the CTDV values are shown in Table 6-8.

Table 6-8: Mean and Standard deviations measured per section for south-easterly and north-westerly flowing CTDVs

SECTION	From NW		From SE	
	μ (m/s)	σ	μ (m/s)	σ
1	0.28	0.27	-0.33	0.43
2	0.23	0.28	-0.37	0.44
3	0.33	0.31	-0.38	0.51
4	0.33	0.38	-0.51	0.60
5	0.50	0.68	-0.57	0.65

From Table 6-8 the magnitude of mean values for south-easterly CTDVs appear to be slightly smaller then north-westerly CTDVs. Over sections 1,3 and 5 there were only small differences between the CTDV measurements i.e. approximately 12%. Larger differences (approximately 38%) were calculated over sections 2 and 4. The largest average drifts measured were measured in section 5 and were about 0.50m/s (1 knot) for south-easterly drifts and 0.57m/s (1.2 knots) for north-westerly drifts. From this data it is concluded that sections 2 and 4 experience somewhat larger north-westerly drifts than south-easterly drifts. These north-westerly drifts thus appear to be more significant to ship manoeuvring over these 2 sections of the approach channel.

6.6.2. Are there strong correlations between drift directions and crosswinds and if so along which sections are these conditions dominant?

This question was addressed using the CTDV data from sections 1 to 5 together with crosswind data. Table 6-9 shows the total number of ships that were used for the analysis per section.

Table 6-9: Total number of ships that were available for analysis along each relevant section of the approach channel

SECTION	1	2	3	4	5
TOTAL = 46	38	44	45	38	29

The CTDV data in each section were first averaged for each ship. The average CTDVs values for each section as well as the maximum CTDV values were then used for a correlation analysis. Normalised cross correlation coefficients (CCC) were used to indicate the statistical relationship between the two data sets. The average and maximum CTDV values for each ship track can be found tabulated in Appendix C for each section.

Table 6-10 shows the cross correlations coefficients between crosswinds and CTDVs. The highest correlations occurred in section 1 (0.33 and 0.40 for average and maximum CTDVs respectively).

Table 6-10: Cross correlations coefficients calculated between CTDV and crosswind data

SECTION	1	2	3	4	5
TOTAL = 46	38	44	45	38	29
Average	0.33	0.09	0.19	0.05	0.11
Maximum	0.40	0.25	0.19	-0.15	0.10

Further analysis was carried out by conditioning the correlations on the direction of the wind components. From the data set twenty-eight of the ships experienced north-westerly crosswinds whilst sixteen experienced south-easterly crosswinds. Table 6-11 and Table 6-12 show the cross correlations coefficients between the CTDV data conditioned on north-westerly or south-easterly crosswinds. From Table 6-11 it is evident that stronger correlations exist in sections 1 and 5. From Table 6-12 there appears to be a stronger correlation between the measured drift and south-easterly crosswinds in sections 3, while lower values were obtained for sections 1,2,4 and 5.

Table 6-11: Correlation values between CTDV and between CTDV and north-westerly crosswind data

SECTION	1	2	3	4	5
TOTAL = 28	22	27	27	23	18
Average	0.57	0.19	0.23	0.14	0.54
Maximum	0.67	0.14	0.11	-0.11	0.49

Table 6-12: Correlation values between CTDV and south-easterly crosswind data

SECTION	1	2	3	4	5
TOTAL = 18	15	17	18	16	11
Average	0.16	0.27	0.41	-0.05	0.03
Maximum	0.18	0.44	0.42	0.04	0.03

Even though sample sizes are small, it seems that it can be tentatively concluded that there is a trend whereby under strong north-westerly crosswinds pilots can expect stronger drifts towards the south-east in sections 1 and 5. These sections are at 1.5 and 4 kilometres from the south breakwater respectively. It is noted that poor correlations exist between south-easterly winds and north-westerly drifts in these two sections, however under prolonged south-easterly crosswinds, pilots can expect stronger drifts towards the north-west over section 3 at a range of 2.7 kilometres.

6.6.3. Does the drift experienced by deeper draught vessels depend on crosswinds or does the drift have other forcing mechanisms?

Specific examples were shown in sections 6.5.1 where the average drift direction experienced by deeper draught vessels were opposite to that of local crosswinds. This motivated the question posed here. The data set was conditioned on the ship draught, by dividing it into two subsets. The first subset was vessels with draughts less than or equal to 8.5 metres (23 ships) and the second for vessels of draughts greater than 8.5

meters (23 ships). Cross correlation coefficients between the CTDV data and crosswinds were determined for these two data subsets. Both the average and maximum CTDVs for each section were used for this analysis.

The cross correlation results are shown in Table 6-13 and Table 6-14. For shallower draught vessels larger cross correlation coefficients were obtained for sections 1 and section 2. For deeper draught vessels the largest cross correlation coefficients were obtained over sections 1 and 5. These correlations are however not high enough to reach any definite conclusions.

Table 6-13: Correlation values between CTDV and crosswind data for ships conditioned for draughts less than or equal to 8.5 metres

SECTION	1	2	3	4	5
TOTAL = 23	21	22	23	20	15
Average	0.37	0.17	0.20	-0.01	0.04
Maximum	0.44	0.36	0.25	-0.33	0.03

Table 6-14: Correlation values between CTDV and crosswind data for ships conditioned for draughts greater than 8.5 metres

SECTION	1	2	3	4	5
TOTAL = 23	16	21	22	19	14
Average	0.39	0.20	0.20	0.20	0.43
Maximum	0.34	0.38	0.12	0.07	0.37

The analysis was repeated with a different depth partition to check the robustness of the results. The data was split into vessels with draughts less than or equal to 7.8 metres (17 ships) and vessels of draughts greater than 9.6 meters (14 ships). The results are presented in Table 6-15 and Table 6-16. From Table 6-15 it is evident that fairly strong correlations for both the average and maximum CTDVs for shallower draught vessels exist, especially in section 1 and to some degree in section 3. It was also noticed that in section 4 for vessels less than 7.6m, there is a large but negative cross correlation coefficient. This may imply that the direction of drift in this section is independent of the local crosswind direction.

With respect to the deeper draught vessels, for both the average and maximum CTDV values, extremely weak correlations appear to exist in sections 2,3 and 4.

The cross correlation coefficients for average CTDVs over section 1 for both deeper and shallower draught vessel are similar. This seems to imply that the drift experienced in this section is to some degree independent of the draught of the vessel.

Table 6-15: Correlation values between CTDV and crosswind data conditioned for ship draughts less than or equal to 7.8 metres

SECTION	1	2	3	4	5
TOTAL = 17	15	17	17	14	10
Average	0.61	-0.09	0.41	-0.31	0.10
Maximum	0.59	0.08	0.39	-0.51	0.03

Table 6-16: Correlation values between CTDV and crosswind data conditioned for ship draughts greater than 9.6 metres

SECTION	1	2	3	4	5
TOTAL = 14	9	12	14	12	11
Average	0.61	0.24	0.05	0.17	0.54
Maximum	0.28	0.49	0.04	0.08	0.48

From the correlation analysis, it appears that correlations are in general poor for all conditions i.e. shallow and deep draught vessels. They are generally smaller for deeper draught vessels. These results thus suggest and provide further evidence for the earlier conclusions in section 6.5.1. Since the data set used is small, the results presented are uncertain.

There seems to be a stronger correlation between CTDV and crosswind data in section 1, which is independent of vessel draught. The pilots can thus expect that under strong crosswinds, they will experience stronger drifts in the direction of the crosswinds along section 1 of the approach channel irrespective of the draught of the ship being steered. This effect may be related to the shallower depths in this region.

6.6.4. Comparison with CSIR results

From the work carried out in CSIR (1999b), conclusions were reached that currents to the north-west, of the order 0.5 m/s (1 knot) appear to be more significant concerning their influence on keeping the ship on course than currents to the south-east, up to 0.8 m/s (1.5 knots). Under the latter conditions pilots appeared to safely manoeuvre a design ship into the port using a ship simulator.

From this investigation the maximum average measured CTDVs calculated were about 0.71m/s (1.4 knots) and 0.81m/s (1.5 knots) for drifts moving to north-westerly and south-easterly directions respectively. If it is assumed that the CTDVs measured in this investigation are representative of the local currents, then by comparing these values to the data from CSIR (1999b) it appears that currents to the north-west, presented by the CSIR appear to be smaller and more conservative then the currents in the same

direction presented here i.e. (by 0.21m/s or 0.4 knots). Currents to the south-east for both cases are similar in magnitude. More ship tracks are however required to further corroborate these comparisons.

6.6.5. Summary

In this section results have been presented which relate drift patterns to, wind speed and direction as well as ship draughts. The maximum correlation coefficient presented was 0.67 (refer Table 6-11). Figure 6-15 (a) and (c) are scatter plots of the data, which produced cross correlation coefficients of 0.67 and 0.14 respectively. From these plots the scatter in the data points is apparent. There appears to be some order for Figure 6-15 (a), but if the outlying points were removed from the data a decrease the overall correlation coefficient results (to 0.57). This scatter plot is shown in Figure 6-15 (b). By removing such outlying data points from the data used for Figure 6-15 (c), an improvement in correlation coefficient is found (to 0.28) as shown in Figure 6-15 (d). These scatter plots illustrate the sensitivity of the correlation coefficients presented in this section. Its sensitivity is increased as the number of data points in the data set decrease. More data points are thus required to substantiate and confirm the conclusions made in this section.

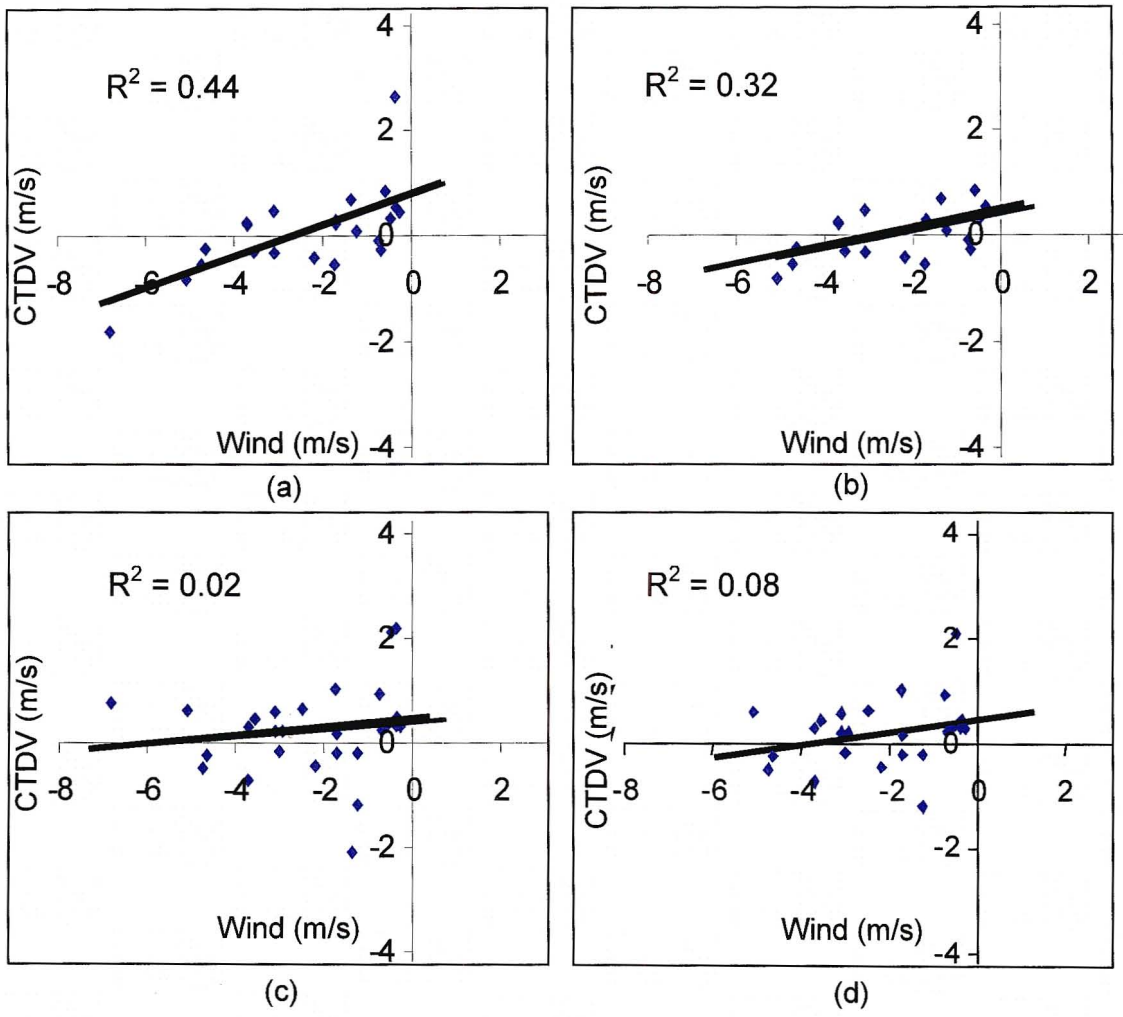

Figure 6-15: Scatter plot diagrams illustrating the maximum (a) and minimum (c) correlation coefficients presented in Table 6-11 for sections 1 (a) section 2 (c). Diagrams without spurious data for the same sections are shown in plots (b) and (d)

CHAPTER 7

SUMMARY AND CONCLUSIONS

7.1. Introduction

This investigation set out to develop and validate a new technology, which uses digital imaging to track ships entering a port and measures the direct effects of winds, waves and crosscurrents on the ships. This technology was then used to investigate the preferred entry patterns of pilots at Durban as well as investigate the spatial structure of the cross track drift experienced by ships along the Durban approach channel.

7.2. Summary

The new technology that is being proposed was explained and illustrated in the Chapter 3. The assumptions and limitations of the technology were discussed. The implementation of the proposed concept was described in the Chapter 4 with examples of actual ship track and CTDV data shown. The results of a key validation exercise were presented i.e. validation of ship track results using GPS's. Chapter 5 describes how this new technology was developed and applied for a real time automated monitoring system. Analysis of the ship track and CTDV data for forty-six ship tracks was presented in Chapter 6. Results were presented illustrating how ship slip, if accounted for in the calculation of CTDVs can be used to provide more accurate data.

7.3. Technological developments

It was initially unclear if the proposed imaging technology would work. The technology has evolved from initially using a digital still camera to a fixed video camera system. Software has been developed which monitors the approach channel, with the software triggering a capture sequence when a ship is detected entering the port and ending the capture sequence once the ship is out of the region of interest. The key function of this software is the feature tracking option, where specified objects can be tracked automatically. With this software, CTDV data as well as ship track plots can be obtained on a real-time basis.

7.4. Key findings regarding Ship Tracks and CTDV data

It was found that an overall bias towards the north-west side of the channel axis existed. For winds from the south-easterly sector, larger offsets towards the north-westerly side of the channel axis were found, with this trend probably reflecting the prevailing wind, current and wave conditions. It was found that deeper draught vessels have a smaller offset from the channel axis then shallower draught vessels. From the CTDV data it appears that harbour pilots steer their vessels from the north-west because they are aware of a dominant drift pattern from the south-east and prefer steering into the drift rather than away from it.

Examples have been found illustrating how currents that vary with depth, can result in the drift experienced by shallower draught ships being in the direction of the local crosswind (and associated surface currents) whilst the drift experienced by deeper draught vessels can be in the opposite direction. This was corroborated by a detailed analysis which showed that poor correlations exist between crosswinds and the CTDVs for deeper draught vessels (greater than 9.6 metres), which implies that the drift experienced by these vessels is generally independent of local crosswind conditions.

However, It was found that the average correlations between crosswinds and CTDVs were higher in section 1 (0 to 570m) of the channel and independent of vessel draught. Thus it appears that in strong crosswinds, harbour pilots will tend to experience stronger CTDVs in the crosswind direction over section 1 of the approach channel.

In general CTDVs from the south-east appear to be more common over sections 2 (570m to 1150m) and 4 (1730m to 2305m) of the approach channel. Fairly strong average correlations (cross correlation = 0.56) exist between CTDVs from the nort-west and crosswinds in sections 1 (0 to 570m) and 5 (2305m to 2880m).

The small sample of available ship tracks reduces the statistical certainty of the above results. Additional data is thus required to substantiate the conclusions.

7.5. CSIR comparison

The deviation results were found to be inconsistent with the findings of CSIR (1999b). The offsets from the channel axis were similar in magnitude but opposite in direction in the case of the simulated ship tracks. It is speculated that the port entry manoeuvres, as simulated by the Durban pilots on the Portsim simulator (CSIR, 1999b), were not representative of the actual conditions. Unfortunately, only one section along the

approach channel could be used where the data overlapped, so the conclusion remains tentative.

From this investigation the maximum sectional average measured CTDVs were about 0.71m/s (1.4 knots) and 0.81m/s (1.5 knots) for north-westerly and south-easterly moving CTDVs respectively. The limiting crosscurrent (north westerly currents) quoted by CSIR (1 knot) appears to be smaller than the drift components determined in this investigation. More ship tracks are however required to substantiate this conclusion conclusion.

7.6. Recommendations

A new innovative technology of measuring the direct affects of winds waves and crosscurrents on ships entering a port has been developed, validated and used to determine ship track and drift information for a wide range of ships and weather conditions. Based on this technological development, it is suggested that this new technology be further developed, into a more robust and commercial software package, which can be used at any port in the world. This type of technology is relatively cheap as compared to a more expensive option like the Acoustic Doppler Current Profilers in the case of current information. Even though ADCPs provide actual current data, they are unable to measure the response of ships to wind, waves and currents as in the case of the proposed technology. The data provided by this technology can therefore be used in conjunction with such a system to compliment and validate conclusions. With long term monitoring the information and data provided by this technology can be useful in making strategic decisions with respect to ship operations at a port.

REFERENCES

1. Aarninkhof, S.G.J (1996), "Quantification of Bar Bathymetry from Video Observations", Delft Hydraulics Report H2443
2. Bijker, E.W and Massie, W.W (1978). Coastal Engineering, Vol II,Chapter 4 : Channel Depth. Coastal Engineering Group, Delft University of Technology
3. Basson, J.F (1999), "Correlation and Neural Network Techniques Applied to Surf Zone Imaging", Master Thesis, University of Natal, p17
4. CSIR (1995),"Macro Sedimentary Dynamics around Durban", *CSIR Report EMAS-C 95080.*
5. CSIR (1999a), "Port of Durban: Entrance Channel Cross Currents Part 1: ADCP Transects". *CSIR Report ENV-S-C 99018A. Stellenbosch*
6. CSIR (1999b), "Port of Durban: Ship Maneuvering Simulations to Determine the Optimum Width of the Port Entrance Channel for Fully Laden Post-Panamax Container Vessels". *CSIR Report ENV-S-C 98127. Stellenbosch*
7. CSIR (1999c), "Port of Durban: Entrance Channel Cross Currents Part 2: ADCP Monitoring". *CSIR Report ENV-S-C 99018B. Stellenbosch,*
8. CSIR (2000), "Port of Durban: Ship Maneuvering Simulations to Determine the Optimum Width of the Port Entrance Channel for Fully Laden Post-Panamax Container Vessels". *CSIR Report ENV-S-C 2000-008. Stellenbosch*
9. CSIR (2001), "Simplex Ship Maneuvering Simulator: Review, Implementation and Potential of a PC-based Bridge-View Simulator for South African Ports". *CSIR Report ENV-S-C 2001-021. Stellenbosch*
10. Crowley, J.L & Coutaz, J. (1995) "Vision for man machine interaction. Proceedings of Engineering Human Computer Interaction", *EHCI'95*, Gran Targhee, USA, August 1995, Chapman & Hall Publ.
11. Demirbilek, Z & Sargent, F (1999). "Deep-Draught Coastal Navigation Channel Practice", *US Army Corps of Engineers, CHETN IX-1.*
12. Gordon, R.L (1996). "Acoustic Doppler Current Profiler, Principles of Operation, A practical Primer", RDI, San Diego
13. Haren, H.V (2001). "Estimates of sea level, waves and winds from a bottom – mounted ADCP in a shelf sea", *Journal of Sea Research Vol 45, p 1-14*
14. Harlow, E (1981). "Harbour/Port Entrance Design", p 13-25
15. Holland K.T; Holman R.A; Lippmann T.C; Stanley J and Plant N (1997). "Practical Use of Video Imagery in Nearshore Oceanographic Field Studies", *IEEE Journal of Oceanic Engineering, Vol 22, No.1, p 81-92*

16. Holman, R.A; Sallenger, A.H; Lippmann, T.C and Haines, J.W (1993). "The application of video image processing to the study of nearshore processes", *Oceanography,* vol.6, *p 78-85*
17. Kriebel, D.L; Alsina, M.V; Godfrey, M.L; Waters J.K and Mayer R.H (2000). "Deep-Draught Navigation Channel Design: A comparison of U.S. and International Practice", *Department of Naval Architecture and Ocean Engineering, United States Naval Academy*, Annaplois, MD 21402
18. Lane, A; Knight, P.J and Player, R.J (1999). "Current measurement technology for near shore waters", *Coastal Engineering 37, p 343-368*
19. Lippmann, T.C & Holman, R.A (1989). "Quantification of Sand Bar Morphology: A video Technique Based on Wave Dissipation". *Journal of Geophysical Research, Vol. 94, p 995-1011.*
20. Mardon, D.W & Stretch, D.D (2002). "The effects of wind speed, direction and duration on crosscurrents at the Port of Durban entrance", to be published in *1st International Conference on Heat Transfer, Fluid Mechanics, and Thermodynamics*, Kruger Park, South Africa, April 2002
21. Martin, J & Crowley, J.L (1995). Experimental Comparison of Correlation Tecniques, *Proceedings of the First International Workshop on Intelligent Adaptive Systems (IAS-95)*, Melbourne Beach, FL, April 26, 1995.
22. Moffit, F.H & Mikhail, E.M (1980), Photogrammetry 3rd Edition.
23. Musatenko, Y (2000), "MST IMAGE C++ LIBRARY SOFTWARE ", C++ library for reading or writing raster images v. 3.34, http://tetis.uazone.net/~yura/.
24. Nundlall, N (2001). "Ship Tracking and Cross-Currents at the Harbour Entrance", *Final year dissertation, School of Civil Engineering, University of Natal.*
25. Patel, S.R (1999), "Effects of Winds, Waves and Currents on Durbans Port Operations". *Final year dissertation, School of Civil Engineering, University of Natal.*
26. Patel, S.R & Stretch, D.D (2001), "Effects of Winds, Waves and Currents on Durbans Port Operations", *Proceedings of the Inaugural International Conference on Port and Maritime R&D and Technology*, Singapore, *Vol 1, p377-381.*
27. PIANC (1997), "Approach Channel: A guide for Design", *Final Report of the joint PIANCE-AIPH Working Group II - Brussels.*
28. PIANC (2002),"Guidelines for the Design of Fenders Systems: 2002", *Report of Working Group 33 of the Maritime Navigation Commission.*
29. Pinkel, R & Smith, R.A (1987). "Open ocean surface wave measurement using Doppler sonar". *Journal of Geophysical Research, 92, p 12967-12973.*

30. Press, W.H; Teukolsky, S.A; Vetterling, W.T and Flannery, B.P (1992). "Numerical Recipes in C - The art of scientific Computing", Second Edition, p 504-510
31. Richardson, P.L (1997). "Drifting in the wind: leeway error in shipdrift data". *Deep-Sea Research, Vol. 44, No. 11, p 1877-1903*
32. Schott, F (1989). "Measuring winds from underneath the ocean surface by upward looking acoustic Doppler current profilers". *Journal of Geophysical Research, 94, p 8313-8321.*
33. Segal, M.P (2000). "South African Metocean Conditions an Overview". The Energy and Geoscience Institute, The University of Utah, Salt Lake City, UT 84108.
34. Stretch, D.D (2001). Personal communication.
35. Tsanis, I.K (1989) "Simulation of Wind-Induced Water Currents". *Journal of Hydraulic Engineering*, ASCE, Vol.115, p 1113-1133.
36. USACE. (1995). "Hydraulic Design Guidance for Deep-Draught Navigation Projects", Engineer Manual 1110-2-1613, Washington DC.
37. Visbeck, M & Fischer, J. (1995). "Sea surface conditions remotely sensed by upward-looking ADCPs". *Journal of Atmospheric Oceanic Technology,12, p 141-149.*
38. Wewetzer, S.F.K, Duck, R.W, Anderson J.M (1998), "Acoustic Doppler current profiler measurements in coastal and estuarine environments: examples for the Tay Estuary", Scotland, *Geomorphology 29, p 21-30*
39. Wolf, P.R (1974), "Elements of Photogrammetry: with air photo interpretation and remote sensing"
40. Wu, J (1975). "Wind Induced Drift Currents". *Journal of Hydraulic Engineering, Vol. 68(1), p 49-70*
41. Wu, J & Tsanis, I.K (1995). "Numerical Study of Wind Induced Drift Currents". *Journal of Hydraulic Engineering*, May 1995, *Vol.121, p 388-395*

APPENDICES

Appendix A: CROSS CORRELATION DERIVATION

The cross correlation is a statistic that can be used to determine whether two sets of data are related. For a positive correlation, large values in one set are associated with larger values in the other. For a negative correlation small values in one set are associated with larger values in the other. Small correlations occur if values in the two data sets are unrelated. The normalised cross correlation coefficient (CCC) is defined as,

$$\rho_{U,V} = \frac{Cov(U,V)}{\sigma_U . \sigma_V}$$

where,

$$Cov(U,V) = \frac{1}{n}\Sigma\left(U_i - \overline{U}\right)\left(V_i - \overline{V}\right)$$

and,

$$\sigma_U^2 = \frac{1}{n}\Sigma\left(U_i - \overline{U}\right)^2$$

$$\sigma_V^2 = \frac{1}{n}\Sigma\left(V_i - \overline{V}\right)^2$$

with *n* the number of values in each data set.

A vector cross correlation coefficient (VCCC) can be similarly defined to measure the relationship between two vector-valued data sets. The vector cross correlation coefficient calculation returns the covariance of the two vector-valued sets divided by the product of their standard deviations. All products are interpreted as scalar products in this case. Whence,

$$Cov(U,V) = \frac{1}{n}\sum\left(\overline{U \cdot V} - \overline{U} \cdot \overline{V}\right)$$

$$Cov(U,V) = \frac{1}{n}\sum\left(\overline{\left[U_R\, U_G\, U_B\right] \cdot \begin{bmatrix} V_R \\ V_G \\ V_B \end{bmatrix}} - \left(\overline{\left[U_R\, U_G\, U_B\right]} \cdot \begin{bmatrix} \overline{V_R} \\ \overline{V_G} \\ \overline{V_B} \end{bmatrix}\right)\right)$$

$$Cov(U,V) = \frac{1}{n}\sum\left(\overline{U_R \cdot V_R + U_G \cdot V_G + U_B \cdot V_B} - \left(\overline{U_R} \cdot \overline{V_R} + \overline{U_G} \cdot \overline{V_G} + \overline{U_B} \cdot \overline{V_B}\right)\right)$$

and:

$$\sigma_U = \sqrt{\left(\frac{1}{n}\sum\left(\overline{(U \cdot U)} - \overline{U} \cdot \overline{U}\right)\right)}$$

$$\sigma_U = \sqrt{\frac{1}{n}\sum\left(\overline{U_R{}^2 + U_G{}^2 + U_B{}^2} - \left(\overline{U_R}^2 + \overline{U_G}^2 + \overline{U_B}^2\right)\right)}$$

where

$$\overline{U_R} = \frac{1}{n}\Sigma(U_R)$$

and similarly for U_G and U_B

and:

$$\sigma_V = \sqrt{\left(\frac{1}{n}\sum\left(\overline{(V \cdot V)} - \overline{V} \cdot \overline{V}\right)\right)}$$

$$\sigma_V = \sqrt{\frac{1}{n}\sum\left(\overline{V_R{}^2 + V_G{}^2 + V_B{}^2} - \left(\overline{V_R}^2 + \overline{V_G}^2 + \overline{V_B}^2\right)\right)}$$

Appendix B: SHIP CHARACTERISTIC DATA

B.1. All Ship data

NO	DATE	TIME	NAME OF SHIP	LENGTH (m)	DRAUGHT (m)	GROSS TONNAGE (tonnes)
1	17/8/99	12:42 PM	Heron	188	8.9	22009
2	20/8/99	12:30 PM	CMBT Tana	113	7	6030
3	23/8/99	12:00 PM	Silver Ying	195	9.8	27117
4	24/8/99	6:20 AM	Del Kalahari	258	10	53000
5	27/8/99	7:30 AM	Silver Star	106	6.6	3731
6	27/8/99	8:23 AM	Anangel Dignity	182.8	11.5	24643
7	31/8/99	8:01 AM	Louis Pasteur	138	7.6	9438
8	31/8/99	8:31 AM	Liberty Star	176	10.4	16000
9	02/9/99	11:15 AM	Alam Tangari	146	9.4	10511
10	02/9/99	9:40 AM	Iran Motahari	197.6	10.8	20471
11	02/9/99	8:34 AM	Sea Spirit K	186	5.4	21228
12	02/9/99	9:25 AM	Socol 6	113	7.8	7000
13	03/9/99	7:40 AM	Frio Hellanic	148	6.6	9997
14	03/9/99	10:20 AM	Salinthip Naree	153	9.9	13000
15	03/9/99	7:10 AM	Glacier Bay	149	6.1	8739
16	17/9/99	8:10 AM	SAS Drakensburg	148	7.8	12500
17	17/9/99	9:30 AM	Corel Mermaid	141.8	8.4	9829
18	04/2/00	6:20 AM	Royal Sphere	258	10	53000
19	10/5/00	7:20 AM	Barrier	140	6.6	8000
20	16/5/00	7:40 AM	Joe Grand	175	10.5	23914
21	16/5/00	6:50 AM	Ned Clarence	204	9.5	33000
22	17/7/00	12:15 PM	Meng Hai	189	11.4	26782
23	17/7/00	1:23 PM	Saigon 5	144	8.8	9114
24	18/7/00	8:00 AM	Msc Melbourne	203	8.5	22589
25	18/7/00	9:20 AM	Jo Lonne	175	9.6	22772
26	19/7/00	6:30 AM	Camboda Star	113	5.6	5000
27	19/7/00	8:50 AM	Master Nicos	179	9.7	17858
28	19/3/01	3:50 AM	Marulaki	193	8.4	22118
29	20/3/01	11:25 AM	Meva	90	9	3297
30	22/3/01	2:36 PM	Ociurance	176	7.3	12284
31	23/3/01	9:55 AM	Evergenius	231	5	37000
32	26/3/01	8:18 AM	Berge Clipper	224	8.7	45032
33	28/3/01	9:11 AM	Prosprim Cont	183	7.8	17125
34	28/3/01	1:01 PM	Jorbony	129	7.9	7915
35	29/3/01	2:52 PM	Lissosm	170	10	18235
36	02/4/01	12:20 PM	SD Truimph	225	11.8	38267
37	02/4/01	1:30 PM	Emirate Star 2	169	6.5	14539
38	03/4/01	1:42 PM	Iran Jamal	190	8.5	25763
39	04/4/01	12:25 PM	Ned Rio Grande	182	10	21600
40	05/4/01	12:54 PM	Barbrite Arrow	199	9	27470
41	09/4/01	10:45 AM	Pride	164	9	14151
42	10/4/01	10:44 AM	Feng Anshan	156	8.5	13367
43	10/4/01	3:07 PM	Namibia	143	5.9	10573
44	30/08/01	11:52 AM	Bella Lontra	190	5.6	n/a
45	11/9/01	9:14 AM	Global Mombasa	113	6.2	n/a
46	18/9/01	6:33 AM	Alam Senang	178	10.5	n/a

B.2. All ships with wind direction speed and crosswind components

No	Date	Name of Ship	Length (m)	Draught (m)	Wind direction (degrees)	Wind Speed (m/s)	Crosswinds (m/s)
1	17/8/99	Heron	188	8.9	161.8	4.4	-3.6
2	20/8/99	CMBT Tana	113	7	44.6	6.0	-1.0
3	23/8/99	Silver Ying	195	9.8	178.5	8.0	-4.8
4	24/8/99	Del Kalahari	258	10	223.9	10.6	1.6
5	27/8/99	Silver Star	106	6.6	304.0	3.1	3.1
6	27/8/99	Anangel Dignity	182.8	11.5	305.9	2.9	2.9
7	31/8/99	Louis Pasteur	138	7.6	297.2	1.3	1.3
8	31/8/99	Liberty Star	176	10.4	297.2	1.3	1.3
9	02/9/99	Alam Tangari	146	9.4	272.8	4.4	3.7
10	02/9/99	Iran Motahari	197.6	10.8	247.9	3.2	1.7
11	02/9/99	Sea Spirit K	186	5.4	247.9	3.2	1.7
12	02/9/99	Socol 6	113	7.8	282.5	0.8	0.7
13	03/9/99	Frio Hellanic	148	6.6	13.7	18.3	6.8
14	03/9/99	Salinthip Naree	153	9.9	21.3	19.0	4.6
15	03/9/99	Glacier Bay	149	6.1	26.9	20.7	3.1
16	17/9/99	SAS Drakensburg	148	7.8	217.0	14.2	0.4
17	17/9/99	Corel Mermaid	141.8	8.4	210.7	13.4	-1.1
18	04/2/00	Royal Sphere	258	10	11.5	7.4	3.0
19	10/5/00	Barrier	140	6.6	274.5	4.1	3.6
20	16/5/00	Joe Grand	175	10.5	297.5	4.8	4.7
21	16/5/00	Ned Clarence	204	9.5	301.3	5.1	5.1
22	17/7/00	Meng Hai	189	11.4	39.9	4.1	-0.3
23	17/7/00	Saigon 5	144	8.8	72.6	2.2	-1.3
24	18/7/00	Msc Melbourne	203	8.5	291.4	3.8	3.7
25	18/7/00	Jo Lonne	175	9.6	346.4	3.3	2.5
26	19/7/00	Camboda Star	113	5.6	209.6	5.8	-0.6
27	19/7/00	Master Nicos	179	9.7	217.9	6.6	0.3
28	19/3/01	Marulaki	193	8.4	80.0	2.8	-2.0
29	20/3/01	Meva	90	9	150.0	2.4	-2.2
30	22/3/01	Ociurance	176	7.3	50.0	5.0	-1.3
31	23/3/01	Evergenius	231	5	30.0	3.8	0.4
32	26/3/01	Berge Clipper	224	8.7	320.0	1.8	1.7
33	28/3/01	Prosprim Cont	183	7.8	190.0	1.6	-0.7
34	28/3/01	Jorbony	129	7.9	120.0	4.3	-4.3
35	29/3/01	Lissosm	170	10	70.0	5.5	-3.1
36	02/4/01	SD Truimph	225	11.8	160.0	4.7	-3.9
37	02/4/01	Emirate Star 2	169	6.5	130.0	3.9	-3.9
38	03/4/01	Iran Jamal	190	8.5	210.0	9.0	-0.9
39	04/4/01	Ned Rio Grande	182	10	220.0	6.2	0.5
40	05/4/01	Barbrite Arrow	199	9	190.0	2.6	-1.1
41	09/4/01	Pride	164	9	30.0	6.2	0.6
42	10/4/01	Feng Anshan	156	8.5	220.0	4.7	0.4
43	10/4/01	Namibia	143	5.9	170.0	5.4	-3.9
44	30/08/01	Bella Lontra	190	5.6	220.0	9.6	0.8
45	11/9/01	Global Mombasa	113	6.2	240.0	5.3	2.2
46	18/9/01	Alam Senang	178	10.5	330.0	1.5	1.4

B.3. Ships with crosswinds from South-East (Total 18)

NO	DATE	NAME OF SHIP	WIND DIRECTION (degrees)	WIND SPEED (m/s)	CROSS-WINDS (m/s)
1	17/8/99	Heron	161.8	4.4	-3.6
2	20/8/99	CMBT Tana	44.6	6.0	-1.0
3	23/8/99	Silver Ying	178.5	8.0	-4.8
17	17/9/99	Corel Mermaid	210.7	13.4	-1.1
22	17/7/00	Meng Hai	39.9	4.1	-0.3
23	17/7/00	Saigon 5	72.6	2.2	-1.3
26	19/7/00	Camboda Star	209.6	5.8	-0.6
28	19/3/01	Marulaki	80.0	2.8	-2.0
29	20/3/01	Meva	150.0	2.4	-2.2
30	22/3/01	Ociurance	50.0	5.0	-1.3
33	28/3/01	Prosprim Cont	190.0	1.6	-0.7
34	28/3/01	Jorbony	120.0	4.3	-4.3
35	29/3/01	Lissosm	70.0	5.5	-3.1
36	02/4/01	SD Truimph	160.0	4.7	-3.9
37	02/4/01	Emirate Star 2	130.0	3.9	-3.9
38	03/4/01	Iran Jamal	210.0	9.0	-0.9
40	05/4/01	Barbrite Arrow	190.0	2.6	-1.1
43	10/4/01	Namibia	170.0	5.4	-3.9

B.4. Ships with crosswinds from the North-West (Total 28)

NO	DATE	NAME OF SHIP	WIND DIRECTION (degrees)	WIND SPEED (m/s)	CROSS-WINDS (m/s)
4	24/8/99	Del Kalahari	223.9	10.6	1.6
5	27/8/99	Silver Star	304.0	3.1	3.1
6	27/8/99	Anangel Dignity	305.9	2.9	2.9
7	31/8/99	Louis Pasteur	297.2	1.3	1.3
8	31/8/99	Liberty Star	297.2	1.3	1.3
9	02/9/99	Alam Tangari	272.8	4.4	3.7
10	02/9/99	Iran Motahari	247.9	3.2	1.7
11	02/9/99	Sea Spirit K	247.9	3.2	1.7
12	02/9/99	Socol 6	282.5	0.8	0.7
13	03/9/99	Frio Hellanic	13.7	18.3	6.8
14	03/9/99	Salinthip Naree	21.3	19.0	4.6
15	03/9/99	Glacier Bay	26.9	20.7	3.1

16	17/9/99	SAS Drakensburg	217.0	14.2	0.4
18	04/2/00	Royal Sphere	11.5	7.4	3
19	10/5/00	Barrier	274.5	4.1	3.6
20	16/5/00	Joe Grand	297.5	4.8	4.7
21	16/5/00	Ned Clarence	301.3	5.1	5.1
24	18/7/00	Msc Melbourne	291.4	3.8	3.7
25	18/7/00	Jo Lonne	346.4	3.3	2.5
27	19/7/00	Master Nicos	217.9	6.6	0.3
31	23/3/01	Evergenius	30.0	3.8	0.4
32	26/3/01	Berge Clipper	320.0	1.8	1.7
39	04/4/01	Ned Rio Grande	220.0	6.2	0.5
41	09/4/01	Pride	30.0	6.2	0.6
42	10/4/01	Feng Anshan	220.0	4.7	0.4
44	30/08/01	Bella Lontra	220.0	9.6	0.8
45	11/9/01	Global Mombasa	240.0	5.3	2.2
46	18/9/01	Alam Senang	330.0	1.5	1.4

B.5. Ship's with draught less then or equal to 8.5 metres (Total 23)

NO	DATE	NAME OF SHIP	LENGTH (m)	DRAUGHT (m)	WIND DIRECTION (m/s)	WIND SPEED (m/s)	CROSS-WINDS (m/s)
2	20/8/99	CMBT Tana	113	7	44.6	6.0	-1.0
5	27/8/99	Silver Star	106	6.6	304.0	3.1	3.1
7	31/8/99	Louis Pasteur	138	7.6	297.2	1.3	1.3
11	02/9/99	Sea Spirit K	186	5.4	247.9	3.2	1.7
12	02/9/99	Socol 6	113	7.8	282.5	0.8	0.7
13	03/9/99	Frio Hellanic	148	6.6	13.7	18.3	6.8
15	03/9/99	Glacier Bay	149	6.1	26.9	20.7	3.1
16	17/9/99	SAS Drakensburg	148	7.8	217.0	14.2	0.4
17	17/9/99	Corel Mermaid	141.8	8.4	210.7	13.4	-1.1
19	10/5/00	Barrier	140	6.6	274.5	4.1	3.6
24	18/7/00	Msc Melbourne	203	8.5	291.4	3.8	3.7
26	19/7/00	Camboda Star	113	5.6	209.6	5.8	-0.6
28	19/3/01	Marulaki	193	8.4	80.0	2.8	-2.0
30	22/3/01	Ociurance	176	7.3	50.0	5.0	-1.3
31	23/3/01	Evergenius	231	5	30.0	3.8	0.4
33	28/3/01	Prosprim Cont	183	7.8	190.0	1.6	-0.7

34	28/3/01	Jorbony	129	7.9	120.0	4.3	-4.3
37	02/4/01	Emirate Star 2	169	6.5	130.0	3.9	-3.9
38	03/4/01	Iran Jamal	190	8.5	210.0	9.0	-0.9
42	10/4/01	Feng Anshan	156	8.5	220.0	4.7	0.4
43	10/4/01	Namibia	143	5.9	170.0	5.4	-3.9
44	30/08/01	Bella Lontra	190	5.6	220.0	9.6	0.8
45	11/9/01	Global Mombasa	113	6.2	240.0	5.3	2.2

B.6. Ships with draught greater than 8.5 metres (Total 23)

NO	DATE	NAME OF SHIP	LENGTH (m)	DRAUGHT (m)	WIND DIRECTION (m/s)	WIND SPEED (m/s)	CROSS-WINDS (m/s)
1	17/8/99	Heron	188	8.9	161.8	4.4	-3.6
3	23/8/99	Silver Ying	195	9.8	178.5	8.0	-4.8
4	24/8/99	Del Kalahari	258	10	223.9	10.6	1.6
6	27/8/99	Anangel Dignity	182.8	11.5	305.9	2.9	2.9
8	31/8/99	Liberty Star	176	10.4	297.2	1.3	1.3
9	02/9/99	Alam Tangari	146	9.4	272.8	4.4	3.7
10	02/9/99	Iran Motahari	197.6	10.8	247.9	3.2	1.7
14	03/9/99	Salinthip Naree	153	9.9	21.3	19.0	4.6
18	04/2/00	Royal Sphere	258	10	11.5	7.4	3.0
20	16/5/00	Joe Grand	175	10.5	297.5	4.8	4.7
21	16/5/00	Ned Clarence	204	9.5	301.3	5.1	5.1
22	17/7/00	Meng Hai	189	11.4	39.9	4.1	-0.3
23	17/7/00	Saigon 5	144	8.8	72.6	2.2	-1.3
25	18/7/00	Jo Lonne	175	9.6	346.4	3.3	2.5
27	19/7/00	Master Nicos	179	9.7	217.9	6.6	0.3
29	20/3/01	Meva	90	9	150.0	2.4	-2.2
32	26/3/01	Berge Clipper	224	8.7	320.0	1.8	1.7
35	29/3/01	Lissosm	170	10	70.0	5.5	-3.1
36	02/4/01	SD Truimph	225	11.8	160.0	4.7	-3.9
39	04/4/01	Ned Rio Grande	182	10	220.0	6.2	0.5
40	05/4/01	Barbrite Arrow	199	9	190.0	2.6	-1.1
41	09/4/01	Pride	164	9	30.0	6.2	0.6
46	18/9/01	Alam Senang	178	10.5	330.0	1.5	1.4

Appendix C: AVERAGE AND MAXIMUM CTDV DATA FOR EACH SECTION

C.1. Section 1

NO	NAME OF SHIP	AVERAGE CTDV (m/s)	MAXIMUM CTDV (m/s)	CROSSWINDS (m/s)	DRAUGHT (m)
1	Heron	n/a	n/a	-3.565	8.90
2	CMBT Tana	0.042	0.264	-0.956	7.00
3	Silver Ying	n/a	n/a	-4.821	9.77
4	Del Kalahari	n/a	n/a	1.560	10.00
5	Silver Star	-0.346	-0.463	3.097	6.60
6	Anangel Dignity	n/a	n/a	2.931	11.54
7	Louis Pasteur	-0.083	-0.083	1.250	7.60
8	Liberty Star	n/a	n/a	1.250	10.40
9	Alam Tangari	-0.162	-0.240	3.706	9.35
10	Iran Motahari	0.004	-0.281	1.709	10.80
11	Sea Spirit K	0.011	-0.227	1.709	7.80
12	Socol 6	0.042	0.260	0.696	7.80
13	Frio Hellanic	1.813	1.813	6.822	6.60
14	Salinthip Naree	0.180	0.247	4.648	9.90
15	Glacier Bay	0.064	0.322	3.089	6.10
16	SAS Drakensburg	n/a	n/a	0.373	7.80
17	Corel Mermaid	-0.150	-0.296	-1.120	8.40
18	Royal Sphere	n/a	n/a	3.007	10.00
19	Barrier	0.044	0.294	3.555	6.60
20	Joe Grand	0.092	0.537	4.741	10.50
21	Ned Clarence	0.204	0.811	5.085	9.50
22	Meng Hai	-0.162	-0.268	-0.315	11.40
23	Saigon 5	-0.375	-0.375	-1.304	8.80
24	Msc Melbourne	-0.165	-0.214	3.699	8.50
25	Jo Lonne	n/a	n/a	2.477	9.60
26	Camboda Star	0.025	-0.267	-0.597	5.60
27	Master Nicos	-0.159	-0.445	0.281	9.70
28	Marulaki	-0.149	-0.586	-1.963	8.40
29	Meva	-0.045	-0.356	-2.184	9.00
30	Ociurance	0.298	0.784	-1.252	7.30
31	Evergenius	-0.342	-0.527	0.364	5.00
32	Berge Clipper	-0.024	0.545	1.743	8.70
33	Prosprim Cont	-0.112	-0.594	-0.689	7.80
34	Jorbony	0.000	-0.486	-4.280	7.90
35	Lissosm	0.039	0.478	-3.115	10.00
36	SD Truimph	-0.174	-0.422	-3.873	11.80
37	Emirate Star 2	-0.281	-0.525	-3.888	6.50
38	Iran Jamal	-0.152	-0.502	-0.863	8.50
39	Ned Rio Grande	-0.038	-0.318	0.486	10.00
40	Barbrite Arrow	0.290	0.652	-1.119	9.00
41	Pride	-0.021	-0.833	0.594	9.00
42	Feng Anshan	-2.051	-2.634	0.369	8.50
43	Namibia	n/a	n/a	-3.852	5.90
44	Bella Lontra	0.059	0.092	0.753	5.60
45	Global Mombasa	0.072	0.417	2.198	6.20
46	Alam Senang	0.217	-0.683	1.365	10.50

C.2. Section 2

NO	NAME OF SHIP	AVERAGE CTDV (m/s)	MAXIMUM CTDV (m/s)	CROSSWINDS (m/s)	DRAUGHT (m)
1	Heron	-0.093	-0.118	-3.565	8.90
2	CMBT Tana	0.144	0.220	-0.956	7.00
3	Silver Ying	n/a	n/a	-4.821	9.77
4	Del Kalahari	n/a	n/a	1.560	10.00
5	Silver Star	-0.118	-0.599	3.097	6.60
6	Anangel Dignity	-0.161	-0.222	2.931	11.54
7	Louis Pasteur	0.052	0.190	1.250	7.60
8	Liberty Star	1.173	1.173	1.250	10.40
9	Alam Tangari	-0.125	0.706	3.706	9.35
10	Iran Motahari	-0.010	-0.175	1.709	10.80
11	Sea Spirit K	0.087	0.195	1.709	7.80
12	Socol 6	-0.060	-0.248	0.696	7.80
13	Frio Hellanic	-0.571	-0.766	6.822	6.60
14	Salinthip Naree	0.096	0.231	4.648	9.90
15	Glacier Bay	0.085	-0.219	3.089	6.10
16	SAS Drakensburg	-0.261	-0.324	0.373	7.80
17	Corel Mermaid	-0.169	-0.265	-1.120	8.40
18	Royal Sphere	-0.021	0.161	3.007	10.00
19	Barrier	0.053	-0.452	3.555	6.60
20	Joe Grand	0.250	0.479	4.741	10.50
21	Ned Clarence	-0.096	-0.619	5.085	9.50
22	Meng Hai	-0.226	-0.706	-0.315	11.40
23	Saigon	-0.389	-0.618	-1.304	8.80
24	Msc Melbourne	-0.033	-0.310	3.699	8.50
25	Jo Lonne	-0.141	-0.644	2.477	9.60
26	Camboda Star	0.021	-0.292	-0.597	5.60
27	Master Nicos	-0.129	-0.320	0.281	9.70
28	Marulaki	-0.144	-0.591	-1.963	8.40
29	Meva	-0.032	-0.567	-2.184	9.00
30	Ocuirance	0.469	1.467	-1.252	7.30
31	Evergenius	-0.130	-0.491	0.364	5.00
32	Berge Clipper	-0.022	-1.025	1.743	8.70
33	Prosprim Cont	-0.025	0.629	-0.689	7.80
34	Jorbony	-0.043	-0.457	-4.280	7.90
35	Lissossm	-0.114	-2.425	-3.115	10.00
36	SD Truimph	-0.109	-0.433	-3.873	11.80
37	Emirate Star 2	-0.320	-1.451	-3.888	6.50
38	Iran Jamal	-0.274	-0.664	-0.863	8.50
39	Ned Rio Grande	-0.399	-2.124	0.486	10.00
40	Barbrite Arrow	-0.029	-0.534	-1.119	9.00
41	Pride	-0.006	-0.315	0.594	9.00
42	Feng Anshan	-1.784	-2.193	0.369	8.50
43	Namibia	-0.432	-1.345	-3.852	5.90
44	Bella Lontra	-0.345	-0.931	0.753	5.60
45	Global Mombasa	-0.095	0.436	2.198	6.20
46	Alam Senang	0.441	2.093	1.365	10.50

C.3. Section 3

NO	NAME OF SHIP	AVERAGE CTDV (m/s)	MAXIMUM CTDV (m/s)	CROSSWINDS (m/s)	DRAUGHT (m)
1	Heron	-0.131	-0.131	-3.565	8.90
2	CMBT Tana	0.515	1.169	-0.956	7.00
3	Silver Ying	-0.298	-0.346	-4.821	9.77
4	Del Kalahari	-0.357	-0.405	1.560	10.00
5	Silver Star	0.103	0.142	3.097	6.60
6	Anangel Dignity	-0.139	-0.164	2.931	11.54
7	Louis Pasteur	0.252	0.844	1.250	7.60
8	Liberty Star	-0.108	-0.179	1.250	10.40
9	Alam Tangari	0.000	0.000	3.706	9.35
10	Iran Motahari	-0.114	-0.462	1.709	10.80
11	Sea Spirit K	-0.062	-0.084	1.709	7.80
12	Socol 6	-0.126	-0.250	0.696	7.80
13	Frio Hellanic	0.158	0.229	6.822	6.60
14	Salinthip Naree	-0.268	-0.418	4.648	9.90
15	Glacier Bay	-0.121	-0.358	3.089	6.10
16	SAS Drakensburg	-0.105	-0.242	0.373	7.80
17	Corel Mermaid	-0.135	-0.200	-1.120	8.40
18	Royal Sphere	-0.509	-1.299	3.007	10.00
19	Barrier	0.102	0.320	3.555	6.60
20	Joe Grand	0.189	1.030	4.741	10.50
21	Ned Clarence	-0.012	-0.564	5.085	9.50
22	Meng Hai	-0.224	-0.639	-0.315	11.40
23	Saigon	-0.380	-0.580	-1.304	8.80
24	Msc Melbourne	-0.102	-0.694	3.699	8.50
25	Jo Lonne	-0.118	0.722	2.477	9.60
26	Camboda Star	-0.073	-0.388	-0.597	5.60
27	Master Nicos	-0.128	-0.336	0.281	9.70
28	Marulaki	-0.153	-0.482	-1.963	8.40
29	Meva	-0.680	-1.661	-2.184	9.00
30	Ocuirance	0.206	0.947	-1.252	7.30
31	Evergenius	0.007	0.956	0.364	5.00
32	Berge Clipper	0.369	1.352	1.743	8.70
33	Prosprim Cont	0.081	0.368	-0.689	7.80
34	Jorbony	-0.046	-0.338	-4.280	7.90
35	Lissossm	0.071	0.681	-3.115	10.00
36	SD Truimph	-0.161	-0.427	-3.873	11.80
37	Emirate Star 2	-0.363	-0.933	-3.888	6.50
38	Iran Jamal	-0.063	1.355	-0.863	8.50
39	Ned Rio Grande	-0.030	-0.713	0.486	10.00
40	Barbrite Arrow	0.159	1.067	-1.119	9.00
41	Pride	0.031	0.813	0.594	9.00
42	Feng Anshan	-2.067	-3.027	0.369	8.50
43	Namibia	-1.029	-3.925	-3.852	5.90
44	Bella Lontra	-0.551	-1.071	0.753	5.60
45	Global Mombasa	-0.223	-0.394	2.198	6.20
46	Alam Senang	0.558	1.014	1.365	10.50

C.4. Section 4

NO	NAME OF SHIP	AVERAGE CTDV (m/s)	MAXIMUM CTDV (m/s)	CROSSWINDS (m/s)	DRAUGHT (m)
1	Heron	-0.081	-0.137	-3.565	8.90
2	CMBT Tana	-0.265	-0.454	-0.956	7.00
3	Silver Ying	-0.390	-0.631	-4.821	9.77
4	Del Kalahari	-0.276	-0.356	1.560	10.00
5	Silver Star	0.058	0.066	3.097	6.60
6	Anangel Dignity	-0.318	-0.361	2.931	11.54
7	Louis Pasteur	-0.319	-0.319	1.250	7.60
8	Liberty Star	-0.075	-0.149	1.250	10.40
9	Alam Tangari	n/a	n/a	3.706	9.35
10	Iran Motahari	n/a	n/a	1.709	10.80
11	Sea Spirit K	0.264	0.447	1.709	7.80
12	Socol 6	-0.396	-1.043	0.696	7.80
13	Frio Hellanic	-0.706	-2.496	6.822	6.60
14	Salinthip Naree	0.098	0.165	4.648	9.90
15	Glacier Bay	n/a	n/a	3.089	6.10
16	SAS Drakensburg	-0.149	-0.236	0.373	7.80
17	Corel Mermaid	0.001	0.289	-1.120	8.40
18	Royal Sphere	n/a	n/a	3.007	10.00
19	Barrier	0.071	0.524	3.555	6.60
20	Joe Grand	0.169	0.519	4.741	10.50
21	Ned Clarence	-0.081	-0.516	5.085	9.50
22	Meng Hai	-0.174	-0.358	-0.315	11.40
23	Saigon	n/a	n/a	-1.304	8.80
24	Msc Melbourne	-0.023	-0.327	3.699	8.50
25	Jo Lonne	-0.167	-0.810	2.477	9.60
26	Camboda Star	-0.002	0.655	-0.597	5.60
27	Master Nicos	-0.390	-0.757	0.281	9.70
28	Marulaki	-1.290	-2.532	-1.963	8.40
29	Meva	-0.957	-2.216	-2.184	9.00
30	Ocuirance	0.543	2.851	-1.252	7.30
31	Evergenius	0.042	0.898	0.364	5.00
32	Berge Clipper	-0.098	-0.098	1.743	8.70
33	Prosprim Cont	-0.047	-0.475	-0.689	7.80
34	Jorbony	0.227	1.554	-4.280	7.90
35	Lissossm	0.206	1.067	-3.115	10.00
36	SD Truimph	0.121	0.121	-3.873	11.80
37	Emirate Star 2	n/a	n/a	-3.888	6.50
38	Iran Jamal	-0.291	0.982	-0.863	8.50
39	Ned Rio Grande	-0.042	0.481	0.486	10.00
40	Barbrite Arrow	0.075	0.869	-1.119	9.00
41	Pride	n/a	n/a	0.594	9.00
42	Feng Anshan	-1.903	-2.553	0.369	8.50
43	Namibia	n/a	n/a	-3.852	5.90
44	Bella Lontra	-0.339	-1.275	0.753	5.60
45	Global Mombasa	0.607	0.607	2.198	6.20
46	Alam Senang	0.447	0.989	1.365	10.50

C.5. Section 5

NO	NAME OF SHIP	AVERAGE CTDV (m/s)	MAXIMUM CTDV (m/s)	CROSSWINDS (m/s)	DRAUGHT (m)
1	Heron	-0.006	-0.006	-3.565	8.90
2	CMBT Tana	n/a	n/a	-0.956	7.00
3	Silver Ying	-0.215	-0.423	-4.821	9.77
4	Del Kalahari	-0.333	-0.333	1.560	10.00
5	Silver Star	0.065	0.102	3.097	6.60
6	Anangel Dignity	-0.143	-0.447	2.931	11.54
7	Louis Pasteur	n/a	n/a	1.250	7.60
8	Liberty Star	-0.229	-0.313	1.250	10.40
9	Alam Tangari	n/a	n/a	3.706	9.35
10	Iran Motahari	n/a	n/a	1.709	10.80
11	Sea Spirit K	n/a	n/a	1.709	7.80
12	Socol 6	-0.559	-0.559	0.696	7.80
13	Frio Hellanic	0.525	1.183	6.822	6.60
14	Salinthip Naree	0.116	0.123	4.648	9.90
15	Glacier Bay	n/a	n/a	3.089	6.10
16	SAS Drakensburg	n/a	n/a	0.373	7.80
17	Corel Mermaid	-0.051	-0.051	-1.120	8.40
18	Royal Sphere	0.001	0.103	3.007	10.00
19	Barrier	0.304	0.793	3.555	6.60
20	Joe Grand	0.125	0.812	4.741	10.50
21	Ned Clarence	-0.130	-0.606	5.085	9.50
22	Meng Hai	-0.152	-0.550	-0.315	11.40
23	Saigon	n/a	n/a	-1.304	8.80
24	Msc Melbourne	-0.201	-0.294	3.699	8.50
25	Jo Lonne	n/a	n/a	2.477	9.60
26	Camboda Star	-0.076	-0.309	-0.597	5.60
27	Master Nicos	-0.147	-0.494	0.281	9.70
28	Marulaki	-0.908	-2.646	-1.963	8.40
29	Meva	-0.724	-1.885	-2.184	9.00
30	Ocuirance	1.505	3.891	-1.252	7.30
31	Evergenius	-0.019	0.291	0.364	5.00
32	Berge Clipper	n/a	n/a	1.743	8.70
33	Prosprim Cont	-0.080	0.652	-0.689	7.80
34	Jorbony	0.506	1.457	-4.280	7.90
35	Lissossm	n/a	n/a	-3.115	10.00
36	SD Truimph	n/a	n/a	-3.873	11.80
37	Emirate Star 2	n/a	n/a	-3.888	6.50
38	Iran Jamal	n/a	n/a	-0.863	8.50
39	Ned Rio Grande	-0.035	0.662	0.486	10.00
40	Barbrite Arrow	n/a	n/a	-1.119	9.00
41	Pride	n/a	n/a	0.594	9.00
42	Feng Anshan	-2.058	-3.052	0.369	8.50
43	Namibia	-0.129	-0.129	-3.852	5.90
44	Bella Lontra	-1.439	-1.940	0.753	5.60
45	Global Mombasa	n/a	n/a	2.198	6.20
46	Alam Senang	0.160	0.160	1.365	10.50

Appendix D: RECTIFICATION VALIDATION RESULTS

D.1. Ground coordinates from the GPS and Video Imaging techniques for the Bella Lontra

GPS		VIDEO IMAGING		VIDEO IMAGING - CURVE FITTED		ERRORS	
Y (m)	X (m)	Y (m)	X (m)	Y (m)	X (m)	|ΔY| (m)	|ΔX| (m)
4871.04	2539.21	4789.92	2537.30	4744.44	2595.10	126.60	55.89
4802.33	2515.97	4784.19	2548.19	4687.10	2563.72	115.24	47.75
4794.58	2514.03	4849.21	2592.25	4682.34	2560.23	112.23	46.20
4693.72	2486.90	4775.92	2563.93	4616.29	2515.82	77.43	28.93
4611.71	2464.61	4514.87	2435.53	4562.71	2480.63	49.00	16.02
4561.84	2447.18	4511.26	2442.41	4521.23	2459.48	40.61	12.30
4492.02	2422.00	4388.32	2388.75	4461.97	2430.04	30.05	8.05
4419.99	2396.82	4442.72	2427.08	4403.50	2399.71	16.49	2.89
4340.19	2379.37	4270.03	2341.14	4363.44	2365.95	23.25	13.42
4267.05	2346.45	4213.70	2317.18	4288.93	2334.66	21.88	11.80
4195.02	2311.61	4212.58	2319.32	4211.53	2303.36	16.51	8.25
4118.57	2268.07	4161.03	2289.58	4116.97	2269.47	1.60	1.40
4043.22	2225.49	4060.11	2235.38	4026.82	2235.25	16.40	9.75
3970.09	2185.82	3965.07	2181.75	3944.86	2201.12	25.23	15.30
3870.37	2113.27	3871.88	2135.57	3800.08	2152.98	70.29	39.71
3735.16	2083.22	3741.97	2066.37	3742.01	2084.35	6.85	1.13
3696.38	2059.03	3618.10	2006.32	3696.07	2063.90	0.31	4.87
3635.44	2007.77	3614.70	2012.79	3601.01	2031.07	34.43	23.29
3544.57	1973.89	3461.88	1938.00	3539.88	1980.42	4.69	6.54
3453.70	1935.17	3389.00	1905.07	3471.63	1927.74	17.93	7.43
3371.70	1894.53	3387.17	1908.54	3401.80	1878.45	30.10	16.08
3286.37	1848.09	3286.61	1855.16	3324.18	1825.40	37.80	22.69
3198.83	1800.68	3174.67	1763.57	3247.25	1769.15	48.42	31.52
3116.84	1747.47	3065.15	1689.60	3163.55	1714.86	46.71	32.61
3032.63	1686.54	3069.67	1681.00	3070.88	1657.58	38.25	28.96
2955.08	1625.61	2994.63	1625.21	2981.34	1603.54	26.26	22.07
2875.30	1567.58	2874.98	1544.35	2898.65	1546.80	23.34	20.78
2795.53	1507.62	2743.29	1457.60	2815.52	1489.01	19.99	18.61
2712.43	1443.79	2708.65	1418.23	2729.21	1427.87	16.77	15.92
2631.55	1379.00	2633.51	1360.32	2643.37	1367.62	11.82	11.38
2550.67	1316.14	2583.01	1313.67	2561.30	1306.85	10.63	9.29
2464.25	1251.35	2496.95	1253.30	2477.35	1241.59	13.10	9.75
2384.47	1191.39	2418.80	1193.52	2399.70	1181.31	15.23	10.08
2298.05	1128.53	2283.43	1110.29	2317.74	1116.26	19.69	12.27
2211.62	1064.70	2220.75	1057.05	2233.26	1051.82	21.64	12.89
2126.31	1003.78	2109.11	985.05	2150.79	989.17	24.49	14.61
2034.34	938.99	2056.10	940.78	2060.36	923.17	26.02	15.81
1951.23	880.00	1950.55	875.29	1974.90	865.32	23.66	14.67
1861.48	821.97	1858.40	812.06	1887.25	805.24	25.77	16.73
1765.08	759.11	1775.37	755.07	1787.54	744.09	22.46	15.02
1679.75	701.09	1670.87	686.37	1690.37	693.45	10.61	7.64
1593.32	641.14	1571.47	624.78	1584.01	646.05	9.31	4.91

D.2. Ground coordinates from the GPS and Video Imaging techniques for the Global Mombasa

GPS		VIDEO IMAGING		VIDEO IMAGING - CURVE FITTED		ERRORS	
Y (m)	X (m)	Y (m)	X (m)	Y (m)	X (m)	|ΔY| (m)	|ΔX| (m)
2340.49	1207.47	2335.57	1195.25	2357.21	1197.25	16.72	10.22
2262.93	1159.10	2249.65	1139.13	2278.37	1149.51	15.44	9.60
2192.75	1113.97	2157.30	1079.41	2208.16	1103.92	15.41	10.05
2002.55	962.48	2050.17	1009.05	1991.18	970.60	11.36	8.12
1904.66	917.33	1978.21	952.03	1930.38	897.97	25.72	19.36
1823.40	852.87	1883.79	879.82	1844.97	836.72	21.57	16.14
1736.61	780.35	1789.43	811.68	1749.03	771.34	12.42	9.01
1653.51	722.33	1713.42	753.87	1670.76	709.84	17.25	12.49
1574.10	667.54	1630.29	693.37	1594.24	653.18	20.15	14.36
1498.38	603.08	1549.10	636.34	1499.28	602.14	0.90	0.94
1422.67	543.46	1448.75	570.50	1404.88	555.10	17.79	11.64

D.3. Ground coordinates from the GPS and Video Imaging techniques for the Alam Senang

GPS		VIDEO IMAGING		VIDEO IMAGING - CURVE FITTED		ERRORS	
Y (m)	X (m)	Y (m)	X (m)	Y (m)	X (m)	|ΔY| (m)	|ΔX| (m)
2965.09	1566.67	2971.15	1543.28	3019.46	1541.14	54.37	25.54
2926.32	1527.03	2869.97	1495.33	2937.34	1521.76	11.02	5.27
2777.81	1474.75	2869.59	1496.05	2826.21	1451.42	48.40	23.33
2714.65	1439.93	2732.35	1425.38	2751.66	1422.31	37.01	17.62
2652.60	1399.30	2709.73	1416.19	2665.30	1393.58	12.70	5.72
2619.37	1361.60	2684.61	1412.56	2586.53	1378.02	32.84	16.42
2547.35	1315.17	2600.42	1374.97	2492.35	1343.59	55.00	28.42
2476.43	1269.71	2525.90	1330.68	2403.99	1308.41	72.44	38.70
2388.89	1219.41	2435.34	1285.32	2311.39	1262.71	77.50	43.30
2327.95	1181.69	2152.24	1121.38	2245.77	1229.14	82.17	47.45
2253.70	1136.23	2101.47	1090.88	2171.11	1186.10	82.59	49.86
2187.22	1086.91	2007.27	1033.64	2095.34	1145.42	91.88	58.51
2114.09	1039.52	1990.25	1010.31	2027.11	1098.27	86.98	58.74
2042.07	989.23	1940.84	970.49	1958.61	1049.37	83.45	60.13
1944.56	922.51	1863.77	917.89	1871.47	979.40	73.09	56.89
1898.02	891.56	1803.43	871.84	1831.41	944.57	66.61	53.01
1823.78	844.17	1755.79	833.56	1768.88	887.28	54.90	43.11

Appendix E: PORTSIM - SIMULATOR SHIP CHARACTERISTICS

E.1. Ship Characteristic data for Car Carrier type vessels

Ship Type : **CAR CARRIER**		
PARTICULAR	UNIT	DIMENSION
Main Particulars :		
Length between perpendiculars	m	190
Maximum water line beam	m	32.26
Draught, aft	m	7.7
Draught, fore	m	7.5
Displacement	m^3	27100
Lateral distance between propellor and CL	m	0
Longitudinal centre of gravity, relative to L/2	m	-5.7
Vertical centre of gravity, above keel	m	3.8
Roll radius of gyration	m	15.2
Yaw radius of gyration	m	47.5
Metacentric height	m	1.5
Area of transom (submerged part)	m^2	0
Rudder Particulars :		
Type of rudder	-	Schilling
Number of rudders	-	1
Total area of rudder	m^2	33.14
Area of horn	m^2	0.01
Rudder height at stock	m	6.8
Rudder rate	deg/s	4.5
Longitudinal position of rudder relative to L/2	m	-93.1
Maximum rudder angle	deg	70
Propeller Particulars :		
Type of propeller	-	Fixed
Number of propellers	-	1
Propeller diameter	m	6.8
Propeller pitch ratio	-	1.15
Thrust deduction factor	-	0.16
Wake fraction	-	0.26
Height of propeller race over rudder	m	6
Design speed of ship	knots	20.02

Design propeller rate	rpm	81.03
Bow Thruster :		
Bow thruster power	kW	1350
Bow thruster reversing rate	/s	20
Stern thruster power	kW	1350
Stern thruster reversing rate	/s	20
Wind Areas :		
Lateral wind area	m^2	5400
Transverse area	m^2	950
Lateral area of superstructure	m^2	50
Perimeter length	m	285
Distance of bow to geometrical centre point	m	104
Number of masts	-	1

E.2. Ship Characteristic data for Post-Panamax Container type vessels

Ship Type : **POST-PANAMAX CONTAINER SHIP**		
PARTICULAR	UNIT	DIMENSION
Main Particulars :		
Length between perpendiculars	m	260,80
Maximum water line beam	m	39,40
Draught, aft	m	12,50
Draught, fore	m	12,50
Displacement	m^3	74 500
Lateral distance between propellor and CL	m	0,00
Longitudinal centre of gravity, relative to L/2	m	5,25
Vertical centre of gravity, above keel	m	16,00
Roll radius of gyration	m	13,80
Yaw radius of gyration	m	65,20
Metacentric height	m	1,00
Area of transom (submerged part)	m^2	1,00
Rudder Particulars :		
Type of rudder	-	conventional
Number of rudders	-	1
Total area of rudder	m^2	65,00
Area of horn	m^2	14,00

Rudder height at stock	m	11,25
Rudder rate	deg/s	4,50
Longitudinal position of rudder relative to L/2	m	126,23
Maximum rudder angle	deg	35,00
Maximum autopilot rudder angle	deg	20,00
Propeller Particulars :		
Type of propeller	-	fixed
Number of propellers	-	1
Propeller diameter	m	8,40
Propeller pitch ratio	-	1,03
Thrust deduction factor	-	0,15
Wake fraction	-	0,24
Height of propeller race over rudder	m	7,56
Design speed of ship	knots	23,09
Design propeller rate	rpm	84,79
Bow Thruster :		
Bow thruster power	kW	2 205
Bow thruster reversing rate	/s	20,00
Winch Characteristics :		
Winch speed	m/s	1,00
Maximum force haul home	ton-force	25
Maximum force without slip	ton-force	40
Wire break load	ton-force	110
Wind Areas :		
Lateral wind area	m^2	6 850
Transverse area	m^2	1 340
Lateral area of superstructure	m^2	100
Perimeter length	m	330,00
Distance of bow to geometrical centre point	m	130,00
Number of masts	-	1

E.3. Ship Characteristic data for Panamax Container type vessels

Ship Type : **PANAMAX CONTAINER SHIP**		
PARTICULAR	UNIT	DIMENSION
Main Particulars :		
Length between perpendiculars	m	247,70
Maximum water line beam	m	32,25
Draught, aft	m	13,10
Draught, fore	m	13,10
Displacement	m^3	71 000
Lateral distance between propellor and CL	m	5,60
Longitudinal centre of gravity, relative to L/2	m	-2,10
Vertical centre of gravity, above keel	m	14,20
Roll radius of gyration	m	11,30
Yaw radius of gyration	m	61,85
Metacentric height	m	1,20
No submerged transom		
Rudder Particulars :		
Type of rudder	-	conventional
Number of rudders	-	1
Total area of rudder	m^2	52,60
Area of horn	m^2	0,10
Rudder height at stock	m	9,32
Rudder rate	deg/s	2,33
Longitudinal position of rudder relative to L/2	m	-119,89
Maximum rudder angle	deg	45,00
Maximum autopilot rudder angle	deg	20,00
Propeller Particulars :		
Type of propeller	-	fixed
Number of propellers	-	2
Propeller diameter	m	6,75
Propeller pitch ratio	-	0,93
Thrust deduction factor	-	0,12
Wake fraction	-	0,13
Height of propeller race over rudder	m	6,07
Design speed of ship	knots	19,50
Design propeller rate	rpm	108,00

Bow Thruster :		
Bow thruster power	kW	2 000
Bow thruster reversing rate	/s	20,00
Winch Characteristics :		
Winch speed	m/s	1,00
Maximum force haul home	ton-force	25
Maximum force without slip	ton-force	40
Wire break load	ton-force	110
Wind Areas :		
Lateral wind area	m^2	4 550
Transverse area	m^2	1 025
Lateral area of superstructure	m^2	570
Perimeter length	m	311,00
Distance of bow to geometrical centre point	M	136,00
Number of masts	-	2

E.4. Ship Characteristic data for Product Tanker type vessels

Ship Type : **PRODUCT TANKER**		
PARTICULAR	UNIT	DIMENSION
Main Particulars :		
Length between perpendiculars	m	264
Maximum water line beam	m	48
Draught, aft	m	15.2
Draught, fore	m	15.2
Displacement	m^3	158000
Lateral distance between propellor and CL	m	0
Longitudinal centre of gravity, relative to L/2	m	5.02
Vertical centre of gravity, above keel	m	2.11
Roll radius of gyration	m	21.12
Yaw radius of gyration	m	66
Metacentric height	m	10
Area of transom (submerged part)	m^2	0
Rudder Particulars :		

Type of rudder	-	Schilling
Number of rudders	-	1
Total area of rudder	m^2	55
Area of horn	m^2	0
Rudder height at stock	m	10
Rudder rate	deg/s	4.5
Longitudinal position of rudder relative to L/2	m	-129.36
Maximum rudder angle	deg	35
Propeller Particulars :		
Type of propeller	-	Fixed
Number of propellers	-	1
Propeller diameter	m	8.2
Propeller pitch ratio	-	0.72
Thrust deduction factor	-	0.23
Wake fraction	-	0.42
Height of propeller race over rudder	m	7.6
Design speed of ship	knots	16.02
Design propeller rate	rpm	89.69
Bow Thruster :		
Bow thruster power	kW	0
Bow thruster reversing rate	/s	20
Stern thruster power	kW	0
Stern thruster reversing rate	/s	20
Wind Areas :		
Lateral wind area	m^2	3600
Transverse area	m^2	1600
Lateral area of superstructure	m^2	1600
Perimeter length	m	320
Distance of bow to geometrical centre point	m	160
Number of masts	-	1

E.5. Data for the varying speeds and rudder settings

POST PANAMAX						
	Rudder					
	10 deg		20 deg		30 deg	
Depth	Crab Angle (deg)	Radius of Curvature (m)	Crab Angle (deg)	Radius of Curvature (m)	Crab Angle (deg)	Radius of Curvature (m)
16m	1.11	1926.01	1.81	1294.44	2.31	1032.59
18m	1.62	1600.26	2.73	1016.20	3.25	825.79
20m	2.35	1363.53	3.55	893.38	4.15	736.69
22m	2.63	1249.53	3.86	828.73	4.63	686.25
24m	3.01	1170.40	4.32	790.11	5.09	656.11
deep	6.41	772.23	8.47	552.70	10.05	456.46

CAR CARRIER						
	Rudder					
	10 deg		20 deg		30 deg	
Depth	Crab Angle (deg)	Radius of Curvature (m)	Crab Angle (deg)	Radius of Curvature (m)	Crab Angle (deg)	Radius of Curvature (m)
16m	5.37	658.11	7.90	432.18	9.95	332.68
18m	5.89	632.83	8.63	419.39	10.87	320.27
20m	6.33	608.45	9.10	407.99	11.48	313.85
22m	6.80	597.65	9.92	400.74	12.34	310.52
24m	6.90	589.33	9.83	391.92	12.61	301.02
deep	10.05	475.37	13.99	320.15	17.87	240.88

CAR CARRIER						
	Rudder					
	10 deg		20 deg		30 deg	
Depth	Crab Angle (deg)	Radius of Curvature (m)	Crab Angle (deg)	Radius of Curvature (m)	Crab Angle (deg)	Radius of Curvature (m)
16m	4.80	490.40	7.57	309.32	10.01	223.62
18m	6.85	400.23	8.73	291.34	11.50	209.13
20m	6.31	438.44	9.45	278.76	12.35	199.68
22m	7.09	424.84	10.45	270.46	13.69	193.08
24m	6.99	415.88	10.28	265.12	13.69	187.87
deep	11.66	325.83	17.37	200.66	24.35	122.13

Appendix F: SHIP TRACK PLOTS

1. HERON

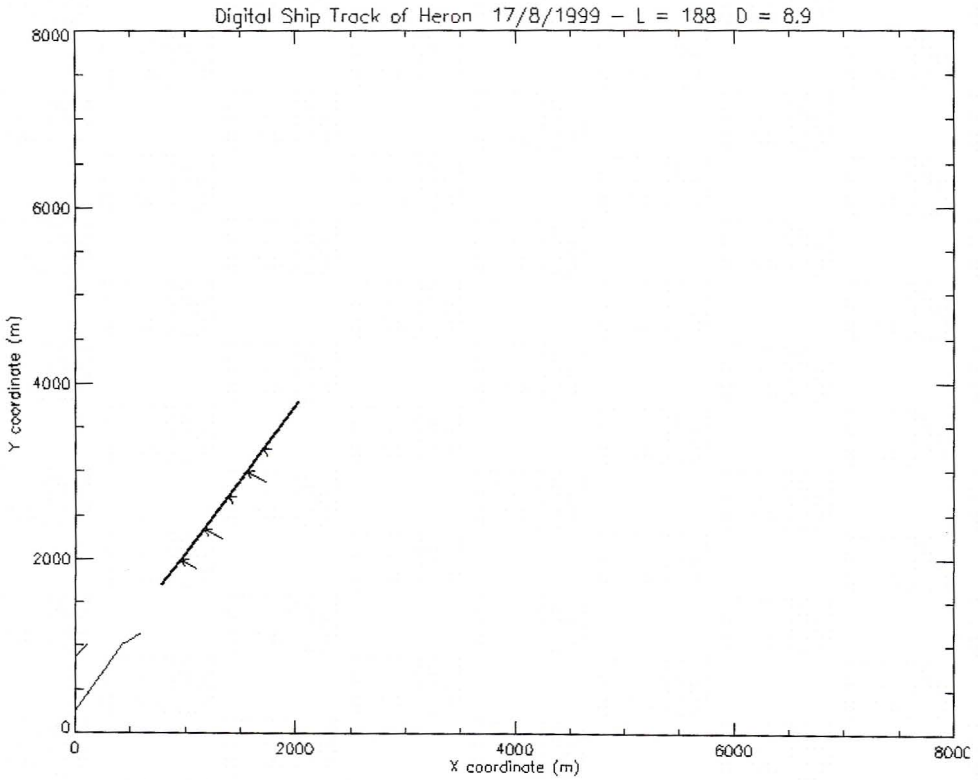

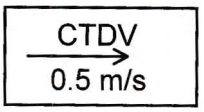

2. CMBT TANA

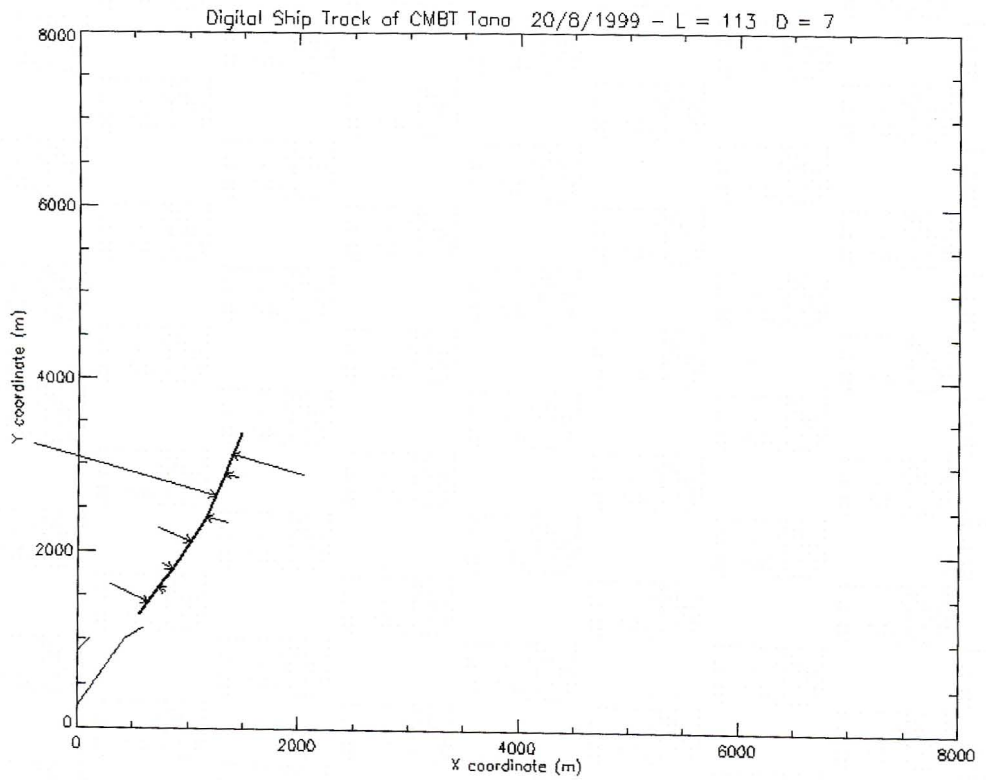

3. SILVER YING

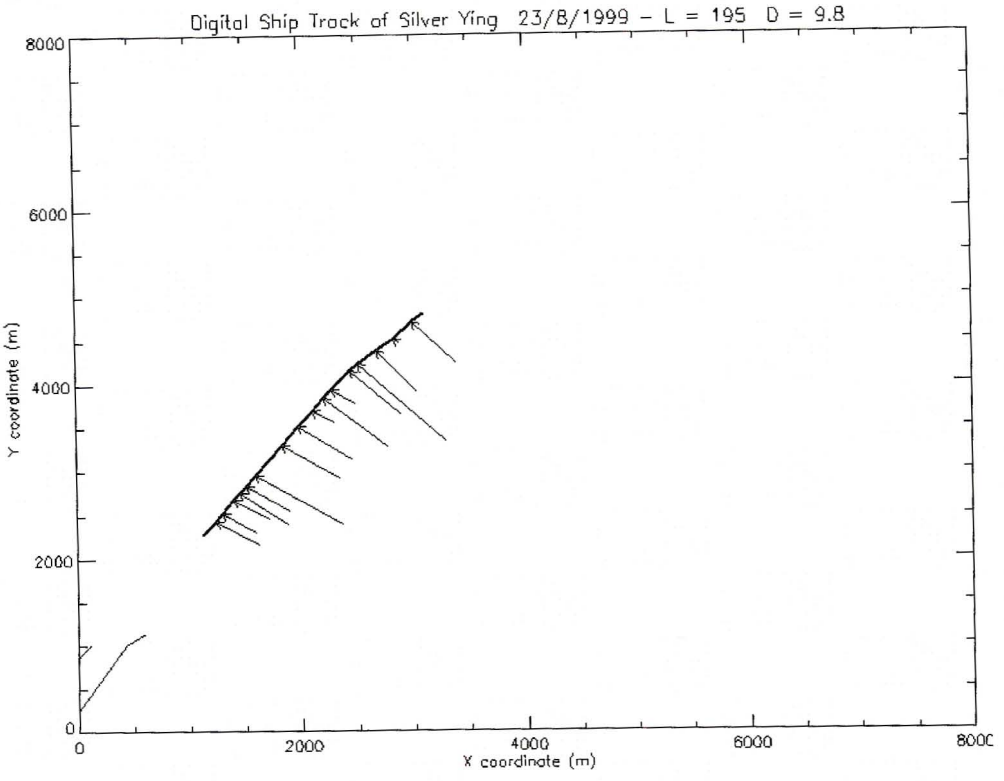

4. DEL KALAHARI

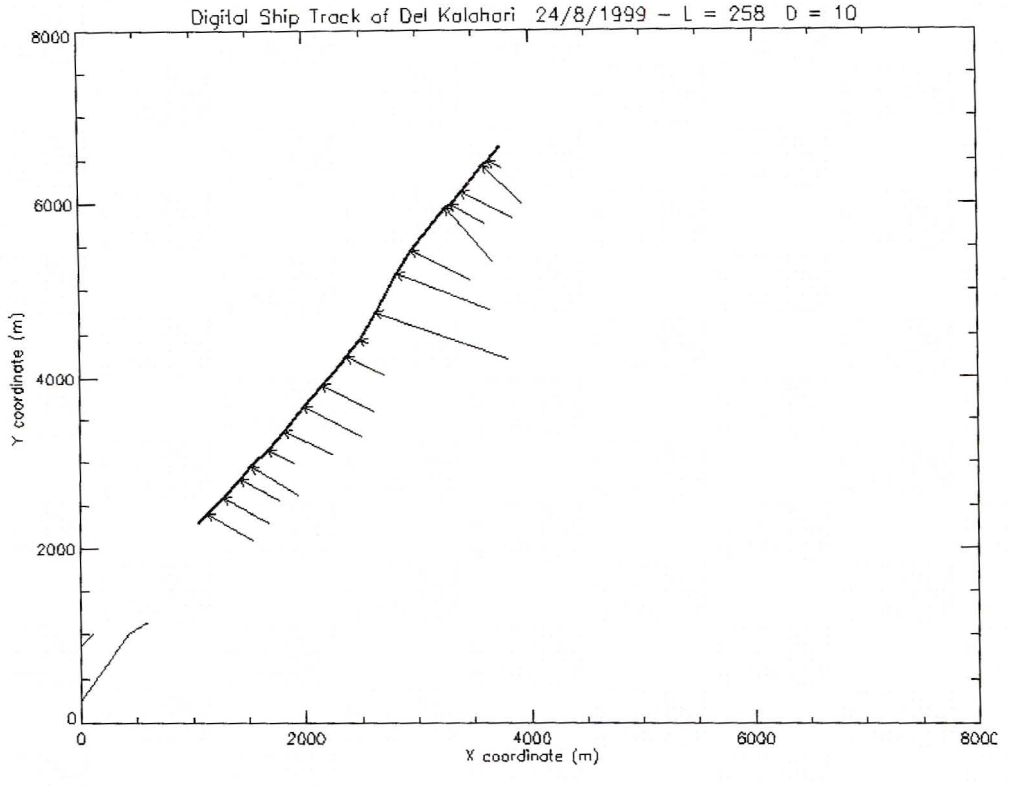

5. SILVER STAR

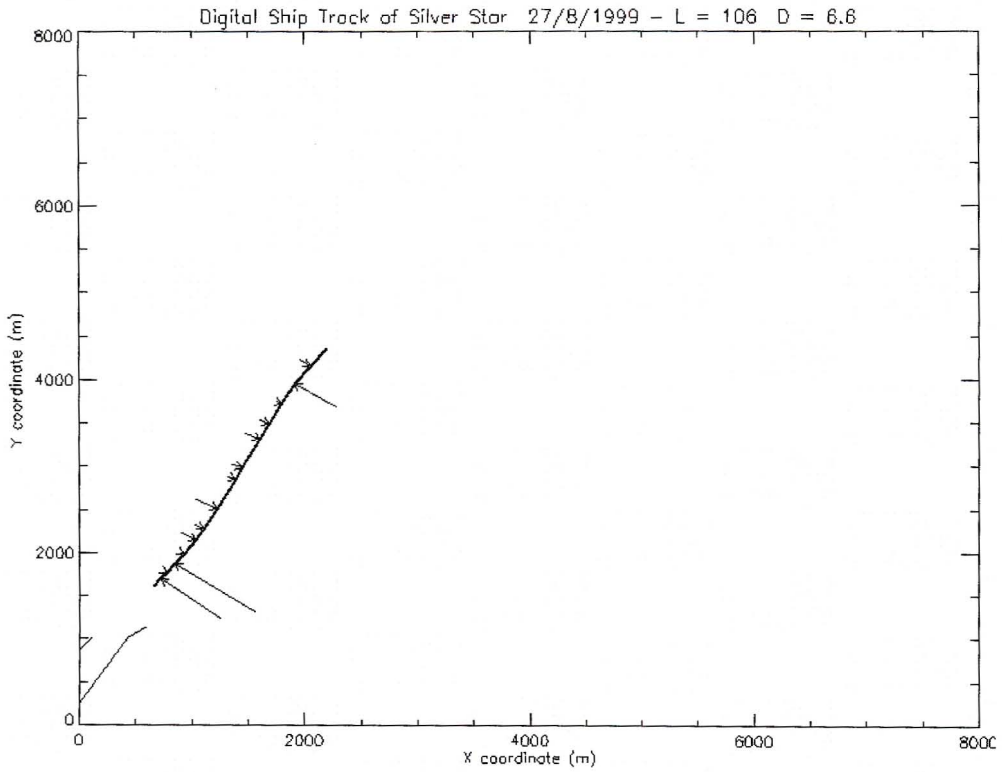

CTDV
0.5 m/s

6. ANANGEL DIGNITY

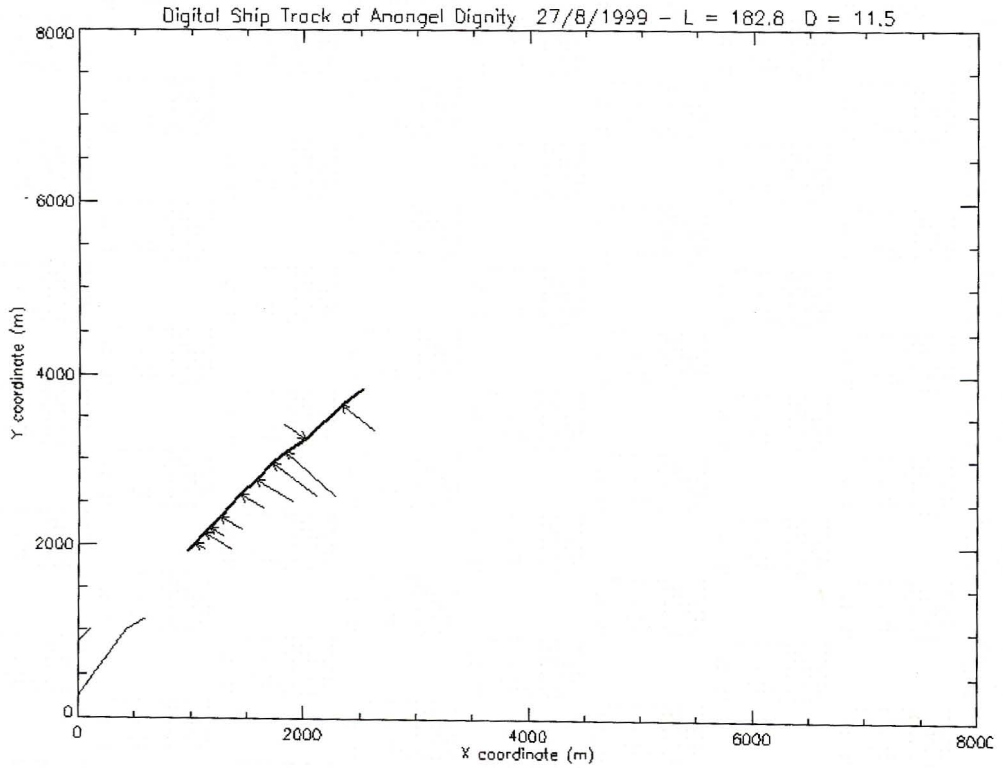

7. LOUIS PASTEUR

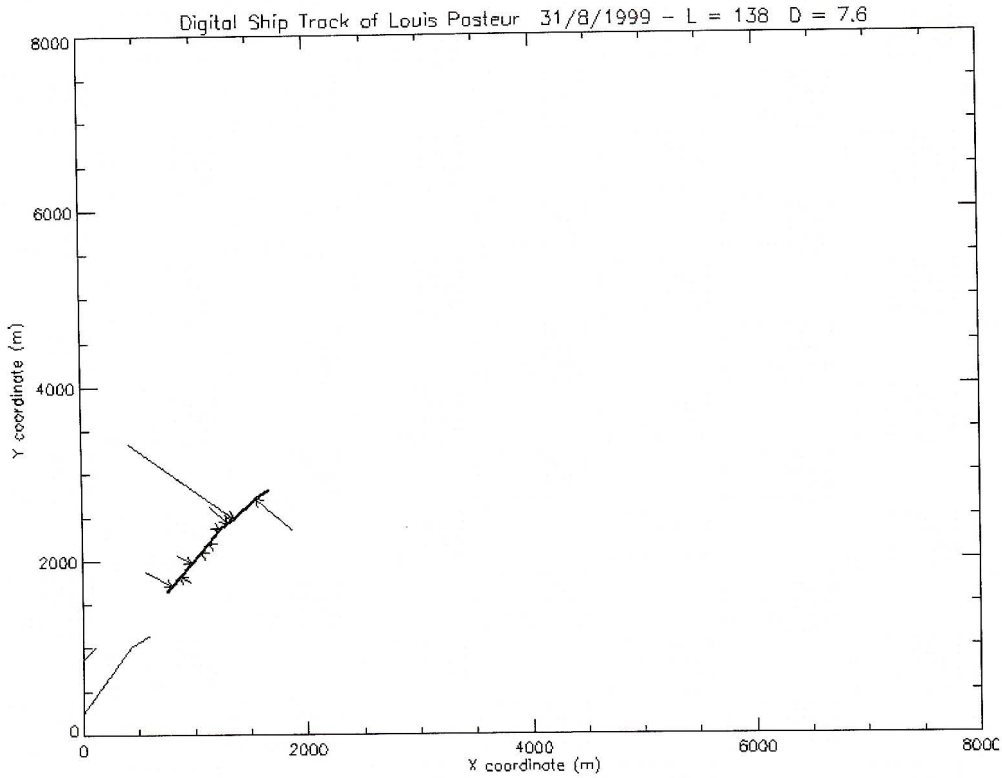

8. LIBERTY STAR

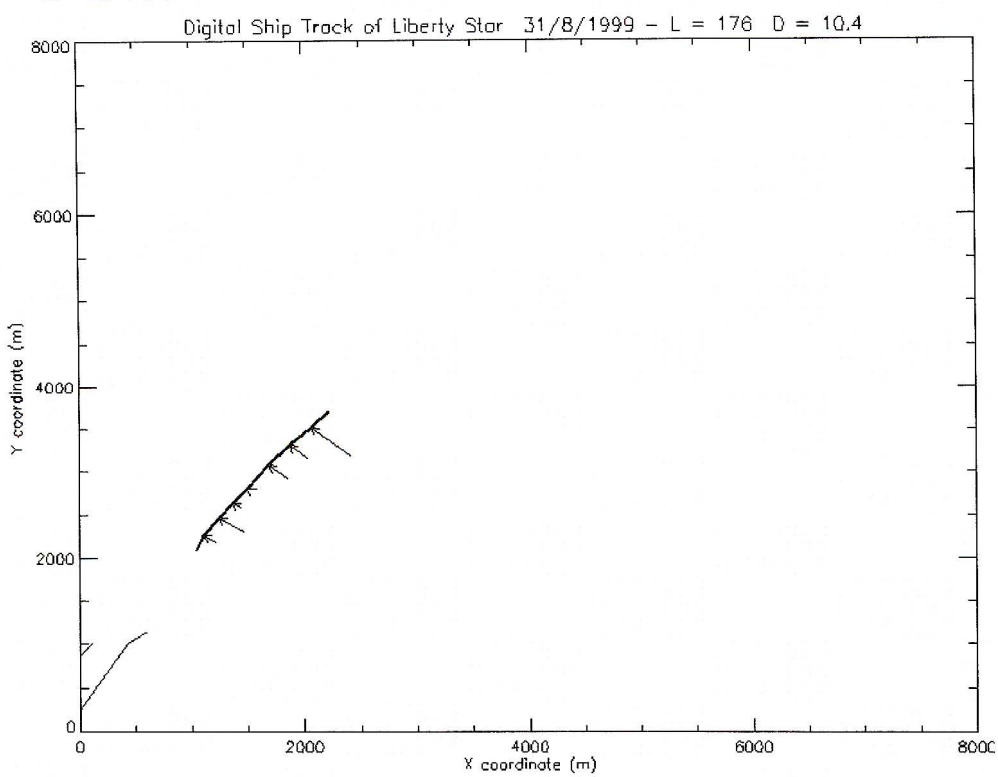

9. ALAM TANGARI

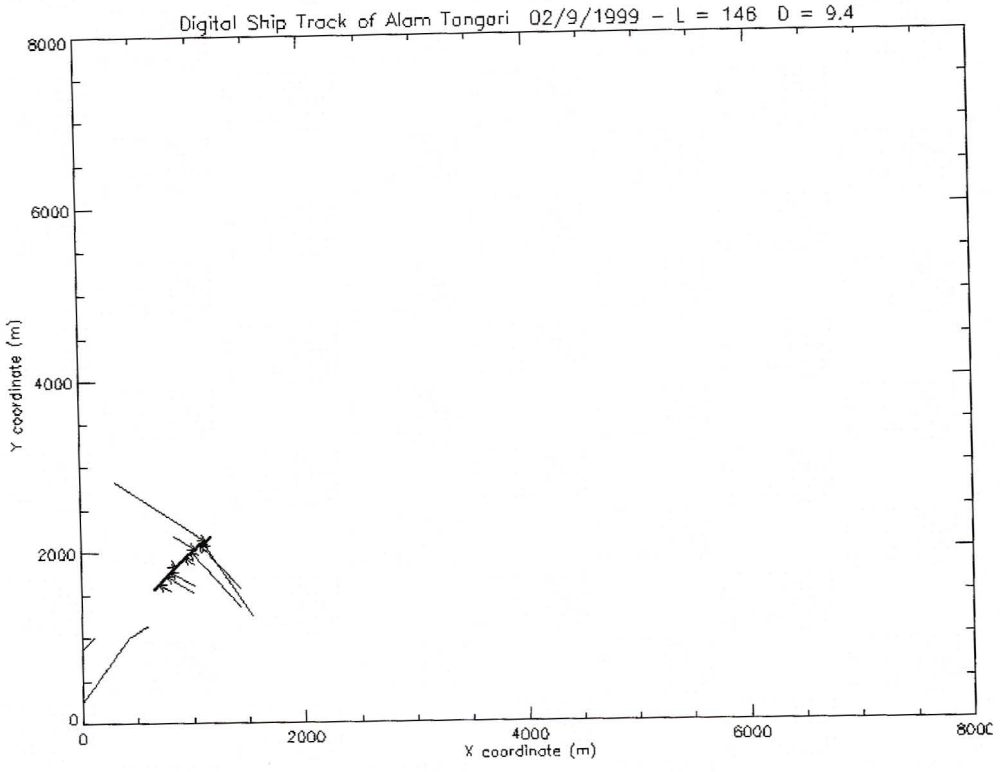

CTDV
0.5 m/s

10. IRAN MOTAHARI

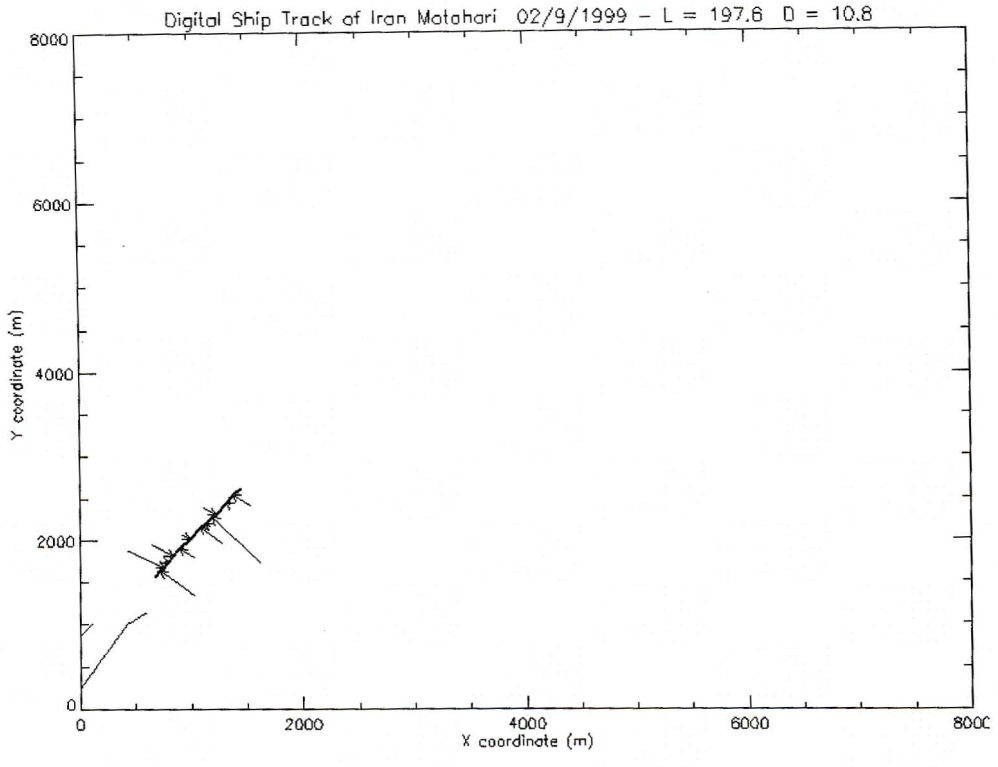

11. SEA SPIRIT K

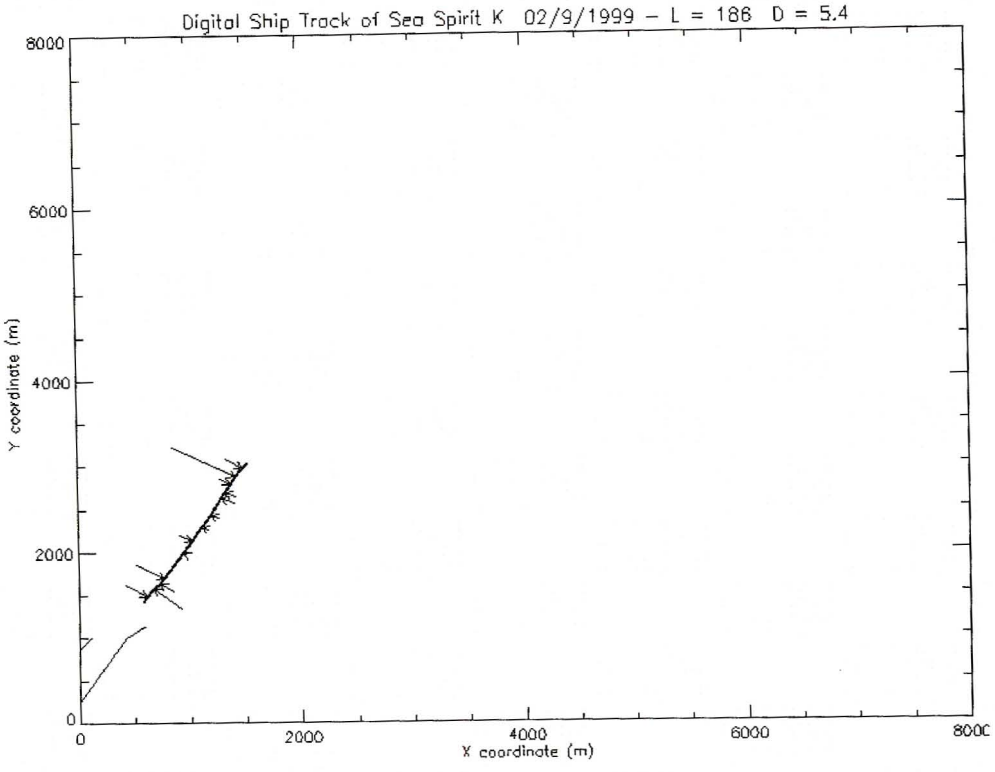

12. SOCOL 6

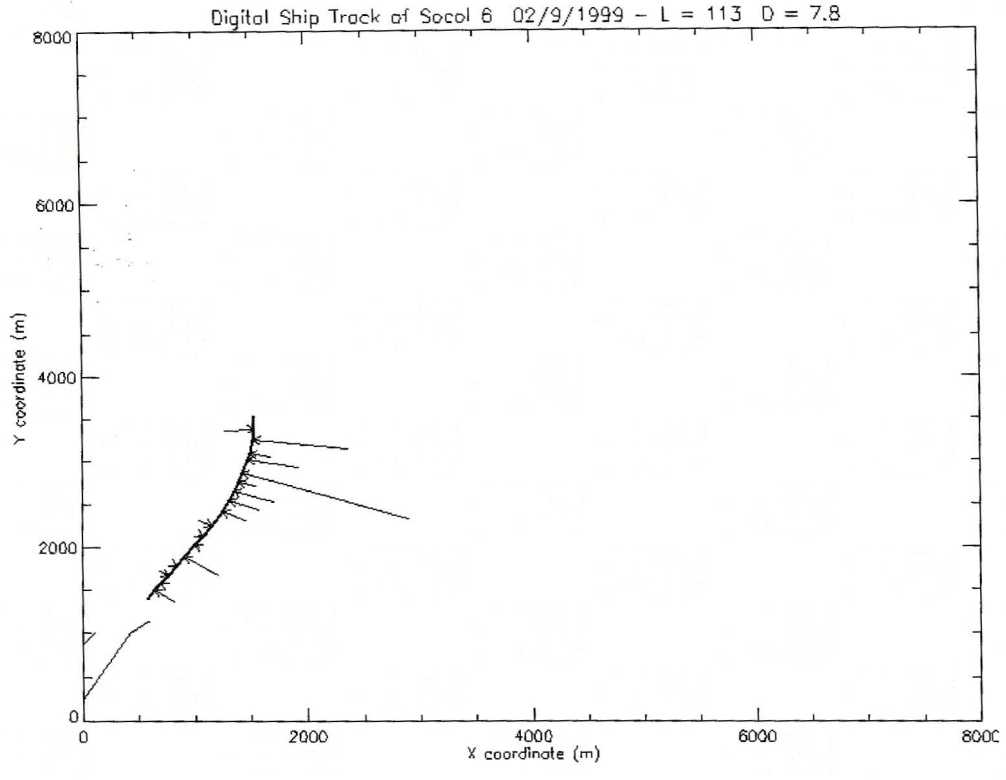

13. FRIO HELLANIC

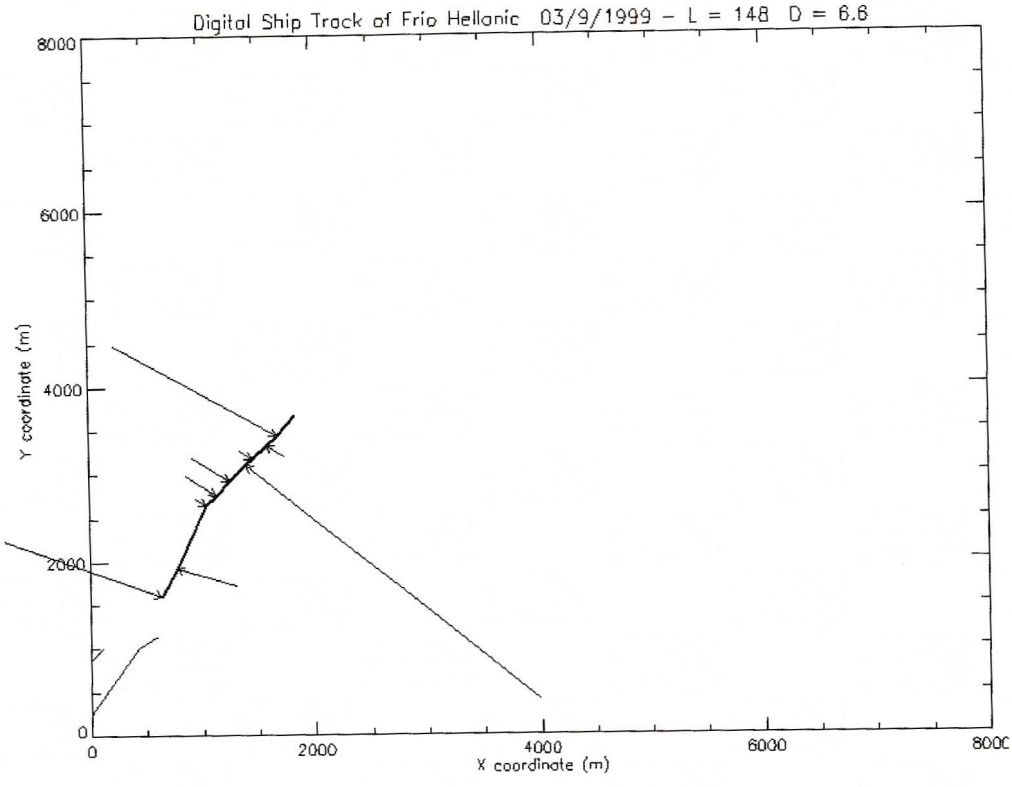

14. SALINTHIP NAREE

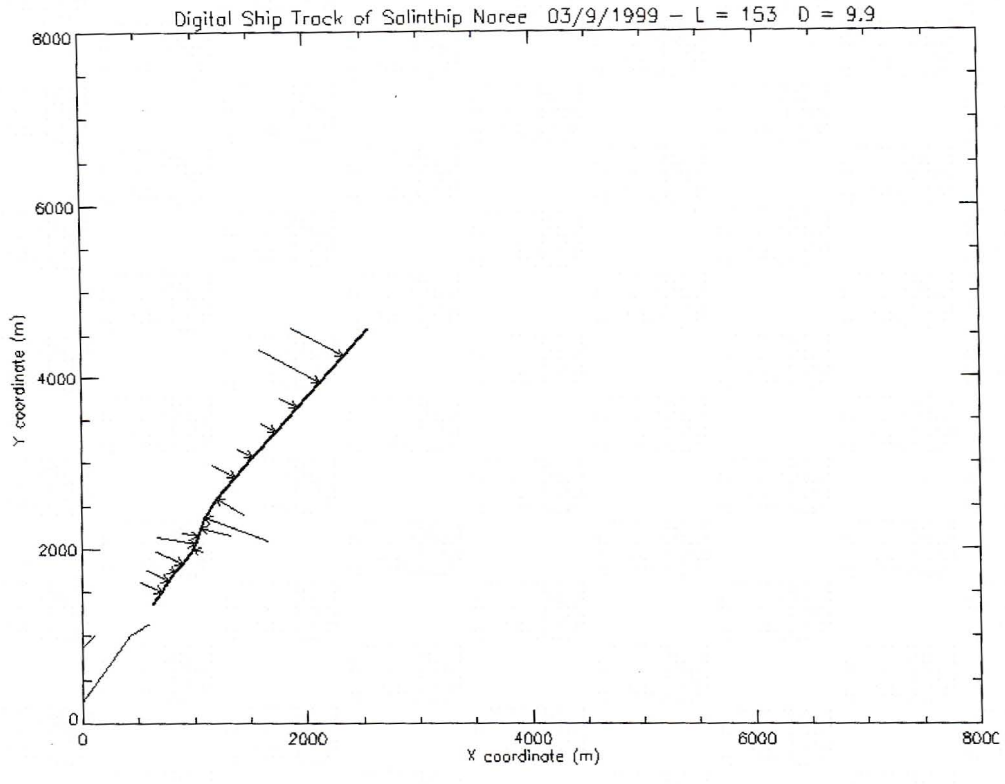

15. GLACIER BAY

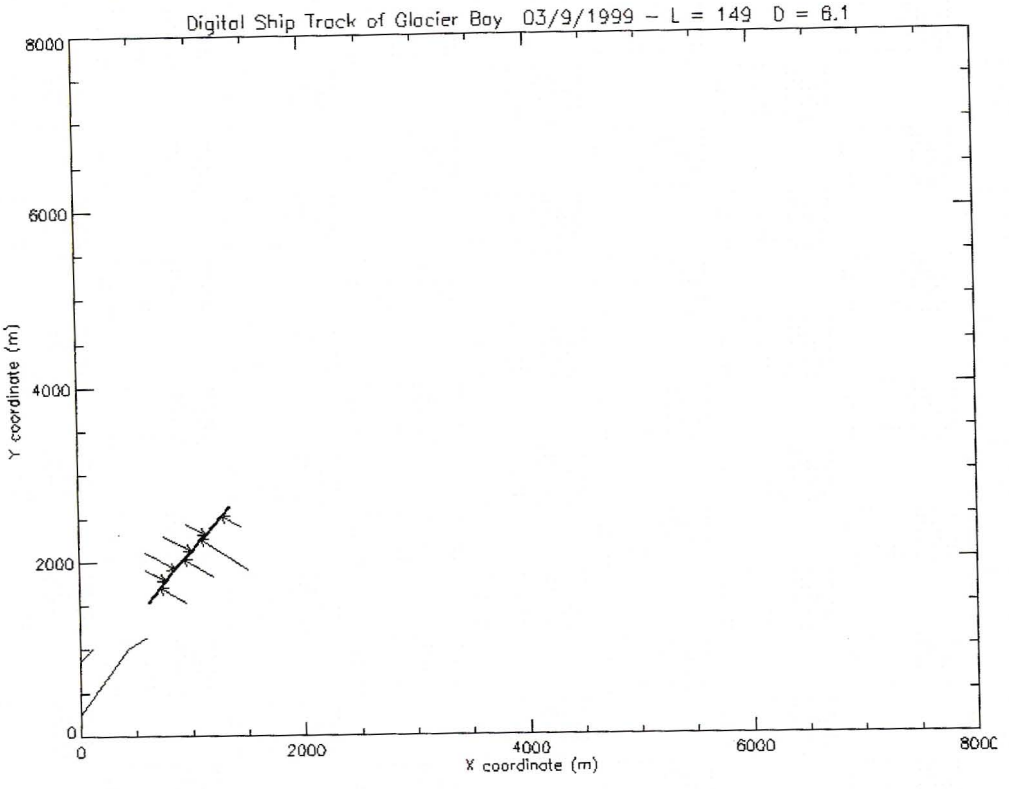

16. SAS DRAKENSBERG

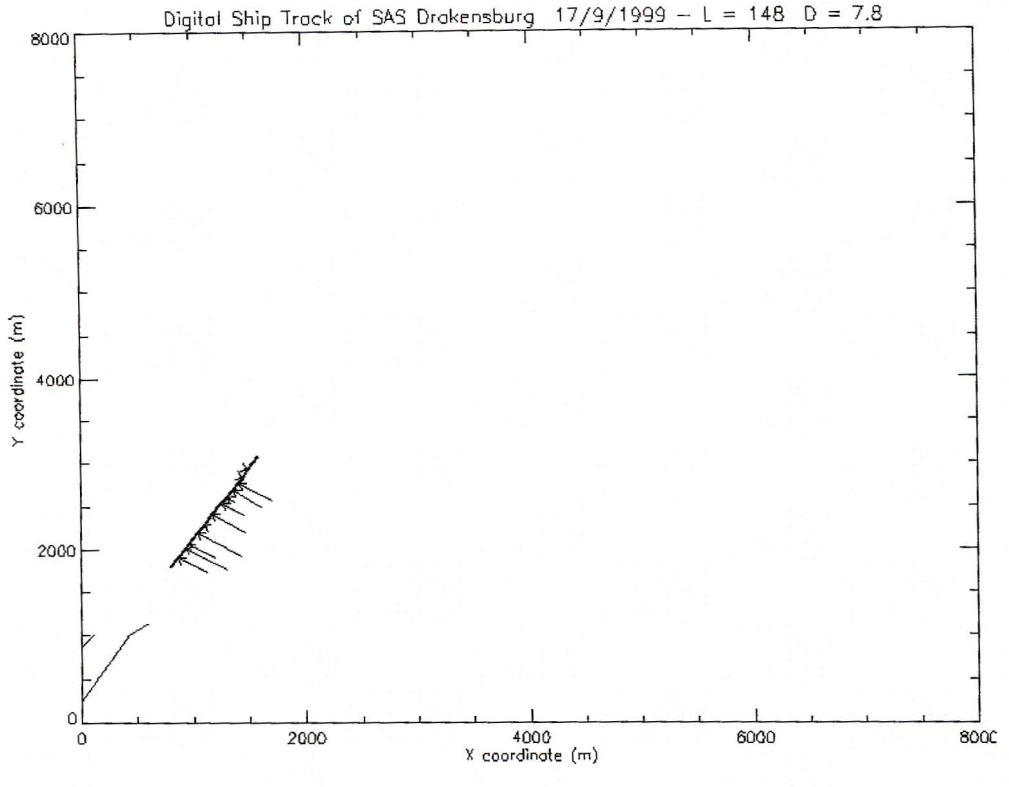

17. COREL MERMAID

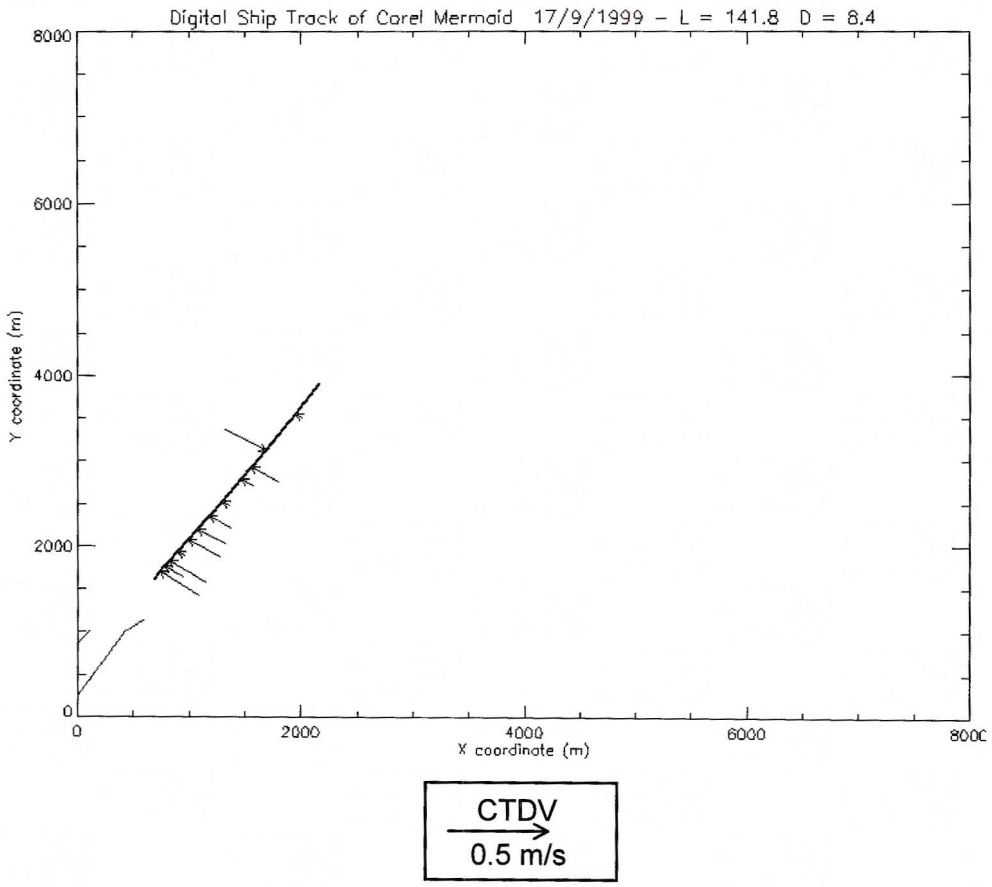

18. ROYAL SPHERE

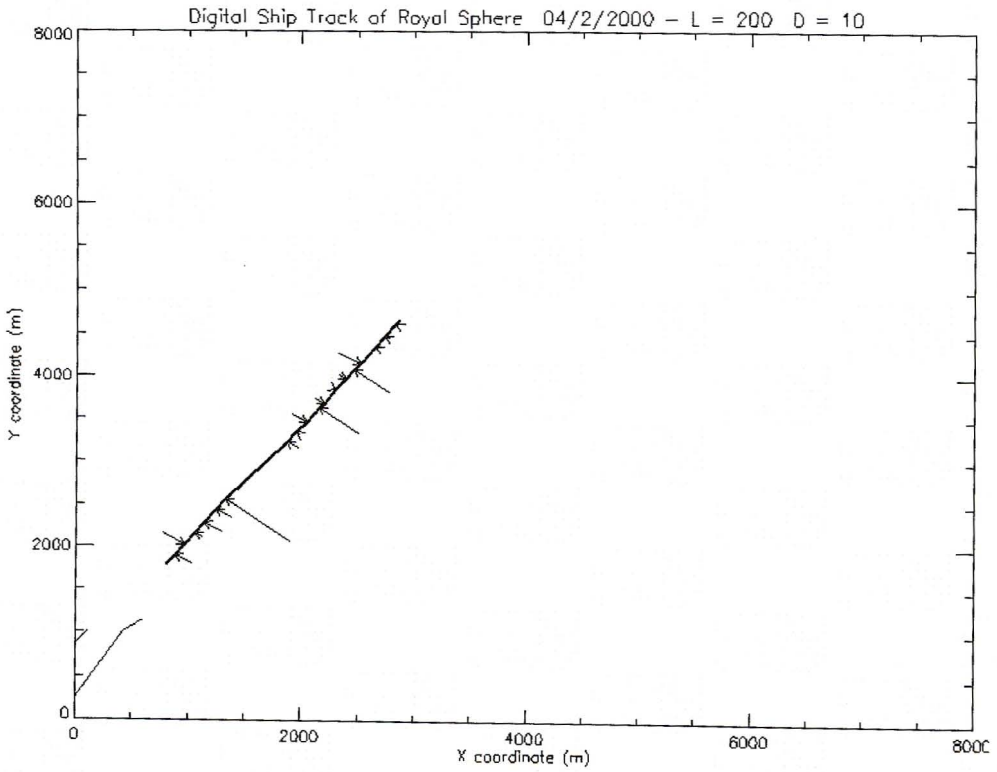

19. BARRIER

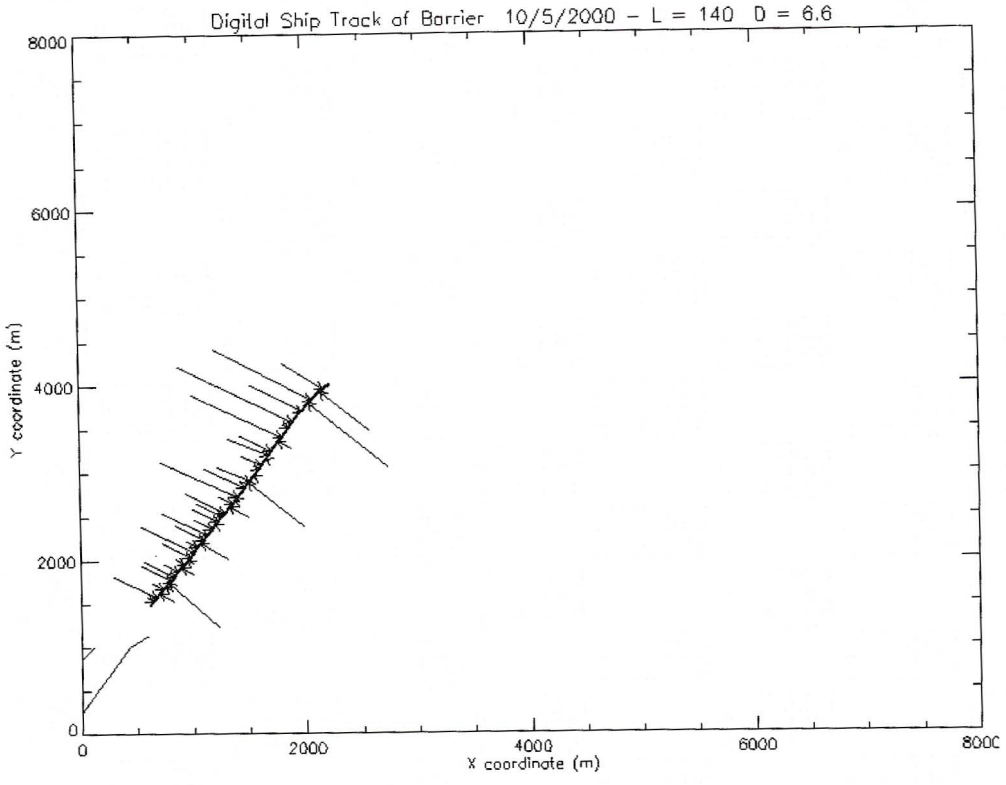

CTDV
0.5 m/s

20. JOE GRAND

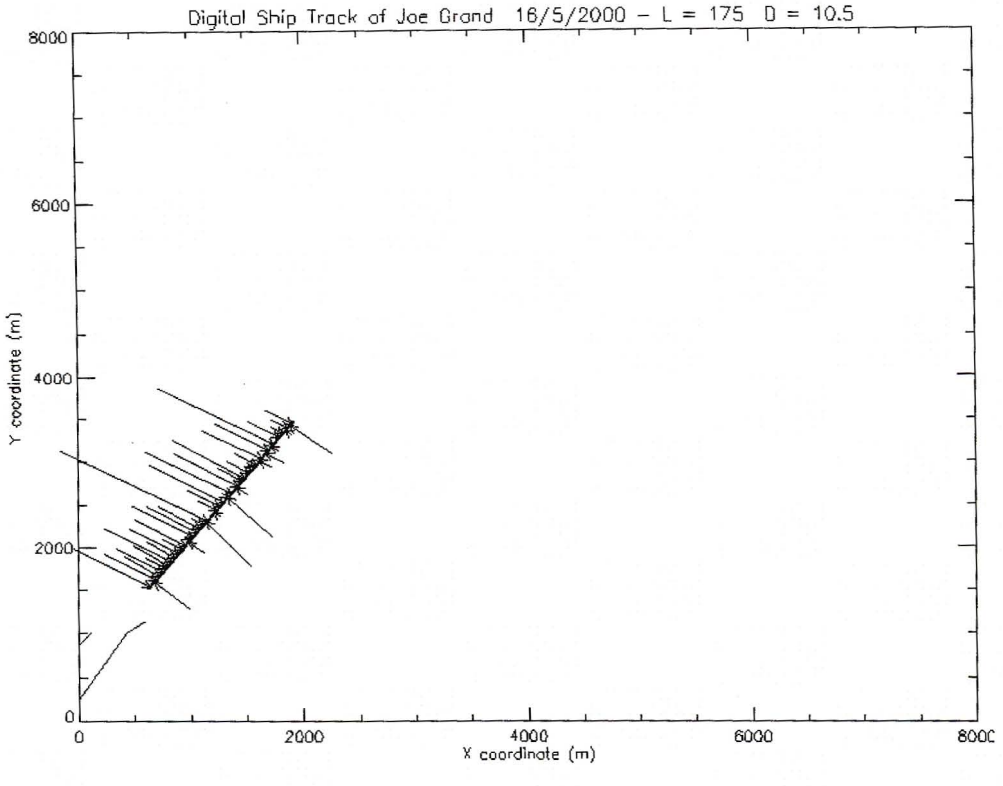

21. NED CLARENCE

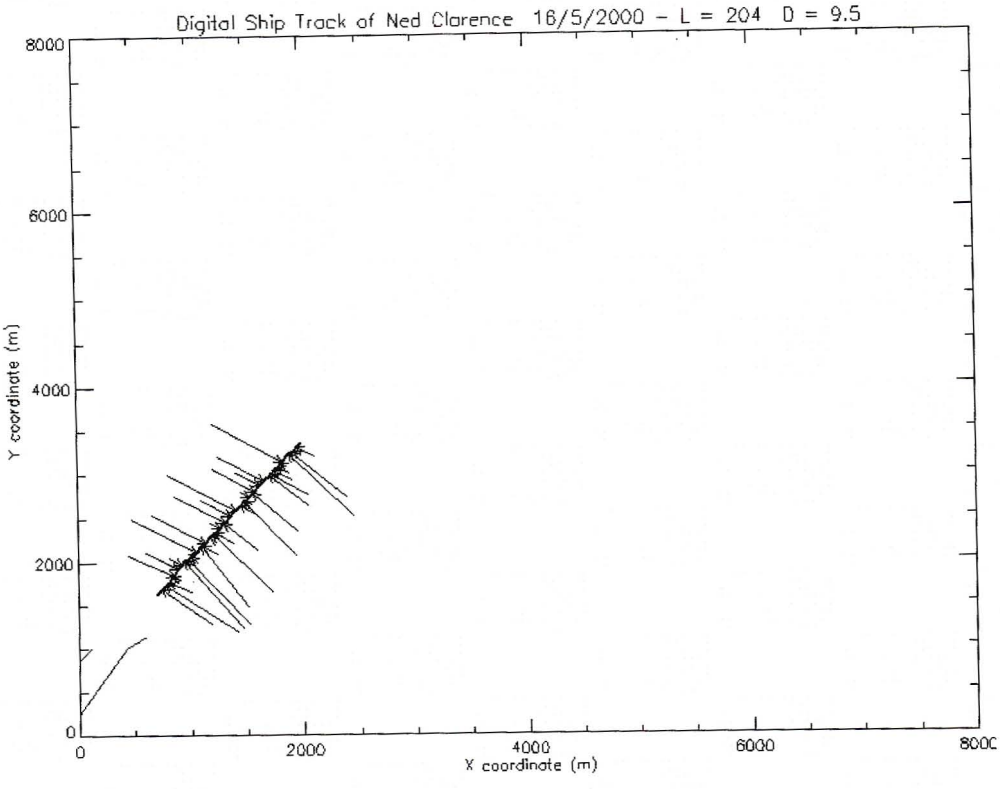

CTDV
0.5 m/s

22. MENG HAI

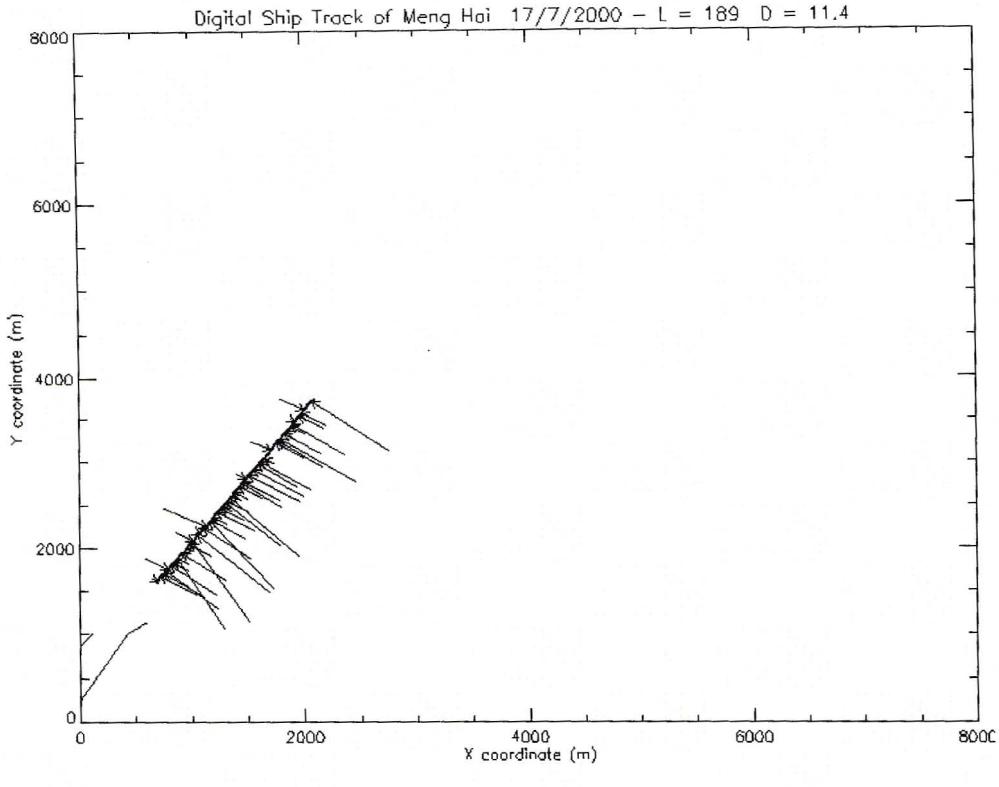

23. SAIGON 5

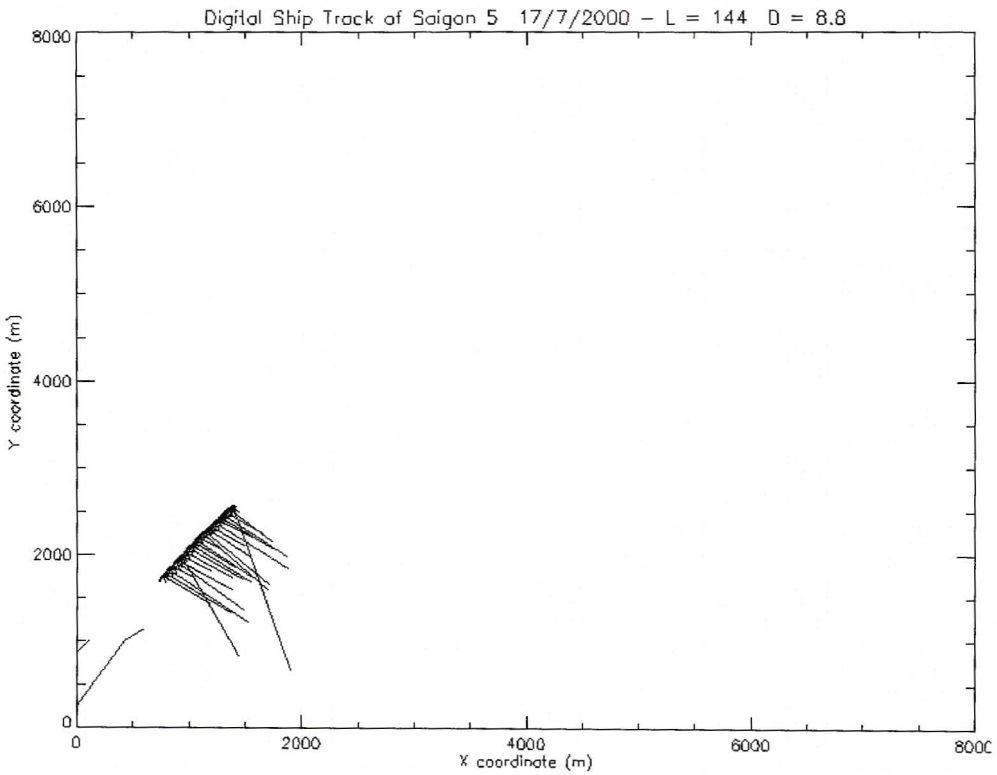

24. MSC MELBOURNE

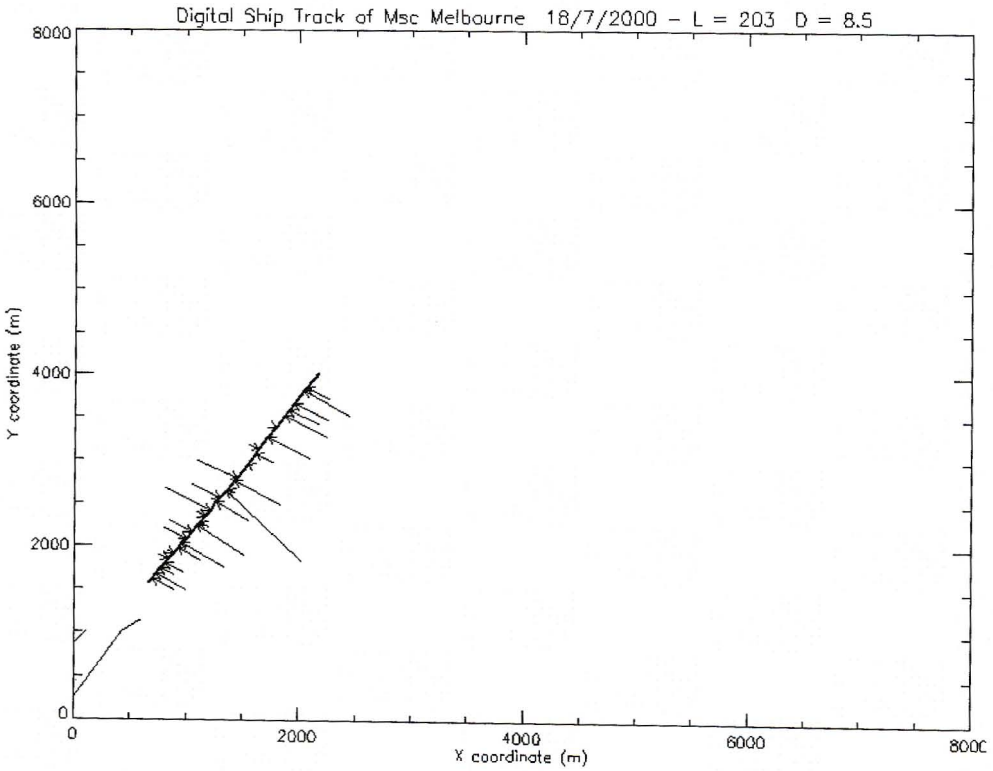

25. JO LONNE

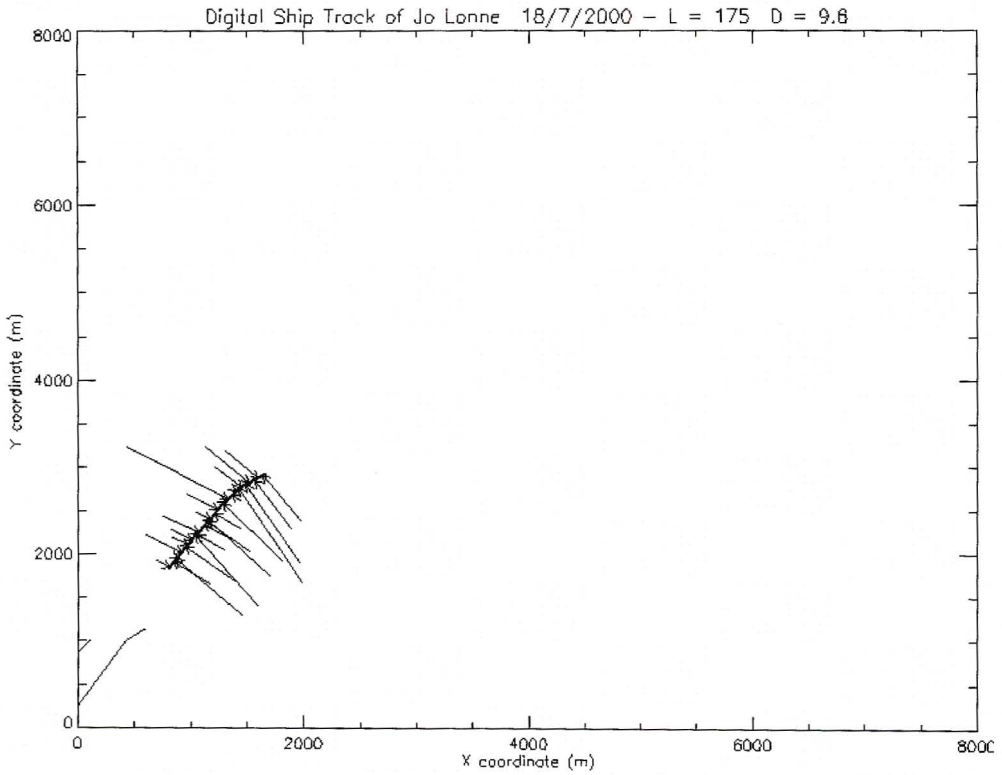

26. CAMBODA STAR

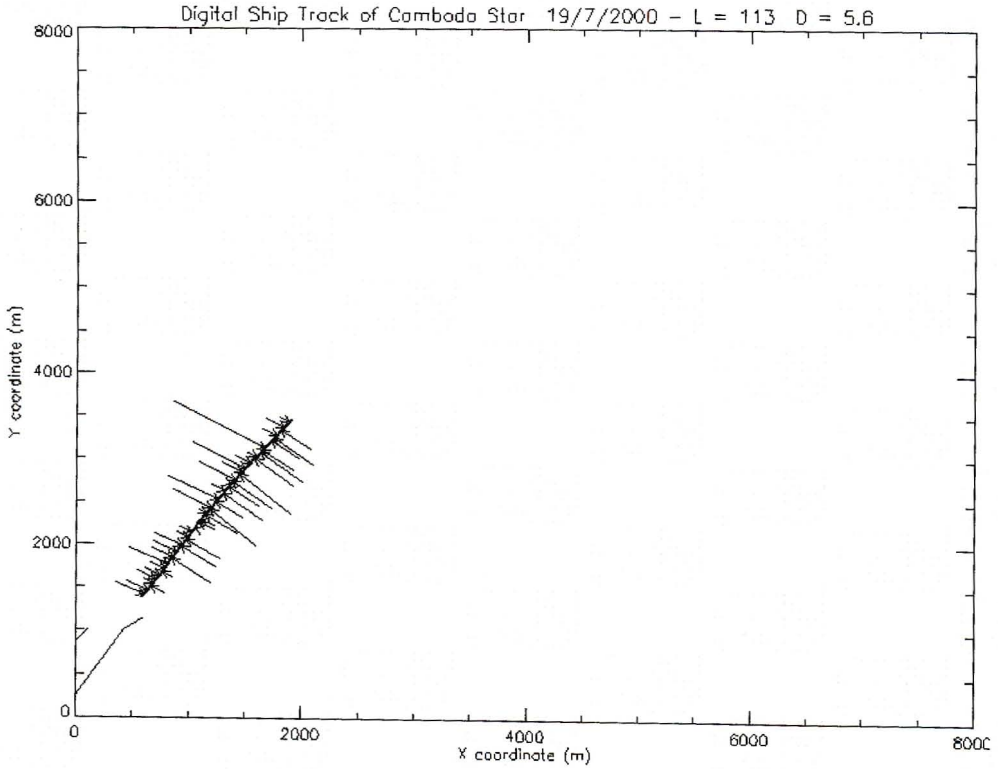

27. MASTER NICOS

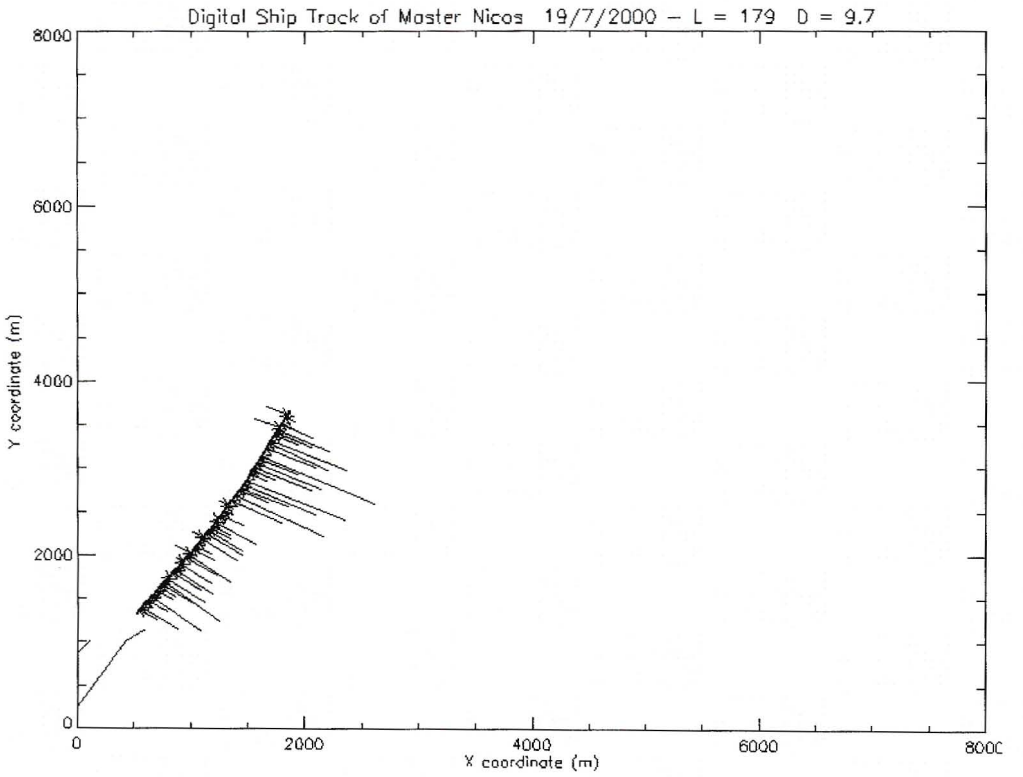

28. MARULAKI

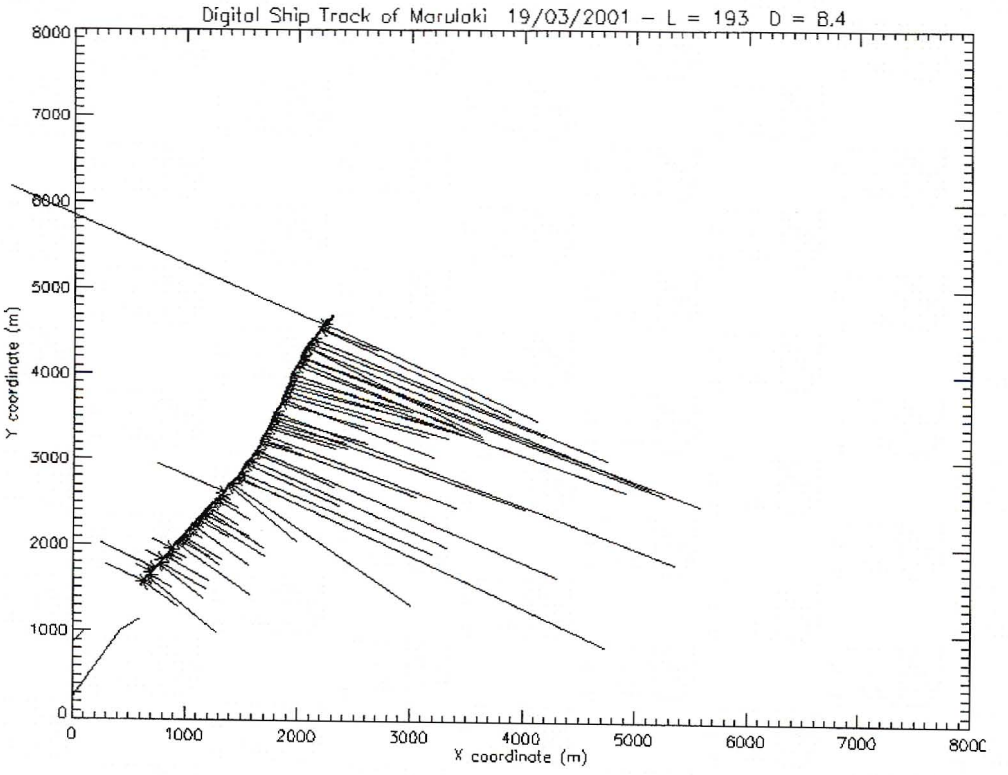

29. MEVA

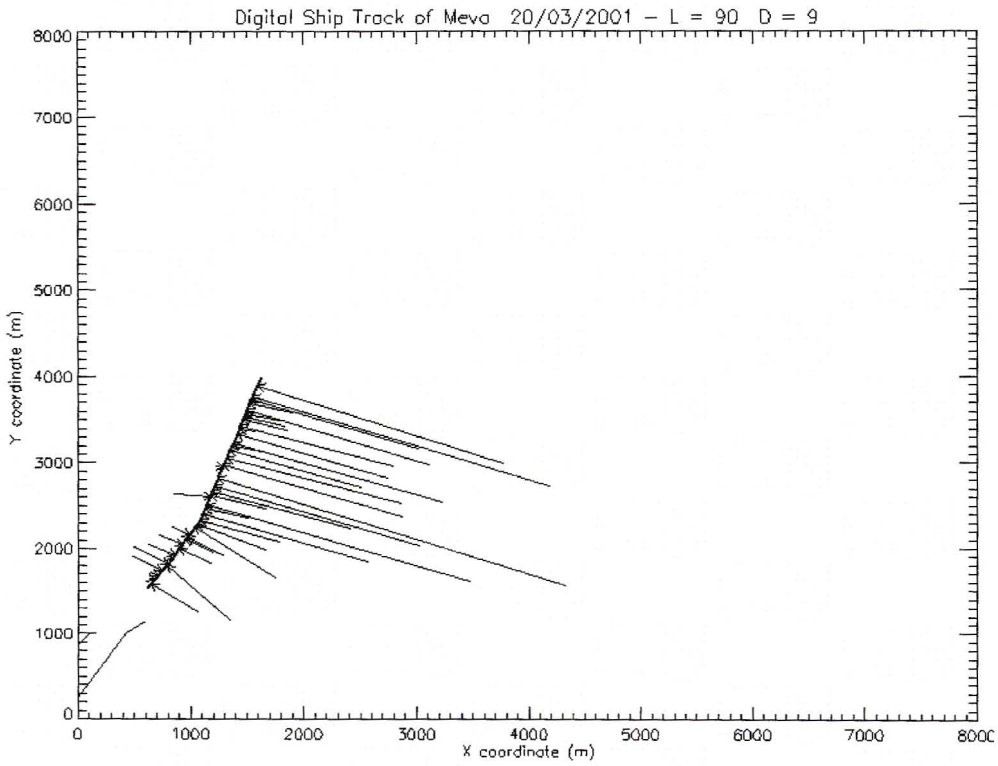

30. OCIURANCE

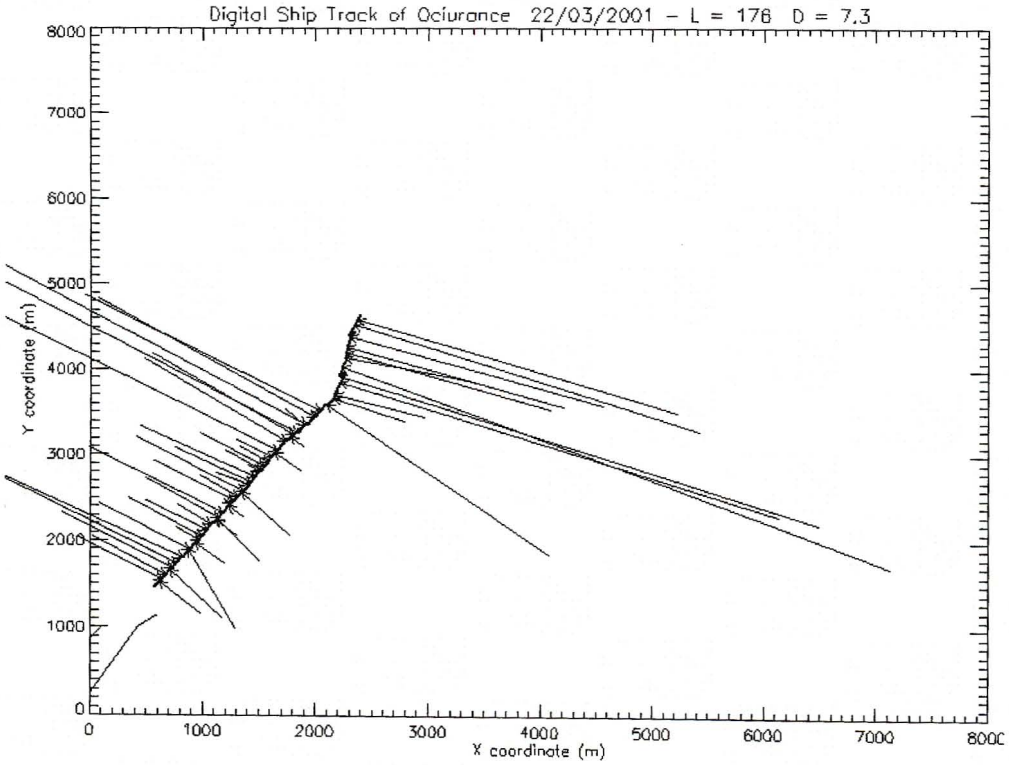

31. EVERGENIUS

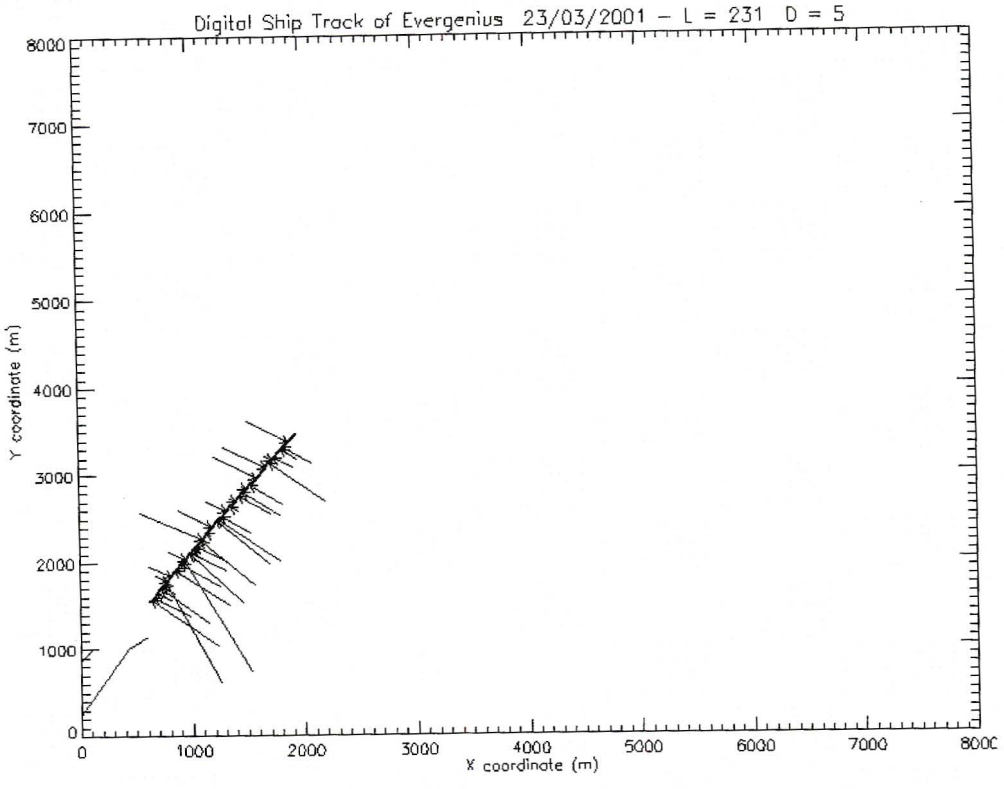

32. BERGE CLIPPER

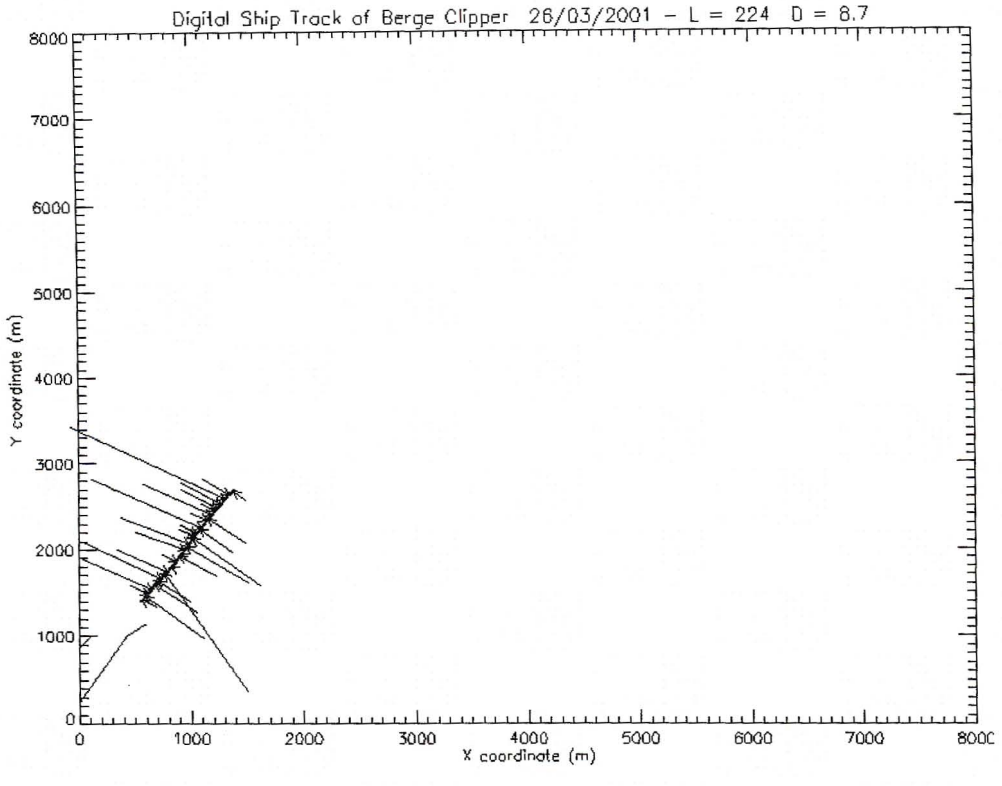

33. PROSPRIM CONT

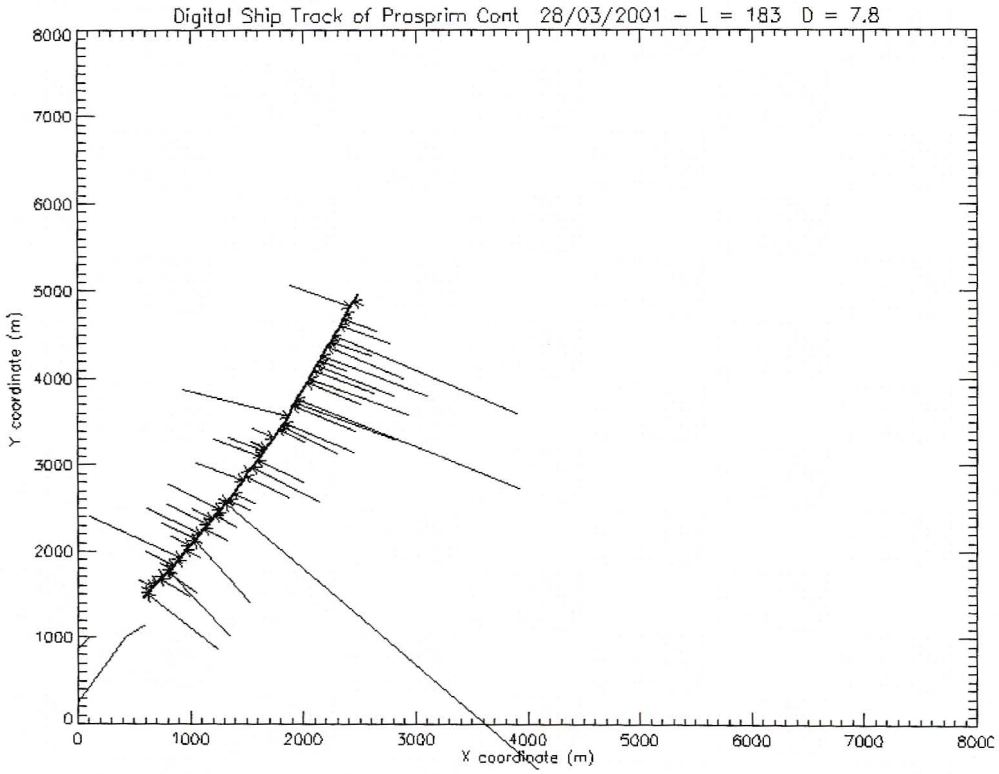

CTDV
0.5 m/s

34. JORBONY

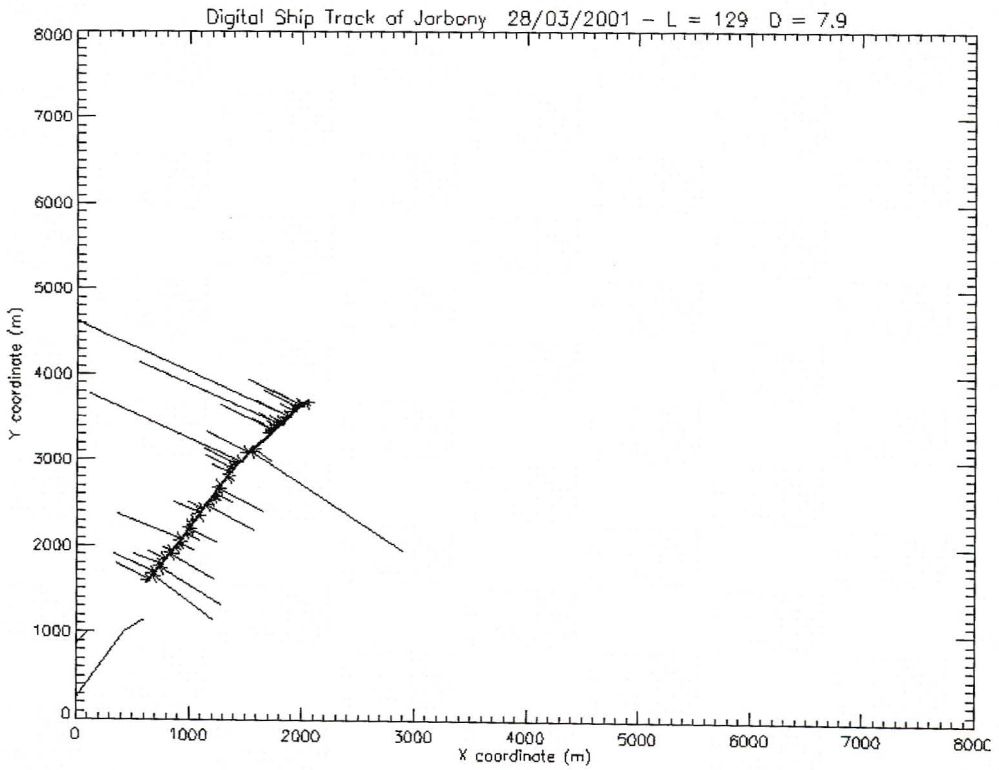

35. LISSOSM

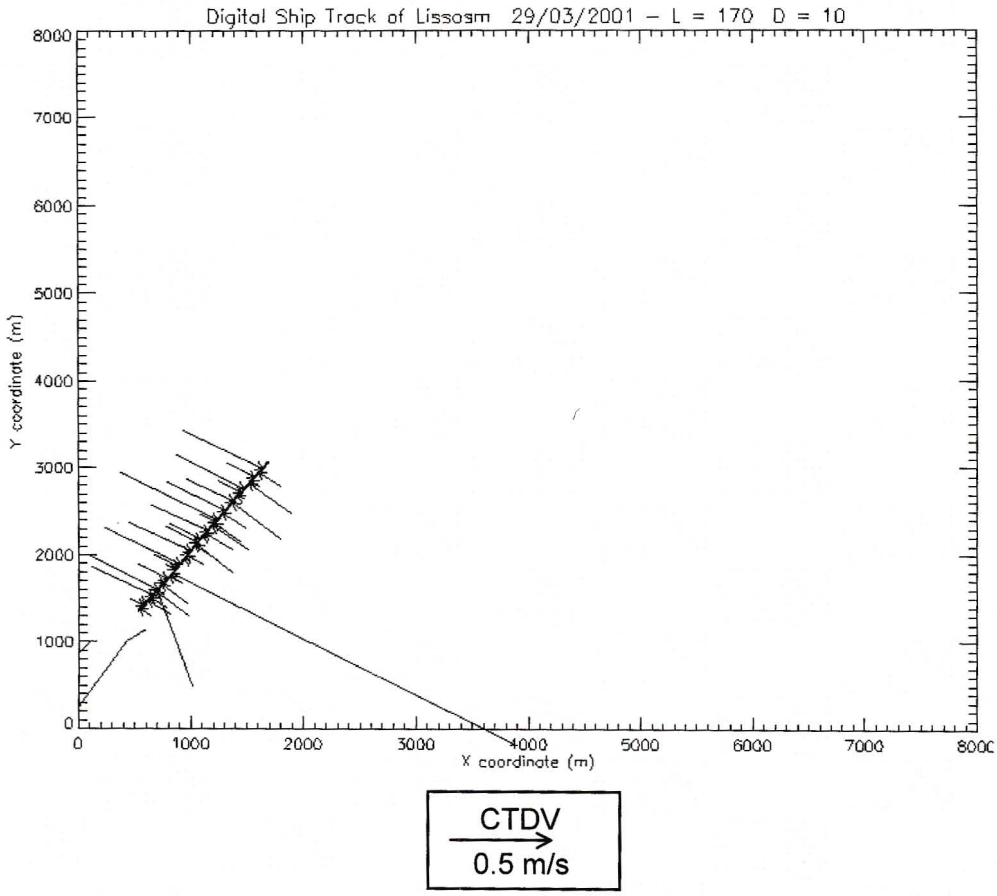

36. SD TRUIMPH

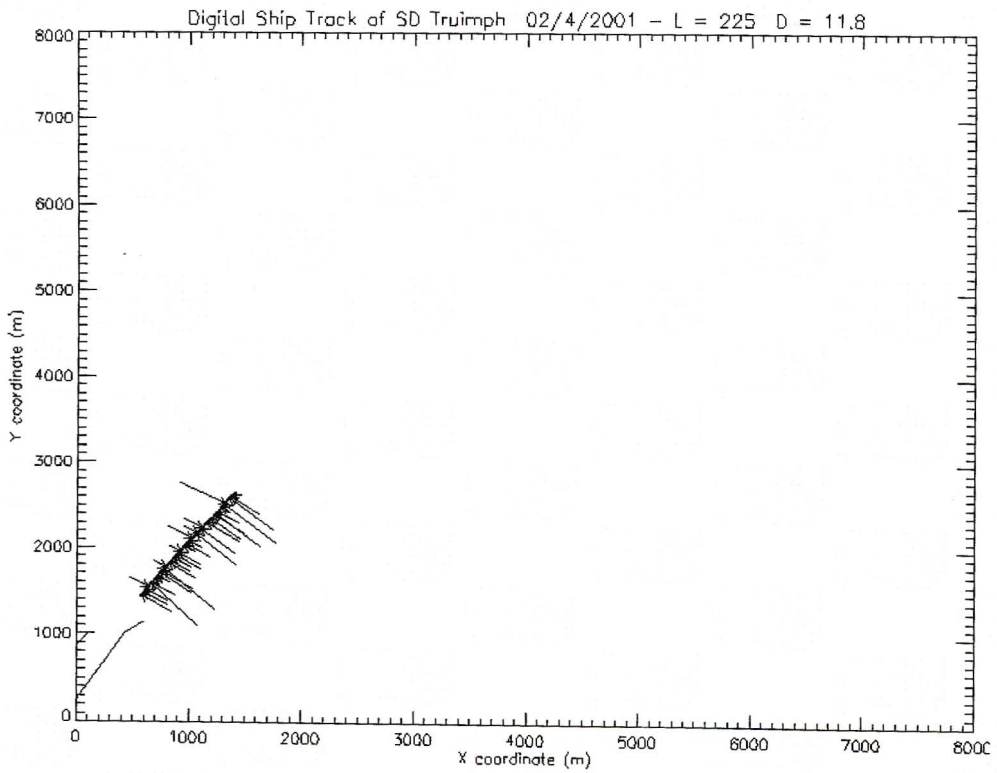

37. EMIRATE STAR

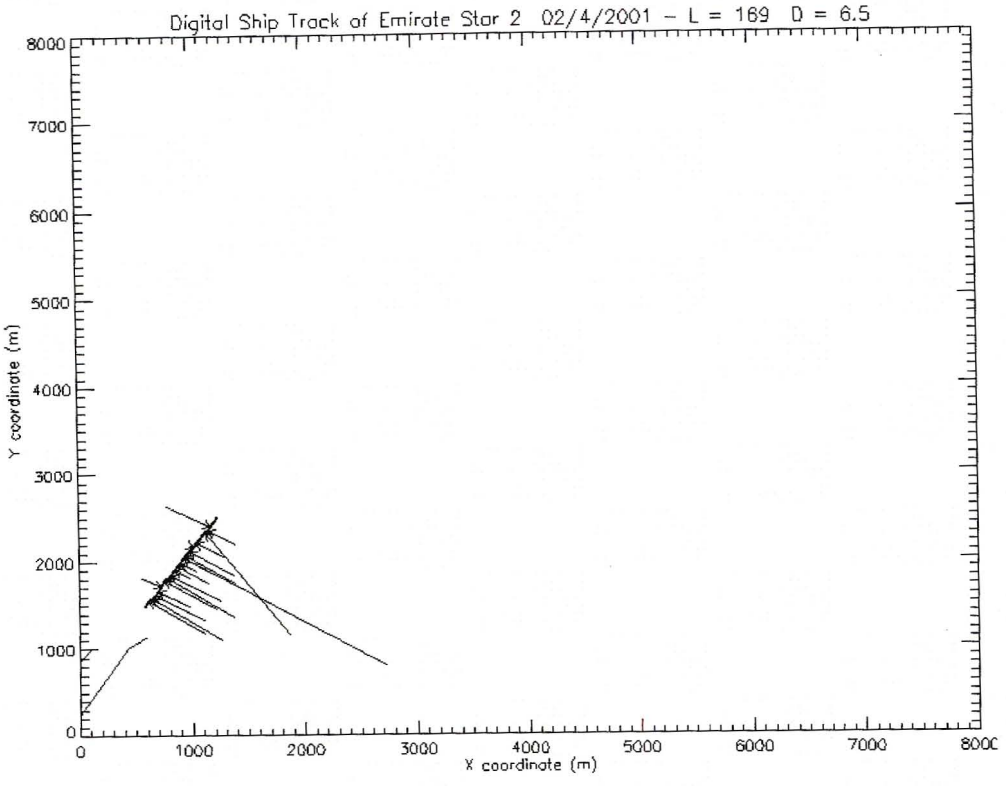

38. IRAN JAMAL

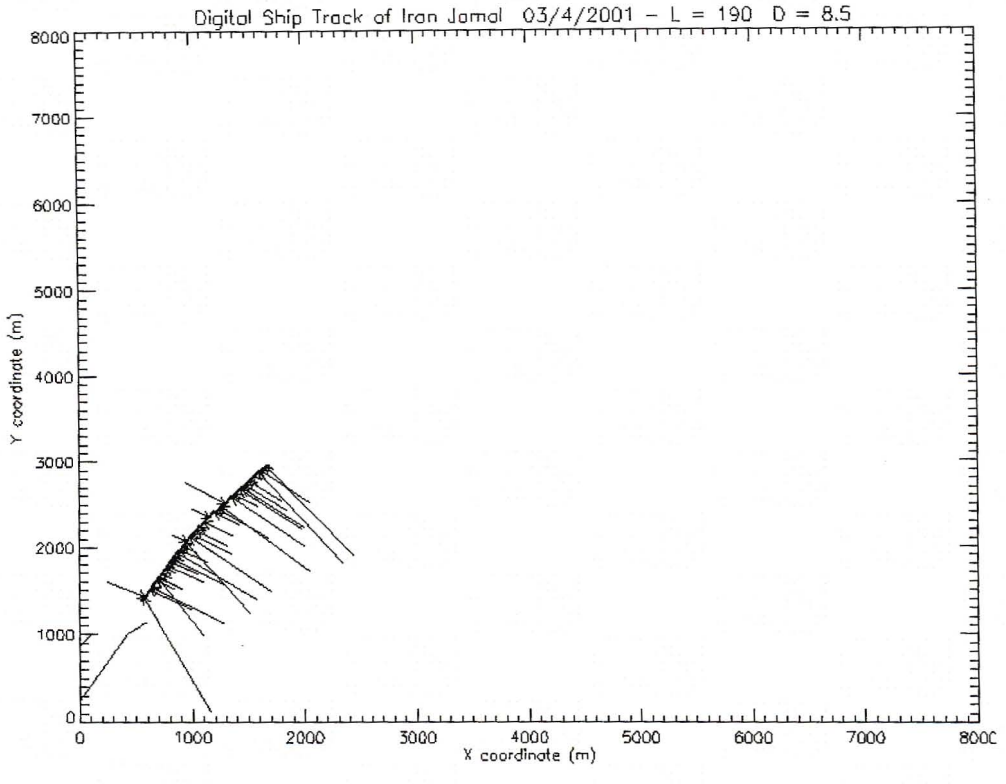

39. NED RIO GRANDE

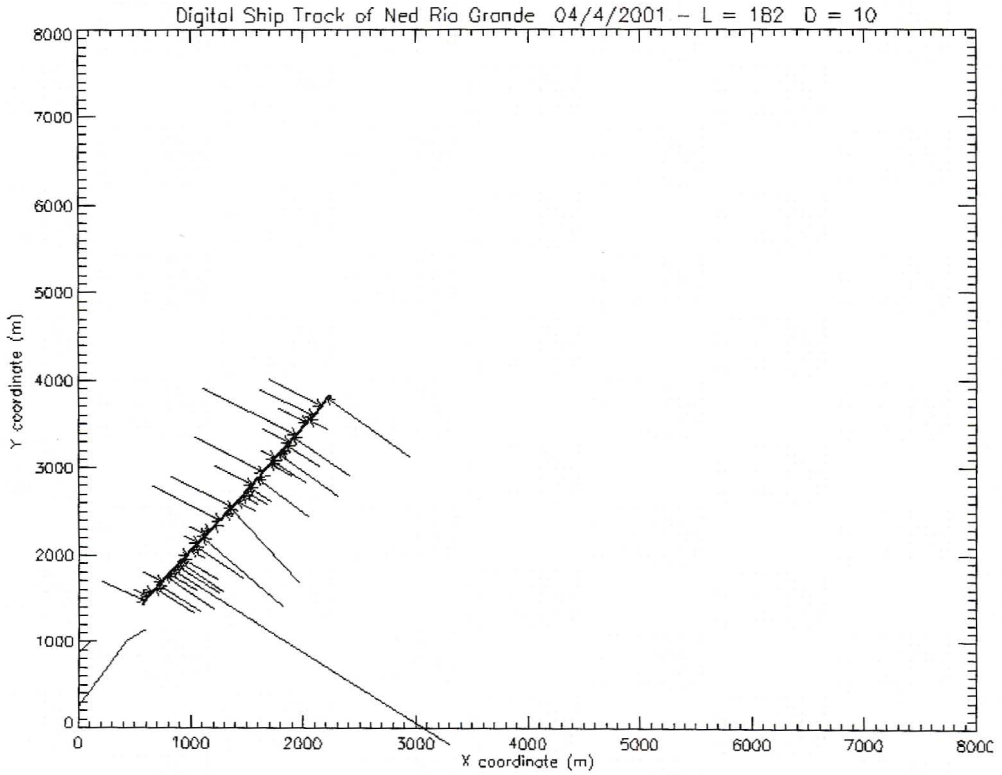

40. BARBRITE ARROW

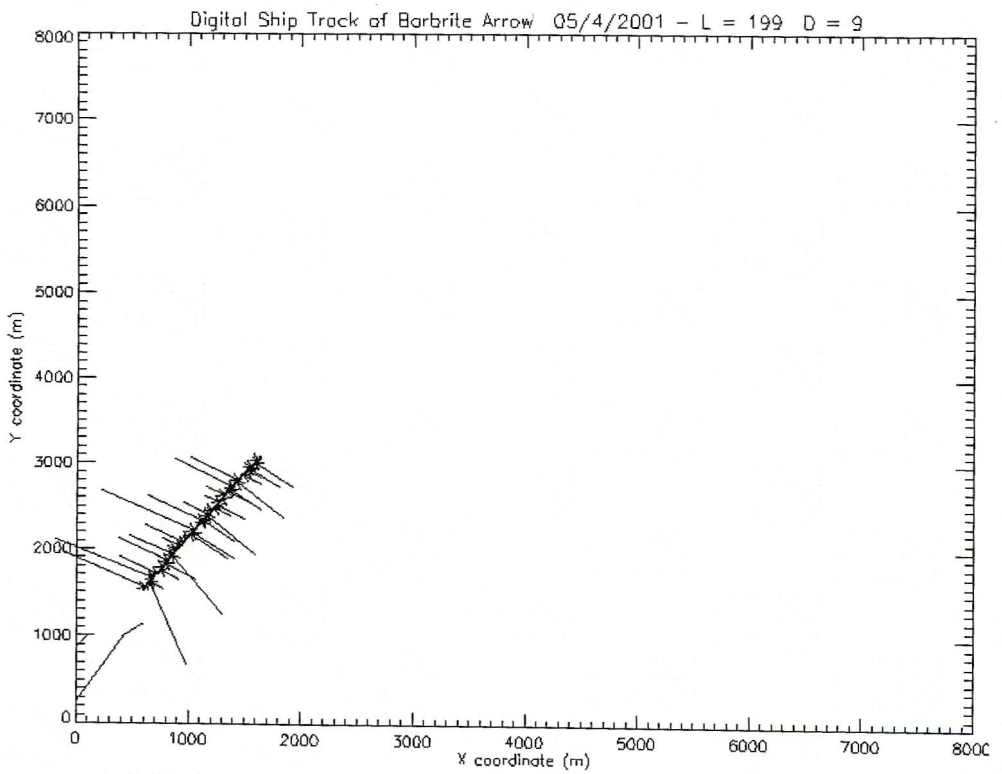

41. PRIDE

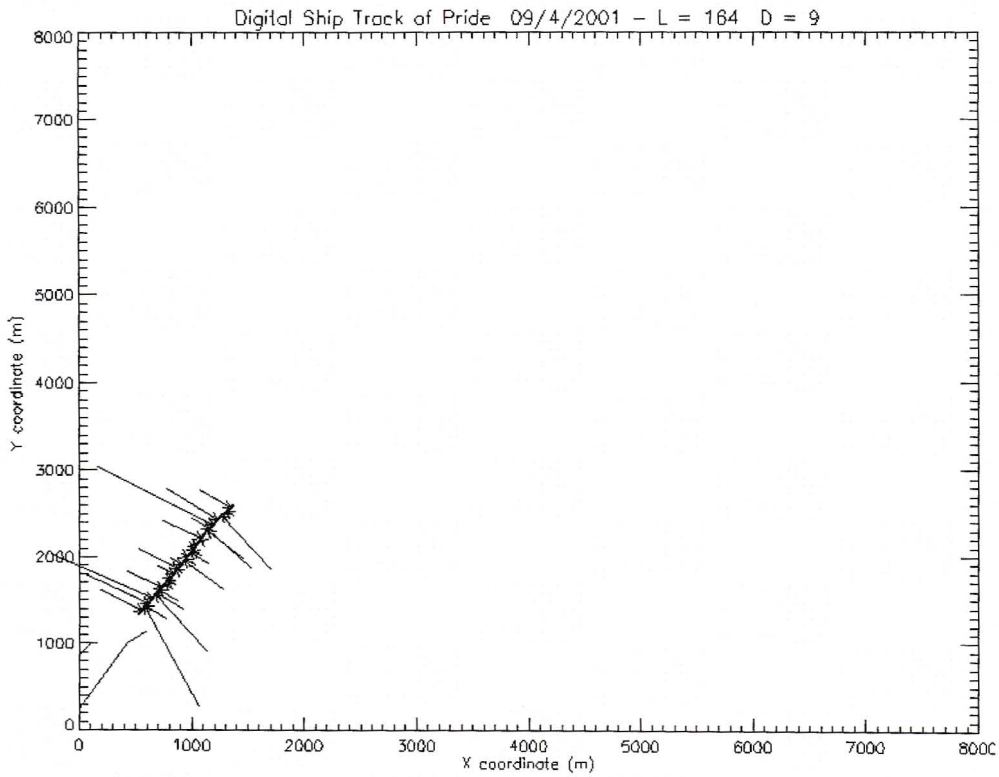

42. FENG ANSHAN

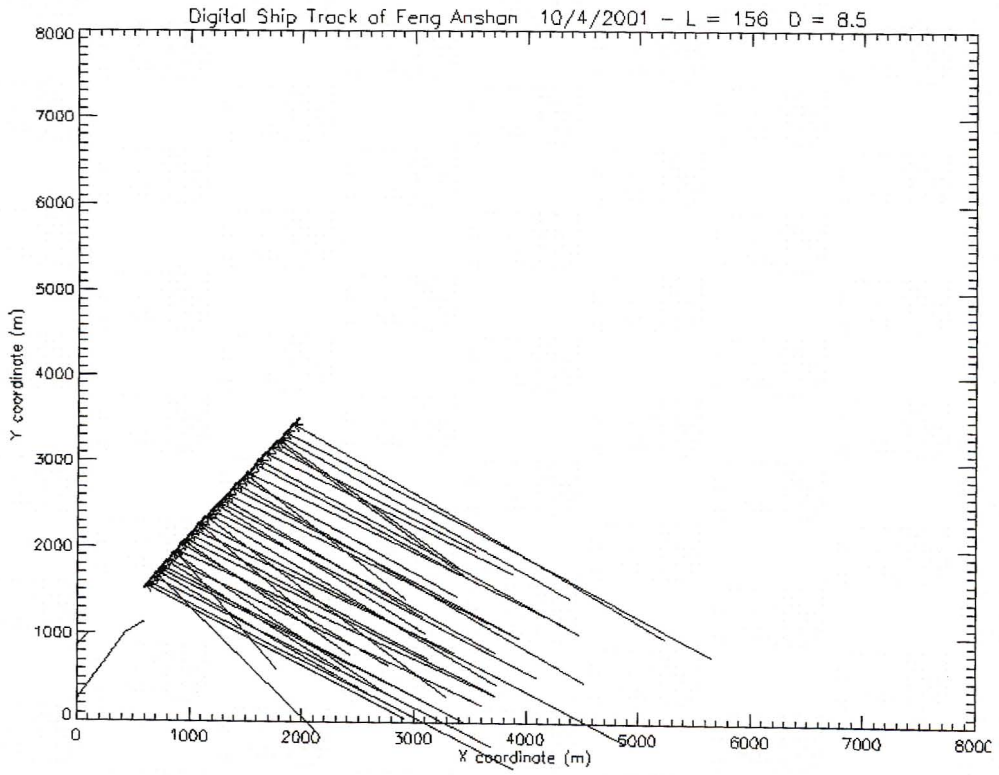

43. NAMIBIA

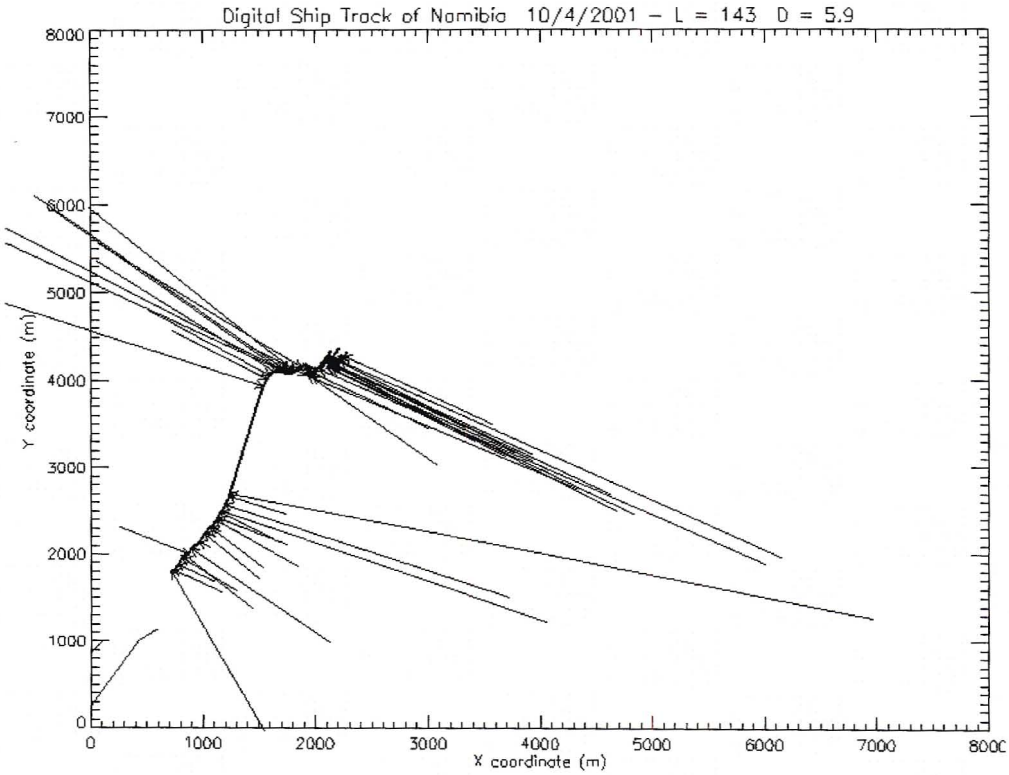

44. BELLA LONTRA

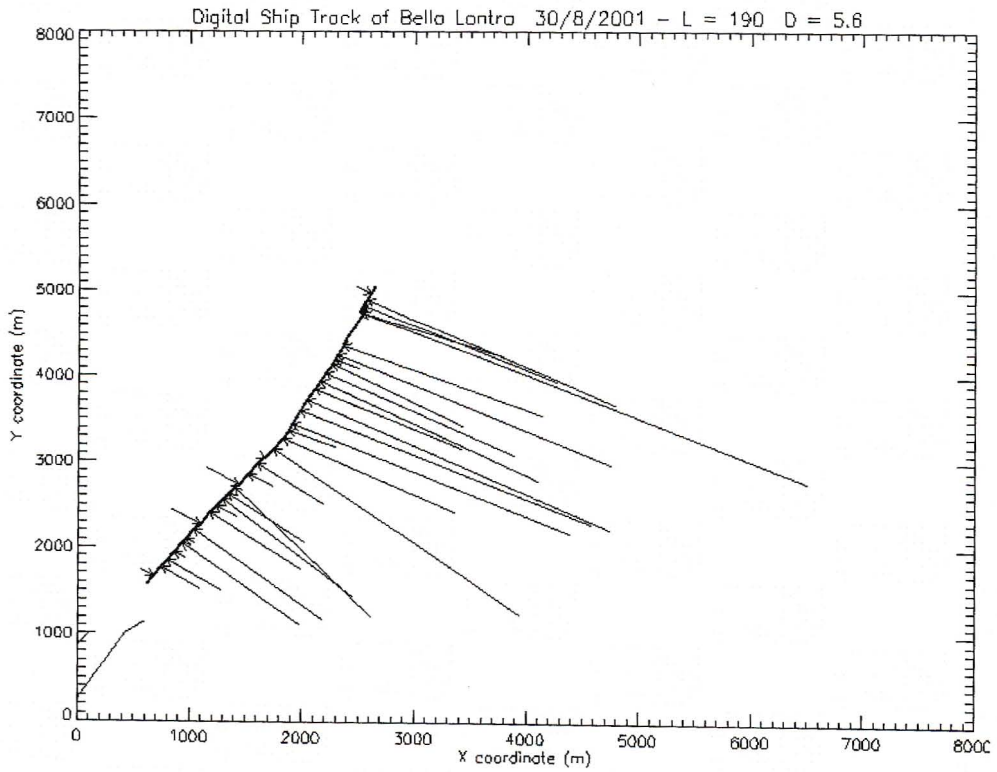

45. GLOBAL MOMBASA

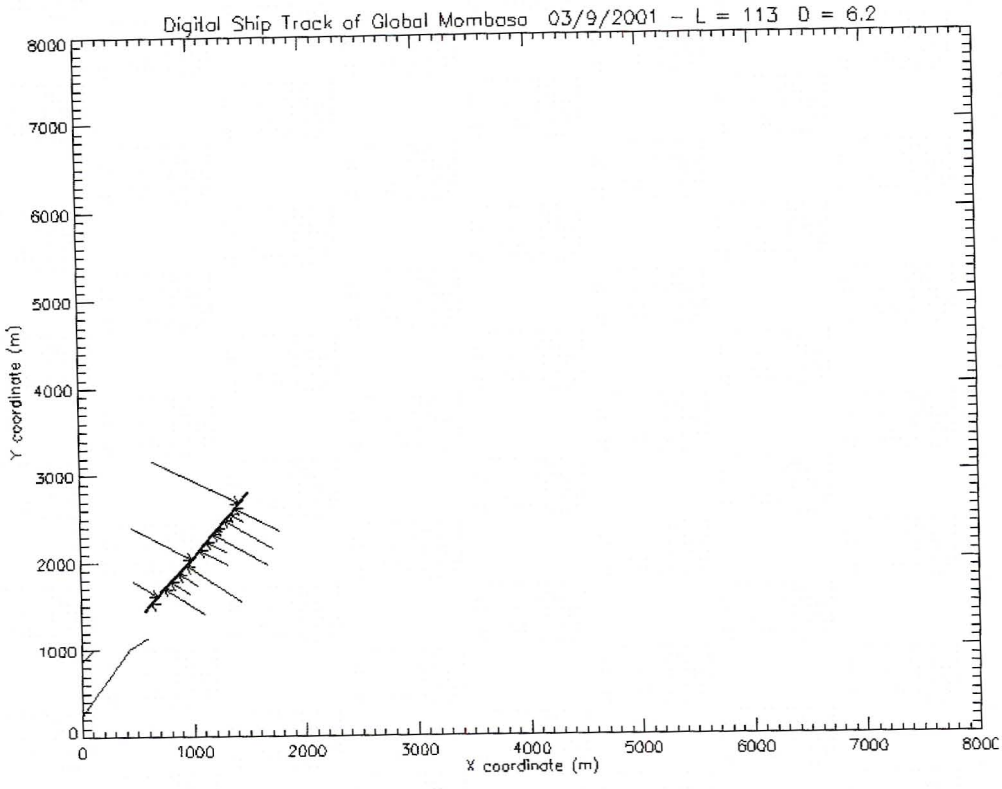

46. ALAM SENANG

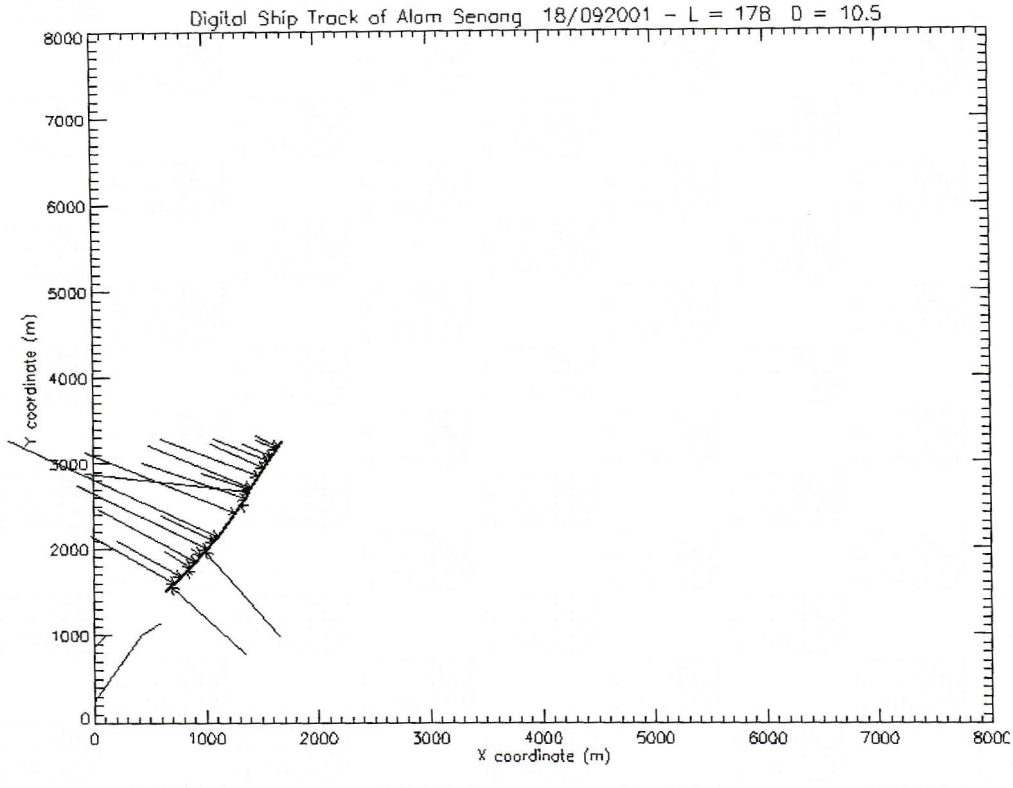

G.1. Saving Routines

```
//this routine accesses the imagebufferhandle and stores the
contents of this handle as a Temp1.bmp file in the working
directory. The programming code presented here was developed by
Sahil Patel and Derek Stretch whom own the copyrights. The MST
Library used was provided by Yurij Musatenko
void SavingTmp0()
{
      int   anu;
      TmstMemoryStream ms;
      TImageEnsemble ens;

      ms.init(&ImageBufferHandle,1327104);
      anu = ens.open(&ms,fiBmpFileInfo(image24BitPerPix,
      FIELD_WIDTH,FIELD_HEIGHT));
      TRGBImage& temp = *ens.getRGBImage();
      TimageEnsemble outputEns
      ("temp0.bmp",fiBmpFileInfo(image24BitPerPix,
      FIELD_WIDTH,FIELD_HEIGHT));
      outputEns.writeRGBImage(0, &temp[2]);
}

//this routine copies the contents of one file (temp0.bmp) to
another file (temp1.bmp)
void TempCopy()
{
      TImageEnsemble ens;
      ens.open("temp0.bmp");
      outputEns("temp1.bmp",fiBmpFileInfo(image24BitPerPix,
      FIELD_WIDTH,FIELD_HEIGHT));
      //read the first image into memory
      TRGBImage& img = *ens.getRGBImage();
      //create new empty image based on first images properties
      TRGBImage& outimg = *outputEns.getEmptyRGBImage();
      //copies the contents of source to destination
       imgcpy(&outimg, &img);
      for( i = 0; i < img.paletteSize(); i++)
      {
         outimg.palette[i] = img.palette[i];
      }
      // save the output image
      outputEns.putImage();
      //free memory correspondent to  the output image
      outputEns.freeImage();
      //free memory correspondent to the input image
      ens.freeImage();
}
```

```
//this routine is called when an image of JPEG OR BMP quality is
required to be saved on the hard disk
void SaveJpeg() OR SaveBmp()
{
      theTime = CTime::GetCurrentTime();
      year = theTime.Format( "%Y" );
      month = theTime.Format( "%b" );
      day = theTime.Format( "%d" );
      //The above 4 statements stores the the time and date
      features into specific strings

      //makes a directory on the local hardrive with the year
      month and day if it doesn't exist that is
      _mkdir( "\\" + year)
      system( "dir\\" + year );
      _mkdir( "\\" + year + "\\"+ month)
      system( "dir\\" + month);
      _mkdir( "\\" + year + "\\"+ month + "\\" + day)
      system( "dir\\" + day);

      //time string of the image
      timest = theTime.Format( "%H%M%S" );
      CString name1 =  "\\"+ year + "\\" + month + "\\"
                     + day + "\\" + timest + jpg OR bmp;
      //full path of where the image will be stored
      const char *name = name1;
      //timestamp of the image with extension
      timestamp= timest+jpg OR bmp;
      TmstMemoryStream ms;
      TImageEnsemble ens;
      int   anu;

      ms.init(&ImageBufferHandle,1327104);//1327104=768*576*3
      anu = ens.open(&ms,fiBmpFileInfo(image24BitPerPix,
                     FIELD_WIDTH,FIELD_HEIGHT));
      TImageEnsemble outputEnsjpeg(
                name,fiJpegFileInfo(image24BitPerPix,
                FIELD_WIDTH,FIELD_HEIGHT,100)); OR
      TImageEnsemble outputEnsbmp(
                name,fiBmpFileInfo(image24BitPerPix,
                FIELD_WIDTH,FIELD_HEIGHT));


      TRGBImage& img = *ens.getRGBImage();
      outputEnsjpeg.writeRGBImage(0, &img[2]); OR
      outputEnsbmp.writeRGBImage(0, &img[2]);
      ens.rejectAllImagesFromMemory();
      ms.clear();
      //close image frees memory
      outputEnsjpeg.close();
}
```

G.2. Correlation Routine

```
//calculates the correlation between temp0 and temp1 in a
specific region. Returns the correlation value which is less
than 1 or greater than -1. The programming code presented here
was developed by Sahil Patel and Derek Stretch whom own the
copyrights.
double Correlation_track(TRGBImage& img0,TRGBImage& img1,int
pxpixel,int pypixel,double ptcorr)
{
      double denxy=0;
      double syy=0,sxy=0,sxx=0,syr=0,sxr=0,syg=0,
        sxg=0,syb=0,sxb=0,ssx=0,ssy=0,ssxy=0;
      double covar,sigx,sigy;
           int ni=0,nj=0;
      int ROIsize_track=zregionsize*zregionsize;

      for(i = y1_d; i < y2_d; i++)//actually y
      {
           for(j = x1_d; j < x2_d; j++)//actually x
           {
                ni=i+pypixel;
                nj=j+pxpixel;
                sxr=sxr+img1.r(i,j);
                sxg=sxg+img1.g(i,j);
                sxb=sxb+img1.b(i,j);
                syr=syr+img0.r(ni,nj);
                syg=syg+img0.g(ni,nj);
                syb=syb+img0.b(ni,nj);
                sxx=sxx+(img1.r(i,j)*img1.r(i,j)+
                         img1.g(i,j)*img1.g(i,j)+
                         img1.b(i,j)*img1.b(i,j));
                syy=syy+(img0.r(ni,nj)*img0.r(ni,nj)+
                          img0.g(ni,nj)*img0.g(ni,nj)+
                         img0.b(ni,nj)*img0.b(ni,nj));

                sxy=sxy+(img1.r(i,j)*img0.r(ni,nj)+
                          img1.g(i,j)*img0.g(ni,nj)+
                          img1.b(i,j)*img0.b(ni,nj));
           }
      }

      ssx=(sxr*sxr+sxg*sxg+sxb*sxb);
      ssy=(syr*syr+syg*syg+syb*syb);
      ssxy=(sxr*syr+sxg*syg+sxb*syb);

      covar=(ROIsize_track*sxy-ssxy);
      sigx=(ROIsize_track*sxx-ssx);
      sigy=(ROIsize_track*syy-ssy);
      denxy=sigx*sigy;

      ptcorr= (covar/sqrt(denxy));
      return ptcorr;
      //correlation value
}
```

G.3. Rectification Procedure

```
//takes in the x and y pixel value and calculates the x and y
ground coordinate of these points. Perform subpixel accuracy
based on quadratic interpolation. The programming code presented
here was developed by Sahil Patel and Derek Stretch whom own the
copyrights.

void Transformation(int pxc,int pyc)
{
      double pxnew;
      double pynew;
      double alpha;
      double DistancetothePier;
      double ActualDistance;
      double Initialangle;
      double DiferenceVpixels;
      double delThetaver;
      double Vtheta;
      double XnewcoordsofPier;
      double YnewcoordsofPier;
      double delThetahor;
      double Rh;
      double T,a1,b1,c1,d1,XS,YS,Fi,Stot,d,w;
      int pixel_ref;
      double angle_main;
      double angle_pier;
      double sub_pxc=pxc+X_offset;
      double sub_pyc=pyc+Y_offset;

      XnewcoordsofPier = XcoordsofLighthouse - XcoordsofPier;
      YnewcoordsofPier = YcoordsofLighthouse - YcoordsofPier;
      DistancetothePier= sqrt(
                        (XnewcoordsofPier*XnewcoordsofPier)+
                              (YnewcoordsofPier*YnewcoordsofPier));

      alpha=fabs(atan(YnewcoordsofPier/XnewcoordsofPier)*180/pi)
      ActualDistance   = DistancetothePier*Hl/(Hl-HeightofPier);
      Initialangle     = 90-(atan((ActualDistance/(Hl-
                              heightofPier)))*180/pi;
      DiferenceVpixels= Yp-Yh;
      delThetaver      = Initialangle/DiferenceVpixels;
      Vtheta           = delThetaver*Ytot;
      delThetaver      = Vtheta/Ytot;
      delThetahor      = Htheta/Xtot;
      Rh               = sqrt((Ro+Hl)*(Ro+Hl)-(Ro*Ro));
      T                = tan((sub_pyc-Yh)*delThetaver*pi/(180));

      a1          = (2*T)*(2*T)*Rh-2*T*Ro;
      b1          = T*T+1;
      c1          = T*T*Rh*Rh-2*T*Ro*Rh;
      d1          = (a1*a1)-4*(b1)*(c1);
      e1          = 2*T*T*Rh-2*T*Ro

      XS          = (-(a1)-sqrt((a1*a1)-4*(b1)*(c1)))/(2*(b1));
      YS          = ((((-(e1)-sqrt(((e1)*(e1))-
```

```
                    4*(b1)*(c1)))/(2*(b1)))-Ro/T+Rh)*(-T));
    Fi          = sqrt((2*(Ro-YS))/Ro);
    Stot        = Ro*Fi;
    d           = Rh-(cos((Fi/2)*pi/(180))*Ro*Fi);
    w           = d/cos(delThetahor*pi/(180)*(Xp-sub_pxc));

    pxnew       = (w*sin((((Xtot-Xp)*delThetahor)+alpha)-
                  (Xtot-sub_pxc)*delThetahor)*pi/(180)));
    pynew       = (w*cos((((Xtot - Xp)*delThetahor) + alpha)-
                  (Xtot - sub_pxc)*delThetahor)*pi/(180)));

    xnew1=pxnew;
    ynew1=pynew;
    distance=sqrt(xnew1*xnew1+ynew1*ynew1);
    pixel_ref=Xtot-Xp;
    angle_main=(pixel_ref*delThetahor)+alpha;
    angle_pier=(Xtot-sub_pxc)*delThetahor;
    //angle from North to the point in reference
    angle=angle_main-angle_pier;

}
```

G.4. Tracking Routine

```
//Tracking algorithm used for tracking features on the ship as
the ship enters the harbour. Use of Cross correlation to
determine best fit. The programming code presented here was
developed by Sahil Patel and Derek Stretch whom own the
copyrights.

void Tracking(int ploop)
{
    int numpixels=0;
    int corr_array;
    double corr = -1.5;
    double oldcorr=-1.5;
    double rcorr = -1.5;

    //variables used to define search strategy
    const int sixe=9;
    int low,high;
    //sub pixel calcs
    int var;
    int centre;
    int xpixel=0;
    int ypixel=0;
    double tcorr=0;
    double rtcorr=0;

    //variables used for velocity vector calcs
    double xnew1old,ynew1old;
    double true_slope1;
    double true_slope;
```

```
//variables used for the left hand mouse button i.e. for
//the bow of the ship
int xpixel1;
int ypixel_old;
int xpixel_new1;
int ypixel_new1;
double tcorr_array[sixe];
double old_tcorr_array[sixe];
int oldx[sixe];
int oldy[sixe];
int newx[sixe];
int newy[sixe];
int oldx1[sixe];
int oldy1[sixe];
//end of variables used for the bow of the ship

//booleans used for operations
BOOL first=TRUE;
BOOL useold=FALSE;
//boolean used to control search strategy of left mouse
//point
BOOL SEARCH=TRUE;

TImageEnsemble ens0;
TImageEnsemble ens1;

ens0.open("temp0.bmp");//opens temp0.bmp image
ens1.open("temp1.bmp");//opens temp1.bmp image

//img0 hold temp0.bmp
TRGBImage& img0 = * ens0.getRGBImage();
//img1 hold temp0.bmp
TRGBImage& img1 = * ens1.getRGBImage();
numpixels=0;
corr_array=0;
//while the crosshairs and spanning crosses are visible
while(SEARCH || rSEARCH)
{
      numpixels=numpixels+1;
      if(numpixels==1)
      {
            first=TRUE;
      }
      else
      {
            first=FALSE;
      }
      if(first)
      {
            xpixel_new1=0;
            ypixel_new1=0;
      }
      else
      {
            xpixel_new1=x1new-x1_d;
            ypixel_new1=y1new-y1_d;
```

```
}
if(first==FALSE && xc!=NULL)
{
      for(int t=0;t<sixe;t++)
      {
            old_tcorr_array[t]=tcorr_array[t];
            oldx[t]=oldx1[t];
            oldy[t]=oldy1[t];
      }
}

//if the center of the ROI for the left point
corresponds to the maximum correlation
found in the previous step then we can stop
correlation as the local max has been found
if(   old_tcorr_array[((sixe-1)/2)]==corr)
{
      SEARCH=FALSE;
}

corr_array=0;
switch(sixe)
{
      case 9:
            low=1;
            break;
      case 25:
            low=2;
            break;
      case 49:
            low=3;
            break;
      case 81:
            low=4;
            break;
      case 121:
            low=5;
            break;
 }

 high=low+1;

 //xpixel and ypixel refer to points in the ROI
 for(xpixel = -low;xpixel<high;xpixel++)
 for(ypixel = -low;ypixel<high;ypixel++)
 {
 if((SEARCH==TRUE || rSEARCH==TRUE) ||
 (ypixel==0 && xpixel==0) && (first==TRUE))
 {
 //BEGINNING OF SEARCH STRATEGY IF LEFT HAND MOUSE
 BUTTON WAS CLICKED
 Do correlation for the point at which left button is
 clicked
 if(xc!=NULL && SEARCH==TRUE)
 {
       //x and y pixel relative to the original image
```

```
        xpixel1=xpixel_new1+xpixel;
        ypixel1=ypixel_new1+ypixel;
        newx[corr_array]=xpixel1;
        newy[corr_array]=ypixel1;
              useold=FALSE;
        if(first==FALSE)
        {
        for(int h=0;h<sixe;h++)
        {
              if((oldx[h]== newx[corr_array]) &&
                        (oldy[h]==newy[corr_array]))
              {
              //map values that have already been
              calculated (to save time)
              tcorr_array[corr_array]=old_tcorr_array[h]
              useold=TRUE;
              }
        }
        if(useold==FALSE)
        {
              tcorr_array[corr_array] =
              Correlation_track(img0,img1,xpixel1,
                                ypixel1,tcorr);
        }
}
//if a tracking point was chosen with the left mouse
button, for the first time when numpixels ==1 then
the correlation will be calculated here
if(xc!=NULL)
{
      if(first==TRUE)
      {
            //stores the correlation for the top left
            hand corner of the ROI when corr_array=0
            the points of the ROI are numbered top
            down left to right
            tcorr_array[corr_array] =
            Correlation_track(img0,img1,xpixel1,
                              ypixel1,tcorr);
      }

}
//if tcorr_array[corr_array] > corr which initially
is -1.5, it will update the corr value and set the 4
boundary points for the ROI box
if(xc!=NULL)
{
      if(tcorr_array[corr_array] > corr)
      {
            corr = tcorr_array[corr_array];
            x1new = x1_d+xpixel1;
            x2new = x2_d+xpixel1;
            y1new = y1_d+ypixel1;
            y2new = y2_d+ypixel1;
            xpixel_old=xpixel;
```

```
                    //if it entered this if statement then it
                    updates the xpixel as the old
                    ypixel_old=ypixel;
                    //if it entered this if statement then it
                    updates the xpixel as the old
               }
          }

          oldx1[corr_array]=newx[corr_array];
          oldy1[corr_array]=newy[corr_array];
     }

     corr_array=corr_array+1;
     }
     }
     }

     centre = (sixe-1)/2;
     var = sqrt(sixe);

     //quadratic interpolation used for subpixel accuracy
     X_offset = (-(old_tcorr_array[centre+var]-
               old_tcorr_array[centre-
               var])/2)/(old_tcorr_array[centre-var]-
               2*old_tcorr_array[centre]+old_tcorr_array[centre
               +var]);
     Y_offset = (-(old_tcorr_array[centre+1]-
               old_tcorr_array[centre-
               1])/2)/(old_tcorr_array[centre-1]-
               2*old_tcorr_array[centre]+old_tcorr_array[centre
               +1]);

     xnew1old=xnew1;
     ynew1old=ynew1;
     if(ploop!=1)
     {
          oldyc=yc;
     }
     if(xc!=NULL)
     {
          x1_d = x1new;
          x2_d = x2new;
          y1_d = y1new;
          y2_d = y2new;
          xc = x1_d+((zregionsize-1)/2);
          yc = y1_d+((zregionsize-1)/2);
          new_Transformation(xc,yc);
     }
     if(oldyc!=yc)
     {
          true_slope1=((ynew1old-ynew1)/(xnew1old-xnew1));
          true_slope=atan(true_slope1)*180/pi;

          if(true_slope<0)
          {
               velocity=(90+true_slope)+180;
```

```
                velocityold=velocity;
            }
            else
            {
                velocity=(90-true_slope)+180;
                velocityold=velocity;
            }
        }
        else
        {
            velocity = velocityold;
            velocityold=velocity;
        }

        if(ploop==1)
        {
            inithordist = distance*tan(Htheta*pi/(180));
            initdistperpixel = inithordist/FIELD_WIDTH;
            initroidist= initdistperpixel*zregionsize;
        }
        else
        {
            hordist = distance*tan(Htheta*pi/(180));
            distperpixel = hordist/FIELD_WIDTH;
            roidist=initroidist;
            zregionsize=floor(roidist/distperpixel);
        }

        if(zregionsize %2 == 0)
        {
            zregionsize = zregionsize+1;
        }
        if(zregionsize <=5)
        {
            zregionsize =5;
        }
        //TRACE("END OF TRACKING\n");
}
```

G.5. Grab Picture Button

```
//camera button that grabs a single image and displays it on gui
this image is saved as file temp1.bmp to the local working
directroy, which is overwritten once this button is repressed.
The programming code presented here was developed by Sahil Patel
and Derek Stretch whom own the copyrights.

void CSingleCapView::OnViewGrabpicture()
{
    BOOL Lock = FALSE;
    //locks memory for DMA transfer
    Lock = RioMemLock();
    //grab image from board and save it to ImageBufferHandle
    RioGrabPicture();
```

```
        //save image in ImageBufferHandle to Temp1.bmp in working
        directory
        SavingTmp1();
        green = TRUE;
        blue= TRUE;
        red=FALSE;
        runstream = FALSE;
        running = FALSE;
        Track=FALSE;
        exitgrabs= TRUE;
        //updates gui
        InvalidateRect(NULL, FALSE);
        //updates latest image on gui
        UpdateWindow();
        //locks memory for DMA transfer
        Lock = RioMemLock();
}
```

G.6. Streaming Button

```
//streaming video button works on a thread which continually
grabs and updates the GUI with the latest image. The user may
decide to save these images to disk or not. Images are saved
with the filenames dependant on the current system time.i.e.
hh:mm:ss. This streaming video may be stopped by the use of the
stop button. The programming code presented here was developed
by Sahil Patel and Derek Stretch whom own the copyrights.

void CSingleCapView::OnViewStream()//blue button
{
        exitgrabs=FALSE;
        Capturing = FALSE;
        BOOL Lock = FALSE;
        BOOL Unlock = FALSE;

        while (runstream)
        {
                //locks memory for DMA transfer
                Lock = RioMemLock();
                //grab image from board and save it to
                ImageBufferHandle
                RioGrabPicture();
                //updates GUI
                InvalidateRect(NULL, FALSE);
                //updates latest image on GUI
                UpdateWindow();
                //if no_trigger = 1 then user has decided to save
                images to disk during streaming capture. If
                no_trigger = 0 then images are not saved to disk.
                Default setting=0
                if(no_trigger==1)
                {
                        //if filetype=1 then user has decided to save
```

```
                images to disk with extension .bmp else if
                filetype=0 then user wants to save images with
                extension .jpg
                if (filetype==1)
                {
                      //routine used to save images with a
                      timestamp (hhmmss.bmp). Images saved in
                      directory default drive
                      year/month/day/timestamp
                      routine found in RioRoutines.cpp
                      SaveBitmap();
                }
                else
                {
                      //routine used to save images with a
                      timestamp (hhmmss.jpg). Images saved in
                      directory default drive
                      /year/month/day/timestamp
                      //routine found in RioRoutines.cpp
                      SaveJpeg();

                }
          }


          if(no_trigger==1)
          {
                //only if images are being saved to disk during
                streaming capture will RioMemLock be required
                Lock = RioMemLock();
          }
          else
          {
                //if images are  not being saved to disk during
                streaming capture, RioMemUnlock will be required
                Unlock = RioMemUnlock();
          }
}
//this is required to ensure that memory is allocated and to
ensure stability in the programme
Lock = RioMemLock();//locks memory for DMA transfer

Capturing = TRUE;
exitgrabs=TRUE;
}
```

G.7. Manual Button

```
//Manual Capture button allows the user to grab images and save
it to the hard disk at specific time intervals. Images will be
saved to disk with the timestamp and in the defaultdirectory.
The programming code presented here was developed by Sahil Patel
and Derek Stretch whom own the copyrights.

void CSingleCapView::OnViewManual()
{
      BOOL Lock = FALSE;
      CTime startTime = CTime();
      CTime endTime = CTime();
      //numerical variables defined here
      int counter=0;
      double correlation_exit,oldcorrelation_exit;
      // booleans used for the buttons
      exitgrabs=FALSE;
      Capturing = FALSE;
      corr_limit_n=(corr_limit/100)*1;
      while (running)
      {
            im = im + 1;
            counter = counter + 1;
            //starttime and endtime in code to capture an image
            at specific time intervals
            startTime = CTime::GetCurrentTime();
            endTime = CTime::GetCurrentTime();
            endTime = endTime + time_interval;
            // when starttime and endtime are equal than proceed
            to lock image in memory else continue until so
            while (startTime < endTime )
            {
                  startTime = CTime::GetCurrentTime();
            }
            //locks image for DMA transfer
            Lock = RioMemLock();

            //grab image from board and save it to
            ImageBufferHandle
            RioGrabPicture();
            //updates gui
            InvalidateRect(NULL, FALSE);
            //updates latest image on gui
            UpdateWindow();
            //if no_trigger = 1 then user has decided to save
            images to disk during streaming capture. If
            no_trigger = 0 then images are not saved to disk.
            Default setting=0
            if(no_trigger==1)
            {
                  //if filetype=1 then user has decided to save
                  images to disk with extension .bmp else if
                  filetype=0 then user wants to save images with
                  extension .jpg
                  if (filetype==1)
```

```
            {
                  //routine used to save images with a
                  timestamp (hhmmss.bmp). Images saved in
                  directory default drive
                  year/month/day/timestamp routine found in
                  RioRoutines.cpp
                  SaveBitmap();
            }
            else
            {
                  //routine used to save images with a
                  timestamp (hhmmss.jpg). Images saved in
                  directory default drive
                  /year/month/day/timestamp routine found in
                  RioRoutines.cpp
                  SaveJpeg();
            }
      }
      //If the user would like to initiate a manual capture
      session but not wait to stop it manually, he/she can
      select radio buttons from the Format dialogue box to
      monitor the exit region, by use of correlations in
      the exit region. The first image captured is used as
      the initial image amongst all other images captured
      are compared to for the correlations. If this feature
      is activated the user will still have functionality
      to manually stop the capture
      if(no_manual!=0)
      {
            //saves file Temp0.bmp to working directory
            SavingTmp0();
            //calculates the correlation
            correlation_exit=Correlation_exit();
            //the oldcorrelation which is the first
            correlation calculated is compared to the
            current correlation value. if this current value
            is less than the old correlation value by 0.1
            then the procedure will be stopped by a call to
            the stop button

            if(correlation_exit < (oldcorrelation_exit-
            corr_limit_n))
            {
                  OnViewStop();
                  counter=0;
            }
            if(counter==1)
            {
                  oldcorrelation_exit=correlation_exit;
            }
      }
      //locks memory
      Lock = RioMemLock();
      Capturing = TRUE;
      exitgrabs=TRUE;
}
```

G.8. Trigger Button

```
//This Trigger subroutine is a routine which allows the user to
put the application into a static mode, which monitors the entry
region for a ship to enter. When a ship enters and passes
through this region the capture sequence is triggered and images
are saved to hard disk. When the same ship enters the exit
region a stop trigger will be initiated which will stop the
sequence all together and wait for further ships to enter for
the process to be repeated. The programming code presented here
was developed and is copyrighted to Sahil Patel and Derek
Stretch.

void CSingleCapView::OnViewTrigger()//GREEN BUTTON
{
      CTime startTime = CTime();
      CTime endTime = CTime();
      //general booleans used
      save= FALSE;
      //boolean used to control memory allocation and
      deallocation
      BOOL Lock = FALSE;
      //numerical variables defined here
      int counter=0;
      double
      correlation_edge,correlation_exit,correlation_entry;
      double oldcorrelation_exit;
      double oldcorrelation_edge;
      double oldcorrelation[16];
      double correl[16];
      // booleans used for the buttons
      exitgrabs=FALSE;
      Capturing = FALSE;
      corr_limit_n=(corr_limit/100)*1;
      //initialize correlation values to be used
      for (int init=0;init<16;init++)
      {
            oldcorrelation[init]=0.0;
            correl[init]=0.0;
      }
      //This routine sets the entry and exit region bounds, and
      can be found in the RioRoutines.cpp file

      SetTrigger(xmax_exit,xmin_exit,ymax_exit,ymin_exit,
      ymax_entry,ymin_entry);
      //while the trigger button is activated and trigger is not
      initiated the while loop will continue until the save
      boolean becomes TRUE. This is done by looking at
      correlation values for image 1 and comparing it to image 1
      plus delta t.(image 2, image 3 etc). If the correlation
      value drops below 0.05 of the initial value then capture
      will be initiated and the save boolean will be set to
      TRUE, thus acquiring images to disk at a fixed interval
      while (running && save == FALSE)
      {
            im = im + 1;
```

```
counter = counter + 1;
// starttime and endtime in code to capture an image
at specific time steps
startTime = CTime::GetCurrentTime();
endTime = CTime::GetCurrentTime();
endTime = endTime + test_interval;
// when starttime and endtime are equal than proceed
to lock image in memory else continue until so
while (startTime < endTime )
{
      startTime = CTime::GetCurrentTime();
}
//locks image for DMA transfer
Lock = RioMemLock();
//grab image from board and save it to
ImageBufferHandle
RioGrabPicture();
//updates gui
InvalidateRect(NULL, FALSE);
//updates latest image on gui
UpdateWindow();
//updates the temp0.bmp file with current
imagebufferhandle image
SavingTmp0();
//correlates the contents of temp0.bmp and temp1.bmp
and compares it with theinitial correlation values
stored in the oldcorrelation[num] array;
wymin = 0;
wymax=wymin;
for(int nums=0;nums<16;nums++)
{
      //sets the region where the correlation will be
      determined
      Setentry(wymin,wymax);

      //every 20 minutes the temp1.nmp will be updated
      and used for the correlation

      if(counter % (20*60/test_interval) == 0)
      {
            //updates the contents of the temp1.bmp by
            copying the current temp0.bmp info
            TempCopy();
            oldcorrelation[nums]=correl[nums];
      }

      correlation_entry = Corellation_entry();
      correl[nums]=correlation_entry;
      if(correl[nums]<(oldcorrelation[nums]-
      corr_limit_n))
      {
            //boolean needed to save images to disk
            (when true)
            save= TRUE;
            //initialise counter
            counter=0;
```

```
                //updates the contents of the temp1.bmp by
                copying the current temp0.bmp info
                TempCopy();
        }

        if(counter==1)
        {
                oldcorrelation[nums]=correl[nums];
        }

        wymin = wymax;
        wymax = wymin+(fieldwidth/16);
}

//if the correlation along the edge of the current
temp0.bmp and temp1.bmp is less than the average by
corr_limit then it will trigger the capturing routine
correlation_edge = Correlation_edge();
if(correlation_edge<(oldcorrelation_edge-
        corr_limit_n))
{
        //boolean needed to save images to disk (when
        true)
        save= TRUE;
        //initialise counter
        counter=0;
        //updates the contents of the temp1.bmp by
        copying the current temp0.bmp info
        TempCopy();
}
if(counter==1)
{
        oldcorrelation_edge=correlation_edge;
}

// this routine will only be executed if save is TRUE
while(running && save==TRUE)
{
        counter=counter+1;
        //starttime and endtime in code to capture an
        image at specific time intervals
        startTime = CTime::GetCurrentTime();
        endTime = CTime::GetCurrentTime();
        endTime = endTime + time_interval;
        // when starttime and endtime are equal than
        proceed to lock image in memory else continue
        until so

        while (startTime < endTime )
        {
                startTime = CTime::GetCurrentTime();
        }
        //locks image for DMA transfer
        Lock = RioMemLock();
        //grab image from board and save it to
        ImageBufferHandle
```

```
RioGrabPicture();
//updates gui
InvalidateRect(NULL, FALSE);
//updates latest image on gui
UpdateWindow();
//if no_trigger = 1 then user has decided to
save images to disk during streaming capture. If
no_trigger = 0 then images are not saved to
disk. Default setting=0
if(no_trigger==1)
{
      //if filetype=1 then user has decided to
      save  images to disk with extension .bmp
      else if filetype=0 then user wants to save
      images with extension .jpg
      if (filetype==1)
      {
            //routine used to save images with a
            timestamp (hhmmss.bmp). Images saved
            in directory default drive
            year/month/day/timestamp routine
            found in RioRoutines.cpp
            SaveBitmap();
      }
      else
      {
            //routine used to save images with a
            timestamp (hhmmss.jpg). Images saved
            in directory default drive
            /year/month/day/timestamp routine
            found in RioRoutines.cpp
            SaveJpeg();
      }
}
correlation_exit=Correlation_exit();
if(correlation_exit < (oldcorrelation_exit -
corr_limit_n))
{
      //boolean needed to stop saving images to
      disk (when false)
      save= FALSE;
      //initialise counter
      counter=0;
      //updates the contents of the temp1.bmp by
      copying the current temp0.bmp info
      TempCopy();
      oldcorrelation_exit=0;
      oldcorrelation_edge=0;
      for(int nums=0;nums<16;nums++)
      {
            oldcorrelation[nums]=0;
            correl[nums]=0;
      }
      //RETURN TO CHECKING FOR NEW SHIPS AND
      STOP SAVING.SAVE OVER
}
```

```
                if(counter==2)
                {
                        oldcorrelation_exit=correlation_exit;
                }
            }
            //so that it continues to search for another ship in
            the entry region
            save=FALSE;
}
//locks memory for DMA transfer
Lock = RioMemLock();
Capturing = TRUE;
exitgrabs=TRUE;
}
```

G.9. Tracking Button

```
void CSingleCapView::OnViewTracking()
{
      //booleans used for operations
      BOOL Lock = FALSE;
      BOOL Unlock=FALSE;
      BOOL first = TRUE;

      const char *filename;
      CString date;
      CString filename1;
      FILE *trackfile;

      //numerical variables defined here
      int counter=0;
      // booleans used for the buttons
      exitgrabs=FALSE;
      Capturing = FALSE;
      save= TRUE;
      //setting up the time variables
      CTime startTime = CTime();
      CTime endTime = CTime();
      //using the current time to get the name of the filename
      where data will be output
      startTime = CTime::GetCurrentTime();
      date = startTime.Format( "%d_%b_%Y" );
      filename1 = date + ".txt";
      filename = filename1;

      //if the file already exists then it will ignore the next
      if statement, but if it doers not exist then it will
      create the file based on the filename generated above and
      write the first line of data in the file which forms the
      header
      if( (trackfile  = fopen(filename, "r")) == NULL )
      {
            trackfile  = fopen(filename, "a+");

            fprintf(trackfile,"No,accurate time,Image,Bow_x_pix,
              Bow_y_pix,Bow_X_Gpos,Bow_Y_Gpos,Dir_Bow,Dist_Bow,
```

```
        Stacks_x,Stacks_y,Dir_Stacks,3rd_x,3rd_y,Dir_3rd,
      Velocity_Vector\n");
      fclose(trackfile);
}
else
{
      trackfile  = fopen(filename, "a+");
      fprintf(trackfile,"\n");
      fclose(trackfile);
}

SetTransformation(horangview,Xcamera_m,Xref_m,xref_p,Ycame
ra_m, yhor_p,Yref_m,yref_p,Zcamera_m,Zref_m,
fieldheight,fieldwidth);

while (Track)
{
      counter = counter + 1;
      //starttime and endtime in code to capture an image
      at specific time intervals
      startTime = CTime::GetCurrentTime();
      endTime = CTime::GetCurrentTime();
      endTime = endTime + time_interval;
      // when starttime and endtime are equal than proceed
      to lock image in memory else continue until so
      while (startTime < endTime )
      {
            startTime = CTime::GetCurrentTime();
      }
      //locks image for DMA transfer
      Lock = RioMemLock();
      //grab image from board and save it to
      ImageBufferHandle
      RioGrabPicture();
      //updates gui
      InvalidateRect(NULL, FALSE);
      //updates latest image on gui
      UpdateWindow();
      //if counter is =1 then it will enter this if
      statement
      if(first)
      {
            //FIRST TIME
            //if no_trigger = 1 then user has decided to
            save  images to disk during streamingcapture. If
            no_trigger = 0 then images are not saved to
            disk. Default setting=0
            if(no_trigger==1)
            {
                  //if filetype=1 then user has decided to
                  save images to disk with extension .bmp
                  else if filetype=0 then user wants to save
                  images with extension .jpg
                  if (filetype==1)
                  {
```

```
                    //routine used to save images with a
                    timestamp (hhmmss.bmp). Images saved
                    in directory default drive
                    year/month/day/timestamp   routine
                    found in RioRoutines.cpp
                    SaveBitmap();
               }
               else
               {
                    //routine used to save images with a
                    timestamp (hhmmss.jpg). Images saved
                    in directory default drive
                    /year/month/day/timestamp
                    //routine found in RioRoutines.cpp
                    SaveJpeg();
               }
          }
          if(no_trigger==1)
          {
               //only if images are being saved to disk
               during streaming capture will RioMemLock
               be required
               Lock = RioMemLock();
          }
          else
          {
               //if images are not being saved to disk
               during streaming capture, RioMemUnlock
               will be required
               Unlock = RioMemUnlock();
          }
          //updates the temp0.bmp file with current
          imagebufferhandle image
          SavingTmp0();
          //actual tracking algorithm
          Tracking(counter);
          //at the end of this if statement first is set
          to false so it will never enter this if part of
          this statement again
          first = FALSE;
     }
     else
     {
          //updates the contents of the temp1.bmp by
          copying the current temp0.bmp info
          TempCopy();
          //if no_trigger = 1 then user has decided to
          save images to disk during streamingcapture. If
          no_trigger = 0 then images are not saved to
          disk. Default setting=0
          if(no_trigger==1)
          {
          //if filetype=1 then user has decided to save
          images to disk with extension .bmp else if
          filetype=0 then user wants to save images with
          extension .jpg
```

```
                if (filetype==1)
                {
                      //routine used to save images with a
                      timestamp (hhmmss.bmp). Images saved in
                      directory default drive
                      year/month/day/timestamp
                      routine found in RioRoutines.cpp
                      SaveBitmap();
                }
                else
                {
                      //routine used to save images with a
                      timestamp (hhmmss.jpg). Images saved in
                      directory default drive
                      /year/month/day/timestamp
                      //routine found in RioRoutines.cpp
                      SaveJpeg();

                }
                      if(no_trigger==1)
                {
                      //only if images are being saved to disk
                      during streaming capture will RioMemLock
                      be required
                      Lock = RioMemLock();
                }
                else
                {
                      //if images are  not being saved to disk
                      during streaming capture, RioMemUnlockwill
                      be required
                      Unlock = RioMemUnlock();
                }
                //updates the temp0.bmp file with current
                imagebufferhandle image
                SavingTmp0();
                //actual tracking algoritm
                Tracking(counter);
          }
          //opens the file created earlier in the day for
          addition
          trackfile  = fopen(filename, "a+");
          fprintf(trackfile,"%d,%.19s.%hu,%s,%d,%d,%.3f,%.3f,
                %.3f,%.3f,%d,d,%.3f,%d,%d,%.3f,%.3f\n",counter,
                timeline, timebuffer.millitm,timestamp,xc,yc,
                xnew1,ynew1,angle,distance,rxc,ryc,rangle,lxc
                ,lyc,langle, velocity);
          fclose(trackfile);
     }
     //locks memory for DMA transfer
     Lock = RioMemLock();
     Capturing = TRUE;
     exitgrabs=TRUE;}
}
```